

A SYSTEMICALLY-DELIVERED STEM CELL THERAPY FOR DRY AGE-
RELATED MACULAR DEGENERATION

S. Louise Pay

Submitted to the faculty of the University Graduate School

in partial fulfillment of the requirements

for the degree

Doctor of Philosophy

in the Department of Medical and Molecular Genetics,

Indiana University

August 2017

Accepted by the Graduate Faculty, Indiana University, in partial
fulfillment of the requirements for the degree of Doctor of Philosophy.

Doctoral Committee

Michael E. Boulton, PhD., Co-Chair

Maria B. Grant, M.D., Co-Chair

Nuria Morral, PhD

June 27 2017

Janaiah Kota, PhD

Hal E. Broxmeyer, PhD

S. Louise Pay

A Systemically-Delivered Stem Cell Therapy for Dry Age-Related Macular
Degeneration

Dry age-related macular degeneration (AMD) is a progressive neurodegenerative disorder characterized by geographical atrophy of the retinal pigment epithelium (RPE), causing irreversible central vision loss. Systemically-delivered bone marrow-derived cells (BMDCs), programmed to RPE-like cells via expression of human *RPE65*, regenerate damaged RPE and preserve vision in murine models of retinal degeneration. *RPE65* rapidly activates adenylate cyclase (AC), which then activates endogenous *Rpe65* and RPE-associated marker *Cralbp*. Previous studies expressed *RPE65* from an integrating lentiviral vector (ILV), which is an unnecessary safety risk due to the potential for insertional mutagenesis, as long-term expression of *RPE65* is not required for BMDC programming. Here, we developed a 3rd generation integrase-defective lentiviral vector (IDLV) for programming both murine and human BMDCs to RPE-like cells, reducing insertional mutagenesis risk and expanding the protocol to include human cells. We enhanced IDLV3-*RPE65* infection of murine and human BMDCs by preloading concentrated vector on RetroNectin at MOI 50, and infecting with low-speed centrifugation, increasing *RPE65* mRNA levels from ~12-fold to ~25-fold ($p < 0.05$). IDLV3-*RPE65* infection initiates expression of endogenous *Rpe65* mRNA expression in murine BMDC and *Cralbp/CRALBP* mRNA in both murine and human BMDCs, indicating programming to RPE-like cells. Inhibiting AC in *RPE65*-infected BMDCs abrogated expression of the endogenous genes, confirming the

role of AC activation in programming. Critically, IDLV3-*RPE65*-infected murine BMDCs are recruited to and incorporate into to the RPE layer, and preserve vision in murine models of retinal degeneration. We conclude that BMDCs programmed with IDLV3-*RPE65* successfully prevent retinal degeneration progression and are appropriate for testing in human cells, with a view to move into human clinical trial for the treatment of dry AMD. This approach significantly increases the safety of the therapy and is, to the best of our knowledge, the first application of a single IDLV in the generation of therapeutic cells from adult stem cells.

Michael E. Boulton, PhD., Co-Chair

Maria B. Grant, M.D., Co-Chair

DEDICATION

Susan Montez

You made me miss my plane.

"Dante named names".

Kimberly Quaid

Thank you. It was an honor to be your friend.

I couldn't have done this without you.

ACKNOWLEDGEMENTS

I would like to express my sincere gratitude to my advisor, Dr. Michael E. Boulton, for his guidance and input throughout my graduate career. Working for Dr. Boulton has been an enlightening experience, and has given me invaluable insight into how best to handle a wide range of challenging situations. He has taught me the value of perseverance and patience when things are not working out as intended. Secondly, I would like to thank my co-PI, Dr. Maria B. Grant, for her support and advice throughout my project, and my research committee members, Drs. Hal E. Broxmeyer, Nuria Morral, and Janaiah Kota for keeping me on track and encouraging me.

I would also like to thank my advisory committee members, Drs. Kenneth Cornetta, Brenda Grimes, Rebecca Chan, Scott Witting, and Brittney-Shea Herbert for their support and advice in my early career as a PhD student, and my previous advisor, Dr. Helmut Hanenberg, who taught me everything I know about lentiviral vectors, along with former colleagues Libby Virts and Stephanie Kelich.

None of the work presented in this study would have been possible without my colleagues in the Boulton lab. In particular, Dr. Xiaoping Qi, who taught me how to measure mouse vision and analyze all my data, Judith Quigley who flat-mounted eyes and took the OCT images of my animals, and Sayak Mitter who taught me how to do qRT-PCR and helped prevent my research from making me crazy (well,

at least no more so than I already was at the start). I am also indebted to the undergraduate interns who worked with me over the past few years, Kavya Sankhavaram, Jeffery Franklin Willard, Ranier Horton, and Sam Macro, and the rest of the Boulton/Grant lab members past and present: Kevin Qian, Zhigang Cai, Ahmed Gomaa, Juliana Godoy, Hongmei Gu, Amanda Fisher, Colin IP, Sunu Mathew, Mark Morrisson, Eleni Beli, Sergio LiCalzi, Yaqian Duan, Thao Trinh, Jimmy Dominguez, Rehae Miller, Tatiana Salazar, and Leni and Nicanor Moldovan.

I would like to thank my department, Medical and Molecular Genetics, for always being encouraging and supportive. In particular, academic advisor Dr. Brittney-Shea Herbert and Department Chair Dr. Tatiana Foroud for helping me get through the program, Dr. Steve Dlouhy for making the coursework engaging and interesting, Dr. Gail Vance, for helping me stay focused, Dr. Kimberly Quaid, who knows why she's on this list; Joan Charlesworth and her predecessor Peggy Knople for handling all our administrative requirements and making sure I never forgot to register for anything, and the department in general for being a wonderful collection of people who I am grateful to have had the opportunity to train with.

Thank you to Susan Rice for sorting millions of cells for me and teaching me about flow cytometry, Keith Condon for sectioning all of my eyes, and Tony Sinn for helping with tail vein injections. Simon Curling, Callum Hill, Clare Taylor and Douglas Fraser-Pitt for their help in preparing me to start a PhD; my friends from

the 2011 IBMG cohort Emrin Horgusluoglu, Esther Bolanis, Baindu Bayon, Rania Sulaiman, without whom I would never have passed my first year, and my qualifying exam study buddies James Butler and Meghan Schellinger.

Thank you to my wonderful parents and family, who have been supportive and encouraging and helpful throughout my entire academic career (and life!). I wouldn't be here without you. My church 'family', Becky, Ed, Rachel & Sarah Chan, and Doug, Valerie, Dan & Jessie Beaver, and friends Nicole Brockmann, Tom Beevers, Stuart Learmonth, Nikki Thompson, Brandi Baros, Debbie Seltzer, Cass Muesing, Angela Gilham, Alanna Cotch, everyone in the BRT Club, Meaghan and Jasper Randall, and Michelle Hamilton-Hibler.

Finally, I would like to thank Aaron Sorkin.

"What's next?"

TABLE OF CONTENTS

List of Tables.....	xii
List of Figures.....	xiii
List of Abbreviations.....	xvi
Chapter I: Introduction.....	1
Introduction.....	1
The Retinal Pigment Epithelium.....	7
Overview of the Eye.....	7
Structure and Function of the RPE.....	13
Regional Variations in the RPE.....	30
Normal Aging Changes in the RPE.....	31
Dry Age-Related Macular Degeneration.....	32
Overview.....	32
Normal Aging Changes in the Retina.....	34
Risk Factors for Dry AMD.....	35
Pathology of Dry AMD.....	36
Therapies for Dry AMD.....	49
Stem Cell-Based Therapy for Dry AMD.....	52
Stem Cells in the Normal Retina/RPE.....	54
Stem Cells in Dry AMD.....	56
Lentiviral Vectors.....	65
Lentiviral Vector Structure.....	67

Integrase-Defective Lentiviral Vectors.....	69
Project Summary.....	71
Chapter II: Materials and Methods.....	75
<i>In Vitro</i> Methods.....	75
<i>In Vivo</i> Methods.....	101
Chapter III: Improving the Infection of Bone Marrow-Derived Cells with an Integrase-Defective Lentiviral Vector.....	107
Introduction.....	107
Results.....	109
Discussion.....	131
Chapter IV: Murine Bone Marrow-Derived Cells Programmed with 3 rd Generation Integrating and Integrase-Deficient Lentiviral Vectors Prevent Retinal Degeneration.....	136
Introduction.....	136
Results.....	140
Discussion.....	173
Chapter V: Pharmacological Treatment of Murine and Human Bone Marrow- Derived Cells Induces Differentiation to RPE-Like Cells <i>In Vitro</i> and Provides Insights into the Mechanism of Programming.....	179
Introduction.....	179
Results.....	181

Discussion.....	206
Chapter VI: Discussion.....	211
Appendices.....	224
References.....	231
Curriculum Vitae	

LIST OF TABLES

Chapter I:

Table 1: Life Expectancy and Leading Causes of Death from 1901 to 2014.

LIST OF FIGURES

Chapter I:

Figure 1.1: The Structure of the Human Eye.

Figure 1.2: The Structure of the Retina.

Figure 1.3: The Retinal Pigment Epithelium.

Figure 1.4: Fundus Photograph of a Normal Human Eye.

Figure 1.5: Diagrammatic Representation of the Location of Drusen in Dry AMD.

Figure 1.6: Fundus Photographs of Dry AMD Progression.

Figure 1.7: Foveal Sparing in Human AMD.

Chapter II:

Figure 2.1: Quantification of Cells in a RPE Flat Mount.

Figure 2.2: Plasmid Maps

Figure 2.3: The Structure of the SOD2-KD Model Ribozymes and Vector

Chapter III:

Figure 3.1: IDLVs Infect Murine BMDCs and Induce Expression of Endogenous mRNA, and Infect HT1080 Cells with Minimal Integration.

Figure 3.2: Optimization of the Use of RetroNectin to Infect BMDCs.

Figure 3.3: Enhancing the Infection of BMDCs with IDLV3-*RPE65*.

Figure 3.4: *In Vitro* Differentiation of Murine and Human BMDCs with IDLV3-*RPE65*.

Chapter IV:

Figure 4.1: ILV3-*RPE65-MITF* and IDLV3-*RPE65-MITF* Express Human *RPE65* and *MITF*, and Initiate Expression of Endogenous *Rpe65* and *Cralbp* mRNA in Murine BMDCs.

Figure 4.2: BMDC-ILV3-*RPE65* Incubated Overnight Following Infection Do Not Preserve Vision or Are Recruited to the RPE Layer.

Figure 4.3: BMDC-ILV3-*RPE65* Are Recruited to the RPE Layer and Preserve Vision in Sodium Iodate-Treated Mice.

Figure 4.4: BMDCs Programmed with IDLV3 Vectors Preserve Vision in Sodium Iodate-Treated Mice.

Figure 4.5: BMDCs Programmed with ILV3 or IDLV3 Vectors Are Recruited to and Integrate at the RPE Layer in SOD2-KD Mice.

Figure 4.6: BMDCs Programmed with ILV3 or IDLV3 Vectors Preserve Retinal Integrity in SOD2-KD Mice.

Figure 4.7: BMDCs Programmed with ILV3 or IDLV3 Vectors Preserve Visual Function in SOD2-KD Mice.

Figure 4.8: Improvement in Visual Function in SOD2-KD Mice Treated with ILV3 or IDLV3 Vectors Persists for At Least Six Months.

Chapter V:

Figure 5.1: Forskolin and Rolipram Induce Expression of *Rpe65* and *Cralbp* mRNA in Murine BMDCs.

Figure 5.2: Forskolin and Rolipram Induce Expression of *RPE65* and *CRALBP* mRNA in Human BMDCs.

Figure 5.3: Adenylate Cyclase Inhibitors Inhibit Expression of *Rpe65* and *Cralbp* mRNA in Forskolin and Rolipram-Treated Murine BMDCs.

Figure 5.4: Adenylate Cyclase Inhibitors Inhibit Expression of *RPE65* and *CRALBP* mRNA in Forskolin and Rolipram-Treated Human BMDCs.

Figure 5.5: Adenylate Cyclase Inhibitors Inhibit Expression of *Rpe65* and *Cralbp/CRALBP* in Murine and Human BMDCs Infected with ILV3-*RPE65*.

Figure 5.6: Forskolin and Rolipram-Treated Murine BMDCs Do Not Preserve Retinal Morphology in Murine Models of Retinal Degeneration.

Chapter VI:

Figure 6.1: An Overview of the Treatment of Retinal Degeneration with BMDCs.

LIST OF ABBREVIATIONS

AMD:	Age-Related Macular Degeneration
BMDC:	Bone Marrow-Derived Cell
<i>CRALBP/Cralbp</i> :	Cellular Retinaldehyde Binding Protein
IDLV:	Integrase-Defective Lentiviral Vector
ILV:	Integrating Lentiviral Vector
MITF:	Microphthalmia Associated Transcription Factor
RPE:	Retinal Pigment Epithelium
<i>RPE65/Rpe65</i> :	Retinal Pigment Epithelium Specific Protein 65 kDa

A SYSTEMICALLY-DELIVERED STEM CELL THERAPY FOR DRY
AGE-RELATED MACULAR DEGENERATION

S. Louise Pay

Submitted to the faculty of the University Graduate School
in partial fulfillment of the requirements
for the degree Doctor of Philosophy
in the Department of Medical and Molecular Genetics,
Indiana University

August 2017

Accepted by the Graduate Faculty, Indiana University, in partial
fulfillment of the requirements for the degree of Doctor of Philosophy.

Doctoral Committee

Michael E. Boulton, PhD., Co-Chair

Maria B. Grant, M.D., Co-Chair

Nuria Morral, PhD

June 27 2017

Janaiah Kota, PhD

Hal E. Broxmeyer, PhD

S. Louise Pay

A Systemically-Delivered Stem Cell Therapy for Dry Age-Related Macular
Degeneration

Dry age-related macular degeneration (AMD) is a progressive neurodegenerative disorder characterized by geographical atrophy of the retinal pigment epithelium (RPE), causing irreversible central vision loss. Systemically-delivered bone marrow-derived cells (BMDCs), programmed to RPE-like cells via expression of human *RPE65*, regenerate damaged RPE and preserve vision in murine models of retinal degeneration. *RPE65* rapidly activates adenylate cyclase (AC), which then activates endogenous *Rpe65* and RPE-associated marker *Cralbp*. Previous studies expressed *RPE65* from an integrating lentiviral vector (ILV), which is an unnecessary safety risk due to the potential for insertional mutagenesis, as long-term expression of *RPE65* is not required for BMDC programming. Here, we developed a 3rd generation integrase-defective lentiviral vector (IDLV) for programming both murine and human BMDCs to RPE-like cells, reducing insertional mutagenesis risk and expanding the protocol to include human cells. We enhanced IDLV3-*RPE65* infection of murine and human BMDCs by preloading concentrated vector on RetroNectin at MOI 50, and infecting with low-speed centrifugation, increasing *RPE65* mRNA levels from ~12-fold to ~25-fold ($p < 0.05$). IDLV3-*RPE65* infection initiates expression of endogenous *Rpe65* mRNA expression in murine BMDC and *Cralbp/CRALBP* mRNA in both murine and

human BMDCs, indicating programming to RPE-like cells. Inhibiting AC in *RPE65*-infected BMDCs abrogated expression of the endogenous genes, confirming the role of AC activation in programming. Critically, IDLV3-*RPE65*-infected murine BMDCs are recruited to and incorporate into to the RPE layer, and preserve vision in murine models of retinal degeneration. We conclude that BMDCs programmed with IDLV3-*RPE65* successfully prevent retinal degeneration progression and are appropriate for testing in human cells, with a view to move into human clinical trial for the treatment of dry AMD. This approach significantly increases the safety of the therapy and is, to the best of our knowledge, the first application of a single IDLV in the generation of therapeutic cells from adult stem cells.

Michael E. Boulton, PhD., Co-Chair

Maria B. Grant, M.D., Co-Chair

DEDICATION

Susan Montez

You made me miss my plane.

"Dante named names".

Kimberly Quaid

Thank you. It was an honor to be your friend.

I couldn't have done this without you.

ACKNOWLEDGEMENTS

I would like to express my sincere gratitude to my advisor, Dr. Michael E. Boulton, for his guidance and input throughout my graduate career. Working for Dr. Boulton has been an enlightening experience, and has given me invaluable insight into how best to handle a wide range of challenging situations. He has taught me the value of perseverance and patience when things are not working out as intended. Secondly, I would like to thank my co-PI, Dr. Maria B. Grant, for her support and advice throughout my project, and my research committee members, Drs. Hal E. Broxmeyer, Nuria Morral, and Janaiah Kota for keeping me on track and encouraging me.

I would also like to thank my advisory committee members, Drs. Kenneth Cornetta, Brenda Grimes, Rebecca Chan, Scott Witting, and Brittney-Shea Herbert for their support and advice in my early career as a PhD student, and my previous advisor, Dr. Helmut Hanenberg, who taught me everything I know about lentiviral vectors, along with former colleagues Libby Virts and Stephanie Kelich.

None of the work presented in this study would have been possible without my colleagues in the Boulton lab. In particular, Dr. Xiaoping Qi, who taught me how to measure mouse vision and analyze all my data, Judith Quigley who flat-mounted eyes and took the OCT images of my animals, and Sayak Mitter who taught me how to do qRT-PCR and helped prevent my research from making me crazy (well,

at least no more so than I already was at the start). I am also indebted to the undergraduate interns who worked with me over the past few years, Kavya Sankhavaram, Jeffery Franklin Willard, Ranier Horton, and Sam Macro, and the rest of the Boulton/Grant lab members past and present: Kevin Qian, Zhigang Cai, Ahmed Gomaa, Juliana Godoy, Hongmei Gu, Amanda Fisher, Colin IP, Sunu Mathew, Mark Morrisson, Eleni Beli, Sergio LiCalzi, Yaqian Duan, Thao Trinh, Jimmy Dominguez, Rehae Miller, Tatiana Salazar, and Leni and Nicanor Moldovan.

I would like to thank my department, Medical and Molecular Genetics, for always being encouraging and supportive. In particular, academic advisor Dr. Brittney-Shea Herbert and Department Chair Dr. Tatiana Foroud for helping me get through the program, Dr. Steve Dlouhy for making the coursework engaging and interesting, Dr. Gail Vance, for helping me stay focused, Dr. Kimberly Quaid, who knows why she's on this list; Joan Charlesworth and her predecessor Peggy Knople for handling all our administrative requirements and making sure I never forgot to register for anything, and the department in general for being a wonderful collection of people who I am grateful to have had the opportunity to train with.

Thank you to Susan Rice for sorting millions of cells for me and teaching me about flow cytometry, Keith Condon for sectioning all of my eyes, and Tony Sinn for helping with tail vein injections. Simon Curling, Callum Hill, Clare Taylor and Douglas Fraser-Pitt for their help in preparing me to start a PhD; my friends from

the 2011 IBMG cohort Emrin Horgusluoglu, Esther Bolanis, Baidu Bayon, Rania Sulaiman, without whom I would never have passed my first year, and my qualifying exam study buddies James Butler and Meghan Schellinger.

Thank you to my wonderful parents and family, who have been supportive and encouraging and helpful throughout my entire academic career (and life!). I wouldn't be here without you. My church 'family', Becky, Ed, Rachel & Sarah Chan, and Doug, Valerie, Dan & Jessie Beaver, and friends Nicole Brockmann, Tom Beevers, Stuart Learmonth, Nikki Thompson, Brandi Baros, Debbie Seltzer, Cass Muesing, Angela Gilham, Alanna Cotch, everyone in the BRT Club, Meaghan and Jasper Randall, and Michelle Hamilton-Hibler.

Finally, I would like to thank Aaron Sorkin.

"What's next?"

TABLE OF CONTENTS

List of Tables.....	xii
List of Figures.....	xiii
List of Abbreviations.....	xvi
Chapter I: Introduction.....	1
Introduction.....	1
The Retinal Pigment Epithelium.....	7
Overview of the Eye.....	7
Structure and Function of the RPE.....	13
Regional Variations in the RPE.....	30
Normal Aging Changes in the RPE.....	31
Dry Age-Related Macular Degeneration.....	32
Overview.....	32
Normal Aging Changes in the Retina.....	34
Risk Factors for Dry AMD.....	35
Pathology of Dry AMD.....	36
Therapies for Dry AMD.....	49
Stem Cell-Based Therapy for Dry AMD.....	52
Stem Cells in the Normal Retina/RPE.....	54
Stem Cells in Dry AMD.....	56
Lentiviral Vectors.....	65
Lentiviral Vector Structure.....	67

Integrase-Defective Lentiviral Vectors.....	69
Project Summary.....	71
Chapter II: Materials and Methods.....	75
<i>In Vitro</i> Methods.....	75
<i>In Vivo</i> Methods.....	101
Chapter III: Improving the Infection of Bone Marrow-Derived Cells with an Integrase-Defective Lentiviral Vector.....	107
Introduction.....	107
Results.....	109
Discussion.....	131
Chapter IV: Murine Bone Marrow-Derived Cells Programmed with 3 rd Generation Integrating and Integrase-Deficient Lentiviral Vectors Prevent Retinal Degeneration.....	136
Introduction.....	136
Results.....	140
Discussion.....	173
Chapter V: Pharmacological Treatment of Murine and Human Bone Marrow- Derived Cells Induces Differentiation to RPE-Like Cells <i>In Vitro</i> and Provides Insights into the Mechanism of Programming.....	179
Introduction.....	179
Results.....	181

Discussion.....	206
Chapter VI: Discussion.....	211
Appendices.....	224
References.....	231
Curriculum Vitae	

LIST OF TABLES

Chapter I:

Table 1: Life Expectancy and Leading Causes of Death from 1901 to 2014.

LIST OF FIGURES

Chapter I:

Figure 1.1: The Structure of the Human Eye.

Figure 1.2: The Structure of the Retina.

Figure 1.3: The Retinal Pigment Epithelium.

Figure 1.4: Fundus Photograph of a Normal Human Eye.

Figure 1.5: Diagrammatic Representation of the Location of Drusen in Dry AMD.

Figure 1.6: Fundus Photographs of Dry AMD Progression.

Figure 1.7: Foveal Sparing in Human AMD.

Chapter II:

Figure 2.1: Quantification of Cells in a RPE Flat Mount.

Figure 2.2: Plasmid Maps

Figure 2.3: The Structure of the SOD2-KD Model Ribozymes and Vector

Chapter III:

Figure 3.1: IDLVs Infect Murine BMDCs and Induce Expression of Endogenous mRNA, and Infect HT1080 Cells with Minimal Integration.

Figure 3.2: Optimization of the Use of RetroNectin to Infect BMDCs.

Figure 3.3: Enhancing the Infection of BMDCs with IDLV3-*RPE65*.

Figure 3.4: *In Vitro* Differentiation of Murine and Human BMDCs with IDLV3-*RPE65*.

Chapter IV:

Figure 4.1: ILV3-*RPE65-MITF* and IDLV3-*RPE65-MITF* Express Human *RPE65* and *MITF*, and Initiate Expression of Endogenous *Rpe65* and *Cralbp* mRNA in Murine BMDCs.

Figure 4.2: BMDC-ILV3-*RPE65* Incubated Overnight Following Infection Do Not Preserve Vision or Are Recruited to the RPE Layer.

Figure 4.3: BMDC-ILV3-*RPE65* Are Recruited to the RPE Layer and Preserve Vision in Sodium Iodate-Treated Mice.

Figure 4.4: BMDCs Programmed with IDLV3 Vectors Preserve Vision in Sodium Iodate-Treated Mice.

Figure 4.5: BMDCs Programmed with ILV3 or IDLV3 Vectors Are Recruited to and Integrate at the RPE Layer in SOD2-KD Mice.

Figure 4.6: BMDCs Programmed with ILV3 or IDLV3 Vectors Preserve Retinal Integrity in SOD2-KD Mice.

Figure 4.7: BMDCs Programmed with ILV3 or IDLV3 Vectors Preserve Visual Function in SOD2-KD Mice.

Figure 4.8: Improvement in Visual Function in SOD2-KD Mice Treated with ILV3 or IDLV3 Vectors Persists for At Least Six Months.

Chapter V:

Figure 5.1: Forskolin and Rolipram Induce Expression of *Rpe65* and *Cralbp* mRNA in Murine BMDCs.

Figure 5.2: Forskolin and Rolipram Induce Expression of *RPE65* and *CRALBP* mRNA in Human BMDCs.

Figure 5.3: Adenylate Cyclase Inhibitors Inhibit Expression of *Rpe65* and *Cralbp* mRNA in Forskolin and Rolipram-Treated Murine BMDCs.

Figure 5.4: Adenylate Cyclase Inhibitors Inhibit Expression of *RPE65* and *CRALBP* mRNA in Forskolin and Rolipram-Treated Human BMDCs.

Figure 5.5: Adenylate Cyclase Inhibitors Inhibit Expression of *Rpe65* and *Cralbp/CRALBP* in Murine and Human BMDCs Infected with ILV3-*RPE65*.

Figure 5.6: Forskolin and Rolipram-Treated Murine BMDCs Do Not Preserve Retinal Morphology in Murine Models of Retinal Degeneration.

Chapter VI:

Figure 6.1: An Overview of the Treatment of Retinal Degeneration with BMDCs.

LIST OF ABBREVIATIONS

AMD:	Age-Related Macular Degeneration
BMDC:	Bone Marrow-Derived Cell
<i>CRALBP/Cralbp</i> :	Cellular Retinaldehyde Binding Protein
IDLV:	Integrase-Defective Lentiviral Vector
ILV:	Integrating Lentiviral Vector
MITF:	Microphthalmia Associated Transcription Factor
RPE:	Retinal Pigment Epithelium
<i>RPE65/Rpe65</i> :	Retinal Pigment Epithelium Specific Protein 65 kDa

CHAPTER I: INTRODUCTION

Introduction

The biological process of aging is associated with an increased risk for developing a number of diseases, including cancers, [1] cardiovascular diseases, [2] arthritis, [3] and neurodegenerative disorders such as Alzheimer's disease and Parkinson's disease. [4, 5] This increased risk is contributed to by a number of external factors. For example, genetic predisposition to disease, [2] environmental factors such as smoking and consumption of alcohol, [6] exposure to carcinogenic agents throughout life, [7] and pre-existing conditions such as diabetes. [8]

The average life expectancy in the USA has increased significantly in the past ~100 years, and we continue to develop life-lengthening treatments for infections, disorders, and diseases that have in the past resulted in a lower average life expectancy (Table 1.). Age-associated diseases are therefore increasingly becoming, and will continue to become, a significant concern.

One of the most prevalent aging-associated diseases is Age-Related Macular Degeneration (AMD). Risk for developing AMD increased from age 50 onwards. [9] By 2020, an estimated 196 million people will be affected by AMD worldwide, increasing to 288 million by 2040. [10] AMD is a neurodegenerative disorder characterized by progressive, severe, and irreversible central vision loss resulting

from degeneration of critical retinal cells at the central region of the eye, known as the macula. [9] There are two forms of AMD: wet AMD, and dry AMD.

Wet AMD is characterized by aberrant formation of blood vessels which invade the retinal pigment epithelial (RPE) layer and cause degeneration. Visual improvement has been observed in ~30% of wet AMD patients treated with anti-VEGF injections. [11] Dry AMD is characterized by geographical atrophy of the RPE at the macula and there are currently no effective treatments available. [12] Due to the nature of dry AMD and the lack of blood vessel invasion of the RPE/retina from the choroid, anti-VEGF therapies are not appropriate. The most viable and attractive option for targeting dry AMD in the early stages of disease is replacement of the damaged RPE. [12, 13]

A number of studies have evaluated the potential for RPE cell transplant or RPE replacement with cells derived from adult RPE, embryonic stem cells (ESCs) and induced pluripotent stem cells (iPSC) in dry AMD. [14] While success has been observed in murine models this, has yet to carry over into human clinical trials. [12] Methods of harvesting RPE cells for transplant and delivering transplants of therapeutic cell sheets are highly invasive, [15] and cells transplanted by subretinal injection have been found to exhibit poor adhesion to the Bruch's membrane. [16] Additionally, there are several safety concerns associated with the use of pluripotent cells. ESCs, and both autologous and non-patient-derived iPSCs, may be immunogenic, [17] and may form teratomas. [18] The first clinical trial using

iPSCs for AMD was interrupted by the discovery of genomic alterations in the iPSCs, which were not present in the patient cells from which the iPSCs were derived. [19] ESCs also have the added complication of well-documented ethical concerns, with their use restricted in several parts of the world due to the fact that their harvest requires the destruction of fertilized embryos.

In this study, we present a minimally-invasive, systemically-delivered cell-based therapy for RPE replacement in dry AMD, using autologous adult bone marrow-derived cells (BMDCs) modified with a single lentiviral (LV) vector.

We assert that our approach will maximize recovery of vision, and delay the progression of the disease, as BMDC-derived RPE cells can be replaced before the neural retina, in particular the photoreceptor layer, has become damaged. Systemically injected cells, which are recruited to the RPE from the blood, integrate uniformly across the RPE layer as opposed to forming a 'clump' in one area, improving the potential for visual recovery. [13] The use of autologous BMDCs also reduces tumorigenic potential in comparison with iPSCs, due to the fact that the cells are not pluripotent. The use of autologous cells also reduces the potential for immunogenicity, and is less ethically problematic than the use of ESCs.

In this chapter, we will review the structure and function of the RPE, the pathology of dry AMD, the application of stem cell-based therapies in AMD, and the use of

LV vectors. Finally, we will present an overview of the background, approach, and outcomes of our study.

TABLE 1	Average Life Expectancy (Years)		³Leading Causes of Death (in order of prevalence)
	Male	Female	
1901¹	47.6	50.6	Pneumonia, influenza, tuberculosis, diarrhea, enteritis, ulceration of intestines, diseases of the heart, intracranial lesions of vascular origin, nephritis, accidents, cancer, senility, diphtheria.
1950¹	65.6	71.1	Diseases of the heart, malignant neoplasms, vascular lesions affecting central nervous systems, accidents, influenza and pneumonia, tuberculosis, arteriosclerosis, chronic and unspecified nephritis and other renal sclerosis, diabetes mellitus.
2014²	76.4	81.2	² Diseases of the heart, malignant neoplasms, unintentional injuries, chronic lower respiratory diseases, stroke, diabetes, suicide, Alzheimer's Disease, influenza and pneumonia, chronic liver disease and cirrhosis, Parkinson's Disease
Sources:	¹ Department of Commerce United States Life Tables, ² National Vital Statistics Reports Volume 65 (5) Deaths: Leading Causes for 2014, ³ National Office of Vital Statistics (lead1900_98.pdf).		

Table 1. Life Expectancy and Leading Causes of Death from 1901 to 2014.

The average life expectancy of males and females has increased from 47.6 and 50.6 to 76.4 and 81.2 respectively between 1901 and 2014. The most prevalent causes of death have changed from predominantly infectious disease to lifestyle and age-related disease due to changes in the availability of treatments and changes in environmental factors which contribute to disease, along with the direct link between an increase in average life expectancy and the development with age-related disease such as Alzheimer's disease.

The Retinal Pigment Epithelium

Overview of the Eye

Almost every organism on Earth has evolved to use the light from the sun as a means of perceiving the world or as a source of energy, with over 95% of the world's living organisms possessing a form of eye or a mechanism by which light can be processed, such as photosynthesis or carbon fixation. [20-22] The human eye is a complex structure consisting of several specialized components (Figure 1.1) which are involved in the processing of light to generate signals which are then processed into images by the brain. At the front of the eye, the cornea, pupil, and iris function to control the entry and focusing of light into the eye. At the back of the eye, the retina, comprised of ten highly specialized layers, processes light into neural impulses, which are then transmitted to the brain via the optic nerve. [23]

The retina, from the innermost to outermost layer, consists of: (1) the inner limiting membrane, (2) the nerve fiber layer, (3) the ganglion cell layer, (4) the inner plexiform layer, (5) the inner nuclear layer, (6) the outer plexiform layer, (7) the outer nuclear layer, (8) the outer limiting membrane, (9) the photoreceptor layer, and, finally (10,) the RPE. [23] (Figure 1.2). Layers 1-9 of the retina collectively comprise the neural retina, which is considered a part of the central nervous system (CNS). The neural retina and RPE layer develop separately, with the neural

retina formed from the inner wall of the optic cup, which is the evaginated optic vesicle that develops as an outgrowth of the diencephalon region of the brain, [24] and the RPE layer formed from the outer wall of the optic cup. [24]

Figure 1.1

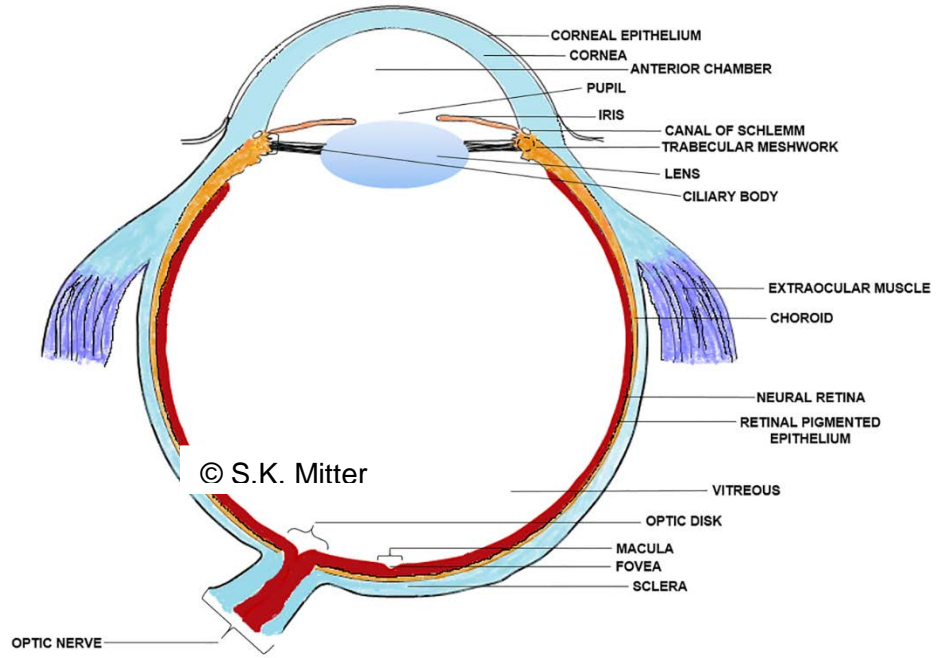


Figure 1.1. The Structure of the Human Eye. Diagram of the human eye with major structures. (Image from: <https://www.intechopen.com/books/autophagy-in-current-trends-in-cellular-physiology-and-pathology/autophagy-in-ocular-pathophysiology>)

Figure 1.2

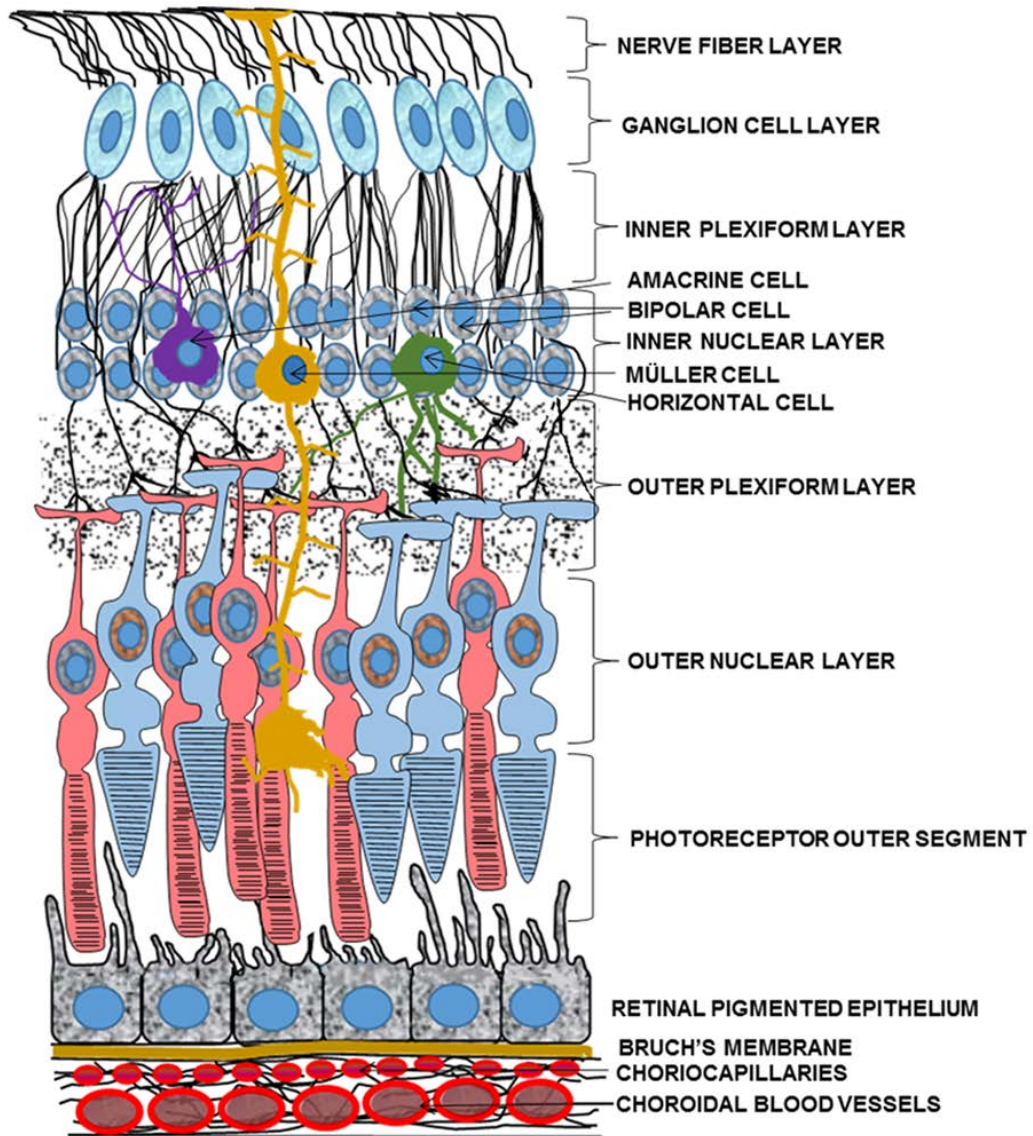


Figure 1.2. The Structure of the Retina. Diagrammatic cross-section of the retina, showing the neural retina layers, the underlying RPE, Bruch's membrane, choroid and the specialized cell types at each layer. (Image from: <https://www.intechopen.com/books/autophagy-in-current-trends-in-cellular-physiology-and-pathology/autophagy-in-ocular-pathophysiology>)

Structure and Function of the RPE

Structure

In humans, RPE cells are found at the highest density in the central macular region of the eye (Figure 1.1) and become less dense as the retina extends into the periphery, [25] with ~ 4220 cells/mm² in the foveal region, decreasing to ~ 3002 /mm² in the midperipheral regions, and ~ 1600 /mm² in the outer peripheral fundus.[26] Overall, the human RPE layer consists of $\sim 3.5 \times 10^6$ ($\pm 4.9 \times 10^5$) cells.[26] Each RPE cell supports, on average, 30-40 photoreceptors. [27]

The RPE is dysfunctional in most retinal degeneration disorders, and is the first cell type to degenerate in AMD. As RPE integrity and viability is critical for the maintenance of photoreceptor cells and, thus, the visual cycle and overall retinal function, we focused on regenerating the RPE layer in models similar to the pathology of dry AMD. The RPE is a highly specialized cell with a number of critical functions, the loss of which all contribute to retinal degeneration.

The RPE consists of a monolayer of hexagonal cells which are held together by lateral tight junctions, adherens junctions, and gap junctions, forming the outer blood/retinal barrier. [28, 29] The RPE cells are polarized, with the apical microvilli extending into the interphotoreceptor matrix [30] of the subretinal space, and the infolded basal membrane tightly adhered to the underlying collagenous, acellular

Bruch's membrane via integrin interaction (Figure 1.3). [29, 31] The apical microvilli of the RPE interact with the apical rod and cone photoreceptor outer segments in the outer nuclear layer of the neural retina. The choriocapillaris of the choroid lies directly beneath the Bruch's membrane and consists of highly fenestrated endothelium and capillaries. [29, 32] Mature RPE cells are traditionally considered to be post-mitotic, meaning they are terminally differentiated and unable to divide; [33] however, it has recently been suggested that the lack of RPE division may be maintained by its close proximity with photoreceptor cells, resulting in contact inhibition as opposed to permanent inability to divide, which may contribute to disease in retinal detachment disorders. [34] While the normal RPE is non-proliferative, the cells do retain the ability to proliferate as they can be stimulated to do so in culture, and become proliferative in some disease such as resulting from RPE injury or proliferative vitreoretinopathy. [35-37]

The apical surface of the RPE is unusual in comparison with other epithelial cells as it is oriented toward the apical surface of the photoreceptors, as opposed to being oriented toward an inner vessel or other lumina. [38] The apical microvilli, approximately 5-7 μm long, [39] are intricately connected with, though not physically attached to, the apical membrane of the photoreceptor outer segments in the interphotoreceptor matrix of the subretinal space, which consists of proteins and other components required for the transport of nutrients to and from the retina and RPE. [30] This interaction is not only required for 'communication' between the photoreceptors and RPE, but also for maintaining retinal attachment to the RPE.

Disruptions in the interaction between RPE and photoreceptor cells in the interphotoreceptor matrix, such as during retinal detachment, results in degeneration of the photoreceptors due to their reliance on the RPE and subsequent loss of retinal integrity. Aquaporin-1 expressed on the RPE apical membrane contributes to maintaining the connection between the RPE and neural retina, aiding retinal attachment. [40]

While specific localization of organelles and protein expression is typical in epithelial cells, some localization in RPE cells and protein expression differs significantly from other epithelial cell types – in contrast to the majority of epithelial cells, the sodium/potassium ATPase and associated ankyrin and fodrin proteins [41] are located at the apical membrane at the RPE. [38] The adhesion molecule N-CAM, [42] the extracellular matrix metalloproteinase inducer EMMPRIN/CD147 [43, 44] and sodium/potassium/chlorine ($\text{Na}^+/\text{K}^+/\text{Cl}^-$) transport proteins [38] are also located apically in the RPE. The difference in localization of channels and proteins is referred to as reverse polarity, [31, 44, 45] which is critical for the function of the RPE [38] as the sodium/potassium ATPase is necessary to maintain an ionic environment in the subretinal space that is conducive to phototransduction. [38]

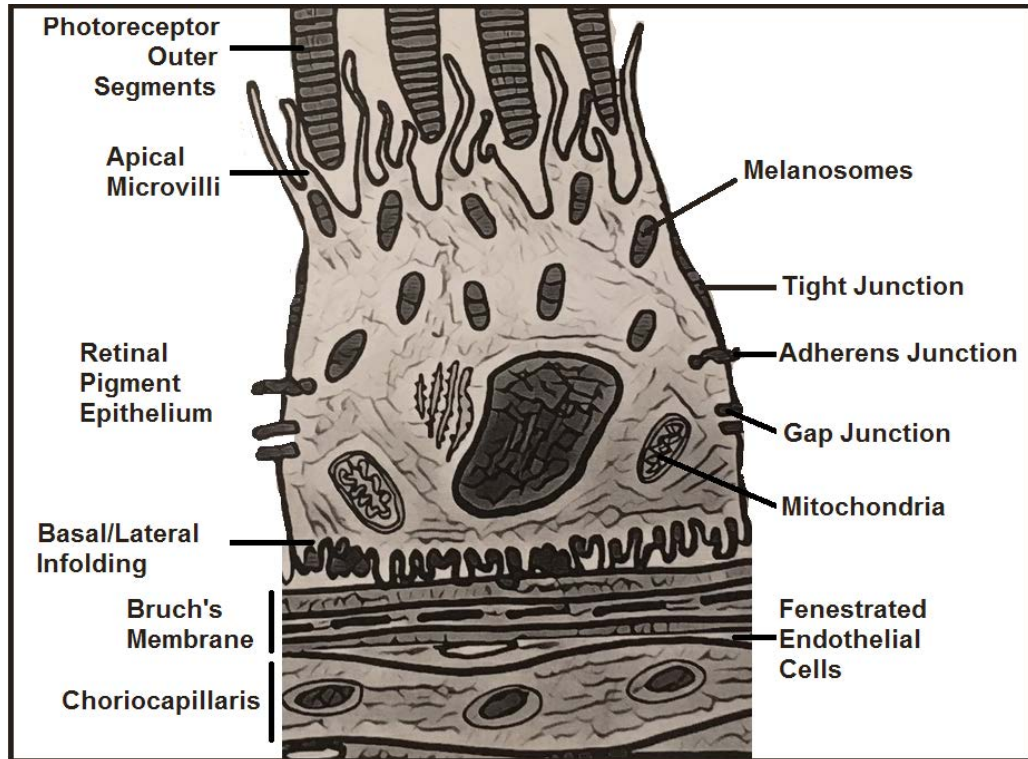
In contrast to the interaction between the apical membranes of the RPE and photoreceptor cells, the basal lamina of the RPE is directly attached to the Bruch's membrane. The basal lamina of the RPE, as is typical for epithelia, is infolded, [46]

and considered to be the outermost layer of the Bruch's membrane, [47] which is a permeable extracellular matrix of proteins that separates the RPE from the choriocapillaris. The basal lamina of the RPE is approximately 0.15 μm thick, [48, 49] and contains an extracellular matrix of filamentous structures including fibronectin, heparan sulfate, proteoglycans, [47] type IV collagen isoforms alpha 1-5. [50, 51] Laminins, for example laminins 1, 5, 10, and 11, are produced by the RPE cells and aid in the attachment of the RPE cell layer to the Bruch's membrane through interaction with integrins. [52] The attachments of the basement membrane and the actin cytoskeleton of the cell, adhering the RPE cell to the Bruch's membrane, are observed as focal adhesions at the base of the RPE. [53] RPE cells are highly pigmented with melanin [54] and lipofuscin, with the former present during development, and the latter accumulating with age. [55] RPE cells contain several organelles including lysosomes, [56] phagosomes, [57] microperoxisomes, [58] and melanosomes. [31] Melanin is localized to elongated melanosomes, which are apically located and can extend into the apical microvilli. [59] Mitochondria and nuclei are basally localized, [31, 32] and the cytoplasm contains a large amount of smooth endoplasmic reticulum (ER) and minimal rough ER. [32]

Finally, the lateral membranes of the RPE function as the outer blood/retinal barrier due to the presence of tight junctions near the apical membrane which control diffusion between cells, [28] adherens junctions, which are cell-cell adhesion molecules that bind cells together through interaction of cadherins with actin

filament,[60] and gap junctions, comprised of connexins, which facilitate the movement of small molecules and ions between the RPE cells. [61, 62] These cell-cell adhesions are necessary for the regulation of transport of nutrients, ions, and water between the neural retina and the choriocapillaris [63] and to maintain the polarity of the RPE cells. [31]

Figure 1.3



© S.L. Pay (source)

Figure 1.3. The Retinal Pigment Epithelium. Diagrammatic representation of an RPE cell and underlying Bruch's Membrane and choriocapillaris.

Function

The specialized structure of the RPE cell contributes to its multiple functions, all of which are necessary to maintain the normal function of both the neural retina and the choroid, which the RPE cells support. As the RPE layer is situated between the photoreceptor layer and the choroid, and forms a tight barrier which is not permeable, the RPE functions to regulate the flow of nutrients, ions, and waste products to and from the choroid and the neural retina, maintain the photoreceptors, and to limit RPE cell damage resulting from its high metabolic activity and exposure to inducers of oxidative stress. [29, 64] While light absorption was one of the earliest elucidated functions of the RPE, and was thought for some time to be the only function of the RPE, it is now known that critical components of RPE functionality also include phagocytosis of the photoreceptor outer segments, the recycling of visual cycle substrates, spatial buffering of potassium, maintenance of the immune privileged status of the eye, and epithelial transport to and from the subretinal space and the choroid. [29, 64]

Light Absorption and Pigments

The pigmented melanin granules of the RPE primarily function to absorb scattered light. These pigmented granules, located in melanosomes, absorb light energy, protecting the photoreceptor cells and the RPE itself from extensive damage from excess light exposure. [65] This is important for maintaining RPE cells, as they are

constantly exposed to factors which contribute to oxidative stress and resulting oxidative damage and are not capable of regenerating in the event that they become damaged, due to their post-mitotic status.[66] RPE cells therefore require mechanisms to protect themselves against several sources of oxidative stress. [67] Melanin also functions as a metal ion scavenger.[68] Melanosomes in the RPE exhibit antioxidant properties against non-light-associated oxidative damage; for example, in cells expressing large numbers of melanosomes, oxidative damage from hydrogen peroxide was reduced in comparison with cells not expressing melanosomes. [67]

In addition to melanosomes, RPE cells also contain lipofuscin and melanolipofuscin. Unlike melanosomes, which form during development and remain during the lifetime of the cell without the capacity to renew, lipofuscin and melanolipofuscin develop during the aging process. These pigments are implicated in age-related disorders of the RPE, and will be discussed in more detail in context with AMD pathology. Lipofuscinogenesis occurs as a result of autophagy [66] and incomplete phagocytosis of photoreceptor outer segments. [69] Melanolipofuscin, a combination of melanin and lipofuscin, has been associated with the cells' post-mitotic status. [70]

Phagocytosis of Photoreceptor Outer Segments

Photooxidative damage to the photoreceptor outer segments results in daily shedding of damaged outer segment disc tips, which are constantly renewed at the base of the outer segment which is distal to the tip in order to maintain correct outer segment length. [71] The full outer segment is replaced in this manner approximately every ten days, with 10% of their length lost daily. [72, 73] Shedding follows a circadian pattern, with the initiation of disc shedding occurring once per day, coinciding with the onset of light. [74] The RPE phagocytoses the shed outer segment discs, and, as extensive photoreceptor degeneration is observed when the ability of RPE cells to phagocytose these discs is removed, this process is one of the most important roles of the RPE in supporting the neural retina. [75] Not only is it necessary for the RPE to remove these waste products to avoid pathological build-up of debris in the subretinal space, it is also necessary for the RPE cells to adequately break down the phagocytosed material to prevent damage to the RPE cells themselves – RPE cells must be capable of sustained, long-term processing of photoreceptor outer segments as they are non-dividing cells. [73] There are several regulated stages of photoreceptor outer segment phagocytosis by the RPE, which differs from traditional phagocytosis as RPE cells are not macrophages. [73, 75]

The first step is the recognition of the photoreceptor outer segment by the RPE, and subsequent binding, which is contributed to by phosphatidylserine, $\alpha\beta_5$ integrin, CD36, and milk-fat-globule-EGF-factor-8 (MFG-E8).[73] Phosphatidylserine expression on the photoreceptor discs has been associated with recognition of these discs by the RPE as material to be phagocytosed, with segments expressing phosphatidylserine, a cell-surface marker indicating cell death, are recognized by the RPE.[73] It has been shown that $\alpha\beta_5$ integrin, which is apically localized in RPE cells, is required for the binding of shed outer segments to the RPE, with binding diminished in the presence of antibodies blocking its function *in vitro* and loss of *in vivo* phagocytosis observed in $\alpha\beta_5^{-/-}$ mice. [76, 77] Binding of $\alpha\beta_5$ integrin is facilitated by tetraspanin CD81, resulting in a decrease in binding when silenced. [78] MFG-E8, which is expressed early in the light cycle, around the same time that photoreceptor outer segment shedding occurs, contributes to the roles of $\alpha\beta_5$ integrin and phosphatidylserine, binding to $\alpha\beta_5$ integrin and facilitating the interaction between the shed photoreceptor discs, $\alpha\beta_5$ integrin, and the RPE. [73] In mice lacking MFG-E8, RPE phagocytosis of shed discs was reduced, and this could be restored by providing soluble MFG-E8, confirming its critical role in the phagocytosis process. [79] MFG-E8 and $\alpha\beta_5$ integrin are not, however, required for the internalization of the segments.[76] This, instead, is mediated by expression of CD 36 receptors on the RPE, which has been reported to be both required and sufficient for the internalization of bound photoreceptor outer segments into the RPE, [76] required for the second step of phagocytosis.

This second step in RPE phagocytosis of photoreceptor outer segments is engulfment and phagosome formation, which is dependent on the expression MER proto-oncogene tyrosine kinase (Mertk), growth arrest-specific 6 (Gas6) or protein S, focal adhesion kinase (Fak), annexin A2, tubby, Tulp1, and myosin II. [73] The role of Fak in engulfment is related to the role of $\alpha_v\beta_5$ integrin in binding, as Fak forms a complex with, and is activated by, apical RPE $\alpha_v\beta_5$ integrin, and blocking this interaction in mice results in a lack of engulfment despite binding to the RPE. [80] Knocking out Annexin A2 delays Fak activation, leading to a buildup of phagosomes in the RPE. [81] Fak is also required for the phosphorylation of Mertk, which is also necessary for engulfment of photoreceptor outer segments by RPE cells. [80] In mice with the *Mertk* gene knocked down, photoreceptor outer segment debris builds up in the subretinal space, an absence of phagosomes, and exhibit retinal degeneration similar to that observed in the Royal College of Surgeons rat, which has an RPE with an inherent inability to phagocytose outer segments due to mutations in *Mertk*, demonstrating a critical role for *Mertk* in outer segment phagocytosis, and highlighting the critical importance of this phagocytosis in the support of the neural retina. [82, 83] Mertk binds to Gas6 and related protein, Protein S, the roles of which were first determined in the retina. [84] Both Gas6 and Protein S are ligands of Mertk [85] and function independently to facilitate RPE phagocytosis of outer segments, as knocking out either gene does not affect the process; however, knocking out both results in a phenotype similar to that observed in the absence of Mertk. [84, 86] Additional Mertk ligands tubby and tubby-like protein 1 (Tulp) also activate Mertk, facilitate the organization of myosin

II in the RPE and colocalization with phagosomes, where tubby and Tulp1 were found to be colocalized with Lamp1, a marker of mature phagosomes. [85]

The final step in RPE phagocytosis of photoreceptor outer segments is degradation, which requires myosin VIIa, caveolin-1, a decrease in lysosomal pH, and an increase in protease activity. [73] Myosin VIIa defects cause Usher syndrome, in which abnormal phagocytosis of photoreceptor outer segments leads to accumulation of disc segments in phagosomes within the RPE, resulting from an inhibition of fusion of the phagosome with the lysosome. [87] Phagosomes must be transported to the lysosome for degradation of the phagocytosed contents to occur. The protease Cathepsin D and Caveolin-1 are required for phagolysosomal degradation of engulfed outer segments,[88] and Caveolin-1 is recruited to the phagolysosome, where, in its absence, Cathepsin D levels decrease and lysosomal pH increases. [88] An acidic pH in the lysosome along with active protease activity is necessary for proper degradation to occur. Therefore, when this pH is increased, material will not be adequately cleared from the RPE. Severe, progressive vision loss occurs in Usher syndrome as a direct result of a build-up of unprocessed outer segment material in the RPE, highlighting the importance of clearing this material post-engulfment for maintaining the integrity and function of the RPE cell layer. Without the clearance of photoreceptor waste material, RPE cells are unable to adequately support the visual cycle.

Recycling of Visual Cycle Substrate 11-Cis-Retinal

Another key mechanism by which RPE cells maintain the visual cycle is in the recycling of 11-cis-retinal for photoreceptor cells. During the visual cycle, the photoreceptor pigment rhodopsin component 11-cis-retinal, which is an isomer of retinaldehyde, is converted to all-trans-retinal, thus converting rhodopsin to its active form, metarhodopsin II. [89-91] This process is the 'start signal' of the visual cycle, which necessitates the rapid overturn of visual cycle substrates. 11-cis-retinal must be available to convert metarhodopsin II back into rhodopsin for the next cycle, otherwise, the photoreceptor cells are no longer able to correctly polarize. Consequently, the ability of the cells to promote the visual cycle cascade is lost. [89-91] Photoreceptor cells, however, are unable to convert all-trans-retinal back to 11-cis-retinal, meaning that they are unable to independently generate the substrates required for the visual cycle to persist. [89-91]

The RPE cells play a vital role in this process, converting all-trans-retinol into 11-cis-retinal for the photoreceptors. All-trans-retinal is first converted to all-trans-retinol in the photoreceptor cell, [92] then transported to the RPE cell, in which it is isomerized to form 11-cis-retinal. [89-91] This process involves six key proteins: the interphotoreceptor retinoid-binding protein (IRPB), the cellular retinol binding protein (CRBP), lecithin-retinol transferase (LRAT), the RPE protein 65kDa (RPE65), retinol dehydrogenases (RDH), and the cellular retinaldehyde-binding protein (CRALBP). [89-91] All-trans-retinol is chaperoned into RPE cell from the

photoreceptor by the interphotoreceptor retinoid-binding protein IRPB, [89-91] from which it is transferred to CRBP and is converted to all-trans-retinyl by LRAT. [89-91] RPE65 converts all-trans-retinyl to 11-cis-alcohol and, facilitated by CRALBP, retinol dehydrogenases convert this to 11-cis-retinal. [89-91] Finally, IRBP transports 11-cis-retinal back to the photoreceptor cells. [89-91]

The photoreceptor pigment rhodopsin conversion to metarhodopsin as a result of the conversion of 11-cis-retinal to all-trans-retinal also necessitates the spatial buffering of potassium by RPE cells. Sodium and calcium decreases in the presence of light and photoreceptor polarization results in an increase in uptake of potassium from the subretinal space by the inner segments via Na^+/K^+ -ATPase. [89] The apical membrane of the RPE first hyperpolarizes in response to the decrease in potassium. [64, 93-95] Following this, the basal membrane first hyperpolarizes, then depolarizes in response to the decrease in potassium, [94] resulting in a release of potassium into the subretinal space. [64] This potassium modulation is enabled by the expression of kir potassium channels on the surface of the apical plasma membrane of RPE cells, [96-98] and the electrical output of the hyperpolarization of the apical and basal membranes of the RPE during potassium channel response to photoreceptor polarization is a component of the c-wave of the electroretinogram. [99, 100]

Trans-Epithelial Transport between the Retina and Choroid

In addition to the previously discussed mechanisms by which the RPE layer supports photoreceptor function, the RPE is also responsible for providing energy, in the form of glucose, and for transporting the fatty acid 22:6 omega 3 from the choriocapillaris to the photoreceptors. [101] Trans-epithelial transport is facilitated by sodium/potassium ATPase. [29] Glucose transport is critical to provide the energy required for phototransduction, and is transported into the subretinal space, for uptake by the neural retina, from the choroid. This is facilitated by the inducible glucose transporter GLUT1, and the constitutive glucose transporter GLUT3. [29] 22:6 omega 3 is required for maintaining the structural integrity of the photoreceptor cells and synaptic membranes, [102] and is both transported to the subretinal space by the RPE and used by the RPE itself to generate neuroprotectin D1. [102, 103] Neuroprotectin D1 is both anti-inflammatory and anti-apoptotic, and has been shown to counteract RPE apoptosis following DNA hydrogen peroxide-induced oxidative stress. [102, 103]

The RPE cells also remove water from the subretinal space to the blood via the choriocapillaris, which is necessary to remove the water produced during phototransduction, and avoid a buildup of water in the retina. [38, 104-106]

Immune Modulation

The microenvironment of the eye, including the subretinal space and the RPE, is protected by the prevention of the free movement of cells from the blood into and out of the eye, and therefore the eye is protected from inflammatory and immune responses through a combination of a physical barrier to entry of cells from the blood, comprised of the inner and outer blood/retinal barrier, inhibition through expression of immunosuppressive peptides, and active regulation of systemic immune cells. [107] The RPE plays several roles in maintaining the immune privileged status of the eye, [108] which is critical for preserving vision by protecting the eye from adverse inflammatory responses.

Firstly, the outer blood/retinal barrier formed by the RPE prevents the entry of immune cells from the blood stream, effectively separating the eye from the systemic immune system. [64] Secondly, RPE cells are capable of directly influencing the adaptive immune response by releasing extracellular vesicles in response to inflammatory cytokines which are capable of inhibiting T-cells. [109] RPE cells express TGF-beta 1 and TGF-beta 2, [110] galectin-1, [111] interleukin 1 receptor agonist (IL-1ra), [112] MHC molecule and adhesion molecules [29] resulting in a down regulation of immune responses. Human RPE cells also express the Fas ligand, which, when interacting with activated T-cells, induces programmed cell death in the T-cells, indicating that RPE cells are capable of directly killing activated T-cells to prevent immune cell invasion of the eye, as

blocking Fas ligand expression in the RPE inhibited FasL-associated T-cell death. [113] RPE cells also suppress the immune response through expression and secretion of complement factor H in response to inflammatory cytokine interferon gamma, [114] suggesting a potential mechanism for the involvement of complement factor H mutations in both promoting and protecting against the development of AMD.

Regional Variations in the RPE

The morphology, function, and size of RPE cells is not consistent across the whole human retina, with the number of RPE cells increasing, and size decreasing, according to location [115] and correlating with the number of photoreceptors requiring the RPE support. [26] Thus, the RPE cells at the macular region, where photoreceptors exist at their highest density, are present in larger numbers but are smaller (~14 μm) than those observed in the peripheral regions (~60 μm). [26, 116] The highest density of RPE cells exists in the fovea. In the peripheral retina, RPE cell density is at its highest in the nasal fundus.[26] Functionally, lysosomal enzymes acid phosphatase, B-glucuronidase, and N-acetyl-B-glucosaminidase have been found to be enriched in peripheral RPE cells in a canine model, [117] whereas in a bovine model, another lysosomal enzyme Cathepsin D was found to be enriched in the central region compared with the peripheral region, [118] indicating that lysosomal function varies across different locations in the eye.

Finally, sodium potassium pump expression varies regionally, with higher expression observed in the peripheral vs. macular region in humans. [119]

Normal Aging Changes in the RPE

Several changes occur in the RPE during aging which are not necessarily pathogenic, but may contribute to the development of retinal degeneration in some individuals. These changes include an overall density loss in RPE cells at a rate of approximately 0.3% per year with age, as determined by a study on 53 normal human eyes. [26] An increase in apoptotic RPE cells is observed in the macular region compared with the peripheral retina with aging; however, interestingly, the cell density in this region remains the same despite a high incidence of apoptotic cells, and it has been suggested that non-apoptotic peripheral RPE may be recruited to compensate for the loss of cells at the macula. [120]

RPE cell pigmentation changes with normal aging, with a loss of melanin, an increase in complex melanin granules, and an increase in lipofuscin observed with age in a study of 50 eyes aged between 1-100, most pronounced in the macular region. [121] The presence of small sub-RPE deposits referred to as drusen is observed during normal aging. Numerous large drusen are considered a hallmark of AMD, but as small (<63 μm) drusen are also present in normal aging eyes, these are not considered indicative of disease in otherwise normal eyes.

Feher *et al.* described a decrease in mitochondrial number and function in normal aging eyes in conjunction with lipofuscin granule accumulation, [122] and it has also been reported that mitochondrial DNA damage accumulates with aging in rodents as a result of a change in the expression of enzymes necessary to repair mitochondrial DNA [123] which has become damaged as a result of exposure to reactive oxygen species, while the majority of the damage was observed in the photoreceptor cells, [124] mitochondrial DNA damage and lack of repair proteins was also observed in rodent RPE. [123]

Collectively, while non-pathogenic in the context of vision loss, these aging-related changes may contribute to the development of RPE-related disorders such as dry AMD.

Dry Age-Related Macular Degeneration

Overview

Senile macular degeneration was first identified by Otto Haab in 1885 as a pathological alteration of pigmentation and loss of retinal integrity around the macular region which correlated with progressive loss of vision in patients over 50 years old. However, the disease was not fully characterized until the 1970s, when it was determined by Donald Gass that a build-up of sub-RPE deposits (referred to as drusen) prior to retinal degeneration at the macular region was a hallmark of

what is now referred to as AMD. AMD is a late-onset disorder, with symptoms typically appearing in adults age 50 and over. [125] In the 60-64-year-old age group, approximately 5% are affected by AMD in its early stages. [9] It is a multifactorial, heterogeneous neurodegenerative disorder characterized by the build-up of drusen, dysfunction and atrophy of the RPE prior to progressive loss of the photoreceptor cells. [125] Two forms of AMD are now known. Wet AMD is characterized by exudative choroidal neovascularization (CNV), whereas dry AMD is characterized by geographic atrophy in the absence of CNV, [125] though in the very late stages of disease, dry AMD can develop into wet AMD in some patients. As progression of dry AMD is considerably slower than progression of wet AMD, the 'time window' for treatment with a cell-based therapy is wider in dry AMD, and may allow for more effective early intervention if at-risk patients can be identified early in the development of RPE dysfunction. As there are no current effective therapeutic interventions available, we have focused on dry AMD in this project, hypothesizing that treatment early in the progression of the disease is more likely to preserve vision loss as it is easier to prevent further degeneration than to address severe vision loss after it has already occurred.

In this section, we will review the normal aging process in the retina, the risk factors and pathology of dry AMD, and an overview of treatments which have been attempted in dry AMD.

Normal Aging Changes in the Retina

The retina undergoes several 'normal' changes during aging in addition to the previously discussed changes in the RPE. In a study of 100 people aged 6-79 (without retinal disease), Alamouti and Funk described an overall annual reduction in the thickness of the whole retina by 0.53 μM . [126] As much as 20% of retinal thinning is attributed to thinning of the retinal nerve fiber layer, [127] observed as a 0.44 μM annual reduction in thickness at this layer, [126] or 2.5 μM per decade of life. [128] This loss of thickness has been attributed to a loss of ganglion cells, with less thinning observed in the optic disc region. [128] The optic nerve itself is affected by aging, with the neuroretinal rim region decreasing by 0.28-0.39% annually. [129] An increase in both the vertical optic cup diameter and optic cup area is also observed during normal aging, resulting in an increase in the cup to disc ratio of 0.1 over a 40 year period in a study of 88 healthy individuals. [129]

The density of cells in the photoreceptor layer also decreases annually with age, with a greater loss of rod photoreceptors in comparison with cone photoreceptors observed in a study of 55 normal eyes, with a mean yearly density loss of 0.37% and 0.18% respectively. [130] Photoreceptor loss occurs predominantly in the periphery of the retina and fovea, with the loss of rod cells preceding the loss of cone cells. [131] Retinal thinning also includes the macular region of the eye, with a loss in retinal thickness at the macular region observed as a loss of macular volume of 0.01mm³ per year. [127]

These age related changes, like those discussed in the RPE, are considered normal and are not typically associated with loss of visual function; however, changes in the thickness of the retina is observed in age-related disorders of the retina, indicating that the loss of retinal cells as part of the aging process may be a precursor to the development of retinal degeneration in people who are exposed to other risk factors.

Risk Factors for Dry AMD

The most significant risk factor for AMD is aging. Risk for developing wet or dry AMD increases from age 50 onwards, with Caucasian people over 75 years old having the greatest risk for developing the condition. [132] Other non-modifiable risk factors include gender, [133, 134] iris color, [135] and genetic susceptibility. [125, 136, 137] Several genetic loci are associated with either risk for, or protection against, developing AMD. [125, 136, 137] However, no single specific gene or mutation has been found to cause the disorder directly. Modifiable risk factors for AMD include smoking, [138] hypertension, [139] excessive alcohol use, [140] obesity, [141] and nutritional deficiencies in antioxidants and zinc. [142]

The complexity of the risk factors, both genetic and environmental, and lack of a clear cause beyond aging itself as a common initiator in the development of either wet or dry AMD, therapeutic strategies are best aimed toward targeting the physiological damage to the retina and underlying RPE as opposed to correcting

the different factors which contribute to disease development. While genetic factors play a significant role in predisposing people to developing AMD, the complexity of the disorder makes it difficult to predict patient outcomes purely on the basis of genetics, or to design therapeutics for targeting a single gene, though identification and characterization of susceptibility alleles does provide insight into pathogenesis of the disease.

Pathology of Dry AMD

The fovea of the macula lutea ('yellow spot': Latin, *macula* = spot; *lutea* = yellow), located at the center of the retina in the human eye, [143] is the primary site of RPE degeneration in dry AMD. [144] It is clearly visible as a dark spot on fundus images of normal eyes (Figure 1.4). This region of the eye contains a dense concentration of cone photoreceptor cells and is responsible for central high acuity color vision. There are several clinical features which encompass dry AMD from the early to the late stages, including the accumulation of large soft drusen, RPE abnormalities, and geographic atrophy of the RPE.

Early AMD

Early dry AMD is largely asymptomatic in terms of altered vision, so it is important for early intervention that the disease is recognized before patients begin to experience vision loss, which typically presents as gradual diminished vision when performing activities such as driving or reading. [145] One or both eyes may be

affected, though in the early stages, unilateral vision loss is more common than bilateral vision loss. Patients with AMD in one eye have an increased risk for developing AMD in the other eye with increased severity where progression and severity in the affected eye can be a predictor for accelerated progression and severity in the unaffected eye in the future. [146]

Early dry AMD features a thickening and breakdown of the Bruch's membrane. [144, 147] Bruch's membrane thickening is contributed to by the accumulation of primarily phospholipid deposits referred to as basal linear and basal laminar deposits within and around the membrane, [148] and also involves an increase in TIMP-3 expression in comparison with that observed with normal aging of the Bruch's membrane [149] along with dysregulation of expression of other extracellular matrix proteins. [150] The earliest detectable signs of dry AMD are visualized as the accumulation of yellow-colored extracellular deposits known as drusen. [144] Drusen can be either 'hard' or 'soft', [151] with hard drusen typically <125 μm in diameter and soft drusen >125 μm in diameter. [152] While drusen are considered a 'hallmark' of AMD, it is important to note that the presence of drusen is not directly linked to AMD as some drusen are present at the macula of almost all eyes as a part of the normal aging process. [153] One subset of drusen, referred to as either pseudodrusen or reticular ('net like') drusen, are particularly associated with the development of late AMD. [154]

Drusen are located between the basement membrane of the RPE and the inner collagenous layer of the Bruch's membrane (Figure 1.5). [155] While it has been established for some time that the number and size of drusen can be predictive of the development of dry AMD, the composition of drusen and the process by which these deposits form is not fully understood. [155] It is generally accepted that drusen contain lipids, carbohydrates, and proteins [156] derived from both the RPE and Bruch's membrane. [157] Interestingly, some drusen have been shown to contain amyloid beta, which is also found in plaques in Alzheimer's disease. [158] Patients are classified as having early, intermediate, or late dry AMD depending on the appearance and features at the macular region. [159] Early dry AMD is characterized by the presence of drusen between 63 and 125 μ m in diameter (Figure 1.6a.). [159] These early presentations of drusen are not associated with vision loss. Changes in the pigmentation of the RPE are also indicative of the onset of dry AMD, [44] with hyperpigmentation observed in the presence of drusen which has been suggested to result from local RPE cell displacement (Figure 1.6a). [155] Intermediate dry AMD is characterized by the presence of medium drusen in combination with RPE abnormalities or large drusen (>125 μ m) [159] (Figure 1.6b), and late-stage dry AMD is characterized by large confluent drusen, central vision loss and the presence of geographic atrophy, which is clearly visible as a large fluorescent spot in the macular region, with clearly visible choroidal vasculature due to regional RPE hypopigmentation. (Figure 1.6c).

Figure 1.4

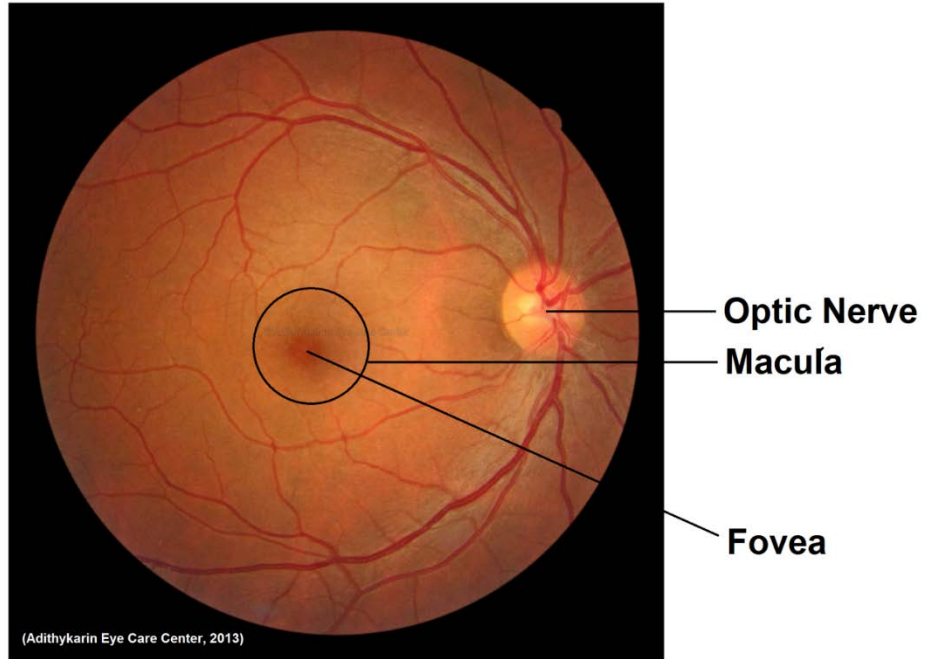
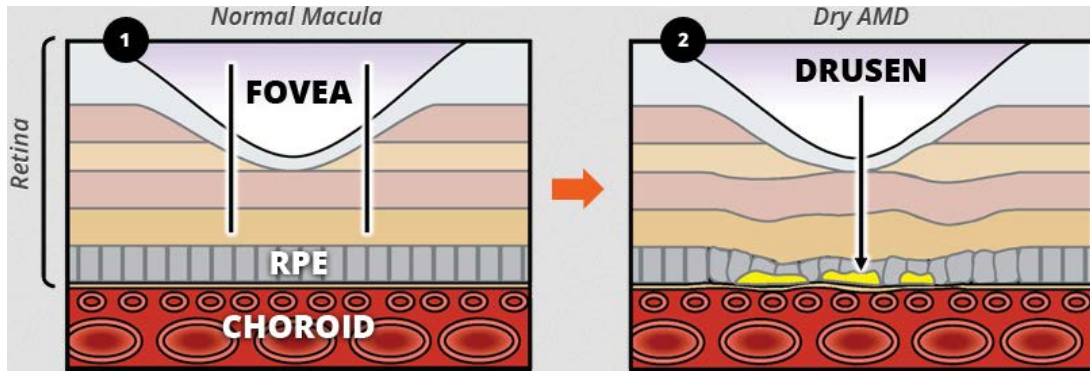


Figure 1.4. Fundus photograph of a normal human eye showing the fovea of the macula and the optic nerve.

Figure 1.5



Source: <http://www.opthotech.com>

Figure 1.5. Diagrammatic Representation of the Location of Drusen in Dry AMD.

Figure 1.6

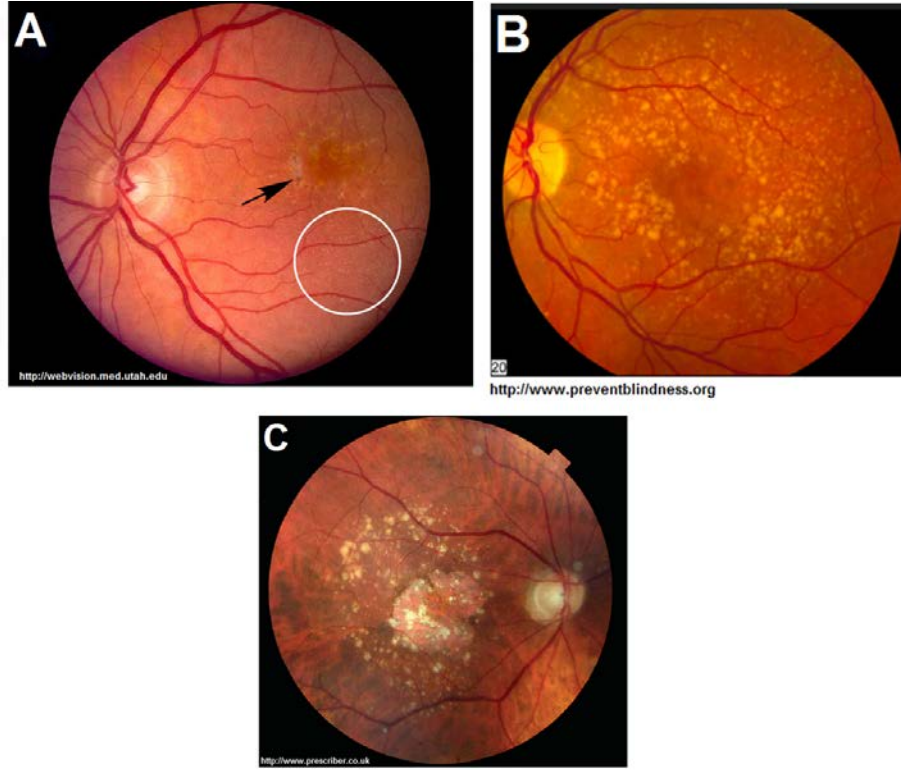


Figure 1.6. Fundus Photographs of Dry AMD Progression. (A) Fundus photograph of a human eye with early dry AMD. Arrow indicates RPE degeneration at the macular region of the eye. Circle indicates the presence of drusen. **(B)** Fundus photograph of a human eye with intermediate AMD. **(C)** Fundus photograph of a human eye with late dry AMD.

Late AMD

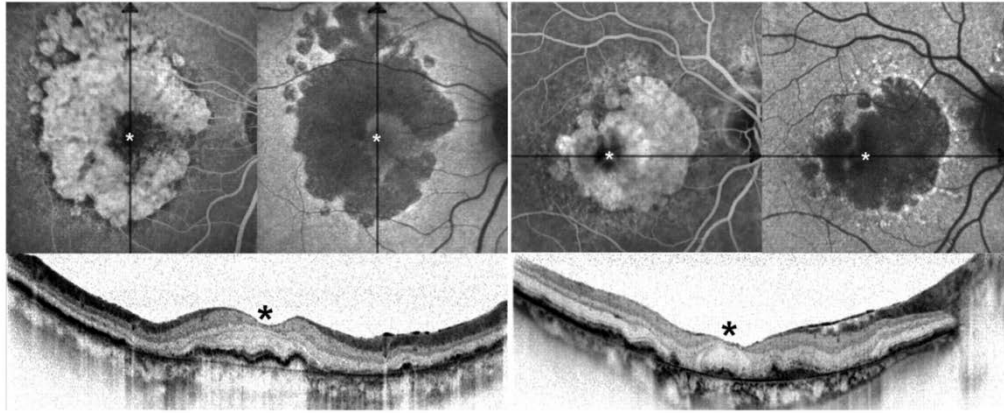
As the disease progresses, geographic atrophy of the RPE results in loss of photoreceptor cells critical for high acuity vision at the macular region, autofluorescent lipofuscin granules accumulate in the RPE cells [160, 161] subretinal microgliosis develops, [162] and retinal morphology deteriorates. [125] The critical role of the RPE in maintaining the retina is first diminished, then lost, and the resulting loss of the photoreceptor cells results in irreversible loss of central high-acuity vision, as the greatest cell loss is observed at the macular region, though peripheral degeneration is also frequently observed. [160]

The presence of geographic atrophy (GA) marks the progression of dry AMD from the early to the late stage of the disease, and is clearly visible by fluorescein angiography (Figure 1.6c). [163] The area of GA presents as a large autofluorescent patch on the fundus photograph, localized around the macular region of the eye.[163] The choroidal vessels are prominently visible around the area of GA as a result of a localized loss of RPE cell pigmentation, and the GA may be surrounded by areas of hyper- and hypo-pigmentation as a result of RPE dysfunction (Figure 1.6c). [163] While GA encompasses much of the macular region, in some cases identified earlier in the progression of the late stage of dry AMD, the area of GA will present in a 'horseshoe' figuration, with GA predominantly forming in the parafoveal area and not in the fovea itself, which is known as foveal

sparing (Figure 1.7), [163] as the involvement of the fovea may occur only in the later stages of late AMD, perhaps due to the migration of RPE cells from the periphery to the fovea as observed in normal aging. [164] Overall retinal thickness is significantly reduced in the region of GA in comparison with retinal thickness loss in normal aging, and RPE degeneration is often present in the periphery of the eye in addition to in the macular region. [163]

At the very end stage of dry AMD, GA may progress to choroidal neovascularization, as observed in wet AMD. [163] This is observed in approximately 10-15% of patients with dry AMD, and involves the formation of abnormal blood vessels which invade the RPE layer and retina from the choriocapillaris, and will eventually lead to the formation of a disciform scar and severe vision loss. [163, 165]

Figure 1.7



(Schmitz-Vacklenberg *et al.*, 2009)

Figure 1.7. Foveal Sparing in Human AMD. Asterisks mark the fovea surrounded by an area of foveal sparing located around the central region of the macula. This indicates areas of undamaged RPE/retina surrounded by areas of extensive damage, responsible for moderate preservation of vision at the very center of the visual field.

Therapies for Dry AMD

As mentioned previously, there are no current effective therapies for dry AMD, though several approaches have been attempted in both animal studies and in human clinical trial. These include, but are not limited to, macular translocation surgery, [166] RPE transplantation, [163] retinal prosthesis implantation, [167] induced pluripotent and embryonic stem cell based therapies (iPSC and ESC), [168] all of which necessitate invasive surgery. Any procedure which involves transplantation into the subretinal space is associated with a significant risk for causing blindness due to intraocular hemorrhage, retinal detachment, or proliferative vitreoretinopathy as a result of retinal detachment. [169] The benefits of these treatments are therefore likely limited to patients in the later stages of disease, in order for the potential benefit to outweigh the potential risk, which limits the outcome in terms of visual recovery in comparison to what may be possible with a less invasive approach such as the one we describe in this study. One non-invasive study by the Age-Related Eye Disease Study Research Group involving treatments with supplements containing a combination of antioxidants and zinc indicates that these may aid in preventing the progression of intermediate to late dry AMD, though little benefit was observed in patients with earlier stage AMD, [170] again making this an option which is unlikely to result in significant visual recovery due to the retinal damage already present.

The concept of macular translocation has predominantly been investigated in the context of wet AMD. Van Meurs *et al.* reported successful translocation of peripheral RPE, but observed deterioration of vision due to vitreoretinopathy in 3 patients. [171] However, this surgery has been attempted in cases of geographic atrophy. The principle of the treatment is to detach and rotate the retina to relocalize the macular region in an attempt to preserve it. [163] This treatment is therefore highly invasive. Cahill *et al.* reported a study in which investigated the recurrence of RPE damage in dry AMD patients treated with macular translocation in 2005, finding that the translocation was insufficient to prevent the new development of pathology in the foveal region, indicating that this treatment is insufficient to preserve vision in dry AMD. [166]

RPE transplantation was considered an attractive possibility in dry AMD due to the fact that it is widely accepted that loss of the RPE precedes damage to the neural retina. Therefore, replacing the damaged RPE with a new sheet of RPE cells was thought to be sufficient to preserve retinal function and, consequently, vision. The majority of human RPE transplantation studies have involved wet AMD with some, albeit limited, vision recovery in a small number of people. [172-175] While it was found that transplanting sections of a fetal RPE layer into the subretinal space of four dry AMD patients did not result in transplant rejection in comparison with results observed in wet AMD patients receiving the same treatment, and that visual function was not reduced as a result of the procedure in the dry AMD transplant recipients, [176] a patient treated with an RPE allograft developed leakage,

fibrosis, and anti-photoreceptor immune responses, indicating that while the eye is 'immune privileged', immunosuppression is likely required for allografts and allogeneic transplants, which may be detrimental to the health of patients over the age of 65. [177] A subsequent trial in wet AMD demonstrated effective engraftment of an RPE allograft with immunosuppression, but no recovery of vision. [178]

More recent advances in the development of organic retinal prostheses in a rat model [179] and the electrode-based Argus II Retinal Prosthesis System, which has been shown to be potentially beneficial in retinitis pigmentosa, [167] present an encouraging possibility for future use in humans, though retinal prosthesis insertion remains an invasive procedure.

In recent years, researchers have been investigating the potential for stem cell treatment in RPE replacement through the subretinal transplant of RPE cells derived from ESC or iPSC, which have been successful in animal models. iPSC are advantageous as they can be derived from autologous cells and therefore do not require immunosuppressant therapy, though the transplant protocol for both of these cell types is, again, invasive as it necessitates invasion of the subretinal space. Unfortunately, while ESC have been shown to be relatively safe in terms of not generating teratomas or tumors, or tissue rejection, in one clinical trial, the visual recovery in the patients was limited, as was the patient number. [180] In terms of iPSC-derived RPE, the results of the first human clinical trial using these cells in AMD by Takahashi's group in Japan revealed encouraging safety data, and

indicated that the treatment does not worsen vision, but again a lack of significant improvement in vision was observed. [181] This study was carried out on wet AMD patients as opposed to dry AMD, therefore it is not currently known if visual improvement can be obtained using these cells in dry AMD. [181] We propose that this lack of success in visual recovery is in part due to the fact that patients have been treated in the later stages of disease, and that subretinally-transplanted cells may not spread out enough to recover vision, as they have been shown to remain in a 'clump' at the site of injection. [180] The success and limitations of stem cell-based therapy for dry AMD, along with our strategy for overcoming these limitations, will be discussed in more detail in the next section.

Stem Cell-Based Therapy for Dry AMD

Stem cell-based therapies for both wet and dry AMD have been under investigation for several years. Multiple sources of cells for cell-based therapy for diseases of the retina have been evaluated in murine models and human clinical trials, including mature cells such as RPE from the patient or a donor (of either fetal or adult origin), [169] iris pigment epithelial cells, [182] Schwann cell, [183] and a wide range of stem cells, including: mesenchymal stem cells, [184] adipose stem cells, [185] RPE cells derived from ESC, [180, 186] iPSC, [181] and bone marrow-derived cells. [13, 187] The majority of recent studies have focused on stem cell-based therapies as opposed to using developed RPE cells as stem cells have the capacity to proliferate, whereas using autologous or donor RPE is limited by the

limited proliferation potential of the cells. Stem cell-derived RPE cells are also easier to isolate and purify in larger numbers than RPE cells from the patient's own eye or from donor eyes.

Although these therapies have shown considerable promise in animal studies, the successful transfer into the clinic for treatment of humans has been limited to date. Several complications with the procedures for developing and delivering the cells contribute to this, including highly invasive cell delivery protocols, immune system rejection of cells where cells are not autologous, the inability of the cells to adequately differentiate and spread out across the RPE layer, inability of cells to adhere to the aged Bruch's membrane, and the fact that most studies address late-stage disease, at a point where replacing the RPE may be insufficient to recover vision as a result of involvement of the neural retina in disease development prior to treatment with cells.

In order to develop a successful stem cell-based therapy for dry AMD, several factors must be considered: (1) the origin of the cells, (2) the cell delivery mechanism, and (3) the ability of the cells to integrate and function at the site of degeneration. The origin of the cell is closely linked to the available delivery mechanisms, of which there are three options: intravitreal, subretinal, and systemic. The majority of stem cells must be delivered subretinally for RPE repair, though improvement of vision has been observed in murine models with intravitreal injections.

Systemic delivery is the least invasive method, and is thought to only be appropriate for cells of bone marrow origin. In order for systemic delivery to result in adequate localization of cells to the RPE, the cells must be able to circulate in the blood stream, and it is not clear that any cell type besides the bone marrow progenitor-derived RPE and mesenchymal stem cells would have the capacity to do this. Bone marrow-derived cells are a particularly attractive cell source for RPE replacement therapy because they are easily obtained and can be delivered with the minimally invasive systemic injection approach, which provides the potential for treating in the early stages of disease. We have therefore focused on bone marrow-derived cells in our study. In this section, we will review the results of stem cell-based therapies in dry AMD to date, and introduce our approach for the use of bone marrow-derived cells, which will be discussed in greater detail in the subsequent section.

Stem Cells in the Normal Retina/RPE

Unlike the retinae of fish [188] and amphibians, [189] mammal retinae possess limited potential for regenerating damaged tissue. [190-192] There are, however, some cell types which contribute to low level neuronal regeneration following injury, which can also be induced by exposure to growth factors or drugs. [190-192] Müller cells, which are neurogenic in fish, [190] have been found to express similarities to neural stem cells when activated following retinal injury [190, 193] or

exposure to an agonist of the alpha-7 nicotinic receptor. [192] Murine and human Müller cells have been found to have potent neurogenic potential when cultured *ex vivo*, indicating that the microenvironment of the mammalian retina actively suppresses its own regeneration potential. [193, 194] RPE cells have also been shown to be able to proliferate while outside of the retinal microenvironment, and a population of cells which have been described as adult RPE stem cells (RPESCs) have been isolated from the human retina. [195] Removing these cells and activating them *ex vivo*, or pharmacologically activating them *in vivo* may be a viable option for repair using endogenous mechanisms. [195]

As RPESCs are a relatively recent discovery, few studies have evaluated their potential in RPE regeneration in retinal degeneration diseases; however, Stanzel *et al.* reported in 2014 that sheets of RPE generated from human RPE stem cells could be transplanted into rabbits and were capable of engrafting and persisting without immune system targeting, [196] suggesting that transplant of cells derived from RPE stem cells may be more capable of restoring visual function than transplant of mature RPE. This is likely to be due to the stem cell status of the cells, as immature RPE are more likely to mimic developing RPE than the transplant of fully differentiated RPE – if attachment of the cells to the Bruch's membrane following transplant is dependent on the age of the cells, [16] it is possible that developing RPE stem cell-derived RPE layers may be able to engraft whereas adult RPE may not as a result of expression of early markers that the adult RPE would no longer express.

Stem Cells in Dry AMD

Embryonic Stem Cell-Derived RPE

ESCs self-renew and can give rise to any cell type. [197] They are associated with significant ethical concerns due to their embryonic origin, [198] and ESC-derived cells are highly immunogenic, [199] which limits their potential in regenerative medicine, especially in cases where giving immunosuppressants to address their immunogenicity would be contraindicated for the patient. Immunosuppressant therapy is associated with an increased risk for developing infection [200, 201] and malignancies. [202, 203] Nevertheless, ESCs have been applied in retinal degeneration disorders such as Stargardt's macular dystrophy and dry AMD in three landmark clinical trials. The first two trials were carried out by Massachusetts company Ocata Therapeutics (formerly Advanced Cell Technology), [180, 186] and the third by a Korean group using cells obtained from Ocata Therapeutics. [204]

In the first Ocata Therapeutics trial, reported by Schwartz *et al.*, ESC-derived RPE cell transplants in one Stargardt's muscular dystrophy patient, and one dry AMD patient, were not rejected and were not tumorigenic over the 4 month period in which patients were monitored. [180] While limited visual recovery was reported, the study was designed to evaluate safety, not therapeutic performance, and therefore the minimal recovery to 20/800 in the Stargardt's muscular dystrophy

patient, and 7-letter improvement in the dry AMD patient, should not be interpreted to indicate that significant visual improvement could not be attained in future studies. [180, 205] In the second study, involving 18 patients (nine with Stargardt's muscular dystrophy, and 9 with dry AMD), the ESC-derived RPE were again found not to be hyperproliferative. Again, minimal improvements in vision were reported, though only in 10 eyes. Additionally, a decrease in visual acuity was observed in one eye. [186] In the third trial, a lack of tumorigenicity and rejection was observed and visual acuity was improved by 9-19 letters in three out of four patients (two with dry AMD and two with Stargardt's muscular dystrophy). [204]

While these trials provide invaluable information on the tolerability and engraftment capacity of transplanted RPE, [180, 186, 204] they have received criticism for the statistical relevance of their findings due to the small sample size (24 patients total), [206] and the majority of observed improvement in visual acuity could be accounted for by the high variability of the mechanisms used to measure vision. [207-209] Larger trials are therefore necessary to determine the accuracy of the findings. Additionally, the patients were monitored from 4 months up to a year, which raises concerns regarding the validity of the authors' claims that the ESC-derived RPE are not tumorigenic, since this has not been investigated long-term.

IPSC-Derived RPE

iPSC were developed by Takahashi and Yamanaka in Japan in 2007, who reported that retroviral vector-mediated expression of *Klf4*, *Sox2*, *Oct4*, and *c-Myc* in human fibroblasts resulted in the dedifferentiation of the cells to an ESC-like cell with pluripotent properties. Later modifications to this protocol eliminated *c-myc*, improving the cells' safety as *c-myc* is a known oncogene. Expression of two additional genes, *NANOG* and *LIN28* in combination with the previously mentioned factors enhances the production of iPSCs. [210] The advantages of iPSC as a source of RPE cells over ESC are clear: there are no ethical concerns associated with their development, and they can be derived from the patients' autologous fibroblasts, reducing their immunogenicity. There are, however, some safety concerns with iPSC – Riggs *et al.* used transcriptome comparisons of iPSC and oncogenic foci to determine that the transcriptional alterations associated with dedifferentiation of fibroblasts to generate iPSCs are similar to the changes associated with the development of cancers. [211] While this in itself should not be taken to indicate that the iPSCs themselves are tumorigenic, it highlights that the potential for iPSCs to become tumorigenic may be higher than that of ESCs or other stem cell types. This may be overcome by screening of iPSCs prior to use in regenerative medicine approaches to filter out any tumorigenic cells prior to delivery. [212]

The most recent study involving iPSC-derived RPE cells was carried out in Japan by Yamanaka and Takahashi, the pioneers of iPSC development. While the study focused only on wet AMD, it provides valuable insight into the use of iPSC in retinal degeneration. First and foremost, the subretinal transplant of a sheet of iPSC-derived RPE was tolerated and not degraded by the immune system. [181] Additionally, no significant adverse effects were observed in any of the patients treated. [181] These findings suggest that, while the procedure was invasive, it was also safe and did not result in any significant loss of vision, which is encouraging for the future potential of iPSC-derived RPE cells in humans. Unfortunately, however, as was the case in previously discussed clinical trials, none of the patients tested had any improvement in their visual function 1 year after the placement of the iPSC-derived sheets. [181] This suggests that lack of immunogenicity and retention of the graft over long periods of time may be insufficient for visual recovery in patients. While it is encouraging that vision was not found to worsen after treatment, the lack of improvement is a significant concern, as theoretically the replacement of the RPE layer should improve vision if no other complications are present. Some potential reasons for the lack of recovery of vision include inadequate 'communication' between the RPE and the photoreceptors or choroid, inadequate RPE function in terms of supporting photoreceptors and the choroid, or, as previously discussed, the photoreceptors, choroid, and/or neural retina may have already been too damaged for any recovery in vision to occur. It would be interesting to compare, in the long term, the use of this technique in patients with early AMD with late-stage AMD patients. Replacing

the RPE layer early in disease may preserve vision by delaying the progression from early to late AMD; however, obtaining approval to carry out iPSC-derived RPE cell sheet transplants on patients who do not yet have substantial vision loss may be difficult to obtain. At present it is not known whether or not the RPE sheets are capable of supporting vision at all, meaning that they could cause immediate and severe worsening blindness in early-stage patients. Further investigation is therefore required to determine whether or not the RPE sheets can be functional in terms of supporting high acuity vision prior to testing in these patients.

Mesenchymal Stem Cells

Mesenchymal stem cells (MSCs) have been shown to differentiate into an RPE-like phenotype, expressing *RPE65* and the RPE-associated *CRALBP* gene following exposure to RPE-conditioned media, or coculture with RPE cells, photoreceptor outer segments, or a combination of these techniques. [213] Rat bone marrow-derived MSCs differentiate into RPE, photoreceptor, and glial cells in a sodium iodate model [214] and retinal neural cells in a mechanical injury model. [215] MSCs have been evaluated in a clinical setting for the treatment of retinitis pigmentosa, which is an inherited disorder of the RPE, in which adipose tissue-derived MSCs which had not been differentiated to RPE-like cells prior to delivery were subretinally injected in 11 patients with advanced disease. [184] Complications included the development of choroidal neovascularization at the site of injection, and five developed epiretinal membranes requiring further treatment,

[184] highlighting the potential damaging effect of subretinal delivery. While none of the patients experienced loss of vision as a result of the treatment, only one reported an improvement in visual acuity. [184]

Adipose Stem Cells

Recently a study which lacked appropriate FDA approval tested the use of autologous adipose tissue-derived stem cells. The cells were injected intravitreally and bilaterally, and resulted in severe and irreversible blindness in both eyes of all 3 patients treated with the procedure within 7 days of treatments. [185] This highlights several important issues: (1) that adequate safety studies must be carried out prior to use in humans, (2) that stem cell-based therapy **must be** regulated more stringently by the FDA, and, (3) that autologous stem cells are not necessarily safe. Autologous cells have long been touted as non-immunogenic. In principle, they are – these cells are ‘self’ and should therefore not be recognized as foreign when injected back into the patient. However, the treatment of autologous cells *ex vivo* has a significant potential to result in an immunogenic cell population when injected back into the patient. ‘Transformation’ of autologous cells to cells with an allogeneic phenotype may occur, for example, due exposure of cells to serum or growth factors that are either not human or not from the patient. Even if the cells themselves are not immunogenic, there is a potential for injecting components of reagents or media used to culture or expand cells along with the cells if the cell preparation protocol is not adequately monitored, as has been

suggested as the reason for the adverse response in the aforementioned clinical trial. While some changes to the cells may result in the cells being killed by the immune system, the presence of components of culture media have the potential to trigger, for example, a type I hypersensitivity reaction in the patient, if injected repeatedly. It is therefore vital that autologous cells are handled in such a way that they do not become immunogenic in order to protect patients treated with these cells.

Bone Marrow Cells

Bone marrow derived cells have traditionally been thought to be limited to differentiating along hematopoietic lineages. In recent years, however, it has been reported in several studies that these cells may be capable of differentiating along non-hematopoietic lineages. [216] Bone marrow-derived cells have an advantage over other cell types due to their ability to home to sites of injury; in particular, their expression of CXCR4 [217] aids migration to areas of cellular injury that involve the release of the cytokine CXCL12/SDF-1, the CXCR4 ligand. [217, 218] Both SDF-1 and CXCR4 have been localized to the photoreceptor layer and the retinal pigment epithelium in AMD, [219] indicating that the migration of bone marrow-derived cells to the site of injury in AMD is a potential mechanism for reparative processes. The critical advantage of using a bone marrow-derived cell approach is that, due to the cells; natural ability to be recruited to sites of injury from the bloodstream, therapeutic bone marrow-derived cells can be delivered systemically.

This eliminates the need for invasive delivery mechanisms such as subretinal injection and subretinal transplant.

It has been shown in two mouse models, one similar to wet AMD involving VEGF overexpression, and one similar to dry AMD, resulting from sodium iodate-induced RPE injury, that unmanipulated bone marrow-derived cells are recruited to the site of injury and regenerate damaged RPE in mice. [220] In this study, GFP LSK cells were transplanted into irradiated wild type mice with retinal injury. GFP+ cells were found in the RPE layer of these mice and were not found to be a result of cell fusion in XY FISH analysis, [220] indicating true incorporation of these cells at the site of injury.

Because unmodified BMDCs are capable of genuine integration at the RPE layer, the potential for modifying these cells and 'exploiting' their regenerative capacity is an attractive prospect for treating dry AMD. BMDCs are advantageous because they are not pluripotent in the same way that ESCs and iPSCs are – these cells will not become any cell type or differentiate into multiple cell types without an external factor such as having been recruited to a site of cellular injury. They are also not able to form teratomas, as they will not form tumors originating from multiple germ layers. These cells are therefore significantly less likely to result in adverse side effects than ESC and iPSC. Additionally, they can be obtained from the patient, eliminating the need for immunosuppressants as autologous cells will not be rejected if handled appropriately *ex vivo* prior to reinjection. While iPSCs

are also autologous, BMDCs have the advantage that they only need to be differentiated from BMDC to RPE, as opposed to being dedifferentiated into iPSC prior to differentiation into RPE. As previously mentioned, this makes them considerably less likely to be tumorigenic as they are being directed to differentiate into a specific cell type from a starting point which is not designed to be able to be pluripotent.

We have therefore focused on BMDCs in dry AMD. Prior to this study, our group published evidence that BMDCs programmed with the *RPE65* gene are recruited to and integrate into the RPE layer of mice with either sodium iodate [216] RPE damage or SOD2 knockdown-mediated RPE damage.[13] In both of these models, expressing the human *RPE65* gene resulted in enhanced migration to and integration into the RPE layer of BMDCs in comparison with mice treated with naïve BMDCs. This approach is thought to work for a number of reasons: (1) expressing the *RPE65* gene provides a critical RPE function to the cells, (2) expressing the *RPE65* gene activates expression of a second gene, *Cralbp*, and, (3) enhancing the BMDCs differentiation into RPE likely enhances their integration at the site of injury. Additionally, the minimally invasive systemic delivery allows for early intervention.

Given that evidence in the literature suggests that mature RPE – either autologous, donor-derived, or stem cell-derived – does not integrate into and adequately adhere to Bruch's membrane whereas immature RPE cells do, our approach offers

a significant advantage over other approaches. The reason for this is that our programming process for differentiating BMDCs results in an immature cell type which fully differentiates into mature RPE *only* in the microenvironment of the retina. This process mimics development, as the cells are incapable of fully differentiating *ex vivo* and likely rely on factors present in the retina itself to form fully functional RPE. These cells are therefore more likely to be functional than cells which have been transplanted after being fully differentiated *ex vivo* such as iPSC and ESC-derived RPE.

Modifying BMDCs to express RPE associated genes prior to delivery likely enhances the therapeutic potential of the cells due to their ability to perform the function of normal RPE following recruitment for the bloodstream, and expression of *RPE65* in the cells may also aid in recruiting the cells to the site of injury. While the lentiviral vector-mediated approach used in the aforementioned studies has proven successful, [13, 187] safety concerns still exist regarding the insertional mutagenesis and subsequent tumorigenic potential of lentiviral vectors. In this study, we therefore aimed to improve the safety of the *RPE65* gene delivery approach.

Lentiviral Vectors

Stable integration of replication-incompetent LVs into the host genome allows for long-term expression of therapeutic transgenes in quiescent and rapidly dividing

cells. [221] However, not all LV transduction applications necessitate stable integration or long-term expression of a transgene. [222-224] Since the *RPE65* transgene activates expression of adenylate cyclase in BMDCs, and this in turn switches on expression of endogenous *Rpe65*, [216] we suggested that transient expression of the *RPE65* transgene may result in sufficient programming in the absence of integration, further enhancing the safety of our approach for human clinical trials.

In this study, we therefore carried out a systematic optimization of a 3rd generation non-integrating lentiviral vector (IDLV) expressing human *RPE65* for programming both murine and human BMDCs.

LV vectors are an attractive mechanism for gene therapy [225] for several reasons, including a high capacity for packaging large amounts of genomic material in comparison with retroviral vectors, [225, 226] low rate of replication-competent virion production capacity in self-inactivating LV vectors, [227] and the ability to generate LV vectors capable of infecting a wide range of cell types. [228, 229] Cell types which have been targeted with LV vectors include, but are not limited to, direct transduction into muscle cells, [230] neurons, [231] photoreceptors, [232] bone marrow-derived cells, [13, 216] hepatocytes, [230] and T-cells. [233] LV vector design has been extensively modified since the first use of the vectors, incorporating several safety features such as the development of self-inactivating vectors and the use of multiple plasmids to generate virions as a means of reducing

the probability of producing replication-competent lentivirus (RCL). [227, 234, 235] Avoiding RCL is critical to avoid off-target and deleterious effects arising from the infection of non-target cell types with the transduced vector, as typically vectors used in LV-based gene therapy have the capacity to infect a wide range of cell types. [236-238] RCL have not been observed in cells transduced with the most commonly used modified LV vectors, referred to as 3rd generation LV vectors. [239]

Lentiviral Vector Structure

The lentiviral vector genome is derived from the naturally occurring human immunodeficiency virus strain 1 (HIV-1).[234] Third generation LV vectors, in contrast with 1st generation LV vectors which utilized all of the HIV-1 genome with the exception of the *env* gene, are generated with only *gag*, *pol*, and *rev*. [234] This significantly improves vector biosafety. [234] Third generation vectors were developed by Dull *et al.*, in 1998 and are generated by the transient transfection of HEK-293T cells with four plasmids: **(a)** an expression vector, containing the transgene under the control of an appropriate promoter along with the Rev responsive element (RRE) for nuclear export, the central polypurine tract (cPPT) to aid transduction into non-dividing cells, [240] the packaging signal (ψ), [234] the Woodchuck Post-Transcriptional Response Element (WPRE) for stabilizing the mRNA, [241, 242] and flanking 5'LTR with a self-inactivating 3'LTR (SIN-LTR) [227, 235], **(b)** a packaging plasmid expressing *gag* and *pol* for capsid formation and integration, [234] an RRE, and a polyA tail, **(c)** an envelope plasmid

expressing the desired envelope for pseudotyping the vector (typically vesicular stomatitis virus G protein, VSV-G), [234, 243] and, finally, **(d)** a *rev*-expressing plasmid. [234] *Rev* binds the RRE to nuclear export machinery and facilitates the nuclear transport of RRE-expressing transcripts. [234, 244] Together, these plasmids provide everything necessary to generate a LV vector expressing the desired expression vector which is capable of vector particle formation and stable integration into the host cell genome, but not replication. [234]

The stable integration of standard LV vectors into the host cell genome in both dividing and non-dividing cells [245] is a significant advantage of LV vector-based therapy for a wide range of diseases. [245] For example, in monogenic disorders such as β -thalassemia, caused by mutations in the *HBB* gene, and adrenoleukodystrophy, caused by mutations in the *ABCD1* gene, the stable integration of LV vectors expressing the normal gene in hematopoietic stem cells (HSCs) used for transplant has yielded positive results in clinical trials. [246, 247] Success has also been achieved in LV vector-based clinical trials targeting Wiskott-Aldrich syndrome, caused by *WASp* mutations, [229, 248] metachromatic leukodystrophy, caused by a deficiency in arylsulfatase A, [249] and blood cancers arising from CD19+ cells such as chronic lymphocytic leukemia, acute lymphoblastic leukemia, and lymphomas. [233, 250-252] LV vectors have been established as considerably safer than other gene therapy approaches such oncogenic gamma retroviral vectors and adenoviral vectors, which have resulted in severe adverse effects such as the development of T-cell leukemia [253] and

fatal inflammatory responses [254] respectively. LV vectors are known to exhibit relatively low activation of immune responses against cells expressing the vector in comparison with other vectors such the adenoviral vector used in the aforementioned clinical trial, [255, 256] making them a safer alternative to these vectors.

Integrase-Deficient Lentiviral Vectors

Despite stable integration being advantageous in many LV vector-based therapies, integration is associated with the risk of insertional mutagenesis. [257] Insertional mutagenesis occurs when the vector inserts within a region of the genome which alters the expression of another gene, either through directly interrupting the coding sequence or through disruption of elements controlling gene expression such as promoter and enhancer regions. [257] Consequences of insertional mutagenesis include the development of cancer due to oncogene activation, loss of tumor suppressor genes, and other dysregulation of the cell cycle and cell death pathways. [258] Additionally, as more and more roles for non-coding regions of the genome are being identified, for example, long non-coding RNA and micro-RNAs, [259-261] it is becoming clear that LV vector integration may result in aberrant gene expression or gene expression control even when not inserted into coding regions of the genome. As a result, in applications where permanent expression of a transgene may not be required, the use of an integration defective LV (IDLV)

vector may significantly reduce the risk of LV vector-based pathologies following treatment.

In order for vectors to integrate into the host genome, several enzymes are required to be present including the reverse transcriptase, polymerase, and protease enzymes generated by the HIV-1 *pol* gene, [262] the viral integrase enzyme, and integrase interactor 1 (INI1/hSNF5). [262-266] A simple modification to one of these enzymes, the integrase enzyme, in the LV packaging plasmid results in the production of a LV vector which retains most of the function of a standard LV vector, but is incapable of integrating into the host genome. [267, 268] This vector remains episomal and is not retained as cells divide as a result of an Aspartic Acid to Asparagine substitution at position 116 in the integrase gene, referred to as D116N, which was first found to diminish integrase in a study in which the integrase gene was mutated in wild-type HIV-1. [267] When packaged with a packaging plasmid, such as the commonly used pMDL [269] or pCD-NL/BH*DDD [270] packaging plasmids containing the D116N mutation, lentiviral particles are no longer capable of integrating into the host cell genome, and transgene expression reduces over time as cells divide. pMDL with the D116N mutation in its integrase enzyme demonstrates significantly reduced integration in comparison with its integrating counterpart, though its efficiency is markedly lower .[271]

Some residual integration does occur with IDLVs as a result of non-integrase-mediated integration; however, the rate of residual integration is significantly lower than that observed with an integrating virus, and therefore the risk associated with insertional mutagenesis is significantly lower. [271] IDLVs have been successfully used in several studies in which transient expression of the transgene was sufficient, for example expression of zinc finger nucleases or gene editing. [222, 224, 272-276]

Project Summary

In this study, we have addressed two major concerns in cell-based therapy for dry AMD. Firstly, we have established a non-integrating lentiviral vector-mediated approach for generating therapeutic cells, significantly reducing the potential for off-target effects resulting from insertional mutagenesis. Secondly, we have demonstrated that BMDCs treated with these non-integrating vectors are recruited to and regenerate damaged RPE *in vivo*. The use of autologous BMDCs is advantageous for four reasons: (1) the cells are not immunogenic as they are derived from the patients' own bone marrow, (2) unlike ESCs, BMDCs are not associated with ethical concerns, (3) the cells are not pluripotent and are therefore less likely to result in tumorigenesis or teratomas formation in comparison with ESC and iPSC, and, (4) the cells can be given to the patient systemically, reducing the invasiveness of the treatment in comparison with strategies that involve

invasion of the subretinal space. Systemic delivery therefore allows for treatment early in the progression of the disease, and thus is more likely to preserve vision. In addition, we have expanded our approach to include human BMDCs *in vitro*, demonstrating that these cells can be induced to express RPE-associated markers in the same way as murine BMDCs, indicating that our approach is suitable for future analysis using human BMDCs in an immune-suppressed murine model of retinal degeneration. Furthermore, we have confirmed that adenylate cyclase activation plays a critical role in the programming of BMDCs to RPE-like cells *in vitro*.

In Chapter III, we present the results of our first specific aim, which was to generate a 3rd generation IDLV expressing *RPE65* (IDLV3-*RPE65*) for programming murine and human BMDCs to RPE-like cells. Our previous observation that expressing *RPE65* induces expression of the endogenous *Rpe65* gene; we therefore hypothesized that transient *RPE65* expression from an IDLV may be sufficient. We demonstrate that IDLV3-*RPE65* successfully infects both murine and human BMDCs and have optimized the infection protocol to address a significant difference in the normal infection efficiency of IDLVs vs. ILVs to include (1) high titer concentration with LentiX Concentration Reagent, (2) preloading of viral particles on RetroNectin, and, (3) spinoculation of cells. We show that BMDCs infected with IDLV3-*RPE65* express the endogenous *Rpe65* gene and RPE-associated *Cralbp* gene at similar levels to that observed in cells infected with the integrating *RPE65* viruses.

In Chapter IV, we present the results of our second specific aim, which was to evaluate the efficacy of systemically-delivered IDLV3-*RPE65*-programmed murine BMDCs in regenerating the RPE layer in models of retinal degeneration. We hypothesized that, as BMDCs infected with IDLV3-*RPE65* expressed RPE-associated genes at a similar level to BMDCs infected with the integrating 3rd generation *RPE65* vector, ILV3-*RPE65*, these cells would be capable of regenerating the RPE and preserving vision *in vivo*. In this set of experiments, we also included a second set of IDLV and ILV vectors expressing both *RPE65* and the development-associated gene microphthalmia-associate transcription factor (MITF), hypothesizing that this would enhance BMDC programming and consequently enhance preservation of vision. Unfortunately, we did not observe any advantage in using vectors expressing *RPE65-MITF* in comparison with *RPE65* alone. However, we have shown that systemically-delivered murine BMDCs programmed *ex vivo* with IDLV3-*RPE65* are recruited to and regenerate damaged RPE in both the acute and chronic models of retinal degeneration in mice, with improved visual function and evidence of RPE regeneration at the RPE layer in mice treated with the vector-modified cells.

Finally, in Chapter V, we present the results of our third specific aim, which was to investigate the potential for pharmacological programming of BMDCs to RPE-like cells. As we have previously demonstrated that adenylate cyclase activation precedes the activation of the endogenous *Rpe65* gene following *RPE65* vector

infection, we hypothesized that activating adenylate cyclase may also promote the programming of BMDCs to RPE-like cells with the ability to travel to and regenerate the RPE when injected systemically. Using inhibitors of adenylate cyclase, we demonstrate that the activation of adenylate cyclase is critical for expression of both *Rpe65* and *Cralbp* mRNA, with minimal expression observed in cells treated with the inhibitors after exposure to either adenylate cyclase activators or lentiviruses expressing *RPE65*. While BMDCs exposed to these drugs were not recruited to the eye in murine models of retinal degeneration, in this study, modifications to the protocol are likely to result in successful application of drug-treated cells in future.

Overall, we have expanded the knowledge of our field by contributing evidence that IDLVs may be sufficient to program BMDCs to RPE-like cells for systemic delivery, and demonstrated that human BMDCs can also be induced to express RPE-associated markers following infection with *RPE65* vectors. This allows us to move the project another step closer to clinical trials in humans, with experiments currently underway to evaluate human BMDCs programmed with *RPE65* in an immune-suppressed murine model of retinal degeneration.

To the best of our knowledge, our study comprises first example of the use of a single IDLV in programming an adult BMDC to differentiate into a cell of non-hematopoietic lineage.

CHAPTER II: MATERIALS AND METHODS

In Vitro Methods

Bacterial Growth

All bacteria were grown in Luria-Bertani (LB) broth or on LB agar. LB broth was prepared with 10 g bacto-tryptone, 5 g yeast extract, and 10 g sodium chloride (NaCl) (Fisher Bioreagents, BP1427-500) in 800 mL dH₂O, mixed using a magnetic stirrer and heat plate set at room temperature for 15 minutes. pH was adjusted to 7.5 with sodium hydroxide (NaOH; Fisher Bioreagents, BP1425-212) prior to adjusting the total volume to 1 L with dH₂O. LB broth was then sterilized by autoclaving for 20 minutes on the Liquid cycle. For LB agar, 15 g of agar was added prior to adjusting the total volume to 1 L. Following sterilization, LB agar was allowed to cool to 50⁰C in a waterbath. The required antibiotics were then added: for Ampicillin (Fisher Scientific, BP1760-25), 100 µg/mL was used; for Kanamycin (Teknova, K2127), 50 µg/mL was used. Agar was mixed well by stirring and 12mL poured into petri dishes using aseptic technique. Where air bubbles formed, the Bunsen burner flame was briefly held over the plate. Plates were then cooled at room temperature for 1-3 hours and stored in plate sleeves at 4⁰C until use.

Transformation into JM110 Bacteria

Prior to cloning, all plasmids were transformed into dam/dcm-negative *Escherischia coli* strain JM110 obtained from Agilent (Catalog #200239) due to the presence of methylation-sensitive restriction sites in the cloning protocols. JM110 bacteria were stored on the bottom shelf of a -80°C freezer (Thermo Scientific) until use. For all transformations, JM110 bacteria were thawed on ice for 30 minutes prior to transferring 50 µL bacteria per transformation to 14 mL polypropylene round-bottom tube (BD Falcon catalog #352059). Two extra tubes containing 25 µL JM110 bacteria were prepared each time a transformation was performed – one for the pUC18 positive control, and one for a negative control (i.e. untransformed). Prior to adding plasmid DNA, 0.85 µL beta-mercaptoethanol was added to each aliquot of cells and mixed gently by swirling. 1-5 µg plasmid DNA was then added to each tube; 0.5 µL pUC18 plasmid DNA was added to the positive control tube, and 0.5 µL dH₂O was added to the negative control tube. Tubes were then incubated on ice for 30 minutes, heat-shocked for 45 seconds in a waterbath preheated to 42°C, and incubated on ice for a further two minutes. 250 mL plain LB broth was then added to each tube, and tubes were incubated for 1h at 37°C at 250 rpm. Transformations were then diluted 1:10 and 1:100 and plated on LB agar containing the required antibiotic (200 µL of the pUC18 control transformations were plated on LB agar containing ampicillin; negative control transformations were plated on plates containing all antibiotics used to propagate the plasmids being transformed). Plates were left to dry for one hour, inverted, and

incubated for 16-20h at 37⁰C. Transformations were considered successful where colonies were obtained on the pUC18 plate (~100 colonies) and no colonies were obtained on the negative control plate. 12-24 colonies were picked immediately after transformation and patched onto a numbered LB agar plate containing the required antibiotic. Patch plates were inverted and incubated overnight at 37⁰C before being transferred to the cold room. Bacteria was then picked off each colony and grown in preparation for miniprepping to screen for the plasmid of interest. Once identified, one colony containing the correct plasmid was maxiprepped and bacteria were stored long-term as a glycerol stock (80% glycerol in plain LB broth).

Transformation into TOP10 Bacteria

Following cloning, plasmids generated using the JM110 strain were transformed into the dam/dcm-positive *E. coli* 'One-Shot TOP10' strain obtained from Thermo Fisher (C404010). TOP10 cells were stored on the bottom shelf of a -80⁰C freezer prior to use. For transformations, cells were thawed on ice for 30 minutes and transferred into pre-chilled 14 mL BD Falcon tubes as previously described, at a volume of 25 μ L cells per tube per transformation, plus a positive (pUC18) and negative (no plasmid) control as previously described. 1-5 μ L plasmid was added to each tube and mixed by swirling gently. Transformations were incubated on ice for 30 minutes, heat-shocked at 42C for 60 seconds, and placed on ice for 1 minute. 250 μ L plain LB broth was added to each tube and tubes were incubated for 1 hour at 37⁰C, at 225 rpm. Transformations were then diluted 1:10 and 1:100

and plated on LB agar containing the required antibiotic (200 μ L of the pUC18 control transformations were plated on LB agar containing ampicillin; negative control transformations were plated on plates containing all antibiotics used to propagate the plasmids being transformed). Plates were left to dry for one hour, inverted, and incubated for 16-20 hours at 37⁰C. Transformations were considered successful where colonies were obtained on the pUC18 plate (~100 colonies) and no colonies were obtained on the negative control plate. 12-24 colonies were picked immediately after transformation and patched onto a numbered LB agar plate containing the required antibiotic. Patch plates were inverted and incubated overnight at 37⁰C before being transferred to the cold room. Bacteria was then picked off each colony and grown in preparation for miniprepping to screen for the plasmid of interest (see: Plasmid Preparation). Once identified, one colony containing the correct plasmid was maxiprepped and bacteria were stored long-term as a glycerol stock (80% glycerol in plain LB broth).

Plasmid Miniprep

Plasmid minipreps were used to obtain plasmid for sequence verification and in the intermediate stages of vector cloning. The QIAGEN Spin Miniprep Kit (QIAGEN, 27106) was used as per manufacturer's instructions with the following specifications/modifications: single colonies were grown in 5 mL LB broth containing the required antibiotic (prepared as previously described) per miniprep for 16 hours at 37⁰C at 220 rpm in 14 mL BD Falcon polystyrene tubes (BD,

352051), and harvested by centrifugation at 5400 g for 10 minutes at 4⁰C. Where JM110 bacteria was used to propagate the plasmid, the extra wash step (step #7 in the QIAprep Miniprep Handbook, pg. 21) was carried out. 30 µL sterile nuclease-free water was used to elute plasmid DNA.

Plasmid Maxiprep

Plasmids used for the production of lentiviruses were prepared by maxiprep to ensure that the DNA obtained was of high quality and high concentration (800 ng/µL – 2 µg/µL). Initially, the PureLink HiPure Plasmid Filter Maxiprep Kit (Invitrogen, K210017) was used as per manufacturer's directions; however, after several kits failed to produce good quality DNA, maxipreps were carried out using the QIAGEN Plasmid Maxi Kit (QIAGEN, 12165). As such, the pcz-VSVG lentiviral vector envelope plasmid, the pMDL 3rd generation lentiviral packaging plasmid, and the pMDL-D116N integrase-deficient lentiviral vector packaging plasmid were prepared using the Invitrogen kit, and all other plasmids were prepared using the QIAGEN kit as per manufacturer's directions with the following specifications/modifications: single colonies were grown in 200 µL LB broth containing the required antibiotic (prepared as previously described) at 37⁰C, 220rpm for 1 hour to generate a starter culture which was then added to 250mL LB broth containing the required antibiotic, which was then incubated for 16h at 37C, 220rpm. Bacterial cells were harvested by centrifugation at 5000 g for 15 minutes at 4⁰C. Pellets were frozen overnight at 20⁰C as we have previously

determined that freezing pellets prior to harvesting plasmids results in a higher plasmid yield. The following day, pellets were thawed at room temperature for an hour. LyseBlue was added to Buffer P1 for all maxipreps. Buffer P3 was stored at 4°C. Following air-drying of the pellet, the pellet was covered in 300-500 µL sterile nuclease-free water and incubated at 4°C overnight as we have previously determined that this increases the DNA concentration obtained. The following day, plasmid DNA was transferred to a sterile microfuge tube and stored at -20°C. Plasmid DNA concentration was measured as described below.

Measurement of Plasmid Concentration

Plasmid concentration was measured on a NanoDrop 2000 Spectrophotometer (Thermo Scientific, SO6497) in the Nucleic Acid>DNA category. Prior to each use, the arm of the NanoDrop was raised, and the upper and lower pedestals were cleaned with water to ensure no nucleic acids were present on the instrument before measurement. The instrument was then blanked using 1 µL sterile nuclease-free water. Water was cleaned from the upper and lower pedestals, and 1 µL plasmid was measured for each preparation. Where multiple plasmids were measured, the upper and lower pedestals were cleaned with water to avoid cross-contamination. DNA was considered to be of suitable quality where the 260/280 ratio of absorbance was between 1.8 and 2.0. Where ratios were considerably lower, plasmid preparation was repeated.

Plasmid Storage

Bacteria containing plasmids plated on LB agar were kept in the cold room at 4°C for up to 1 month. Plasmid DNA was stored at -20°C in sterile nuclease-free dH₂O for up to 6 months and at -80°C indefinitely. Glycerol stocks of bacteria containing plasmids were stored at -80°C. 200 µL of an overnight culture of bacteria was combined with 200 µL 80% glycerol (prepared in sterile dH₂O) in a 2 mL cryovial and mixed by inverting. Cryovials were then flash-frozen in liquid nitrogen and stored at -80°C for up to 1 year.

Plasmids

The 3rd generation lentiviral vector expression plasmid pCDH-EF1-T2A-copGFP was obtained from Systems Biosciences (CD823A-1), and the packaging plasmids pMDL and pMDL-D116N along with helper plasmid Rev were obtained from the IU Vector Production Facility. The pcz-VSVG envelope plasmid was obtained from Dirk Lindemann (University of Dresden). The *RPE65* gene and the *MITF* cDNA inserts were obtained from GeneArt Gene Synthesis Service. The pTYF-*RPE65* and pTYF-LacZ lentiviral vectors were provided by Lung-Ji Chang (University of Florida), packaged with pHP-VSVG.[13, 216]

Restriction Enzyme Digests

Restriction enzymes were obtained from New England Biolabs. For cloning of the MITF gene into the GeneArt RPE65 plasmid, 1 µg of GeneArt RPE65 (Appendix 1) and 1 µg of the GeneArt MITF (Appendix 1) plasmid were digested with 1 unit each of BamH1 (R3136) and EcoR1 (R3101) in 5 µL CutSmart Buffer and dH₂O to 20 µL for 1 hour at 37⁰C. For cloning the RPE65 gene and the combined RPE65-T2A-MITF construct into pCDH-EF1-T2A-GFP (Appendix 1), 1 µg GeneArt RPE65 and 1 µg pCDH-EF1-T2A-GFP plasmids were digested with 1 unit each of Xba1 (R0145S) and Sal1 (R3138) in 5 µL CutSmart Buffer and dH₂O to 20 µL for 1 hour at 37⁰C. Following digest with restriction enzymes, all enzymes were inactivated as per manufacturer's directions and bands separated on a gel.

Agarose Gel Separation of Digested DNA Fragments

To separate required bands from undesired bands, entire restriction digests were run on a 0.8% agarose gel containing 10 µL ethidium bromide/100 µL agarose for 1 hour after enzymes were inactivated with an appropriate DNA ladder to determine the size of the correct band(s) to be excised. Bands were excised under UV light using a razor blade.

Gel Extraction of Digested DNA Fragments

Digested bands separated by agarose gradient were extracted from agarose gel using a Gel Extraction Kit (QIAGEN, 28704) as per manufacturer's directions with no protocol modifications. Fragments were eluted in 30 μ L dH₂O.

Ligation

T4 DNA ligase was used for all ligations (New England Biolabs, M0202S) as per manufacturer's directions with a 3:1 ratio of insert to vector as calculated using the New England Biolabs Online Ligation Calculator. Ligations were transformed into TOP10 bacteria as previously described, screened, and verified as previously described. The resulting plasmid pCDH-*RPE65* was used to generate vectors ILV3-*RPE65* and IDLV3-*RPE65*. The plasmid pCDH-*RPE65-MITF* was used to generate vectors ILV3-*RPE65-MITF* and IDLV3-*RPE65-MITF*. (Figure 2.1).

Figure 2.1

A

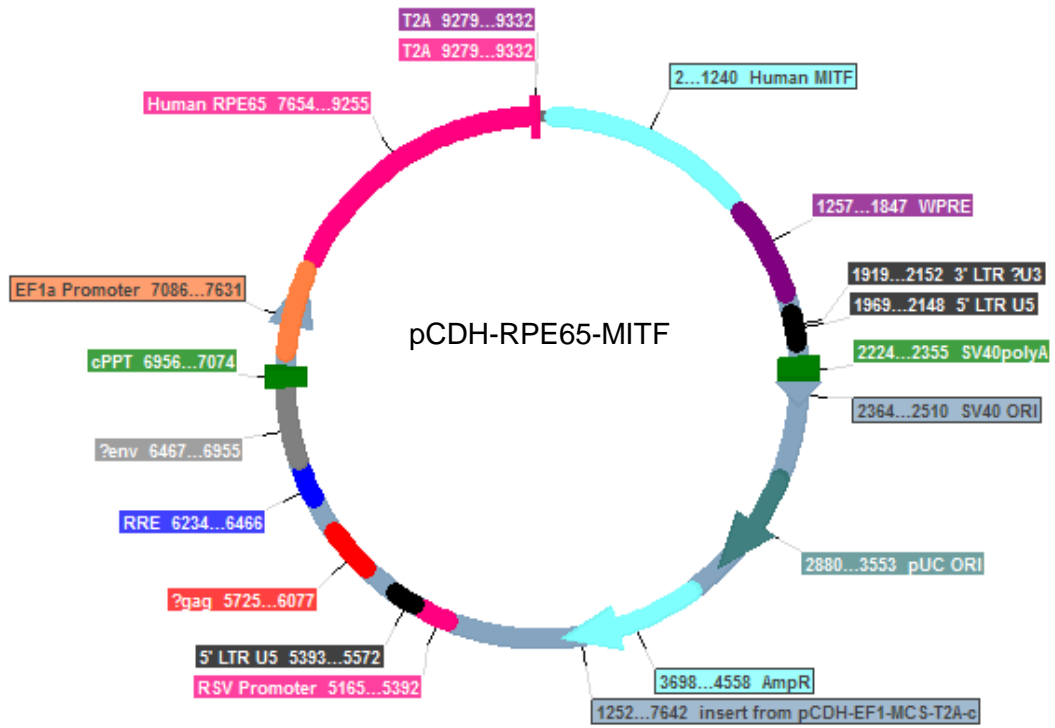


Figure 2.1. Plasmid Maps for pCDH-RPE65 (A) and pCDH-RPE65-MITF (B).
Generated in Serial Cloner.

Lentiviral Production and Titer

All lentiviral vectors were produced by transfection of HEK-293T cells (ATCC, HEK 293T/17 ATCC-CRL-11268) at IU School of Medicine with the exception of the 1st generation vector LV-RPE65, obtained from Lung-Ji Chang (University of Florida). HEK-293T cells were maintained in high glucose DMEM containing L-Glutamine, sodium pyruvate (ThermoFisher, 11995-081), 10% heat-inactivated fetal bovine serum (HI-FBS; ThermoFisher, 10437-010) and 1% penicillin/streptomycin (Gibco, 15070-063), referred to as 'complete DMEM'. Cells were split every 2-3 days and maintained under 80% confluence for no more than 45 passages.

On Day One, HEK-293T cells were plated for infection. Seven 10 cm tissue culture dishes (Corning, CLS430167) per viral vector were coated with 6ml Attachment Factor (ThermoFisher, S006100) for 3 hours at 37^oC. Attachment Factor was then aspirated and 8×10^6 HEK-293T cells were plated per plate in 10 mL complete DMEM. Plates were swirled to ensure even distribution of the cells across the plates. Plates were then incubated for 16-24 hours at 37^oC. On Day Two, media was aspirated from all plates and replaced with 4 mL high glucose DMEM containing L-Glutamine, sodium pyruvate, 15% HI-FBS and 1% penicillin/streptomycin. For each plate, one 2 mL cryogenic vial containing 955 μ L plain DMEM and 45 μ L of 1 mg/mL polyethylenimine (PEI; Sigma Aldrich, 9002-98-6 diluted in PBS, Sigma Aldrich 46-013-CM) was prepared. DNA mixture for each plate was then prepared in 2 mL cryogenic vials as follows: 1 mL plain DMEM

with 5 µg pcz-VSV-G envelope plasmid, 10 µg lentiviral vector (pCDH-RPE65 or pCDH-RPE65-MITF), 5 µg packaging plasmid (pMDL or pMDL-D116N), and 1 µg Rev. DNA mixture was added to one cryovial of PEI mixture per plate and mixed well by vortexing for 30 seconds. Tubes were then incubated at room temperature in the dark for 20 minutes. One tube (containing 2mL DNA/PEI mixture) was then added to each plate containing HEK-293T cells for a final volume of 6 mL per plate and a final HI-FBS concentration of 10%. Cells were incubated for 16 h at 37⁰C. On Day Three, media was aspirated and replaced with 5 mL fresh complete DMEM and plates were incubated for 20-24 hours. To titer the virus, 50,000 HT1080 cells obtained from Dr. David Gilley (IU School of Medicine) were plated per well in two 6-well plates, coated with 1 mL Attachment Factor for 3 hours prior to plating of cells, in 3 mL complete DMEM. On Day Four, the viral supernatant (media on the plates containing the DNA/PEI mixture added on Day Two) was harvested and filtered through a polyethersulfone membrane with a mesh size of 0.45 µm (ThermoScientific Nalgene Filter Unit, 166-0045). Viral supernatant was then concentrated by centrifugation at 10,000 g for 2 hrs, or mixed with Lenti-X Concentrator (ClonTech, PT4421-2), 1 volume Lenti-X per 3 volumes viral supernatant. Lenti-X/viral supernatant mixture was then incubated for 1 hour at 4⁰C, and centrifuged at 1500 g for 45 minutes. Supernatant was poured off and pellet was resuspended to yield a 10-20x concentration by resuspending in sterile PBS by carefully pipetting up and down 50x without generating air bubbles. Virus-containing PBS was then aliquoted in 20-50 µL aliquots and snap-frozen in liquid nitrogen. Aliquots were stored at -80⁰C until use.

Immediately after freezing, one vial of virus was thawed and titered on HT1080 cells plated on Day Three. 1.8 mL complete DMEM containing 8 µg/mL Polybrene was added to each of 11 sterile Eppendorf tubes. 200 µL viral supernatant was added to the first tube to bring the volume to 2 mL and vortexed to mix, to generate a 10x dilution. 200 µL was then taken from tube 1 and added to tube 2 and repeated until tube 11 to serially dilute the virus for titer measurement. 1 mL of each dilution was added to 1 well per tube of the 6-well plates of HT1080, with one well as a negative control. After incubating for 16-24 hours at 37°C, 3mL complete DMEM without Polybrene (Specialty Media, TR-10003-9) was added to each well. Plates were then incubated for 48 hours at 37°C. Viral titer was determined by qRT-PCR for the gene expressed (e.g. *RPE65*). Titer was confirmed by qRT-PCR in murine BMPCs by adding 2.5 µL or 10 µL viral supernatant to 50,000 cells as described below.

Calculation of Viral Titer

As the lentiviral vectors used in this study lack a reporter gene, viral titers cannot be obtained via FACS. Instead, a standard curve was generated by comparing $2^{-\Delta\Delta CT}$ values with flow cytometric data for GFP positive cells, to allow a comparison between $2^{-\Delta\Delta CT}$ values and viral titer. The pCDH-EF1-GFP virus was serially diluted and titered as previously described. The viral titer was determined using the following equation:

$$(\#cells\ plated \times 2 \times \%GFP + / 100 \times dilution\ factor)$$

The titer was considered accurate where linear with the dilution factor. The virus was then serially diluted and GFP expression was measured by qRT-PCR (as described below) to obtain $2^{-\Delta\Delta CT}$ values corresponding with viral titer. A $2^{-\Delta\Delta CT}$ value of 30 where 10 μ L viral supernatant was added per well containing 50,000 cells was considered to represent a viral titer of 10^8 at MOI 50; where a $2^{-\Delta\Delta CT}$ value of 30 was obtained with 2.5 μ L viral supernatant, viral titer was $\sim 10^9$ at MOI 50.

Lineage Negative Cell Enrichment

All lineage depletion was carried out using the EasySep Mouse Hematopoietic Progenitor Cell Enrichment Kit (StemCell Technologies, 19856), which removes non-hematopoietic and non-progenitor cells using an antibody cocktail of anti-CD5, anti-CD11b, anti-CD19, anti-CD45R/B220, anti-Ly6G/C, and anti-TER119. Manufacturer's directions were followed without modification. The additional wash step was not carried out. Following isolation, cells were counted on a 1:10 dilution and prepared for Sca1+ cell isolation by FACS.

Sca1 Positive Cell Selection

Cells were resuspended at a concentration of 1×10^8 cells/mL in flushing buffer. 20 μ L Sca1 PE Positive Labeling Reagent (StemCell Technologies, 18756) was added per mL of cells and cells were mixed well by pipetting and incubated for 20

minutes at room temperature in the dark. Cells were then washed 2x in flushing buffer by centrifugation at 350 g for 5 minutes, 1x in PBS by centrifugation at 350 g for 5 minutes, and finally resuspended at a concentration of 10 million cells per mL for FACS sorting. Where GFP cells were used, cells were sorted for double positive GFP(cells)/PE(Sca1+) with a 7-12% recovery. Where wild-type cells were used, cells were sorted for PE (Sca1+) with a 7-12% recovery. Sorted cells were post-sorted to verify purity and were typically >95% pure. For the majority of experiments in which cells were not injected back into mice, the Sca1+ isolation was carried out using the StemCell Technologies Sca1+ Isolation Kit (18756).

Isolation of BMDCs from Human Blood

Cord blood CD34+ were isolated by the IU AngioBiocore with a purity of >99% by flow cytometry assisted cell sorting (FACS) or were obtained from cord blood isolations performed in other laboratories. Where CD34+ cells were obtained from blood bank samples or healthy donors, white blood cells were first isolated in the laboratory by Ficoll gradient followed by flow cytometry assisted cell sorting (FACS) for CD34+ cells stained with AlexaFluor488 anti-human CD34 antibody (BioLegend, 344518) or bead separation (StemCell Technologies EasySep Human CD34 Positive Selection Kit, 18056). For Ficoll separation, blood was aliquoted into 25 mL aliquots in 50mL conical tubes and diluted by topping off with 25 mL PBS containing 2% FBS. A gradient for separation consisting of 1 part Ficoll to 2 parts diluted blood was prepared by adding 12.5mL Ficoll to empty 50mL tubes

and gently adding diluted blood to the Ficoll, ensuring that the blood sits on top of the Ficoll with no mixing. Samples were then centrifuged for 30 minutes at 2300 rpm in an Eppendorf Centrifuge #5804 with the centrifuge brake off. The interphase layer was then transferred to new 50 mL tubes (10-20 mL per tube) and topped off with PBS containing 2% FBS and 1 mM EDTA. Samples were centrifuged for 10 minutes at 350 *g*. (Eppendorf Centrifuge 5804). Pellets were resuspended in 1 mL PBS containing 2% FBS and 1 mM EDTA. Red blood cells were then lysed by adding ammonium chloride (5-9 mL) to the sample and incubating on ice for 15 minutes. Samples were then washed three times with PBS containing 2% FBS and 1mM EDTA by centrifugation at 350 *g* (Eppendorf Centrifuge 5804). Cells were counted on a 1:100 dilution and prepared for isolation of CD34+ cells. Where the EasySep Kit was used, cells were isolated as per manufacturer's directions with no modifications. Where FACS was used, cells were resuspended at 10 million cells/mL and incubated for 20 minutes at room temperature in the dark with 5 μ L/million cells of Alexa Fluor 488 anti-human RPE65 antibody. Cells were then washed 3x with PBS by centrifugation at 350 *g* and resuspended at a volume of 10 million cells/mL for flow sorting.

Lentiviral Vector Infection of Primary Cells for Injection

Where cells were injected into mice, and unless otherwise specified in the text, all infections were done by 2 hour spinoculation at 150 *g*, 21⁰C on RetroNectin (ClonTech, T100B) as per manufacturer's directions with the exception of the

concentration used: tubes and plates were coated with RetroNectin at a concentration of $2 \mu\text{g}/\text{cm}^3$. All cells were infected at a concentration of 1×10^5 cells per mL at an MOI of 50 in tubes with all integrating vectors, unless a higher or lower MOI is indicated. Following infection, cells were immediately washed 3x in PBS and resuspended in PBS at a concentration of 50,000 cells/100 μL for injection into mice.

Lentiviral Infections for Optimization of Protocols

Infections were carried out using a number of different methods to identify the optimum procedure. Briefly, BMDCs were infected overnight for 16 hour or by 2 hour spinoculation at 150 g, 21°C , with no reagent, Polybrene, Protamine, RetroNectin at a concentration of 0-12 $\mu\text{g}/\text{mL}$ added to media, or on RetroNectin at 0-12 $\mu\text{g}/\text{cm}^3$. RetroNectin was either pre-loaded with virus for 30 min at 37°C prior to infection, or cells and virus were added together at the same time as the infection. RetroNectin was used to coat up to 4 plates per preparation. 5000-100,000 cells per well were infected at an MOI of 50 unless a higher or lower MOI is indicated in the text. Where Polybrene or Protamine Sulfate was used for *in vitro* experiments, Polybrene was used at a concentration of $8 \mu\text{g}/\text{mL}$, and Protamine Sulfate was used at a concentration of $10 \mu\text{g}/\text{mL}$. Where RetroNectin plates or tubes were pre-loaded with either cells or viral particles, pre-loading was carried out for 30 min at 37°C in the lowest volume of medium required to cover the surface of the plates. Where RetroNectin was added to the media instead of being used to

coat plates, the same volume that would have been used should the plates have been coated was added to the media.

RNA Isolation from Cells

The RNeasy Mini Kit was used for all RNA isolations. Cells were harvested by centrifugation for 5 minutes at 350 g and resuspended in 350 μ L buffer RLT. 1 volume of freshly prepared 70% ethanol in RNase-free water was added to each sample and mixed well by pipetting. Samples were then added to a RNeasy Mini Spin Column in a 2 mL collection tube (contained in the kit) and centrifuged for 30 seconds at >8000 g. Samples were then prepared as per the manufacturer's directions and eluted in 20 μ L RNase-free dH₂O in the final step. RNA concentration was measured on the Nano-Drop as described below.

NanoDrop RNA Quantification

All RNA was measured on the NanoDrop 2000 Spectrophotometer (Thermo Scientific, SO6497) in the Nucleic Acid>RNA setting. Prior to each use, the arm of the NanoDrop was raised, and the upper and lower pedestals were cleaned with water to ensure no nucleic acids were present on the instrument before measurement. The instrument was then blanked using 1 μ L sterile RNase-free water. Water was cleaned from the upper and lower pedestals, and 1 μ L RNA was measured for each preparation. Where multiple RNAs were measured, the upper

and lower pedestals were cleaned with water to avoid cross-contamination. RNA was considered to be of suitable quality where the 260/280 ratio of absorbance was around 2.0. Where ratios were considerably lower (<1.6), the experiment was repeated.

Synthesis of cDNA

All RNA was converted to cDNA immediately after isolation as cDNA is more stable than RNA, allowing for storage at -20°C until use without the risk of degradation. RNA was prepared to yield 25 ng of cDNA per microliter to allow for adding 1 μL cDNA per well of subsequent qRT-PCR experiments as the SsoFast Advanced qRT-PCR kit recommends use of a concentration of 0.00005-50 ng cDNA per reaction. cDNA at a concentration of 25 ng per microliter was generated using 500 ng RNA in a 20 μL reaction of cDNA synthesis iScript kit (BioRad, 1708891). cDNA syntheses were set up in Hard-Shell 96-well PCR plates (BioRad, HSP9601) from a sealed bag. Mastermixes of iScript and reverse transcription mix were set up containing 4 μL reaction mix and 1 μL reverse transcriptase per reaction. Mastermixes were mixed well and 5 μL mastermix was added to one well of the plate per reaction. Wells were labeled directly on the plate. 500 ng RNA was then added to each well as required and mixed well by pipetting. The total volume of each well was then brought to 20 μL using RNase-free dH_2O . Plates were then sealed by rubbing a Kim wipe in a circular motion around the wells to ensure a tight seal with Microseal 'A' PCR Plate Sealing Film (BioRad, MSA5001). Plates were

briefly centrifuged to collect sample at the bottom of the wells with no air bubbles. The plates were then transferred to a PCR machine set to: 5 minutes at 25⁰C, 30 minutes at 42⁰C, 5 minutes at 85⁰C, hold at 4⁰C. Samples were then stored at -20⁰C until use. cDNA concentration was calculated from the amount of RNA added as opposed to using the NanoDrop to measure cDNA concentration directly as cDNA concentration cannot be accurately measured. Unless specified, all cDNA was prepared as 25 ng/μL from 500 ng RNA per 20 μL reaction.

qRT-PCR Reaction

A BioRad CFX96 or CFX384 Touch Real-Time PCR Detection System (BioRad catalog #1855195) was used for all qRT-PCR experiments. BioRad SSoFast Advanced Universal Probes Supermix (BioRad catalog, 1725284) was used for all qRT-PCR experiments. Where available, BioRad PrimePCR validated primers were used for all qRT-PCR experiments. Mastermixes were set up containing (per reaction) 5 μL SsoFast Supermix, 500 nM forward primer, 500 nM reverse primer, and nuclease-free water to a total volume of 9 uL mastermix per reaction. 9 uL mastermix was then added to each well of a Hard-Shell 96-well PCR plate as required – each sample was prepared in triplicate and each measurement was made in triplicate to allow for statistical analysis, so 9 wells per treatment were set up (3 samples, in triplicate). 25 ng cDNA was then added to each well of mastermix as required. Positive PCR controls for RPE65 experiments consisted of cDNA prepared from low-passage ARPE19 cells; for GFP experiments, positive controls

consisted of cDNA prepared from the bone marrow of GFP+ mice. Negative controls for qRT-PCRs consisted of a no-template control (1 μ L d H₂O instead of 25 ng cDNA); negative controls for experiments consisted of uninfected or untreated cells. GAPDH or beta-Actin was used as internal controls for all qRT-PCR experiments. Wells were mixed by pipetting and plates sealed using Microseal 'A' PCR Plate Sealing Film, and centrifuged briefly prior to running on the CFX96 machine set to cycle as follows: 98C for 2 minutes (1 cycle), 98⁰C 1-5 seconds & 60-65⁰C 1-5 seconds (30-40 cycles), 65-95⁰C (in 0.5C inc) 2-5 seconds/step, hold at 4⁰C. The CT values per well in the FAM setting (for SsoFast Advanced) were then recorded and analyzed using the comparative CT ($2^{-\Delta\Delta CT}$) method to compare the CT value of the target gene with the internal control gene. Internal control values were considered to be good where CT values were <20, with 16-18 being optimum. Negative controls typically resulted in CT values between 36-39; positive controls typically resulted in CT values between 17 and 20. Experiments were considered successful where no amplification was observed in the no-template control. If the no-template control produced a CT value, the PCR was repeated.

Whole Eye Flat Mounts

Eyes were enucleated, cleaned of fat and muscle, and the lens, vitreous, and cornea were carefully removed. Four shallow incisions were then made in the eyeball, allowing for separation of the retina from the RPE/choroid with minimal

cross-contamination. The RPE/choroid was then flattened on a glass slide with the RPE facing upward and gently covered with a glass coverslip. Flat mounts were imaged using a ZEISS confocal microscope. The relative number of cells per eye was calculated by counting the number of cells in set areas of each section of the flat mount, corresponding to approximately 10% of the whole flat mount surface, as shown below (Figure 2.2).

Figure 2.2

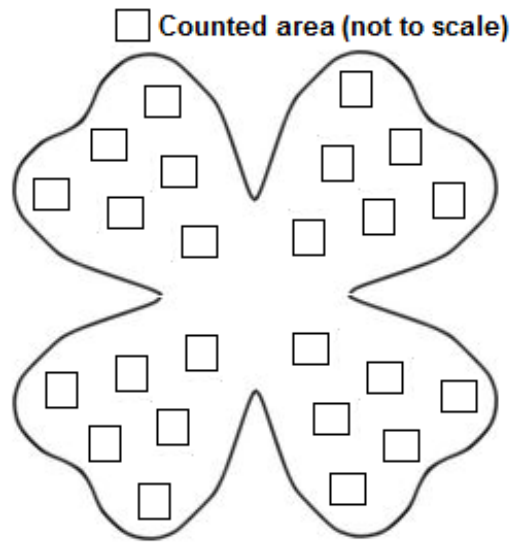


Figure 2.2 Areas of tissue quantified for GFP+ cells per flat mounted eye.

Tissue Sectioning

Eyes were enucleated and fixed in 4% Paraformaldehyde overnight, then washed 3x with PBS and transferred to 70% ethanol for sectioning. Whole eyes were paraffin-embedded, sectioned, and stained with H&E at the Histology Core of the Department of Anatomy and Cell Biology at IU School of Medicine. Sections were imaged with a ZEISS fluorescence microscope.

Pharmacological *In Vitro* Differentiation of BMDCs and Inhibition

Mouse and human BMDCs were isolated as previously described. 5000-50,000 cells per well were added to flat bottomed 96-well plates in 100 μ L complete DMEM. DMEM was supplemented with Forskolin (10 μ mol/l; Tocris Biosciences 1099), Rolipram (1 μ mol/l; Sigma Aldrich, 61313-54-5), KH7 (50 μ mol/l; Tocris Biosciences 3834), BPIPP (50 μ mol/l; Tocris Biosciences 3635), or NKY80 (50 μ mol/l Tocris Biosciences 5071) as required. Cells were cultured for 1-7 days as required before being harvested and prepared for qRT-PCR as previously described.

In Vivo Methods

Animals

All animal studies were conducted under protocols approved by the Institutional Animal Care and Use Committee (IACUC) of IU School of Medicine and according to National Institutes of Health and the Association for Research in Vision and Ophthalmology guidelines. Adult (6–8 week old; or 12 month old) female C57BL/6J mice and homozygous GFP transgenic (C57BL/6-Tg (UBC-GFP)) mice were purchased from Jackson Laboratories, Bar Harbor, ME.

Calculation of Number of Mice Required

The number of mice needed for each isolation was calculated based on the average number of BMPCs (Lin-/Sca1+) obtained per mouse minus 50,000 to allow for isolation of fewer cells than expected. In general, 200,000 Lin-/Sca1+ cells were isolated from each mouse, therefore the cell number was calculated as #cells required/150,000.

Sacrifice of Mice

Mice were sacrificed by isoflurane (Aldrich, CDS019936) sedation followed by cervical dislocation.

Bone Marrow Cell Harvest

Immediately after sacrifice, both hind legs were removed and dipped in 70% ethanol. Tissue was then cleaned off the tibiae and fibiae using Kimwipes. Bone marrow was then flushed out of each bone using a 15mL syringe with a 27g needle in room temperature flushing buffer (PBS containing 2% FBS and 1mM EDTA). Bone marrow was then filtered through a 100uM mesh cell strainer into 50mL conical tubes. Tubes were topped up with flushing buffer to 45mL and centrifuged at 350 *g* (Eppendorf Centrifuge 5804) for 5 minutes at room temperature. Supernatant was carefully poured off and 2 mL ammonium chloride red blood cell lysis buffer was added per mouse to each tube. Tubes were then incubated on ice for 15 minutes and centrifuged at 350 *g* (Eppendorf Centrifuge 5804) for 5 minutes at 4⁰C. Supernatant was removed and cells were resuspended in 4 mL flushing buffer and counted on a 1:100 dilution. Cells were then resuspended at a volume of 1x10⁸ cells/mL as required for lineage depletion.

Sodium Iodate Murine Model

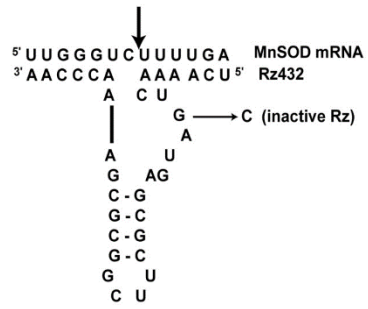
Sodium iodate (Fisher Scientific, S322100) in water at a concentration of 100 mg/kg was injected intraperitoneally to acutely ablate the RPE layer. Cells were injected 8 hours after sodium iodate injection. Control mice received sodium iodate but no cells or 100 μ L water by IP injection and no cells.

Superoxide Dismutase 2 Knockdown Model

Wild-type C57BL/6J mice were injected subretinally with 1 μ L of 2.5×10^{12} particles/mL of recombinant AAV1 construct AAV1-Rz-SOD2 in the right eye. The left eye remained untreated. AAV1-Rz-SOD2, based on the pTR-UF2 vector, expresses the Rz432 SOD2-specific ribozyme Rz432 driven by the RPE-specific promoter VMD2, leading to chronic degradation of the RPE layer as described in Justilien *et al.*, 200.[277] and was obtained from the University of Florida. 3-4 SOD2-KD mice were used for each treatment group. Control injections consisted of rAAV-inactive ribozyme (AAV1-Rz-inactive), also obtained from the University of Florida in one group of mice per experiment. (Figure 2.3).

Figure 2.3

A.



B.

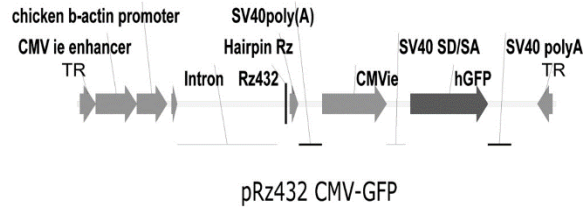


Figure 2.3. The Structure of the Mn-SOD and Inactive Hammerhead Ribozymes (A) and rAAV Vectors (B) for the SOD2-KD mouse model. The Mn-SOD ribozyme degrades SOD2 messenger RNA. The control (inactive) ribozyme consists of the same structure with a G→C mutation which blocks the ability of the ribozyme to target SOD2 mRNA. Source: Justilien *et al.* [277]

Systemic Delivery of Cells into Mice

One month following SOD2-KD, mice received a systemic injection of 5×10^4 Lin⁻/Sca1⁺/GFP⁺ BMDCs (either naïve BMDC, BMDC-ILV3-*RPE65*, BMDC-ILV3-*RPE65-MITF*, BMDC-IDLV3-*RPE65*, BMDC-IDLV3-*RPE65-MITF*) in 100 μ L of PBS, via the tail vein (n=3 or n=4 per group). Injections were performed by the IU *In Vivo* Therapeutics Core. Negative controls consisted of naïve BMDCs and mice injected with PBS (vehicle control), and the untreated left eye in the SOD2-KD model mice was the normal positive control.

Measurement of Visual Function

Two visual function tests, electroretinogram (ERG) and optokinetic nystagmus (OKN) were performed three months following injection of BMDCs as previously described. [13, 216]

Statistical Analysis

Experiments were carried out in triplicate. Results are expressed as mean \pm SEM. ANOVA with Tukey post hoc tests were carried out to determine significance of results. Statistical analysis was performed using Prism 5 ver. 5.01 (GraphPad Software, Inc., La Jolla, CA) with $p < 0.05$ considered statistically significant

.

**CHAPTER III: IMPROVING THE INFECTION OF BONE MARROW-DERIVED CELLS
WITH AN INTEGRASE-DEFECTIVE LENTIVIRAL VECTOR.**

Introduction

We have previously demonstrated that systemic delivery of immature bone marrow-derived cells (Lin-/Sca1+; BMDC), programmed *ex vivo* by inserting a stable *RPE65* transgene using an integrating LV vector, can regenerate an efficient and functional retinal pigment epithelial (RPE) cell layer that restores visual function in mouse models of retinal degeneration. [13, 216] This has significant implications for the treatment of dry age-related macular degeneration (AMD), which is a major cause of vision loss in the elderly. [10] The primary defect in dry AMD is believed to be at the RPE, which shows cellular dysfunction, atrophy, and cell loss, particularly in the central retina. [221, 278] The most viable and attractive option for targeting dry AMD is in the early stages by replacement of damaged RPE using a minimally invasive approach, such as systemic delivery of programmed BMDC, as we have shown in animal models. [13, 216] As success has been observed in murine models with murine cells, it is necessary to optimize and further develop our BMDC programming technique for safe and efficient application in human cells.

Since we have previously found that the expression of *RPE65* mRNA activates expression of adenylate cyclase in BMDCs within hours of infection, [216] and this in turn switches on expression of endogenous *Rpe65* and RPE-associated marker

Cellular Retinaldehyde-Binding Protein-1 (*Cralbp*), [216] we hypothesized that transient expression of *RPE65* from an IDLV may result in sufficient programming in the absence of integration. Limiting integration significantly reduces the risk of insertional mutagenesis, which can result in deleterious effects resulting from LV insertion in coding regions or regulatory elements). [224, 257, 258, 271, 279] This vector is ideal for programming BMDCs for use in human clinical trials.

IDLVs are known to be less efficient than ILVs for a number of reasons, including low infection rates and episomal silencing. [224, 271, 280] Silencing post-transduction is a significant concern for long-term expression of a transgene from IDLVs in non-dividing cells. [280] For our application, however, short term expression of *RPE65* is thought to be sufficient for the programming of BMDCs, as we have shown that cells express the endogenous *Rpe65* and *Cralbp* mRNAs within hours of infection with the integrating *RPE65* vector. [13, 216] This study, therefore, focused on improving the protocol for infecting BMDCs with IDLV-*RPE65* to maximize the number of cells infected with the virus.

We demonstrate that IDLV3-*RPE65* infection can be increased by: (a) increasing the concentration of the viral supernatant to reduce the volume required to obtain a high MOI, (b) pre-loading viral supernatant on RetroNectin prior to infection, and, (c) using a spinoculation method to infect the cells. In the process of optimizing the protocol IDLV3-*RPE65* infection, we included measures to reduce the costs associated with RetroNectin use for LV transduction can be minimized by: (a)

confirming that using 2 $\mu\text{g}/\text{cm}^2$ to coat plates is sufficient to achieve transduction with LV vectors, as has been reported in retroviral vectors, [281] and (b) re-using the 2 $\mu\text{g}/\text{cm}^2$ preparation to coat up to three wells. IDLV3-*RPE65* infected in this manner induces activation of the endogenous RPE-associated genes *Rpe65* and *Cralbp* in murine BMDCs and *CRALBP* in human BMDCs at a similar level to ILV3-*RPE65* infection. This indicates that IDLV3-*RPE65* is capable of initiating the differentiation of both mouse and human BMDCs to RPE-like cells *in vitro*, rendering them suitable for therapeutic transplantation in dry AMD.

Results

Infection of BMDCs with Third Generation ILV and IDLV Vectors.

Infection of murine BMDCs with ILV3-*RPE65* at a multiplicity of infection of 50 (MOI; 50 viral particles per cell) resulted in a ~30-fold ($p < 0.05$) increase in expression of human *RPE65* mRNA compared with the null control (Figure 3.1A). Expression of murine *Rpe65* mRNA was increased ~6-fold, and *Cralbp* ~5-fold (Figure 3.1A). As expression of these endogenous murine mRNAs is a critical step in BMDC programming, [216] we concluded that ILV3-*RPE65* is appropriate for use in programming BMDCs, and for packaging as an IDLV. The average expression of human *RPE65* mRNA from ILV3-*RPE65* in murine BMDCs was ~28-fold ($p < 0.05$) higher than expression in the uninfected control, and expression of human *RPE65* mRNA from IDLV3-*RPE65* was ~3.6-fold ($p < 0.05$) lower than

expression obtained with *ILV3-RPE65* at the same MOI (Figure 3.1B). We therefore focused on improving *IDLV3-RPE65* infection.

To confirm that *IDLV3* vectors have limited integration potential, we infected HT1080 cells with *IDLV3-GFP* and monitored the percentage of GFP+ cells for 12 days. Expression of GFP from *IDLV3-GFP*-infected cells was significantly decreased ($p < 0.05$) at day 6 in comparison with day 1, with a 2.1-fold decrease in expression of GFP at day 6 compared with day 1 (Figure 3.1C). Expression of GFP was almost absent by day 12 (Figure 3.1C), with a 14.9-fold decrease in expression compared with day 1 and a 7.2-fold decrease compared with day 6 ($p < 0.05$). Overall, between day 1 and day 12, the percentage of cells expressing GFP decreased from ~13% to ~1% ($p < 0.05$). The residual expression of GFP retained at the end of the experiment is likely a result of a small number of viral integrations, as some residual integration does occur with *IDLVs*. [282] In contrast, *ILV3-GFP* stably integrates into the genome, with expression rising from ~65% to ~82% ($p < 0.05$) from day 1 to day 4 before stabilizing at ~75% from day 5 through day 12 (Figure 3.1D). Together, Figure 3.1 shows that infection with *IDLV3-RPE65/GFP* or *ILV3-RPE65/GFP* results in low integration and stable integration respectively – as expected, the starting percentage of GFP+ cells where the *IDLV-GFP* vector was transduced into HT1080 cells was considerably lower than that of HT1080 cells infected with *ILV-GFP* (Figure 3.1C-D). HT1080 fibroblasts were used in this experiment as the BMDCs cannot be maintained in culture for long periods of time without the addition of growth factors, which would have altered the

cells in comparison with the cells kept in culture for a short period of time as used for future *in vivo* experiments. The HT1080 cell line was chosen as this cell line is traditionally used for titering lentiviral vectors.

Figure 3.1

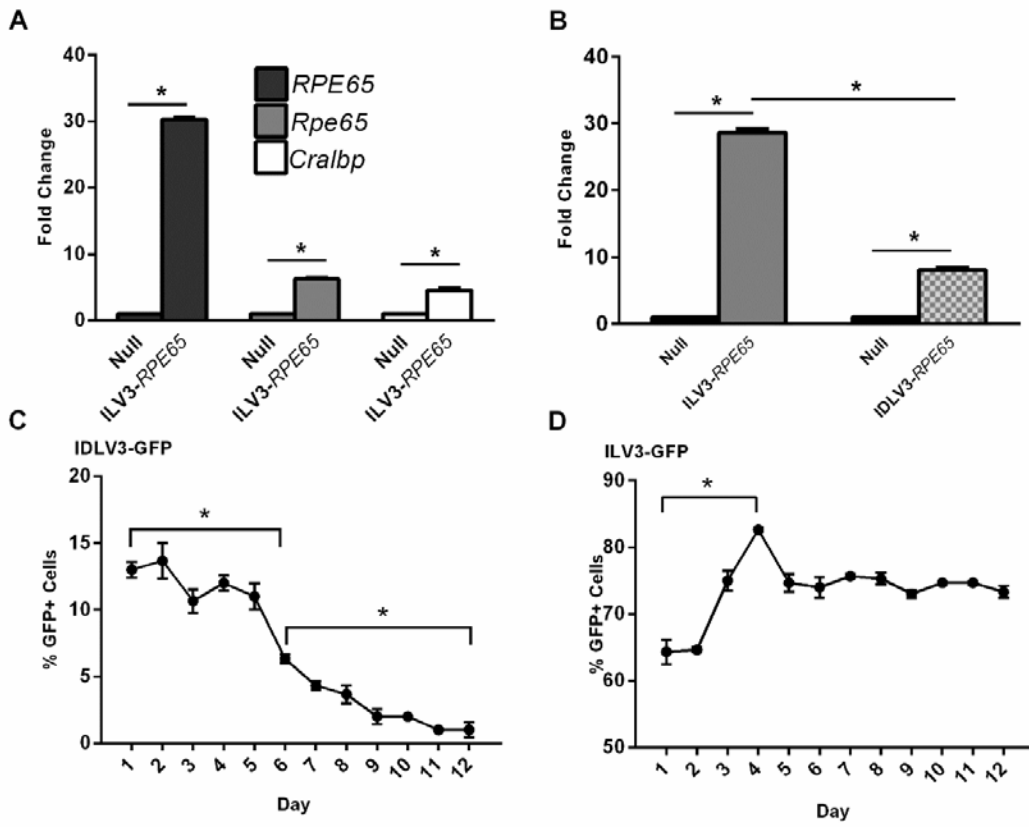


Figure 3.1: IDLVs Infect Murine BMDC and Induce Expression of Endogenous mRNA, and Infect HT1080 Cells with Minimal Integration.

Murine Lin⁻/Sca1⁺ cells were isolated from whole bone marrow of C57BL6/J mice, and infected at an MOI of 50 with ILV3-*RPE65* (A) or IDLV3-*RPE65* (B) on RetroNectin-coated plates (2 $\mu\text{g}/\text{cm}^2$ RetroNectin in PBS, incubated at 4°C overnight) by centrifugation for 2h at 150 g prior to harvest for qRT-PCR analysis. 50,000 HT1080 cells per well were infected with IDLV3-*GFP* (C) or ILV3-*GFP* (D) at an MOI of 50 with Polybrene for 16h and cultured for 1-12 days with GFP expression measured each day by counting the number of positive and negative cells and calculating the percentage of cells expressing GFP. Uninfected cells were used as a negative control. For the GFP assays, cells stably expressing GFP were used as a positive control. In order to achieve the MOI of 50 for integrating vectors, 10 μL of viral supernatant was added as the vector titer was 10^9 . For non-integrating vectors, 250 μL of viral supernatant was added as the vector titer was $\sim 10^7$. (A) Expression of *RPE65* mRNA from ILV3-*RPE65* was ~ 30 -fold higher than in untreated cells respectively. Cells also expressed the endogenous *Rpe65*, and *Cralbp* mRNA ~ 6 and ~ 4 -fold higher than uninfected cells respectively ($p < 0.05$). (*= $p < 0.05$; n(per experiment)=3, n(experiments)=9). (B) Expression of *RPE65* mRNA from ILV3-*RPE65* was ~ 28 -fold higher than expression in the negative control ($p < 0.05$). Expression of *RPE65* mRNA from IDLV3-*RPE65* was ~ 8 -fold higher than in the negative control ($p < 0.05$). Expression of *RPE65* was significantly lower from IDLV3-*RPE65* than ILV3-*RPE65* ($p > 0.05$). (*= $p < 0.05$; n(per experiment)=3; n(experiments)=3). (C) The percentage of cells expressing GFP

was measured each day. Between Day 1 and Day 6, expression of GFP reduced from ~13% to ~6% ($p < 0.05$). Expression further reduced between Day 6 and Day 12 from ~6% to ~1% ($p < 0.05$). (*= $p < 0.05$; n(per experiment)=3; n(experiments)=3). (D) The percentage of cells expressing GFP was measured each day. Between Day 1 and Day 4, GFP expression increased from ~64% to 82% ($p < 0.05$) before stabilizing at ~75% through Day 12.

(*= $p < 0.05$; n(per experiment)=3; n(experiments)=3)

Optimization of the Use of RetroNectin in BMDCs

The colocalization of cells and LV particles is critical for efficient infection, and the goal of infection-promoting reagents such as polycations and the recombinant human fibronectin fragment RetroNectin is to enhance the nonspecific adhesion of the virions to the target cell surface. [281, 283] Previously published experiments were carried out using Polybrene; [13, 216] however, as Polybrene is known to be toxic to some cell lines and primary cells, we first compared infection efficiencies with Polybrene, the less toxic polycation Protamine Sulfate, and RetroNectin.

ILV3-*RPE65* and IDLV3-*RPE65* infection with Protamine Sulfate was significantly less efficient than infection in the presence of Polybrene or RetroNectin ($p < 0.05$; Figure 3.2A, B). Protamine Sulfate yielded an ~8-fold and ~11-fold increase in *RPE65* mRNA from ILV3-*RPE65* in murine and human BMDCs respectively, whereas Polybrene or RetroNectin yielded a ~25-fold and ~24-fold increase in ILV3-*RPE65*-infected cells ($p < 0.05$; Figure 3.2A). In IDLV3-*RPE65* infected cells, a ~5 and ~4-fold increase in *RPE65* mRNA was observed with Protamine Sulfate in murine and human BMDCs respectively, compared with a ~14 and 13-fold increase in the presence of RetroNectin, and ~12-fold and ~13-fold increase in the presence of Polybrene ($p < 0.05$; Figure 3.2B). Interestingly, combining RetroNectin and Polybrene together resulted in a lower infection efficiency than when each reagent was used individually, with an average fold increase of ~28 ($p < 0.05$) in *RPE65* mRNA from ILV3-*RPE65* when used individually compared with an average fold increase of ~21.5 ($p < 0.05$) when used together (Figure 3.2C). A

similar effect was observed with IDLV3-*RPE65*, with a ~16-fold ($p < 0.05$) increase in *RPE65* mRNA with both Polybrene and RetroNectin individually compared with a ~13-fold ($p < 0.05$) increase in expression when used in combination (Figure 3.2D).

The infection efficiency of ILV3-*RPE65* and IDLV3-*RPE65* vectors on increasing concentrations of RetroNectin was compared to determine the lowest concentration required to yield high levels of infection. The instruction manual suggests a concentration of 4-20 $\mu\text{g}/\text{cm}^2$, but it has been reported that cells can be infected with retroviral vectors on 2 $\mu\text{g}/\text{cm}^2$ RetroNectin. [281] A >25-fold ($p < 0.05$) increase in *RPE65* mRNA from ILV3-*RPE65* in both murine and human BMDCs was observed when infected on 2 $\mu\text{g}/\text{cm}^2$ RetroNectin (Figure 3.2E). Infection was not significantly enhanced by transducing the cells on 4 $\mu\text{g}/\text{cm}^2$ or 12 $\mu\text{g}/\text{cm}^2$ RetroNectin (Figure 3.2E). Similarly, infection with the IDLV results in a ~12-fold ($p < 0.05$) increase in mRNA in murine and human BMDCs infected on 2 $\mu\text{g}/\text{cm}^2$ RetroNectin, which is not significantly enhanced when the concentration of RetroNectin is increased, with a similar fold increase observed when cells are infected on 4 $\mu\text{g}/\text{cm}^2$ or 12 $\mu\text{g}/\text{cm}^2$ RetroNectin (Figure 3.2F). We have therefore confirmed that the use of 2 $\mu\text{g}/\text{cm}^2$ RetroNectin is appropriate for infecting murine and human BMDCs with ILV3-*RPE65* and IDLV3-*RPE65*.

Next, we investigated the binding capacity of RetroNectin when used to coat multiple plates. Instead of discarding the RetroNectin after coating the first plate,

we transferred it to a new plate and repeated the coating procedure up to three times. As shown in Figure 2G, *RPE65* mRNA in both human and murine BMDCs was found to be ~27-fold ($p < 0.05$) higher than in the control in cells infected on RetroNectin used 1, 2, and 3 times. In contrast, on the 4th use of RetroNectin, *RPE65* mRNA levels dropped to ~8-fold over the control, indicating that RetroNectin cannot be used more than three times.

Finally, we investigated whether or not adding RetroNectin to the media could also facilitate infection. RetroNectin was added to the media at a concentration of 0-12 $\mu\text{g}/\mu\text{L}$ and human *RPE65* mRNA levels were compared to those achieved on plates coated with 2 $\mu\text{g}/\text{cm}^2$ RetroNectin following infection with ILV3-*RPE65*. Adding RetroNectin to the culture media does not facilitate ILV3-*RPE65* infection murine or human BMDCs, with no significant *RPE65* mRNA increase observed (Figure 3.2H). In comparison with cells infected on a RetroNectin-coated plate, cells infected with 2, 4, or 12 $\mu\text{g}/\text{mL}$ RetroNectin in the media were found to express *RPE65* mRNA ~16, ~10, and ~8-fold ($p < 0.05$) less respectively (Figure 3.2H).

Figure 3.2

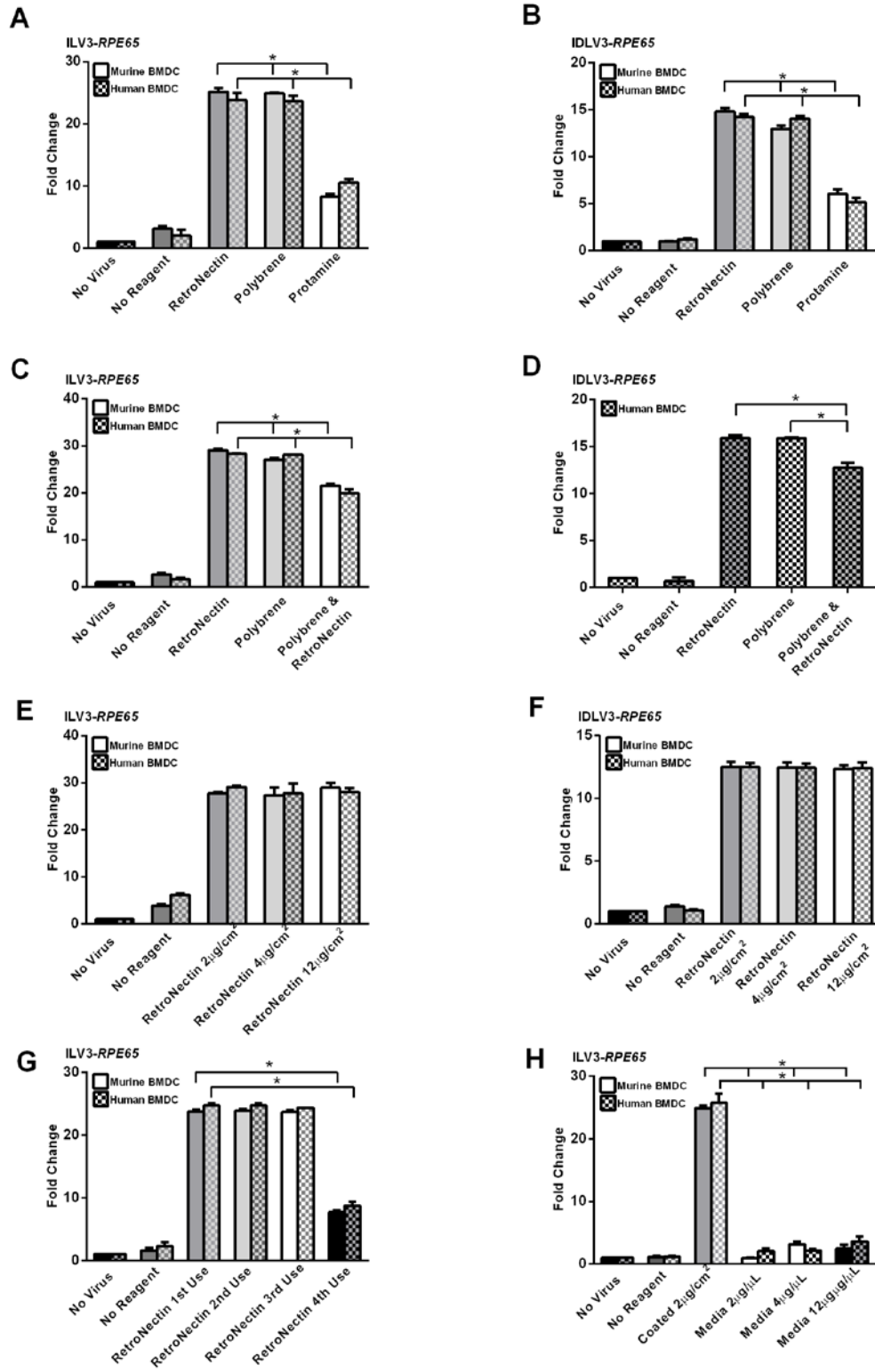


Figure 3.2. Optimization of the Use of RetroNectin in BMDCs

Murine (Lin-/Sca1+) or human (CD34+) BMDCs were infected at an MOI of 50 with ILV3-*RPE65* or IDLV3-*RPE65* with Polybrene (8 $\mu\text{g}/\mu\text{L}$), Protamine Sulfate (10 $\mu\text{g}/\mu\text{L}$), or RetroNectin (2, 4, or 12 $\mu\text{g}/\mu\text{L}$; or 2, 4, or 12 $\mu\text{g}/\text{cm}^3$), or a combination of Polybrene and RetroNectin (2 $\mu\text{g}/\text{cm}^3$). Cells were infected for 12 h and harvested for qRT-PCR analysis at 16 h. (A) Human *RPE65* mRNA levels were increased ~25-fold over control in murine BMDCs and ~23-fold in human BMDCs infected with ILV3-*RPE65* using RetroNectin. Similar levels were observed in BMDCs infected with ILV3-*RPE65* using Polybrene, with a 24-fold ($p < 0.05$) increase in murine BMDCs and a 23-fold ($p < 0.05$) increase in human BMDCs. Expression in cells infected with ILV3-*RPE65* with Protamine Sulfate was lower than that observed with RetroNectin or Polybrene, with an ~8-fold ($p < 0.05$) increase in murine BMDC and a ~10-fold ($p < 0.05$) increase in human BMDCs. (B) Human *RPE65* mRNA levels were increased ~15-fold ($p < 0.05$) over control in murine BMDCs and ~14-fold ($p < 0.05$) in human BMDCs infected with IDLV3-*RPE65* using RetroNectin. Similar levels were observed in BMDCs infected with IDLV3-*RPE65* using Polybrene, with a 13-fold ($p < 0.05$) increase in murine BMDCs and a 14-fold ($p < 0.05$) increase in human BMDCs. Expression in cells infected with IDLV3-*RPE65* with Protamine Sulfate was lower than that observed with RetroNectin or Polybrene, with a ~6-fold ($p < 0.05$) increase in murine BMDC and a ~5-fold increase in human BMDCs ($p < 0.05$). (C) Human *RPE65* mRNA levels were increased ~29-fold over control in murine BMDCs and ~28-fold in human BMDCs

infected with ILV3-*RPE65* using RetroNectin. Similar levels were observed in BMDCs infected with ILV3-*RPE65* using Polybrene, with a 27-fold ($p < 0.05$) increase in murine BMDCs and a 28-fold ($p < 0.05$) increase in human BMDCs. Expression in cells infected with ILV3-*RPE65* with Polybrene and RetroNectin in combination was lower than that observed with RetroNectin or Polybrene, with a ~21-fold ($p < 0.05$) increase in murine BMDC and a ~20-fold ($p < 0.05$) increase in human BMDCs. (D) Human *RPE65* mRNA levels were increased ~16-fold over control in human BMDCs infected with ILDV3-*RPE65* using RetroNectin. Similar levels were observed in BMDCs infected with ILVD3-*RPE65* using Polybrene, with a 16-fold ($p < 0.05$) increase vs. control. Expression in cells infected with IDLV3-*RPE65* with Polybrene and RetroNectin in combination was lower than that observed with RetroNectin or Polybrene, with a ~13-fold ($p < 0.05$) increase vs. control. (E) Murine and human BMDCs infected with ILV3-*RPE65* in the presence of $2\mu\text{g}/\text{cm}^2$ RetroNectin expressed human *RPE65* mRNA 27- and 28-fold over control ($p < 0.05$) respectively. Expression was not increased in either cell type with an increase in RetroNectin concentration to $4\mu\text{g}/\text{cm}^2$ or $12\mu\text{g}/\text{cm}^2$. (F) Murine and human BMDCs infected with IDLV3-*RPE65* in the presence of $2\mu\text{g}/\text{cm}^2$ RetroNectin expressed human *RPE65* mRNA 13-fold over control ($p < 0.05$) in both cell types. Expression was not increased in either cell type with an increase in RetroNectin concentration to $4\mu\text{g}/\text{cm}^2$ or $12\mu\text{g}/\text{cm}^2$. (G) Murine and human BMDCs infected with ILV3-*RPE65* in the presence of $2\mu\text{g}/\text{cm}^2$ RetroNectin used to coat 1 plate expressed human *RPE65* mRNA 23- and 24-fold over control ($p < 0.05$) respectively. Levels did not increase or decrease in cells infected with ILV3-*RPE65*

in the presence of $2\mu\text{g}/\text{cm}^2$ RetroNectin used to coat 2 or 3 plates. In contrast, where $2\mu\text{g}/\text{cm}^2$ RetroNectin was used to coat a 4th plate, *RPE65* mRNA levels were only 7- and 8-fold over control ($p<0.05$) in murine and human cells respectively. (H) Murine and human BMDCs infected with ILV3-*RPE65* on $2\mu\text{g}/\text{cm}^2$ RetroNectin-coated plates expressed human *RPE65* mRNA 24- and 25-fold over control respectively ($p<0.05$). Cells infected with media containing 2, 4, or $12\mu\text{g}/\mu\text{L}$ RetroNectin did not significantly express *RPE65* mRNA.

(*= $p<0.05$; n(per experiment)=3; n(experiments)=3).

Enhancing the Infection of BMDCs with IDLV3-*RPE65*

IDLV3-*RPE65* transduces murine and human cells at a lower efficiency than ILV3-*RPE65* (Figure 3.1, 3.2). *RPE65* mRNA levels IDLV3-*RPE65* are approximately 8-15-fold higher than control in IDLV3-*RPE65*-infected cells, whereas in ILV3-*RPE65*-infected cells, mRNA levels are 27-30-fold higher than control. This is consistent with previously reported findings that IDLVs do not infect as efficiently as ILVs.[271] As maximizing the number of infected cells is, we investigated methods by which IDLV3-*RPE65* infection of BMDCs could be enhanced.

Increasing the MOI does not significantly enhance expression in HT1080 cells infected with IDLV3-GFP, with GFP mRNA remaining at ~8-fold over control in IDLV3-GFP-infected cells, despite an increase of the MOI from 50 to 500 (Figure 3.3A). In contrast, increasing the MOI of ILV3-GFP from 50 to 500 significantly enhances GFP mRNA levels, with a ~27-fold ($p < 0.05$) increase over the control with MOI 50, and a ~150-fold increase at MOI 500 ($p < 0.05$). As increasing the MOI did not enhance infection, we next modified the procedure by which the viral particles were concentrated. Increasing the centrifugation time from 1 hour to 2 hours increased the virion recovery of IDLV3-*RPE65*, with an increase in human *RPE65* mRNA in cells infected with 20 μ L supernatant from ~8-fold over control at 1h to ~12-fold over control at 2h (Figure 3.3B). Further increasing the concentration time to 3 hours did not enhance virion recovery. Additionally, centrifuging the viral

particles for 4 hours significantly reduced recovery, with *RPE65* mRNA observed at less than 5-fold over the control in BMDCs infected with 20 μ L IDLV3-*RPE65* supernatant.

To further investigate whether the concentration protocol could be modified to enhance IDLV3-*RPE65* infection, we concentrated the viral supernatant with LentiX Lentiviral Vector Concentrating Reagent (Catalog #PT4421-2, ClonTech). Concentrating the viral supernatant 10x with LentiX resulted in a ~12-fold ($p < 0.05$) increase in expression over the control when infected at an MOI of 50. IDLV3-*RPE65* concentrated at 20x resulted in a significant increase in *RPE65* mRNA, with a ~20-fold ($p < 0.05$) increase at the same MOI (Figure 3.3C).

While Lenti-X concentration of IDLV3-*RPE65* enhanced infection efficiency in comparison with the centrifugation-concentrated vector, the efficiency was still lower than that of ILV3-*RPE65*, with a ~20-fold increase with IDLV3-*RPE65* compared with an average 27-fold increase with ILV3-*RPE65*. It has been reported that preloading retroviral vectors onto RetroNectin, either once or up to five times, significantly enhances gene transfer.[281] We therefore evaluated the use of preloading in ILV3-*RPE65* and IDLV3-*RPE65* infections. *RPE65* mRNA levels after ILV3-*RPE65* infection remained at ~27-fold ($p < 0.05$) over control when murine BMDCs were infected with or without preloading (Figure 3.3D). In contrast, *RPE65* mRNA increased from ~13-fold ($p < 0.05$) over control on RetroNectin alone to ~23-fold ($p < 0.05$) in murine BMDCs infected with IDLV3-*RPE65* preloaded on

the RetroNectin (Figure 3.3D). Preloading the plate twice enhances IDLV3-*RPE65* infection ($p < 0.05$) (Figure 3.3E). No significant improvement is observed between 2 and 3 preloads. (Figure 3.3E).

As RetroNectin binds to both the virus and the cells, we also looked at infection on plates that had been preloaded with cells prior to the addition of the virus. No advantage in preloading cells in comparison with preloading viral supernatant was observed (Figure 3.3F).

Despite the increase in IDLV3-*RPE65* infection with preloading, *RPE65* mRNA levels were still lower (~23-fold over control) than those obtained with ILV3-*RPE65* (~27-fold over control). As a final modification to the protocol, we combined RetroNectin preloading with infection by centrifugation, referred to as spinoculation. Spinoculating murine BMDCs with preloaded IDLV3-*RPE65* results in a ~27-fold increase in expression of the vector when combined with preloading on RetroNectin without spinoculation ($p < 0.05$) (Figure 3.3G).

We have therefore demonstrated that concentrating IDLV3-*RPE65* 20x with LentiX followed by infection of cells on $2\mu\text{g}/\text{cm}^2$ RetroNectin, pre-loaded with the virus at an MOI of 50, with spinoculation, increases *RPE65* mRNA at a similar level to ILV3-*RPE65*.

Figure 3.3

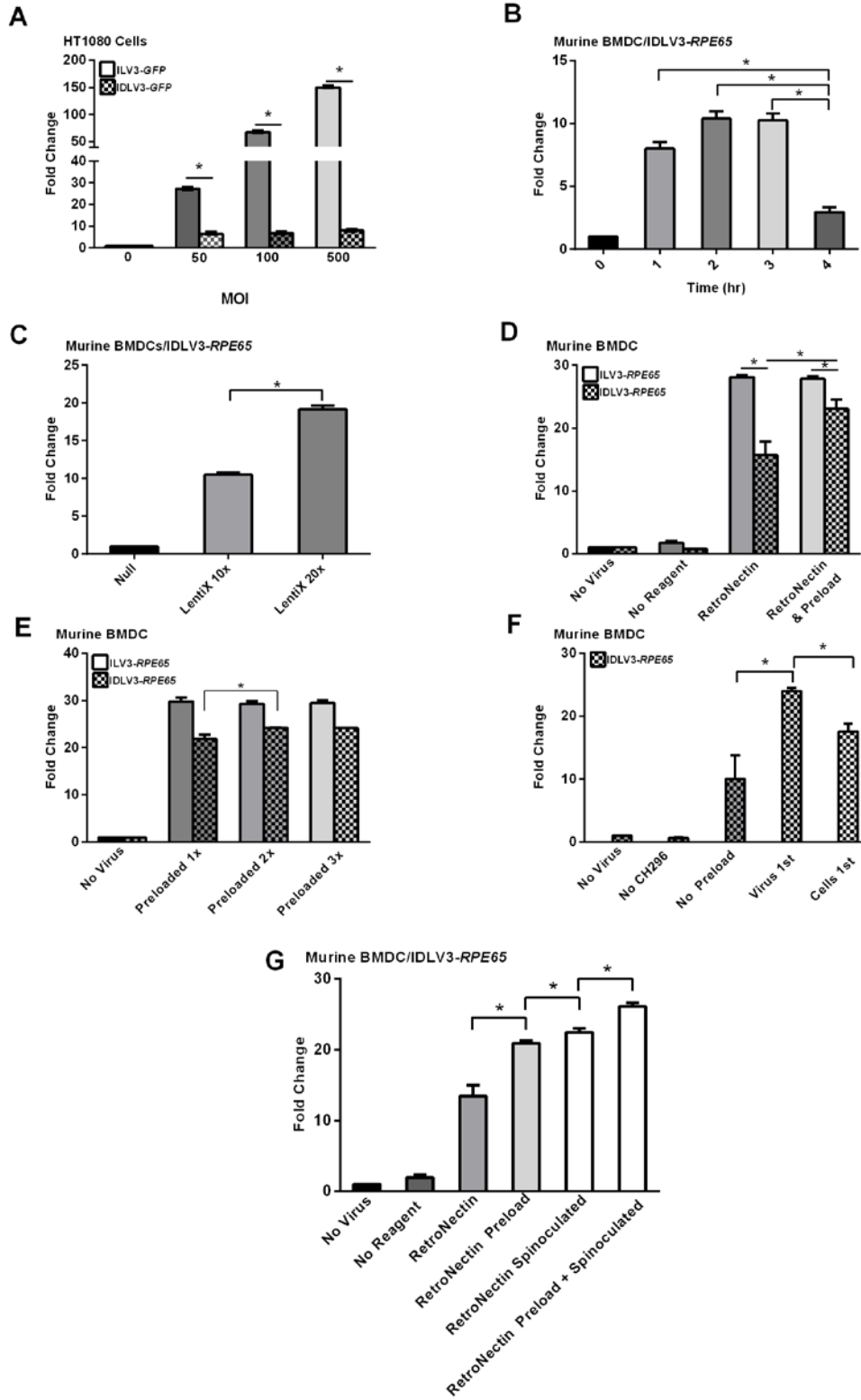


Figure 3.3. Enhancing the Infection of BMDCs with IDLV3-*RPE65*

HT1080, murine (Lin-/Sca1+), or human (CD34+) BMDCs were infected with ILV3-*GFP* (A), ILV3-*RPE65* or IDLV-*RPE65* (B-G) at an MOI of 50 (A, C-G), 100 (A), or 500 (A), or with 20 μ L concentrated viral supernatant (B). RetroNectin at 2 μ g/cm³ was used for all infections, and was either used by itself (A-C) or with preloading of vectors (D-G) or cells (F). Cells were infected for 12 h and harvested for analysis at 16 h unless spinoculated (G), where cells were infected for 2h at 150 g and harvested for analysis at 4h. **(A)** Increasing the MOI of ILV3-*RPE65* increased *RPE65* mRNA levels from ~27-fold over control ($p < 0.05$) at MOI 50 to ~68-fold over control ($p < 0.05$) at MOI 100 and ~150-fold over control ($p < 0.05$) with MOI 500. Increasing the MOI of IDLV3-*RPE65* did not have a significant effect on expression, with *RPE65* levels remaining at ~7-fold over control ($p < 0.05$). **(B)** Centrifugation of IDLV3-*RPE65* supernatant for 2 hours increased recovery of virions, with a ~10-fold increase in infection of murine BMDCs with concentrated supernatant at the same volume in comparison with 8-fold observed at 1 hour. Centrifugation for 3 hours did not enhance infection efficiency, and centrifuging for 4 hours reduced the viability of virions, with *RPE65* expression only 3-fold over control ($p < 0.05$). **(C)** Concentrating viral supernatant 20x enhanced the infection of IDLV3-*RPE65* in comparison with concentrating 10x and infecting at the same MOI, with a 19-fold ($p < 0.05$) increase in *RPE65* mRNA observed at MOI 50 with the 10X concentrated vector and 10-fold ($p < 0.05$) with the 20X concentrated vector at the same MOI. **(D)** Preloading ILV3-*RPE65* on RetroNectin for 30 minutes prior

to adding murine BMDCs did not enhance infection, with a 28-fold increase ($p < 0.05$) observed with or without preloading. In contrast, with IDLV3-*RPE65*, preloading increased *RPE65* expression from 15-fold over control ($p < 0.05$) to 23-fold over control ($p < 0.05$). **(E)** Preloading ILV3-*RPE65* on RetroNectin up to three times did not result in an increase in human *RPE65* expression. Preloading IDLV3-*RPE65* twice increased infection, with *RPE65* mRNA levels increasing from 21-fold to 24-fold over control ($p < 0.05$). No increase was observed with three preloads. **(F)** Murine BMDCs infected with IDLV-*RPE65* expressed *RPE65* the highest level when viral particles were preloaded onto RetroNectin, with a 24-fold increase ($p < 0.05$) in expression vs 10-fold with no preload ($p < 0.05$). Preloading the cells instead of the virus yielded an increase in *RPE65* expression, with a 17-fold increase vs. control ($p < 0.05$); however, this was lower than observed when viral particles were preloaded, indicating no advantage in preloading cells **(G)** IDLV-*RPE65* infects murine BMDCs at the highest efficiency when the virus is preloaded onto RetroNectin followed by infection by spinoculation, with an 26-fold increase ($p < 0.05$) in expression over control in comparison with 20-fold with preload alone ($p < 0.05$), and 22-fold with spinoculation alone ($p < 0.05$).

(*= $p < 0.05$; n(per experiment)=3; n(experiments)=3).

***In Vitro* Differentiation of Human and Murine BMDCs with IDLV3-RPE65**

We have previously reported that pTYF-*RPE65* infection of murine BMDCs initiates expression of the endogenous murine *Rpe65* and *Cralbp* mRNAs.[216] Murine BMDCs infected with either ILV3-*RPE65* or IDLV3-*RPE65* vectors express endogenous *Rpe65*, and *Cralbp* mRNAs 5-10-fold ($p < 0.05$) over control (Figure 3.4A). This indicates that IDLV3-*RPE65* is likely to be sufficient for promoting the expression of the RPE-associated genes that contribute to the programming of the BMDCs to RPE-like cells.

In human BMDCs, a ~5-fold increase in expression of *CRALBP* mRNA is observed in cells infected with either ILV3-*RPE65* or IDLV3-*RPE65* (Figure 3.4B). This indicates that IDLV3-*RPE65* may also be capable of promoting differentiation of human BMDCs to RPE-like cells.

Figure 3.4

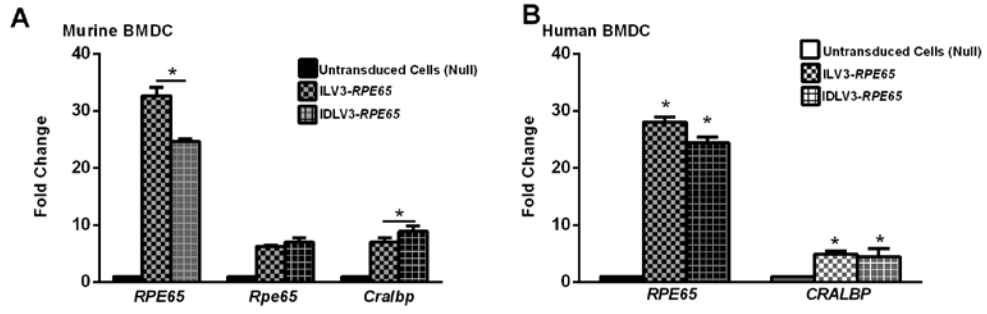


Figure 3.4. *In Vitro* Differentiation of Human and Murine BMDCs with IDLV3-*RPE65*.

Murine Lin-/Sca1+ BMDCs (A) or human CD34+ cells (B) were infected at MOI 50 with ILV3-*RPE65* on RetroNectin (2 $\mu\text{g}/\text{cm}^2$) by spinoculation for 2h at 150g, or with IDLV3-*RPE65* pre-loaded on RetroNectin (2 $\mu\text{g}/\text{cm}^2$) prior to spinoculation. Cells were then harvested and lysed for qRT-PCR analysis. *RPE65* expression was ~32-fold over control and ~28-fold over null control in murine (A) and human (B) BMDCs infected with ILV3-*RPE65* respectively ($p < 0.05$). *RPE65* mRNA levels were ~13,4-fold over control in both murine (A) and human (B) BMDCs infected with the IDLV vector respectively ($p < 0.05$). In murine BMDCs, endogenous *Rpe65* mRNA levels were increased ~6- and ~7-fold vs control in cells infected with ILV3-*RPE65* and IDLV3-*RPE65* respectively, and *Cralbp* mRNA levels were increased 7- and 8-fold vs control in cells infected with ILV3-*RPE65* and IDLV3-*RPE65* respectively (A). In human BMDCs, *CRALBP* mRNA levels were 5-fold over control in cells infected with either vector.

(*= $p < 0.05$; n(per experiment)=3; n(experiments)=12 [murine BMDC, ILV3-*RPE65*]; n(per experiment)=3; n(experiments)=3 [human BMDC, ILV3-*RPE65*; murine and human BMDC, IDLV3-*RPE65*]).

Discussion

We have previously shown in two murine models of RPE damage that adult BMDCs modified *ex vivo* with an ILV expressing *RPE65* are recruited to and preserve the RPE and retina following systemic delivery. [13, 216] Compounding factors facilitating the lack of visual recovery in humans after cell-based therapy for dry AMD to date [180, 181, 186] include treatment in the late stages of disease, limited motility of cells across the RPE layer post-injection, and side effects of invasive cell delivery.[13, 216] [219, 220]

Transient expression of *RPE65* is likely to be sufficient, as we previously reported that the endogenous *Rpe65* and *Cralbp* genes are activated within hours of *RPE65* vector infection. [13, 216] IDLVs lack the integrase gene, and integrate at a 500-1250-fold lower rate than integrating vectors, [282] with residual integration likely occurring through integrase-independent mechanisms, such as DNA break-induced non-LTR-mediated integration. [284] In a clinical setting, inclusion of a suicide gene in the transducing vector would allow for rapid elimination of cells containing integrated virus if off-target effects resulting from insertional mutagenesis were to occur. Suicide gene-mediated inducible apoptosis has been demonstrated to be safe and effective in human clinical trials.[285, 286] Our findings are consistent with observations that low-level transgene expression is maintained 10-14 days post-infection. [287-289]

It has been well established in the literature that IDLVs are less efficient than ILVs. [224, 271] Critical difficulties in the application of IDLVs have arisen for a number of reasons, primarily a low number of virions entering cells, [224] and downregulation of transgene expression due to episome inhibition, [280] which has been shown to be counteracted by a deletion in the U3 region of the virus. [280] Several groups have published modifications to the transducing vector which improve the stability of expression from episomal IDLV particles. These modifications include codon-optimization of the transgene, [290, 291] the use of a strong promoter such as SV40 [292] instead of the CMV promoter which is susceptible to silencing, [293] and inhibiting viral life cycle proteins. [294, 295] We have utilized some of these modifications here through the use of the EF-1 α promoter, which is constitutively expressed at a similar level in all cell types, and codon-optimization of the *RPE65* cDNA for use in human cells.

Overall, we focused on increasing the number of virions entering cells as opposed to further modifying the transducing vector, as retention of transgene expression was not thought to be required for our application. The critical difference between our use of IDLV3-*RPE65* and the majority of IDLV3-based studies published to date is that we only require expression of *RPE65* at a high level for a few hours post-infection for the vector to activate the endogenous genes, and are therefore using it as a molecular 'switch' as opposed to a long-term modification. Consequently, we measure expression at 4 hours post-infection, in contrast with typical lentiviral vector expression studies which measure transgene expression

after several days in culture. [222, 224, 231, 262, 265, 267, 268, 271-273, 275, 280, 282, 289, 291, 292, 295] This time point was chosen as we have previously demonstrated that *RPE65* induces *Rpe65* and *Cralbp* expression within the first few hours of infection. [216]

We propose that the method outlined here is optimal for the application of IDLVs in studies in which short-term (1-12 hrs) expression is sufficient, as the increase in expression in the early stages post-infection may not be sustained – our success in improving expression through increasing viral number per cell is likely to precede silencing of the episome. [280] For studies in which longer-term expression of the transgene is required, vector modifications such as U3 deletions may be necessary to maintain transgene expression after increasing the infection efficiency. [280]

To improve IDLV3-*RPE65* infection efficiency, the infection protocol was systematically modified. Infection is dependent on direct virion-cell interaction. Viral particles have a half-life of around 4-8hrs, [296, 297] during which they are capable traveling 580-610 microns, [298] and are negatively charged. It is therefore necessary to enhance the localization of cells and virions using reagents which either bind both, or eliminate the negative charge of both the cells and the virions. RetroNectin enhances infection efficiency via co-localization of virions and cells [299, 300] through binding by a heparin binding domain and VLA5/VLA4 binding domains respectively, [281, 283] and is frequently used to maintain retroviral gene transfer in hematopoietic stem cells (HSCs) derived from primates, canines, and humans. [301-303] It has advantages over the commonly used

polycation Polybrene, which facilitates gene transfer by counteracting the negative charge of the cells and virions, in that it is less toxic to cells, yet produces similarly efficient infections. Protamine Sulfate has been shown to be as effective as Polybrene with the mouse SAX retroviral vector; [304] however, we found it to be significantly less effective than Polybrene or RetroNectin in BMDCs. Therefore, we focused on using RetroNectin to enhance infection with IDLV3-*RPE65*.

Efficient infection of the HEL cell line and human CD34+ cells with retroviral vectors has been reported on plates coated with 2 $\mu\text{g}/\text{cm}^2$ RetroNectin, [281] despite the instruction manual indicating a requirement for 4-20 $\mu\text{g}/\text{cm}^2$. Our findings support this data, indicating that lentiviral vectors also transduce both human and mouse BMDCs on 2 $\mu\text{g}/\text{cm}^2$ RetroNectin. Additionally, we show that a single preparation of 2 $\mu\text{g}/\text{cm}^2$ RetroNectin can be removed and used to coat up to three wells before any reduction in efficiency. Both of these findings minimize the cost of LV approaches using RetroNectin. Also consistent with the literature, in which it has been reported that preloading of retroviral vectors on RetroNectin enhances gene transfer, [281] preloading of IDLV on RetroNectin prior to infection of cells resulted in a higher infection efficiency, [281] indicating that preloading is effective for infection with lentiviral as well as retroviral vectors.

Expression of the endogenous *Rpe65* and *Cralbp* genes in murine BMDCs infected with IDLV3-*RPE65* confirm that the IDLV is functioning in a similar way to the ILV. Expression of *CRALBP* in human BMDCs infected with ILV3-*RPE65* or

IDLV3-*RPE65* indicates that expression of *RPE65* in these cells is functioning in a similar way as expression in murine BMDCs, and suggests that expression of this is likely to result in human BMDC differentiation into RPE-like cells. This is of significant importance for the therapeutic potential of this technique in humans, which will be the focus of our future studies.

To summarize, use of IDLV3-*RPE65* significantly reduces the risk of our LV-based approach, as the number of viral integrations per cell and the subsequent risk of insertional mutagenesis is markedly reduced. IDLV3-*RPE65* successfully initiates the expression of endogenous genes, which we believe to be responsible for the ability of *RPE65*-infected BMDCs to integrate into and regenerate damaged RPE in mouse models of RPE degeneration, in both murine and human BMDCs. Efficacy is significantly enhanced by modifying the infection protocol with RetroNectin. Our approach is quick and ideal for applications in which short term transient expression may be sufficient, avoiding time-consuming and costly modifications of the transducing vector.

**CHAPTER IV: MURINE BONE MARROW-DERIVED CELLS PROGRAMMED
WITH 3RD GENERATION INTEGRATING AND INTEGRASE-DEFICIENT
LENTIVIRAL VECTORS PREVENT RETINAL DEGENERATION.**

Introduction

In order to verify that murine BMDCs programmed with ILV3-*RPE65* or IDLV3-*RPE65* are functional in terms of regenerating damaged RPE, it was necessary to evaluate the ability of these cells to repair RPE in murine models of retinal degeneration. We have previously demonstrated that pTYF-*RPE65*-infected BMDCs prevent retinal degeneration and preserves visual function in an acute [216] and a chronic [13] model of RPE damage. Critically, in these studies, the cells were administered systemically, either via the retro-orbital sinus vein [216] or the tail vein, [13] eliminating the need for invasive subretinal transplant of the cells and making the treatment considerably more desirable and feasible for use in human patients with early-stage retinal degeneration. [216]. It was demonstrated that the *RPE65*-expressing lentiviral vector was critical for the process of programming regeneration-capable BMDCs as the cells which were infected with the same lentiviral vector expressing a control *LacZ* gene did not result in significant recovery of vision or preservation of retinal morphology. This indicates that it is the expression of *RPE65* from the vector that results in cellular differentiation, as opposed to the process of infecting the cells with the lentiviral vector and/or the integration of viral particles into the host cell genome. [13, 216]

In this current study, we evaluated BMDCs infected with ILV3-*RPE65* and IDLV3-*RPE65* in the two previously published models, the acute injury sodium iodate model, [216] and the chronic injury superoxide dismutase 2 knock-down (SOD2-KD) model of retinal degeneration. [13] We also evaluated BMDCs infected with two additional vectors, ILV3-*RPE65-MITF* and IDLV3-*RPE65-MITF*. The rationale for this is that microphthalmia-associated transcription factor MITF isoforms are both involved in the development of the retina and RPE cells, [305] and expressed in terminally differentiated RPE cells. [306] MITF-M is expressed in differentiated RPE. [306] MITF-A and J are present during the development of the retina and RPE, and MITF-H and MITF-D are present in the RPE, with MITF-D expressed only in the RPE [305]. Defects in MITF isoforms have been found to result in microphthalmia [307] and hyperproliferation of hypopigmented RPE cell and lack of RPE layer formation, [308] along with other non-ocular phenotypes resulting from deficiency in melanin production such as white fur in mice with MITF aberrations. [307] In addition to being expressed in terminally differentiated RPE cells, the M isoform of MITF has been found to be activated following exposure to an inhibitor of cAMP degradation, which in turn stimulates the production of melanin. [309] As we have consistently been unable to observe the development of pigmented RPE *in vitro* following infection with pTYF-*RPE65* or ILV3/IDLV3-*RPE65*, [13] and as we have previously demonstrated the involvement of the cAMP/adenylate cyclase pathway in the differentiation of BMDCs with pTYF-*RPE65*, [216] we hypothesized that including MITF-M in the infecting vector may enhance the differentiation process.

The sodium iodate model consists of an intraperitoneal injection of 100mg/kg sodium iodate per mouse, which selectively and immediately results in necrosis of the RPE, photoreceptor cell death, and activation of the immune response in the retina. [310] As this model results in rapid, severe retinal degeneration, it is not the most accurate representation of the process of pathogenesis in human AMD. It is, however, valuable in initial studies into the efficacy of the 3rd generation vector-treated cells, as results are available within 7-28 days [216] as opposed to 3-6 months in the chronic SOD2-KD model. [13] The sodium iodate damage resembles the pathology of human AMD in the late stages, though cell death is necrotic whereas in human AMD death occurs mainly through apoptosis. [277, 310] The SOD2-KD model closely resembles human AMD in the early stages, with the exception that retinal degeneration is widespread across the retina in mice as opposed to being central as it is in humans, as mice do not have a macula. [277] Therefore, it is advantageous to evaluate the cells in both models in order to determine their suitability for treatment in both late and early-stage disease, though our ultimate goal is to treat early in disease to maximize retinal protection. When other cell types such as photoreceptors have already begun to degenerate, visual recovery via RPE replacement will be limited.

The SOD2-KD model involves subretinally injecting an adeno-associated viral vector (AAV) containing a hammerhead ribozyme to SOD2 mRNA, expressed under the control of a chicken beta-actin (CBA) promoter and the cytomegalovirus (CMV) enhancer. (Figure 2.4). [277] This vector results in progressive oxidative

damage, due to a lack of the manganese superoxide dismutase required for the conversion of superoxide in the mitochondria to hydrogen peroxide and oxygen. This in turn leads to an increase in reactive oxygen species in the mitochondria, which initiates apoptotic cell death. [277] SOD2-KD-induced retinal degeneration progresses slowly over a period of 4 months. [277] This model is a close representation to early dry AMD, as it results in progressive loss of retinal function, the vacuolation and depigmentation and degeneration of the RPE cells, thickening of Bruch's membrane, and a progressive shortening of the photoreceptor outer and inner segments which eventually leads to the death of photoreceptor cells by apoptosis. [277] As we have previously determined that recovery of vision is optimal in SOD2-KD mice when BMDCs infected with pTYF-*RPE65* were given at the 1 month time point, [13] we selected this time point for treatment in the current study.

Here, we investigated the ILV3-*RPE65* and IDLV3-*RPE65* treated cells in the sodium iodate model prior to the SOD2-KD model and determined that cells treated with either vector (a) are recruited to the eye, (b) integrate into the RPE layer, and, (c) preserve visual function as measured by electroretinography, which determines the electrical response of the retina to light, and by optokinetic nystagmus analysis (OKN), which measures the visual acuity of the mouse. In the SOD2-KD model, we observed similar results and further expanded the analysis to include a 6-month measurement of visual acuity in these mice. We determined that RPE recovery following injection with BMDCs programmed with either the

ILV3-*RPE65* or IDLV3-*RPE65* is maintained for at least 6 months. The timing of injection of BMDC post-infection with ILV3-*RPE65* is of particular importance for cellular recruitment to the RPE, with cells injected 16h post-infection failing to be recruited to the RPE. We hypothesize that the BMDCs need to be in an early stage of programming when injected, retaining characteristics of bone marrow-derived cells, in order to effectively circulate in the blood to travel to the intended area of the eye.

Results

ILVs and IDLVs Expressing Both *RPE65* and *MITF* Activate Expression of Endogenous Murine *Rpe65* and *Cralbp* mRNA.

ILV3-*RPE65* and IDLV3-*RPE65* were compared with the new vectors, ILV3-*RPE65-MITF* and IDLV3-*RPE65-MITF*, to confirm that the inclusion of the *MITF* gene in these vectors did not have a detrimental effect on the expression of the endogenous *Rpe65* and *Cralbp* mRNAs. Expression of *RPE65* and *MITF* via infection of the same cells with two vectors each expressing one gene, as opposed to one vector expressing two genes, results in an approximately 50% reduction in expression of both genes in comparison to expression when cells are transduced with either vector alone. BMDCs infected with *RPE65* or *MITF* independently expressed the genes 40-fold and 20-fold over control respectively, which reduced to 22-fold and 13-fold over control when BMDCs were infected with both viruses

together (Figure 4.1A). We therefore expressed MITF from the same vector as *RPE65*, linked by a T2A site, resulting in similar expression of *RPE65* and *MITF* at ~33-fold and ~35-fold over control from the ILV3 vectors and ~5-fold and ~6-fold from the IDLV3 vectors respectively ($p < 0.05$) (Figure 4.1A). Additionally, expression of *RPE65* was similar in BMDCs infected with both ILV3 vectors, with an approximately 33-fold increase in expression over control, and ~5-fold and ~7-fold over control in BMDCs infected with IDLV3 vectors ($p < 0.05$) (Figure 4.1A).

Inclusion of *MITF* in the vector did not reduce expression of *Rpe65* in infected BMDCs. Expression of *Rpe65* was 3-fold over control in ILV3-*RPE65*-infected cells, ~7-fold over control in ILV3-*RPE65*-*MITF*-infected cells, and ~5-fold over control in BMDCs infected with either of the IDLV3 vectors ($p < 0.05$) (Figure 4.1B). Expression of *Cralbp* was 8-fold over control in BMDCs infected with either ILV3 vector, and ~4-fold and ~3-fold over control in BMDCs infected with IDLV3-*RPE65* and IDLV3-*RPE65*-*MITF* respectively ($p < 0.05$) (Figure 4.1B). It is important to note for continuity that this experiment was performed prior to the experiments outlined in Chapter 1, which accounts for the low infection efficiency observed with the IDLVs in Figure 4.1B.

Figure 4.1

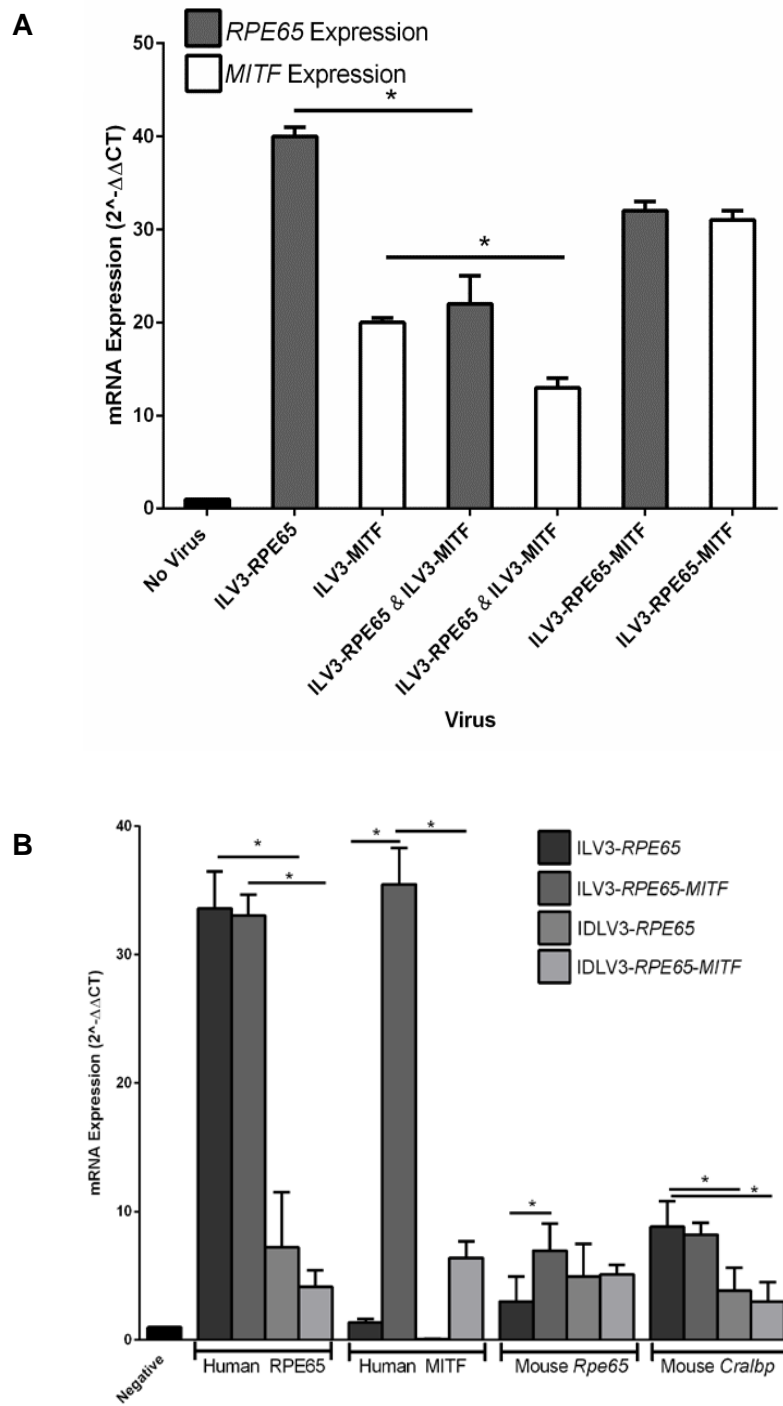


Figure 4.1. ILV3-*RPE65-MITF* and IDLV3-*RPE65-MITF* Initiate Expression of human *Rpe65* and *Mitf* mRNA in Murine BMDCs.

(A) Murine Lin⁻/Sca1⁺ BMDCs were isolated from whole bone marrow of C57BL6/J mice infected at an MOI of 50 on RetroNectin (2 µg/cm²) with ILV3-*RPE65*, ILV3-*MITF*, either alone or in combination, or with ILV3-*RPE65-MITF* by spinoculation for 2h at 150 g, 21°C, prior to harvest for mRNA analysis. Expression of *RPE65* was ~40-fold over control when infected alone, dropping to ~22-fold when infected with ILV3-*MITF* (p<0.04). ILV3-*MITF* infected alone resulted in a ~20-fold increase in expression, dropping to ~13-fold when infected with ILV3-*RPE65* (p<0.05). ILV3-*RPE65-MITF* infection resulted in a ~33-fold increase in expression of both mRNAs. (*=p<0.05, n(per experiment)=3; n(experiments)=3) (B) Murine Lin⁻/Sca1⁺ BMDCs were isolated from whole bone marrow of C57BL6/J mice infected at an MOI of 50 on RetroNectin (2 µg/cm²) with ILV3-*RPE65*, IDLV3-*RPE65*, ILV3-*RPE65-MITF*, or IDLV3-*RPE65-MITF* for 2 hrs at 150 g, 21°C, and harvested for qRT-PCR analysis after 4 hrs. Human *RPE65* mRNA was expressed ~33-fold over control in ILV3-*RPE65* and ILV3-*RPE65-MITF*-infected cells (p<0.05), and human *MITF* mRNA was expressed ~35-fold over control in ILV3-*RPE65-MITF*-infected cells (p<0.05). Human *RPE65* mRNA was 7- and 4-fold over control in IDLV3-*RPE65* and IDLV3-*RPE65-MITF*-infected cells respectively, and human *MITF* mRNA was ~7-fold over control in IDLV3-*RPE65-MITF*-infected cells. Cells infected with all viruses expressed the endogenous *Rpe65* and *Cralbp* mRNAs, with expression in ILV3-*RPE65* and ILV3-*RPE65-MITF*-infected cells 3-fold and 6-

fold, and ~8-fold respectively. In IDLV3-*RPE65* and IDLV3-*RPE65-MITF*-infected cells, *Rpe65* expression was ~5-fold over control and *Cralbp* expression was ~4-fold and ~3-fold over control respectively. (n(per experiment)=3, n(experiments)=12; *=p<0.05).

Timing of Injection of *RPE65*-Programmed BMDCs is Critical for Preserving Retinal Morphology and Visual Function

In the previously published studies, *RPE65*-BMDCs were injected into sodium iodate or SOD2-KD mice immediately after infection with pTYF-*RPE65*. [216] However, as expression of lentiviral vectors increases as the vectors integrate into the genome, it was thought that injecting the cells up to 24 hours after transducing may increase retinal preservation and visual function. Surprisingly, we found that culturing murine BMDCs for 16-20 hours after infection with ILV3-*RPE65* significantly diminished the ability of the cells to regenerate damaged RPE or preserve retinal function.

As shown in Figure 4.2A, sodium iodate treated mice injected with 50,000 BMDCs infected with ILV3-*RPE65* via the tail vein had almost 'flat' ERG traces in comparison with the untreated mice, which had normal A-wave and B-wave patterns. The B-wave was almost absent in all sodium iodate treated mice treated with BMDC-ILV3-*RPE65*. These results were observed consistently in all three treated mice (Figure 4.2A). The average A-wave in normal mice was ~275 (+/- 25), decreasing significantly to ~12 (+/- 3) in sodium iodate treated mice injected with BMDC-ILV3-*RPE65* ($p < 0.05$) (Figure 4.2B). Similarly, while the average B-wave in normal mice was ~650 (+/- 50), the average B-wave in treated mice was ~5 (+/- 2) ($p < 0.05$), demonstrating a significant decrease in retinal function (Figure 4.2B).

ERG data was backed up by OCT, with significant areas of damage visible in the retinas of treated mice in comparison with the wild type normal control. Finally, we found that no GFP+ cells were present in the RPE layer of these mice (Figure 4.2D). Overall, we found that injecting cells that have been cultured overnight after infection with ILV3-*RPE65* do not rescue RPE damage *in vivo* and likely are not recruited to the RPE layer, as no cells were found in the RPE of these mice. Consequently, for the remainder of these studies, we injected the BMDCs immediately after transducing them with lentiviral vectors.

Figure 4.2

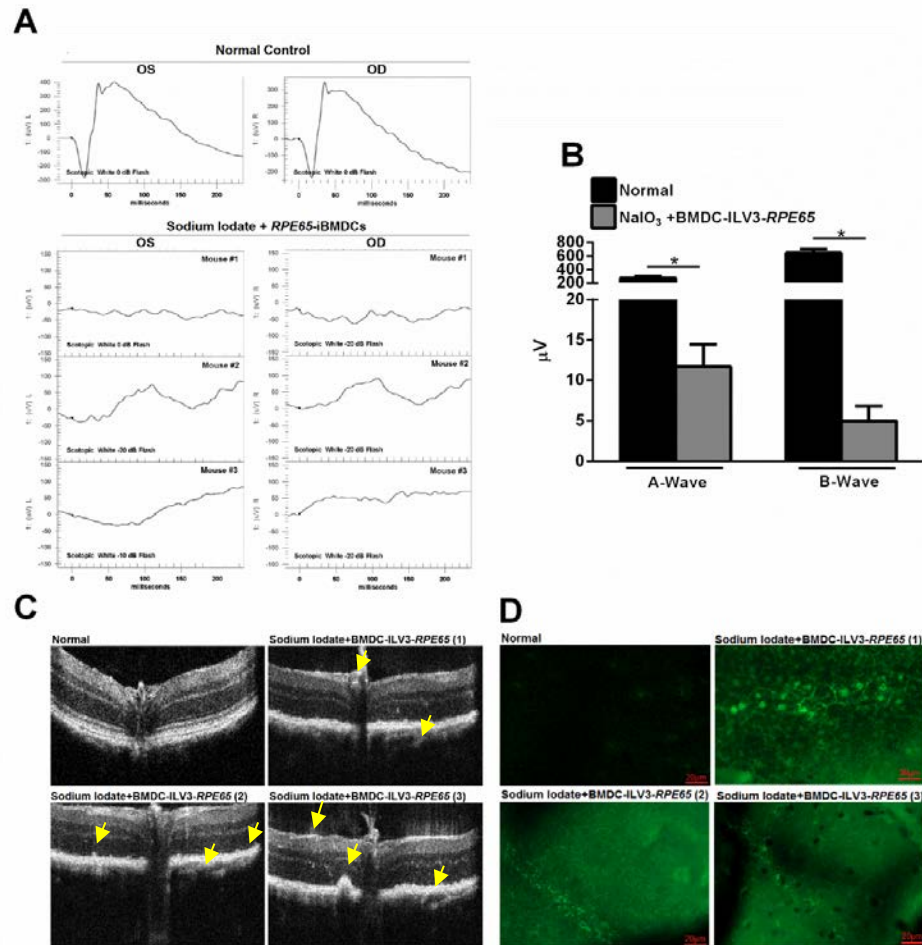


Figure 4.2. BMDC-ILV3-RPE65 Incubated Overnight Following Infection Do Not Preserve Vision or Are Recruited to the RPE Layer. Lin⁻/Sca1⁺ cells were isolated from the femurs and tibiae of ~8-week-old GFP⁺ mice and infected at MOI 50 with ILV3-RPE65 by spinoculation with Polybrene and incubated for 16 hrs post-infection. 50,000 cells were injected via the tail vein per mouse in C57BL6/J mice which had been given a 100mg/kg IP injection 1 day prior to injection of BMDC-ILV3-RPE65. OCT and ERG was carried out approximately 7 days after treatment with cells. Mice were then sacrificed and eyes enucleated, fixed in paraformaldehyde, and flat mounted for analysis. **(A)** Scotopic ERG traces in the OS and OD of the normal control mice show typical pattern for normal mice, with a well-defined A-wave and B-wave. In contrast, the A-wave and B-wave is almost absent in Sodium Iodate treated mice treated with BMDC-ILV3-RPE65. **(B)** Normal mice had an average A-wave of 275 μ V and an average B-wave of 650 μ V. Sodium Iodate-treated mice treated with BMDC-ILV3-RPE65 had an average A-wave of 12 μ V and an average B-wave of 5 μ V. **(C)** Retinae of Sodium Iodate treated mice treated with BMDC-ILV3-RPE65 is clearly visible with OCT. Arrows show areas of pathology. **(D)** No GFP⁺ cells are visible in flat mounted eyes of Sodium Iodate-treated mice treated with BMDC-ILV3-RPE65. (n=3, *=p<0.05)

BMDCs Infected ILV3-*RPE65* Immediately After Infection Are Recruited to the RPE and Preserve Retinal Function in Sodium Iodate-Treated Mice.

To confirm that the lack of recruitment observed in Figure 4.2 was in fact a direct result of the 16 hr time point used, and not a deficiency in the programming of BMDCs with ILV3-*RPE65*, we conducted a short term experiment with the acute sodium iodate model of retinal degeneration. This was necessary to confirm the ability of ILV3-*RPE65*-infected cells to be recruited to and restore vision in our mouse models as BMDCs used in all of the previous studies were infected with pTYF-*RPE65* as opposed to ILV3-*RPE65*. Mice injected with ILV3-*RPE65*-infected GFP+ BMDCs immediately after spinoculation of the BMDCs as opposed to 16 hr later demonstrated significant recovery of vision in comparison with mice injected with null (uninfected Lin-/Sca1+) cells. Electroretinography demonstrated near-normal pattern in mice injected with ILV3-*RPE65*-infected BMDCs in comparison with an almost flat ERG trace observed in mice injected with null BMDCs. The A-wave was improved from ~44 μV in the null BMDC-treated mice to ~104 μV in BMDC-ILV3-*RPE65*-treated mice, in comparison with ~146 μV in the normal control (Figure 4.3A). The B-wave showed similar recovery, with an improvement from ~88 μV in the null BMDC-treated mice to ~236 μV in BMDC-ILV3-*RPE65*-treated mice, in comparison with ~330 μV in the normal control (Figure 4.3B).

We also injected a group of mice with 200k ILV3-*RPE65*-infected cells as opposed to the usual 50k, hypothesizing that an increase in cell number may enhance

migration and recovery of vision. While it was found that mice injected with 200k cells had greater coverage of GFP+ cells at the RPE layer, with ~40% coverage in eyes from mice injected with 200k cells compared with ~20% in mice injected with 50k cells (Figure 4.3C), injecting with 200k cells did not significantly improve visual function over mice injected with 50k cells, with optokinetic nystagmus analysis demonstrating a spatial frequency of 0.482 c/d in the former and 0.505 c/d in the latter, in comparison with normal and vehicle control mice, which had spatial frequencies of 0.643 c/d and 0.593 c/d respectively (Figure 4.3D). We therefore carried out the remainder of the *in vivo* studies with 50k cells.

Figure 4.3

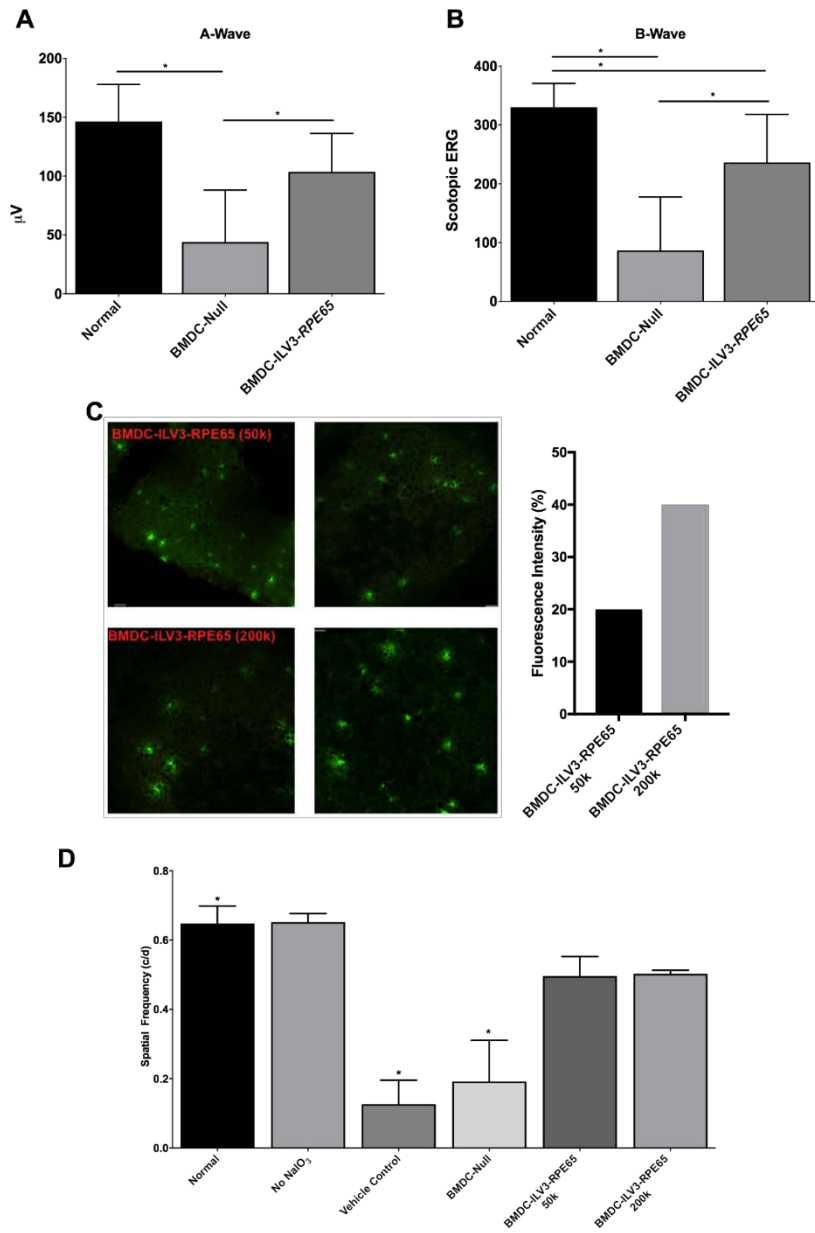


Figure 4.3. BMDC-ILV3-*RPE65* Cells Are Recruited to and Preserve Vision in Sodium Iodate Treated Mice.

Wild-type C57BL6/J mice were injected with 100 mg/kg sodium iodate in water 1 day prior to systemic delivery of GFP+ cells isolated from C57BL6/J GFP+ mice. Cells injected were either null (uninfected) GFP+ BMDCs, 50k GFP+ BMDCs infected at an MOI of 50 with ILV3-*RPE65*, or 200k GFP+ BMDCs infected at an MOI of 50 with ILV3-*RPE65*. All infections were done on RetroNectin (2 $\mu\text{g}/\text{cm}^2$) by spinoculation at 150 g for 2h at 21C. Cells were injected into mice immediately after infection. For the sodium iodate control, mice were injected with water instead of sodium iodate. For the vehicle control for the cell injections, mice were injected with PBS instead of cells. 7 days after injection, with cells, mice were evaluate by electroretinography and OKN. Eyes were then enucleated and the RPE/Choroid layers whole-mounted onto slides to determine the presence of GFP cells in the RPE layer.; (A) Electroretinography (ERG) demonstrates improvement of the A-wave in BMDC-ILV3-*RPE65*-treated mice in comparison with null BMDC treated mice. The average A-wave of normal mice was $\sim 146 \mu\text{V}$, $\sim 44 \mu\text{V}$ in null BMDC-treated mice, and $\sim 103 \mu\text{V}$ in BMDC-ILV3-*RPE65*-treated mice. (n=4) (B) ERG also demonstrates an improved B-wave in BMDC-ILV3-*RPE65*-treated mice in comparison with null BMDC treated mice. The average A-wave of normal mice was $\sim 330 \mu\text{V}$, $\sim 87 \mu\text{V}$ in null BMDC-treated mice, and $\sim 236 \mu\text{V}$ in BMDC-ILV3-*RPE65*-treated mice. (n=4) (C) GFP+ cells were observed in the flat-mounted RPE layer of mice injected with BMDC-ILV3-*RPE65*, with a fluorescence intensity of

approximately 20% in one eye from a mouse injected with 50k cells, and 40% in an eye from a mouse injected with 200k cells. Images show two different areas of the same eye. (n=1) (D) Optokinetic nystagmus analysis (OKN) revealed improved spatial frequency in sodium iodate treated mice treated with either 50k or 200k cells in comparison with BMDC-null or vehicle control treated mice. Normal and sodium iodate control (water-injected) mice had an average spatial frequency of 0.648 c/d and 0.652 c/d respectively. Vehicle control and null mice had an average spatial frequency of 0.126 c/d and 0.192 c/d respectively. Mice treated with 50k or 200k BMDC-ILV3-*RPE65* had an average spatial frequency of 0.496 c/d and 0.503 c/d respectively, with no significant difference between these two groups (n=3, *=p<0.05).

BMDCs Infected with Non-Integrating IDLV Are Recruited to and Preserve Retinal Function in Sodium Iodate-Treated Mice.

Having confirmed that BMDC-ILV3-RPE65 recover vision in sodium iodate treated mice when injected at the correct time point, we injected sodium iodate-treated mice with BMDCs infected with *ILV3-RPE65-MITF* and the two IDLV3 vectors as a preliminary study. ERG results show clear improvement in both the A-wave and B-wave of mice treated with the IDLV3 vectors. The normal A-wave was measured at $\sim 140 \mu\text{V}$, dropping to $\sim 40 \mu\text{V}$ in mice treated with null BMDCs (Figure 4.4A). In contrast, the A-wave was $\sim 100 \mu\text{V}$ and $80 \mu\text{V}$ in mice treated with BMDC-*ILV3-RPE65* or BMDC-*IDLV3-RPE65*, and $\sim 120 \mu\text{V}$ and $\sim 70 \mu\text{V}$ in mice treated with BMDC-*ILV3-RPE65-MITF* and BMDC-*IDLV3-RPE65-MITF* respectively (Figure 4.4B). Similarly, improvement in the B-wave was also observed, with normal mice having an average B-wave of $\sim 320 \mu\text{V}$, mice treated with null cells $\sim 20 \mu\text{V}$, BMDC-*ILV3-RPE65* $\sim 230 \mu\text{V}$, BMDC-*IDLV3-RPE65* $220 \mu\text{V}$, BMDC-*ILV3-RPE65-MITF* $170 \mu\text{V}$, and BMDC-*IDLV3-RPE65-MITF* $190 \mu\text{V}$. Optokinetic nystagmus analysis confirmed that the presence of GFP+ cells in the RPE layer of these mice contributed to a recovery in vision, with a spatial frequency average of 0.192 c/d in null-BMDC-treated mice increasing to 0.496 c/d, 0.415 c/d, 0.315 c/d, and 0.453 c/d in BMDC-*ILV3-RPE65*, BMDC-*ILV3-RPE65-MITF*, BMDC-*IDLV3-RPE65*, and BMDC-*IDLV3-RPE65-MITF*-treated mice respectively (Figure 4.4C).

Figure 4.4

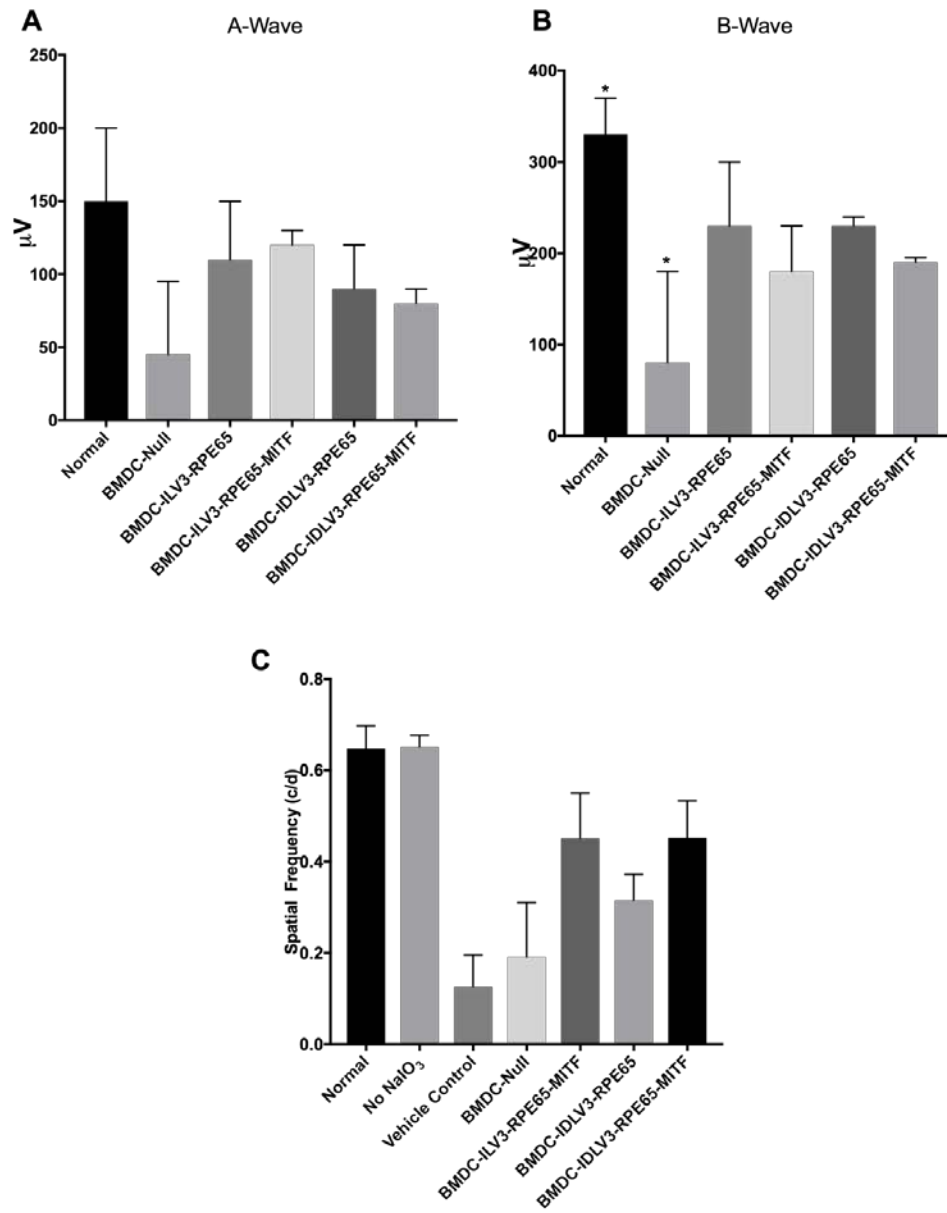


Figure 4.4. BMDCs Programmed with IDLV3 Vectors Preserve Vision in Sodium Iodate-Treated Mice.

Wild type C57BL6/J mice were treated with 100 mg/kg sodium iodate in water or water (control) 1 day prior to tail vein delivery of BMDC-null, BMDC-ILV3-*RPE65*, BMDC-ILV3-*RPE65-MITF*, BMDC-IDLV3-*RPE65*, or BMDC-IDLV3-*RPE65-MITF*. All infections were done on RetroNectin (2 $\mu\text{g}/\text{cm}^2$) by spinoculation at 150 g for 2h at 21C. Cells were injected into mice immediately after infection. (A) The A-wave was improved in BMDC-ILV3-*RPE65*, BMDC-ILV3-*RPE65-MITF*, BMDC-IDLV3-*RPE65*, or BMDC-IDLV3-*RPE65-MITF*-treated mice in comparison with BMDC-null-treated mice, with an average of 100 μV , 120 μV , 80 μV , and 70 μV respectively, compared to 40 μV in the null-treated mice. (B) The B-wave was improved in BMDC-ILV3-*RPE65*, BMDC-ILV3-*RPE65-MITF*, BMDC-IDLV3-*RPE65*, or BMDC-IDLV3-*RPE65-MITF*-treated mice in comparison with BMDC-null-treated mice, with an average of 230 μV , 220 μV , 170 μV , and 190 μV respectively, compared to 20 μV in the null-treated mice. (C) The visual acuity of BMDC-ILV3-*RPE65*, BMDC-ILV3-*RPE65-MITF*, BMDC-IDLV3-*RPE65*, or BMDC-IDLV3-*RPE65-MITF*-treated mice in comparison with BMDC-null-treated mice, with an average of 0.496 c/d, 0.415 c/d, 0.315 c/d, and 0.453 c/d respectively, compared to x in the null-treated mice. (n=2-3)

BMDCs Infected with Non-Integrating IDLV Are Recruited to and Preserve Retinal Function in SOD2-KD Mice.

The primary goal of our study was to evaluate IDLV3-based vectors in the chronic SOD2-KD model of retinal degeneration, as this model is as similar to human AMD as is possible in a mouse. After confirming that the IDLV3-based vectors are capable of generating BMDCs which are recruited to and recover vision in the sodium iodate model, we next tested these cells in the SOD2-KD model. As we are primarily interested in applying this treatment in early AMD, and as our previously published studies indicate that early treatment yields the best results, we injected all mice with 50k BMDCs 1 month after subretinal injection of the right eye (OD) with an adeno-associated virus containing a ribozyme to SOD2 (rAAV-SOD2). The untreated left eye (OS) acted as an internal normal control. OCT was performed at the 3 month time point after BMDC injection. Electroretinography and OKN were performed 3 and 6 months after treatment with BMDCs. After visual function testing, eyes were enucleated and either flat mounted to quantify integrated BMDCs at the RPE layer, or sectioned to observe RPE and retinal morphology.

In all mice injected with BMDCs infected with ILV3 or IDLV3-based vectors, GFP+ cells were found at the RPE layer of the rAAV-SOD2-injected eye (Figure 4.5A). Mice injected with BMDC-ILV3-RPE65 had the greatest number of cells in the RPE layer, with an average of 976 cells across 10% of each flat mounted eye (Figure

4.5B). Mice injected with BMDC-ILV3-RPE65-MITF had an average of 637 cells across 10% of each flat mounted RPE, BMDC-IDLV3-RPE65 645 cells, and BMDC-IDLV3-RPE65-MITF 557 cells, and null-BMDCs 20 cells (Figure 4.5B). In addition, GFP+ cells observed at the RPE layer in BMDC-ILV3-*RPE65*-treated mice were found to co-express ZO-1 (experiment performed by Dr. Xiaoping Qi)[13] a marker of tight junctions that are characteristic of RPE cells (Figure 4.5C), and rhodopsin (experiment performed by Dr. Xiaoping Qi),[13] which indicates that the cells are capable of phagocytosing photoreceptor outer segments (Figure 4.5D), further confirming that these BMDCs take on an RPE-like phenotype *in vivo*. These markers will also be stained for in BMDC-IDLV3-treated cells in future experiments.

Figure 4.5

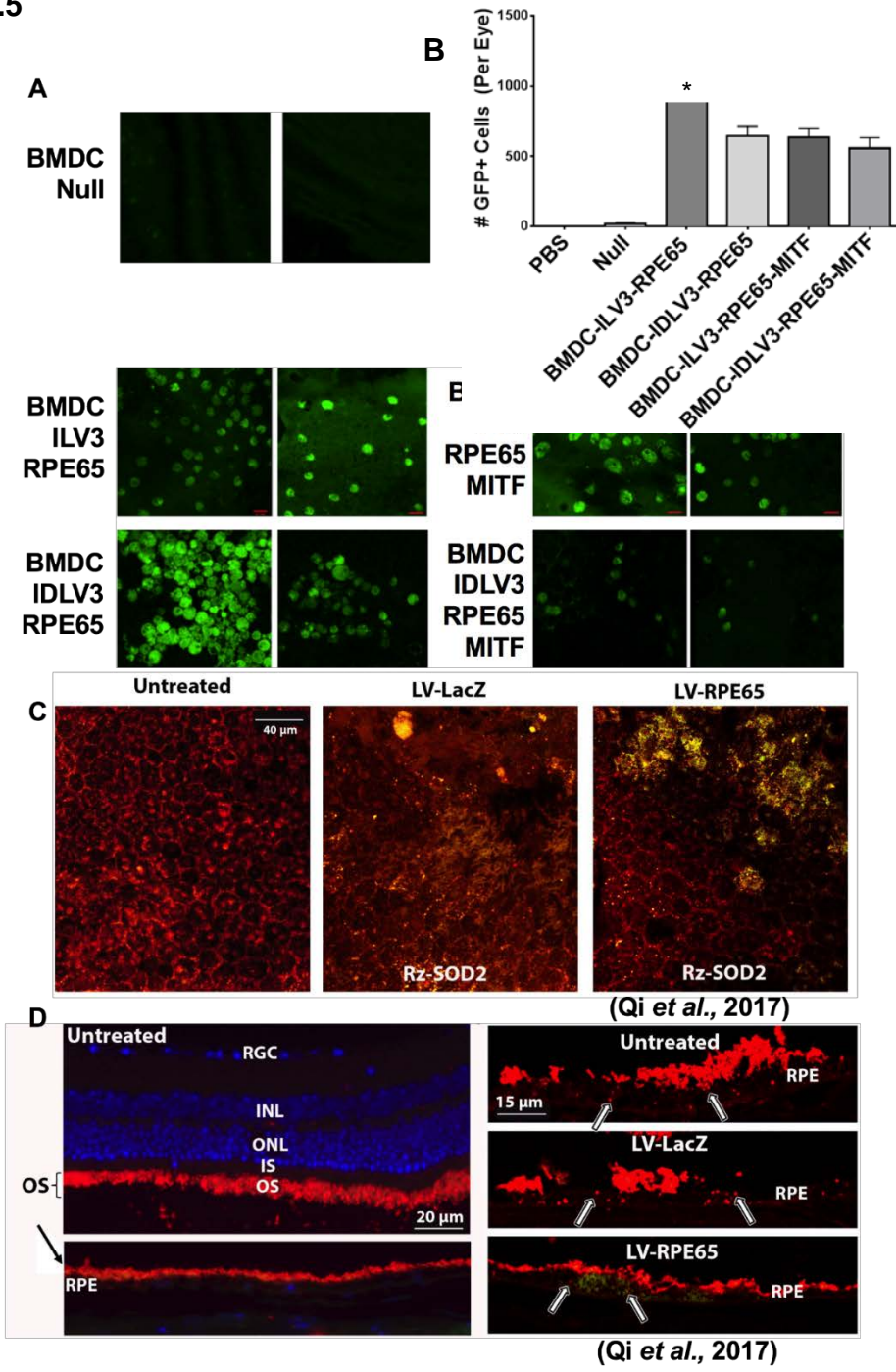


Figure 4.5. BMDCs Programmed with ILV3 or IDLV3 Vectors Are Recruited to and Integrate at the RPE Layer in SOD2-KD Mice.

Vector-Infected BMDCs are Recruited to the RPE Layer in SOD2-KD Mice, where they Integrate and Adopt an RPE-Like Phenotype. Wild-type C57BL6/J mice were injected subretinally with AAV-SOD2 or AAV-inactive 1 month prior to tail vein injection with 50k GFP+ *lin*⁻/*Sca1*⁺ BMDCs infected at an MOI of 50 with ILV3-*RPE65*, IDLV3-*RPE65*, ILV3-*RPE65-MITF*, or IDLV3-*RPE65-MITF*. All infections were carried out on 2 $\mu\text{g}/\text{cm}^2$ RetroNectin by spinoculation at 150g for 2h at 21°C. Eyes were enucleated, fixed in 4% PFA overnight, and the RPE/Choroid layer was flat mounted on slides 3 months after injection with cells. Eyes were also fixed and paraffin embedded followed by cross sectioning and staining for the presence of rhodopsin. Recruitment of injected cells to the RPE layer was visualized as GFP+ cells at the RPE/Choroid layer using confocal microscopy and quantified as the number of cells present in ~10% of the total flat mount. To observe expression of tight junctions, flat mounts were stained with an antibody to ZO-1. Experiments for figure 6 C and D were performed by Dr. Xiaoping Qi. (A) GFP cells were observed in the RPE layers of mice treated with BMDC-ILV3-*RPE65*, BMDC-IDLV3-*RPE65*, BMDC-ILV3-*RPE65-MITF*, or BMDC-IDLV3-*RPE65-MITF*. Each panel shows areas of the RPE/Choroid from the eyes of two mice per group (B) Quantification of cell number was carried out using a confocal microscope. Approximately 10% of the surface of each eye was quantified by counting the number of cells present in a visual field through the microscope using the 10x objective. Mice injected with

BMDC-ILV3-*RPE65*, BMDC-IDLV3-*RPE65*, BMDC-ILV3-*RPE65-MITF*, or BMDC-IDLV3-*RPE65-MITF* had an average of 976, 637, 645, and 557 GFP+ cells in the RPE layer respectively. The average number of GFP+ cells in the RPE layer of BMDC-null-treated mice was 20. (n=3) (C) Integrated GFP+ BMDCs infected with ILV3-*RPE65* co-expressed ZO-1, a marker of tight junctions characteristic to RPE cells (data: Dr. Xiaoping Qi). (D) Integrated GFP+ BMDCs infected with ILV3-*RPE65* co-expressed Rhodopsin, present in photoreceptor outer segments, indicating that the cells are functioning as RPE cells in phagocytosing photoreceptor outer segments (data: Dr. Xiaoping Qi).

(* $p < 0.05$; n=3).

Histology demonstrated significant regeneration of the RPE layer in comparison with mice treated with null-BMDCs in mice treated with BMDCs infected with all 4 vectors (Figure 4.6, A-G). While pathology in some of the eyes and in parts of the RPE were present in mice treated with vector-infected BMDCs, RPE morphology was consistently improved, with a clear monolayer of pigmented cells present in comparison with the vacuolated degenerating RPE cell layer observed in mice treated with null BMDCs (Figure 4.6 A-G). In these mice, significant pathology was observed along with areas of normal retina, though the RPE was degenerated throughout, which is consistent with the progressive nature of the SOD2-KD model (Figure 4.6C).

Electroretinography at the 3-month time point revealed significant preservation of visual function in mice treated with ILV3 or IDLV3-based vectors in comparison with mice treated with null BMDCs (control), with near-normal ERG traces in the vector-infected BMDC-treated mice compared with an almost flat ERG trace in null-BMDC-treated mice (Figure 4.7A). The A-wave in the normal eyes averaged at 132 μ V, 46 μ V in null-BMDC-treated mice, and 116 μ V, 140 μ V, 93 μ V, 86 μ V in BMDC-ILV3-*RPE65*, BMDC-LV3-*RPE65-MITF*, BMDC-IDLV3-*RPE65*, and BMDC-IDLV3-*RPE65-MITF*-treated SOD2-KD eyes respectively (Figure 4.7B). The B-wave demonstrates a similar pattern, with an average of 286 μ V in normal mice, 80 μ V in null-BMDC-treated mice, and 240 μ V, 315 μ V, 266 μ V, 243 μ V in BMDC-ILV3-*RPE65*, BMDC-ILV3-*RPE65-MITF*, BMDC-IDLV3-*RPE65*, and BMDC-IDLV3-*RPE65-MITF*-treated SOD2-KD eyes respectively (Figure 4.7C).

The inactive ribozyme (positive control for the SOD2 ribozyme) did reduce both the A-wave and the B-wave (73 μ V and 173 μ V respectively), indicating that some of the injury to the RPE observed may be due to the injection procedure itself in addition to the SOD2-KD.

As ERG does not necessarily correspond with visual acuity in mice, OKN was carried out to back up the ERG results. The spatial frequency of the normal eye consistently averaged at around 0.6 c/d. rAAV-inactive-injected eyes had a reduction in spatial frequency to \sim 0.5, thought to result from lack of recovery at of the injection site, due to the invasive nature of subretinal delivery (Figure 4.7D). In SOD2-KD eyes of mice injected with null BMDCs, the spatial frequency averaged at 0.06 cd, considerably lower than that observed in SOD2-KD eyes which received vector-infected BMDCs (Figure 4.7D). In BMDC-ILV3-RPE65-treated mice, the average spatial frequency was 0.524 c/d (Figure 4.7D). In BMDC-ILV3-RPE65-MITF-treated mice, the average spatial frequency was 0.498 c/d (Figure 4.7D), in BMDC-IDLV3-RPE65-treated mice 0.538 c/d, and finally in BMDC-IDLV3-RPE65-MITF-treated mice, 0.489 c/d (Figure 4.7D). While all spatial frequencies remained significantly lower than normal ($p < 0.05$), they were also significantly higher than that observed in null-BMDC-treated mice, demonstrating that this improvement is a result of the infection of the BMDCs with the vectors.

Figure 4.6

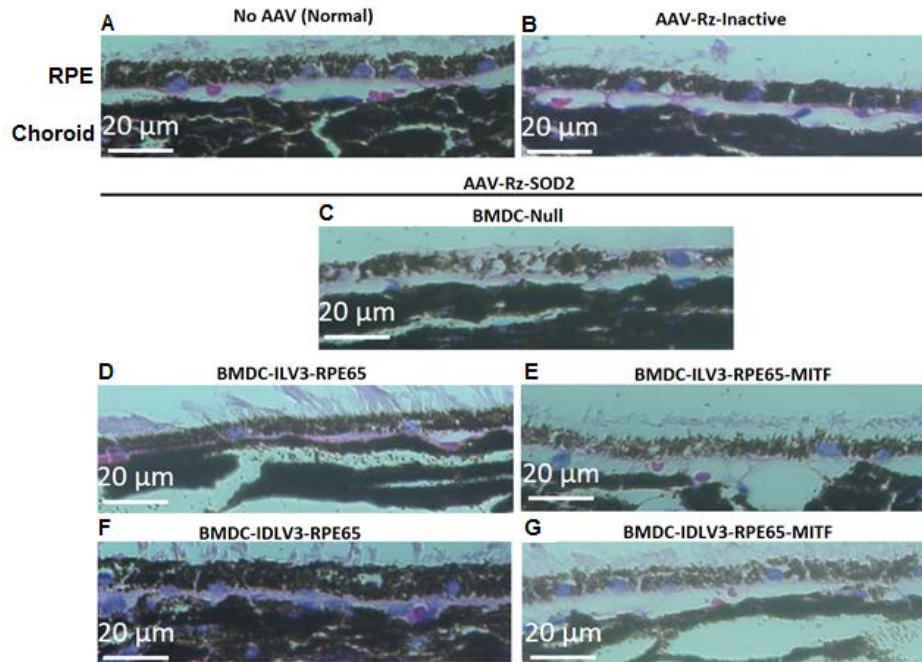


Figure 4.6. BMDCs Programmed with ILV3 or IDLV3 Vectors Preserve Retinal Integrity in SOD2-KD Mice.

Wild-type C57BL6/J mice were injected subretinally with AAV-SOD2 or AAV-inactive 1 month prior to tail vein injection with 50k GFP+ lin-/Sca1+ BMDCs infected at an MOI of 50 with ILV3-*RPE65*, IDLV3-*RPE65*, ILV3-*RPE65-MITF*, or IDLV3-*RPE65-MITF*. All infections were carried out on 2 $\mu\text{g}/\text{cm}^2$ RetroNectin by spinoculation at 150g for 2h at 21°C. Eyes were enucleated, fixed in 4% PFA overnight, and sectioned 3 months after injection with cells. Haematoxylin and Eosin-Stained Cross Sections of Retinae Show Improved Morphology in SOD2-KD Mice Treated with Vector-Infected BMDCS. Eyes were enucleated and immediately transferred to 4% paraformaldehyde for fixing for approximately 72 hrs, paraffin-embedded, and sectioned by the IU Histology Core. Sections were imaged on a Zeiss upright microscope with a color camera and images captured using Zeiss Zen software. All main images were taken with the 20x objective; insets were taken with the 40x objective. (A) RPE layer of a normal retina (*oculus sinister* [OS]; left eye, untreated), with normal pigmentation and morphology. (B) RPE of a retina of a mouse injected with the control AAV containing an inactive ribozyme (*oculus dexter* [OD]; right eye), which has normal pigmentation and morphology. (C) RPE of retina from a mouse injected with the AAV containing a ribozyme to SOD2 followed by systemic injection of null BMDCs, which appears highly depigmented, vacuolated, and degenerated. (OD) (D-G) RPE from the retina of mice injected with AAV-Rz-SOD2 followed by systemic treatment with

BMDCs infected with (D) *ILV3-RPE65*, (E) *IDLV3-RPE65*, (F) *ILV3-RPE65-MITF*, or (G) *IDLV3-RPE65-MITF*. RPE cells demonstrating significant pigmentation in comparison with the null control are shown in K-N. RPE recovery is most pronounced in mice treated with *BMDC-ILV3-RPE65* or *BMDC-IDLV3-RPE65*, with highly pigmented cells in particular observed in the *BMDC-IDLV3-RPE65*-treated eye.

(* $p < 0.05$; $n = 3$)

Figure 4.7

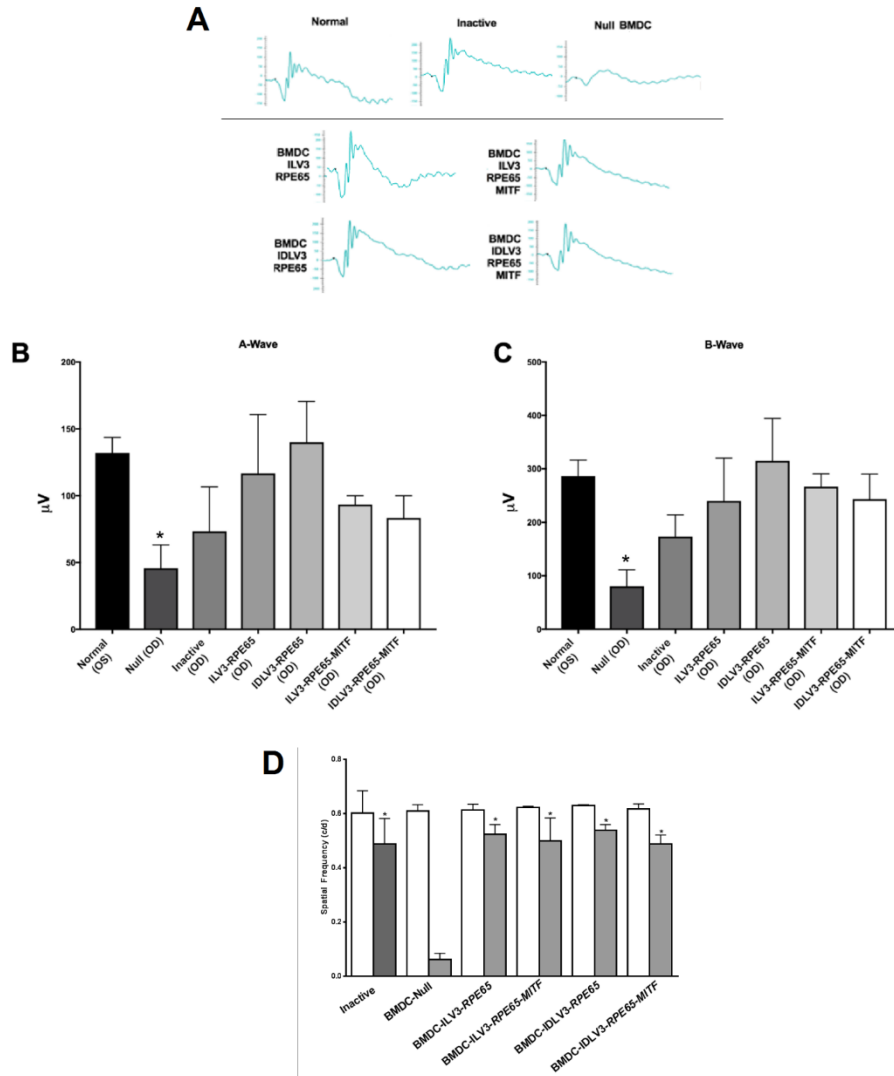


Figure 4.7. BMDCs Programmed with ILV3 or IDLV3 Vectors Preserve Visual Function in SOD2-KD Mice.

Wild-type C57BL6/J mice were injected subretinally with AAV-SOD2 or AAV-inactive 1 month prior to tail vein injection with 50k GFP+ lin-/Sca1+ BMDCs infected at an MOI of 50 with ILV3-*RPE65*, IDLV3-*RPE65*, ILV3-*RPE65-MITF*, or IDLV3-*RPE65-MITF*. All infections were carried out on 2 $\mu\text{g}/\text{cm}^2$ RetroNectin by spinoculation at 150g for 2h at 21°C. Electroretinography and Optical Nystagmus testing was carried out 3 months after injection of the cells. Mice demonstrated improved visual function in mice treated with AAV-Rz-SOD2 following injection with vector-infected BMDCs but not in mice treated with null BMDCs. (A) ERG trace patterns in mice treated with vector-infected BMDCs show a normal pattern with reduced amplitude. In null mice, the ERG trace was flattened. Mice injected with the inactive ribozyme also had reduced amplitude. (B) The A-wave amplitude in normal mice was 132 μV . In SOD2-KD mice treated with BMDC-null, it was reduced to 46 μV . In mice treated with BMDC-ILV3-*RPE65*, BMDC-ILV3-*RPE65-MITF*, BMDC-IDLV3-*RPE65*, or BMDC-IDLV3-*RPE65-MITF*, the A-wave was 116 μV , 140 μV , 93 μV , and 86 μV respectively. (B) The B-wave amplitude in normal mice was 286 μV . In SOD2-KD mice treated with BMDC-null, it was reduced to 80 μV . In mice treated with BMDC-ILV3-*RPE65*, BMDC-ILV3-*RPE65-MITF*, BMDC-IDLV3-*RPE65*, or BMDC-IDLV3-*RPE65-MITF*, the A-wave was 240 μV , 315 μV , 266 μV , and 243 μV respectively. (C) The spatial frequency in BMDC-null treated mice was reduced to 0.06 c/d compared with an overall average of 0.6 in the normal eye across all groups. In mice treated with BMDC-ILV3-*RPE65*, BMDC-ILV3-*RPE65-MITF*, BMDC-IDLV3-*RPE65*, or BMDC-IDLV3-

RPE65-MITF, spatial frequencies averaged at 0.524 c/d, 0.498 c/d, 0.538 c/d, and 0.489 c/d respectively. (* $p > 0.05$, $n = 3$)

At 6-months post-injection of BMDCs, visual recovery was largely retained, though significant variation was observed between mice in each group at this time point in the ERG measurements, including in the normal mice (Figure 4.8A). In normal eyes, the A-wave was $\sim 124 \mu\text{V}$ and the B-wave was $\sim 289 \mu\text{V}$, and in null control SOD2-KD mice, the A-wave was $\sim 27.5 \mu\text{V}$ and the B-wave was $\sim 70 \mu\text{V}$. In BMDC-ILV3-RPE65-treated mice, the A-wave was $\sim 150 \mu\text{V}$ and the B-wave was $\sim 353 \mu\text{V}$. In BMDC-ILV3-RPE65-MITF-treated mice, the A-wave was $\sim 90 \mu\text{V}$ and the B-wave was $\sim 205 \mu\text{V}$. In BMDC-IDLV3-RPE65-treated mice, the A-wave was $\sim 100 \mu\text{V}$ and the B-wave was $\sim 220 \mu\text{V}$. In BMDC-IDLV3-RPE65-MITF-treated mice, the A-wave was $\sim 52.5 \mu\text{V}$ and the B-wave was $\sim 137.5 \mu\text{V}$. (Figure 4.8A).

OKN results were less variable and in the normal eyes, the average spatial frequency was $\sim 0.650 \text{ c/d}$, in null-BMDC-treated SOD2-KD eyes it was $\sim 0.15 \text{ c/d}$, in ILV3 and IDLV3-BMDC treated mice, the average was around 0.600 c/d (Figure 4.8B).

Figure 4.8.

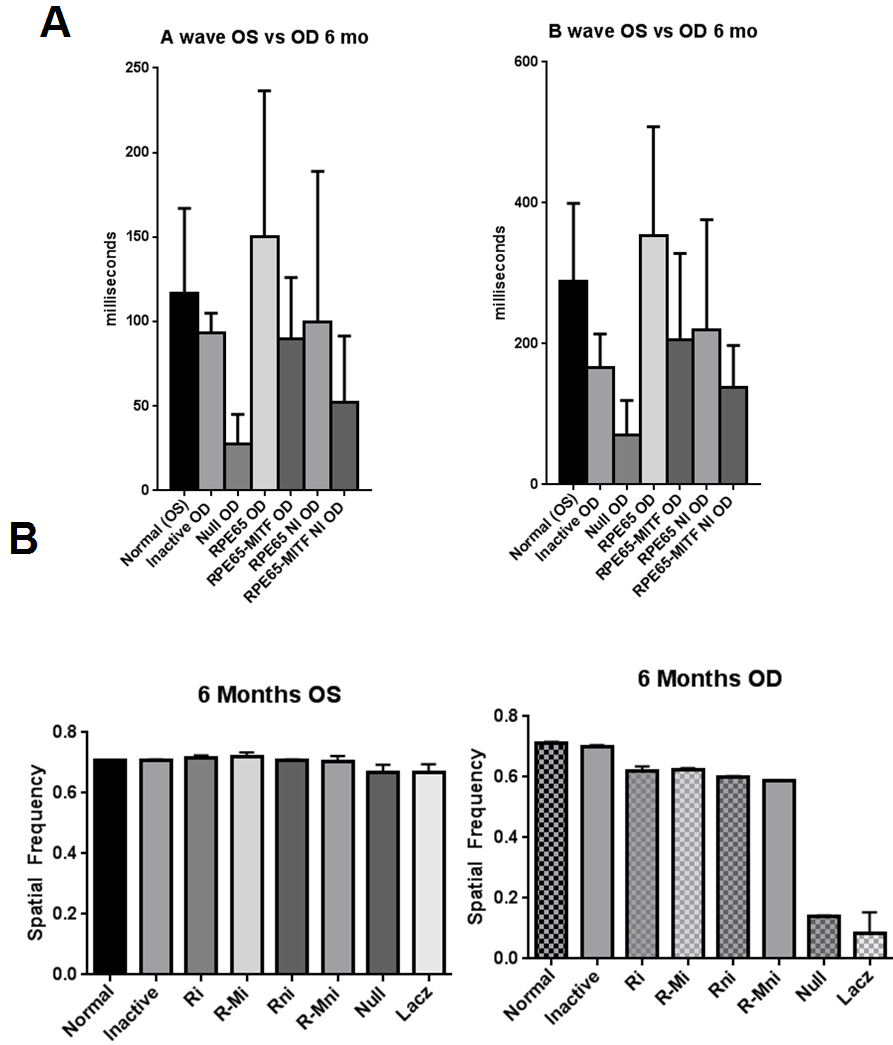


Figure 4.8. Improvement in Visual Function in SOD2-KD Mice Treated with ILV3 or IDLV3 Vectors Persists for At Least Six Months. A group of mice treated with SOD2-KD followed by vector-infected BMDC tail vein injection (50k cells) were retained for 6 months for a later ERG and OKN time point. (A, B) In normal eyes, the A-wave was $\sim 124 \mu\text{V}$ and the B-wave was $\sim 289 \mu\text{V}$, and in null control SOD2-KD mice, the A-wave was $\sim 27.5 \mu\text{V}$ and the B-wave was $\sim 70 \mu\text{V}$. In BMDC-ILV3-RPE65-treated mice, the A-wave was $\sim 150 \mu\text{V}$ and the B-wave was $\sim 353 \mu\text{V}$. In BMDC-ILV3-RPE65-MITF-treated mice, the A-wave was $\sim 90 \mu\text{V}$ and the B-wave was $\sim 205 \mu\text{V}$. In BMDC-IDLV3-RPE65-treated mice, the A-wave was $\sim 100 \mu\text{V}$ and the B-wave was $\sim 220 \mu\text{V}$. In BMDC-IDLV3-RPE65-MITF-treated mice, the A-wave was $\sim 52.5 \mu\text{V}$ and the B-wave was $\sim 137.5 \mu\text{V}$. (C) In normal mice, the spatial frequency was $\sim 0.7 \text{ c/d}$ in all normal eyes. In BMDC-ILV3-RPE65, BMDC-ILV3-RPE65-MITF, BMDC-IDLV3-RPE65, and BMDC-IDLV3-RPE65-MITF-treated mice, the spatial frequency was 0.621 c/d , 0.622 c/d , 0.602 c/d , and 0.586 c/d respectively. In BMDC-null treated mice, the spatial frequency was 0.140 c/d . (* $p > 0.05$, $n = 3$)

Discussion

Insertion of a lentiviral vector in the *HMGA2* gene in a lentiviral vector-based therapy for beta-thalassemia [247] highlights the importance for considering the safety of lentiviral vectors when using them to manipulate therapeutic cells. Due to the risk of insertional mutagenesis, it is advantageous to use a vector which does not integrate where possible. [311] Here, we have focused on an approach which exploits the transient nature of IDLV expression, as programming BMDCs in this context does not require permanent expression of the transgene. Other applications in which this is advantageous include the use of CRISPR/Cas9, where IDLVs can be used to deliver gene-editing sequences (Chang *et al.*, personal correspondence) and also as a tool for detecting off-target cleavage in both CRISPR/Cas9 and TALENs-based approaches. [312] IDLVs are also advantageous for *in vivo* gene therapy in non-dividing cells, where the transgene can be stably and persistently expressed. [282]

We have shown that IDLV3-*RPE65* is sufficient to program BMDCs to RPE-like cells, which are then capable of migrating to the retina, integrating into the RPE layer, and preserving vision in mice with retinal degeneration. The SOD2-KD mice were injected with BMDC-derived RPE-like cells programmed using IDLV3s infected with the modified protocol. Despite this difference in the programming of the BMDCs with the IDLV3s between these two models, visual preservation was not markedly lower in mice treated with cells that had been infected at a

significantly lower efficiency. This suggests that either (a) additional mechanisms, on top of infection itself, promote the programming of the cells, for example cell-cell communication *in vitro* during or after infection, or (b) visual recovery is attainable with a smaller number of cells than injected. It is more likely that our finding is due to the latter, as the cells are not kept *in vitro* for more than 30 minutes prior to injection following infection, on top of the fact that in the initial study by Sengupta *et al.*, [216] mice only received 5K cells, whereas in our later [13] and current studies, mice were given 50K cells. This indicates that as little as 10% of the injected cells may be necessary for visual recovery – which is, coincidentally, the approximate number of cells expressing the viral construct when IDLV3-based vectors are used to infect without the modifications made to the infection protocol outlined in Chapter 3.

There is, however, a potential for infected cells to influence the programming of neighboring un-infected cells. Conditioned medium has been shown in several studies to enhance cellular differentiation or regeneration. [313-318] Experiments to determine whether or not conditioned medium from ILV3 or IDLV3-based vector-infected BMDCs is capable of inducing differentiation of naïve BMDCs to an RPE-like cell would provide further insights into this as a potential mechanism in the programming of our cells. Indeed, should exposure to conditioned media be sufficient to promote BMDC programming, future applications could avoid injection of infected cells altogether, using the vectors only as a means to generate the medium required to program the cells for therapeutic application. [316]

Our finding that visual preservation with IDLV3-programmed BMDCs is not significantly lower in mice treated with the IDLV3-programmed cells in comparison with ILV3-programmed cells strongly supports the use of IDLV3-*RPE65* for reprogramming BMDCs for application in human cells. Although adding *MITF-M* to the infecting vector in the current study did not provide any measurable advantage over using vectors containing *RPE65* alone, this does not necessarily suggest that inclusion of *MITF* overall cannot improve BMDC programming, as we have only tested one isoform of *MITF*. Instead of using MITF-M, expressed in differentiated RPE, isoforms H and D, which are present in developing retina and/or RPE cells, may function to enhance BMDC programming at a greater level than MITF-M. For future studies, the inclusion of MITF-D in the infecting vector as opposed to MITF-M may yield better results – preferential over MITF-H, as MITF-D is only expressed in the RPE, whereas MITF-H is present in both the RPE and neural retina, and A and J are mainly localized in the neural retina. [305-308] It would be interesting to determine whether or not expression of the MITF isoform involved in development, MITF-D, is capable of activating expression of the differentiated RPE isoform, MITF-M *in vitro*, as we did not observe significant or consistent expression of *Mitf* in murine or human BMDCs infected with vectors expressing human *RPE65* or *RPE65-MITF* (data not shown).

The relatively lower number of cells found in the RPE layer in mice injected with BMDCs programmed with IDLV3-based vectors in comparison with mice injected with the ILV3-*RPE65* programmed BMDCs raises an interesting question about

the mechanism of action of the BMDC-derived RPE-like cells *in vivo*. If the cells themselves were solely responsible for preserving vision, we would have expected to have observed a proportionately lower recovery of vision in mice with fewer cells at the RPE layer. Instead, however, we observed very similar ERG and OKN data in mice treated with cells programmed with either ILV3-*RPE65* or IDLV3-based vectors. As a result, it is likely that the BMDC-derived RPE-like cells not only function to support the retina/choroid independently of the existing RPE, but also act in a neuroprotective manner, preserving the existing RPE in addition to regenerating it. Paracrine activity by stem cells has been widely reported [319]. In the eye, it has been shown in a study on glaucoma, in which mesenchymal stem cells were injected intravitreally, that the presence of these cells is neuroprotective, enhancing the protection of the retinal ganglion cell layer in rats. [320] Another study used a lentiviral vector approach to generate neuroprotective neural stem cells for intravitreal delivery in retinal degeneration disorders, showing rescue of degenerating photoreceptor cells in murine models. [321]

The consistency between this study and our previously published studies, [13, 216] along with our findings that human BMDCs infected with the *RPE65* viruses also express the endogenous markers believed to be necessary for cellular programming, indicates that this approach is ready to be applied with human BMDCs *in vivo*. Sustained visual improvement at the 6-month time point is encouraging, as our previously published models only measured vision up to the 3-month time point. Although multiple injections with autologous BMDC-derived

RPE-like cells are technically feasible and safe, should visual recovery be temporary, the ability to address the problem with a single delivery of cells is advantageous for a number of reasons. Firstly, obtaining large numbers of cells for multiple treatments increases the invasiveness of the therapy, which is ideally avoided. Secondly, while autologous cells are generally thought to be non-immunogenic, any *ex vivo* modification of cells has the potential to increase the immunogenicity in terms of 'priming' the immune system to respond in the event of a second exposure. This type of reaction would be rare, but potentially fatal in the case of an allergic response to repeated injections of the cells. A 'one shot' therapy is therefore desirable, and sustained vision to the 6-month time point in mice indicates that long-term recovery from one treatment may be viable.

While beyond the scope of the focus of this study, since the completion of testing murine BMDC-derived RPE-like cells in murine models, our laboratory has demonstrated improvement of vision, as measured by ERG, in a preliminary study with NOD-SCID-gamma-null SOD2-KD mice injected with human CD34+ cells infected with ILV3-*RPE65* (Godoy *et al.*, personal communication), further backing up our claim that the techniques outlined in the current study are appropriate for further development for use in human clinical trials for dry AMD.

As a final note on the safety of this application in humans, is generally accepted that stem cell-based therapies that are delivered to the eye via intravitreal or subretinal injection should be applied in one eye at a time, to ensure that, should

patients have an adverse reaction to the treatment resulting in worsening of vision or blindness, one eye remains unaffected. A recent treatment given by a US “stem cell” company involving intravitreal injection of adipose-derived stem cells resulted in blindness in three women who received simultaneous bilateral injections.[185] Systemic delivery of cells does not allow for the treatment of one eye at a time. However, the risk associated with a systemically-delivered therapy is significantly smaller than the risk associated with injections into the eye itself. Firstly, any components of cell culture medium – which is likely to have contributed to the severe damage observed in the aforementioned patients[185] – will not be directly delivered to the eye and therefore are unlikely to cause damage to the eye. Secondly, our model relies on injury-based recruitment of cells from the bloodstream, meaning that large numbers of cells that are not required are not likely to be recruited to the retina, unlike in intravitreal and subretinal injection where the cells are directly delivered to the eye. We have also consistently demonstrated throughout our studies that the normal eyes of mice which have received systemic injections with our cells retain normal vision and normal retinal morphology, and that the injected cells are recruited primarily to the injured eye in the same mice, suggesting that this recruitment is largely tissue-specific and that the cells are very unlikely to be recruited to the eye in numbers large enough to cause pathology in areas in which significant damage is not present. We therefore believe that systemic delivery of this cell type is not a safety concern, and does not constitute ‘bilateral treatment’ in the same way as giving injections of cell preparations directly into the eye.

**CHAPTER V: PHARMACOLOGICAL TREATMENT OF MURINE AND HUMAN
BONE MARROW-DERIVED CELLS INDUCES DIFFERENTIATION TO RPE-
LIKE CELLS *IN VITRO* AND PROVIDES INSIGHTS INTO THE MECHANISM
OF PROGRAMMING.**

Introduction

We have previously demonstrated using Ingenuity Pathway Analyses that adenylate cyclases 1, 3, and 5 are upregulated in murine BMDCs following expression of the human *RPE65* gene from the 1st generation ILV-*RPE65*. [216] In this study, it was also found that exposure of murine BMDCs to adenylate cyclase activator Forskolin, and cAMP degeneration inhibitor Rolipram, resulted in expression of the RPE-associated protein CRALBP, [216] indicating a potential critical role for adenylate cyclase activation in the differentiation of these cells to an RPE-like phenotype.

In the current study, we have further analyzed the role of adenylate cyclase in murine and human BMDC differentiation to an RPE-like phenotype. As adenylate cyclase activation appeared to be directly involved in the differentiation of BMDCs to RPE-like cells, we postulated that inhibiting adenylate cyclase expression would prevent the expression of RPE-associated markers in both murine and human BMDCs treated with either Forskolin/Rolipram or the *RPE65*-expressing LV vector. To test this hypothesis, we compared expression of *Rpe65/RPE65*,

Cralbp/CRALBP, and *Mitf/MITF* in murine and human BMDCs exposed to either Forskolin/Rolipram or the 3rd generation ILV-*RPE65*, with or without inhibitors of adenylate cyclase. The inhibitors used included BPIPP, a non-competitive inhibitor of both adenylate cyclase and guanylate cyclase which inhibits Forskolin-induced adenylate cyclase activation,[322] NKY 80 which primarily inhibits adenylate cyclase 5 but also inhibits adenylate cyclases 2 and 3,[323, 324] and KH 7, an inhibitor of the soluble adenylate cyclase 10 which was intended as a control inhibitor due to its inert activity against the transmembrane adenylate cyclases observed as upregulated in the previously published study. [216]

We observed that the presence of all the inhibitors tested reduced the expression of RPE-associated genes in Forskolin/Rolipram-treated BMDCs of both mouse and human origin, with BPIPP and NKY 80 resulting in the most efficient inhibition of these genes. KH 7 resulted in some downregulation of expression, suggesting that soluble adenylate cyclase may also be involved in BMDC to RPE-like cell differentiation. We also observed almost 100% inhibition of RPE-associated gene expression in mouse and human BMDCs treated with the inhibitors following ILV3-*RPE65* infection. Collectively, these data confirm that activation of adenylate cyclase plays a critical role in the programming of BMDCs to RPE-like cells.

Finally, we attempted to evaluate the regenerative potential of Forskolin/Rolipram-derived RPE-like cells from murine BMDCs in both the sodium iodate and SOD2-KD models of retinal degeneration. Unfortunately, little success was observed with

no cells found in the retina or RPE of mice treated with these cells. We hypothesize that modifications to the timing of our cell treatment and injection protocol for the delivery of these cells will be critical to obtain sufficient cell migration and in the RPE.

Results

Exposure of Murine and Human BMDCs to Adenylate Cyclase Activators Initiates Expression of Endogenous RPE-Associated Genes

Exposure of murine BMDCs treated once with 10 $\mu\text{mol/l}$ Forskolin and maintained in culture for 3 days resulted in a ~5-fold increase ($p < 0.05$) in expression of the *Rpe65* gene and a ~3.5-fold ($p < 0.05$) increase in expression of *Cralbp* in comparison with the control untreated cells (Figure 5.1A). No significant difference in expression of either *Rpe65* or *Cralbp* was observed in cells treated twice with 10 $\mu\text{mol/l}$ Forskolin and maintained in culture for a total of 6 days. Fold increase in expression of *Rpe65* and *Cralbp* in these cells was also ~5-fold and ~3.5-fold higher respectively.

In contrast with the result observed with Forskolin, treating murine BMDCs with 1 $\mu\text{mol/l}$ Rolipram twice did increase expression of both *Rpe65* and *Cralbp* in comparison with BMDCs treated only once. Murine BMDCs treated twice with 1 $\mu\text{mol/l}$ Rolipram and cultured for a total of 6 days expressed *Rpe65* and *Cralbp*

~4.8 and ~3.8-fold higher than the untreated control respectively ($p < 0.05$), whereas BMDCs treated once with $1\mu\text{mol/l}$ Rolipram and cultured for 3 days expressed ~3.8-fold and ~2.5-fold more *Rpe65* and *Cralbp* in comparison with the negative control (Figure 5.1B). However, the overall fold change in expression of both genes in BMDCs treated with Rolipram, whether the cells received one treatment or two, was lower than overall fold change in expression of both genes when the cells were exposed to one or two treatments of Forskolin.

When Forskolin ($10\mu\text{mol/l}$) and Rolipram ($1\mu\text{mol/l}$) were combined and added to murine BMDCs together, again either as a single treatment for 3 days or as two treatments for a total of 6 days, expression of both *Rpe65* and *Cralbp* increased ~5-fold and ~3.8-fold over the untreated control respectively with no significant difference between expression of either gene in the cells treated once compared with the cells treated twice (Figure 5.1C).

Figure 5.1

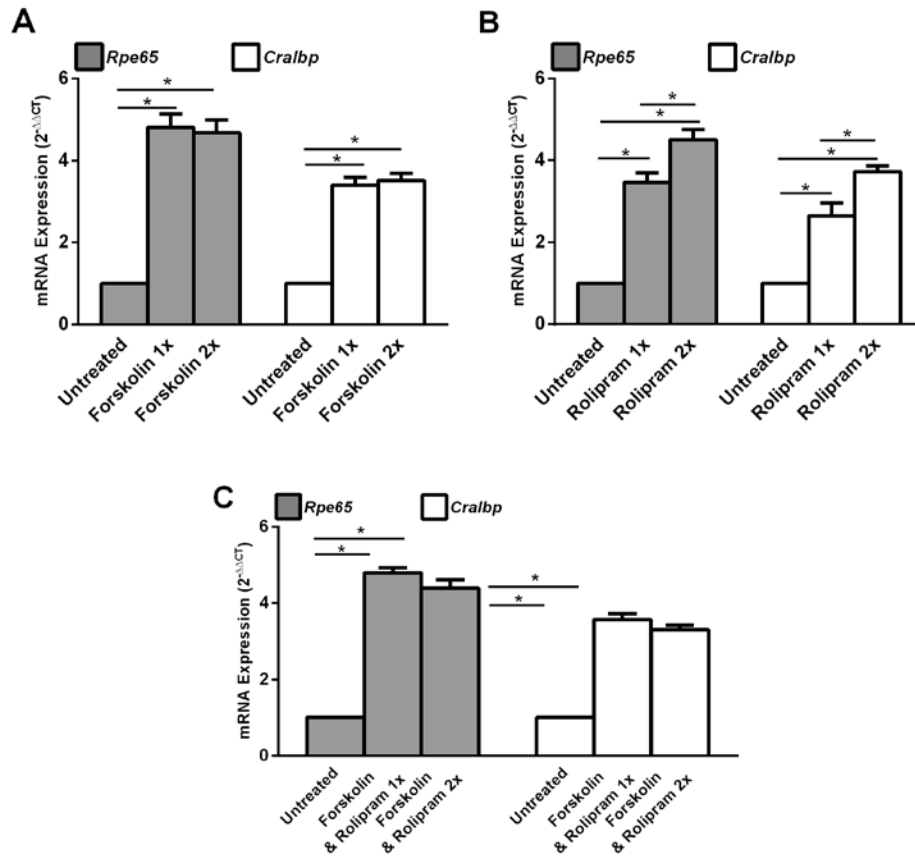


Figure 5.1. Forskolin and Rolipram Induce Expression of *Rpe65* and *Cralbp* mRNA in Murine BMDCs. Murine (lin-/Sca1+) BMDCs were exposed to 10 μ mol/l Forskolin, 1 μ mol/l Rolipram, or a combination of 10 μ mol/l Forskolin and 1 μ mol/l Rolipram. Cells were either treated once, with drug-containing media left on the cells for 1 day prior to replacement with complete DMEM, or twice, with media replaced with a second treatment after 1 day and replaced with complete DMEM on the 3rd day. All cells were cultured for a total of 3 days. (A) Cells treated with Forskolin once expressed *Rpe65* mRNA ~5-fold over control and *Cralbp* mRNA ~3-fold over control ($p < 0.05$) with no increase or decrease in expression when treated twice. (B) Cells treated with Rolipram once expressed *Rpe65* mRNA ~3.5-fold over control and *Cralbp* mRNA ~2.5-fold over control ($p < 0.05$). Cells treated twice expressed *Rpe65* mRNA ~4.5-fold over control and *Cralbp* mRNA ~4-fold over control ($p < 0.05$). (C) Cells treated with Forskolin and Rolipram once expressed *Rpe65* mRNA ~5-fold over control and *Cralbp* mRNA ~3.5-fold over control ($p < 0.05$) with no significant increase or decrease in expression when treated twice.

Experiments carried out in murine BMDCs were repeated with human BMDCs. Significant variation in expression of *RPE65* was observed in cells treated twice with 10 $\mu\text{mol/l}$ Forskolin, and in expression of *CRALBP* in cells treated once with 10 $\mu\text{mol/l}$ Forskolin (Figure 5.2A), though expression of *RPE65* and *CRALBP* was significantly higher in all cells treated with Forskolin despite individual variation within the samples. *RPE65* was upregulated ~ 4 -fold in human BMDCs treated once with 10 $\mu\text{mol/l}$ Forskolin and ~ 6 -fold in cells treated twice ($p < 0.05$); *CRALBP* expression was increased ~ 4.5 -fold (± 3) in cells treated once, and ~ 3 -fold in cells treated twice with 10 $\mu\text{mol/l}$ Forskolin (Figure 5.2A). Rolipram significantly increased expression of both genes in human BMDCs ~ 6.8 -fold and 3.8-fold in cells treated once, and ~ 7.4 and 3.9-fold in cells treated twice (Figure 5.2B). No significant advantage was observed in treating the cells with Rolipram twice (Figure 5.2B).

In contrast with data observed in murine BMDCs, human BMDCs express significantly more *RPE65* when treated with Rolipram than when treated with Forskolin (Figure 5.2A and B), though *CRALBP* expression remains similar. Combining Forskolin and Rolipram treatments, either treating once or twice, results in *RPE65* and *CRALBP* expression with significantly less variation than when Forskolin is used alone (Figure 5.2A and C), with an average fold increase in *RPE65* of ~ 5.3 -fold and ~ 5.9 -fold in Forskolin/Rolipram treated cells treated once or twice respectively, and a correlating increase in *CRALBP* of ~ 3 -fold and ~ 4 -fold (Figure 5.2C).

Our findings that expression of the murine *Rpe65* gene is upregulated following exposure of murine BMDCs to Forskolin and/or Rolipram confirms the role of the endogenous *Rpe65* gene in the programming of murine BMDCs with the lentiviral vector approach. The consistency in expression of both *Rpe65* and *Cralbp* in murine BMDCs whether treated with the adenylate cyclase activator Forskolin or the cAMP degradation inhibitor Rolipram, either independently or in combination, is consistent with our previously published data[216] and our belief that adenylate cyclase activation plays a critical role in BMDC differentiation to RPE-like cells. Our observations that Forskolin/Rolipram treatment also result in expression of the *RPE65* and *CRALBP* genes in human BMDCs further solidify this hypothesis, and indicate that the programming process of human BMDCs may be very closely related to the programming process of murine BMDCs.

Figure 5.2

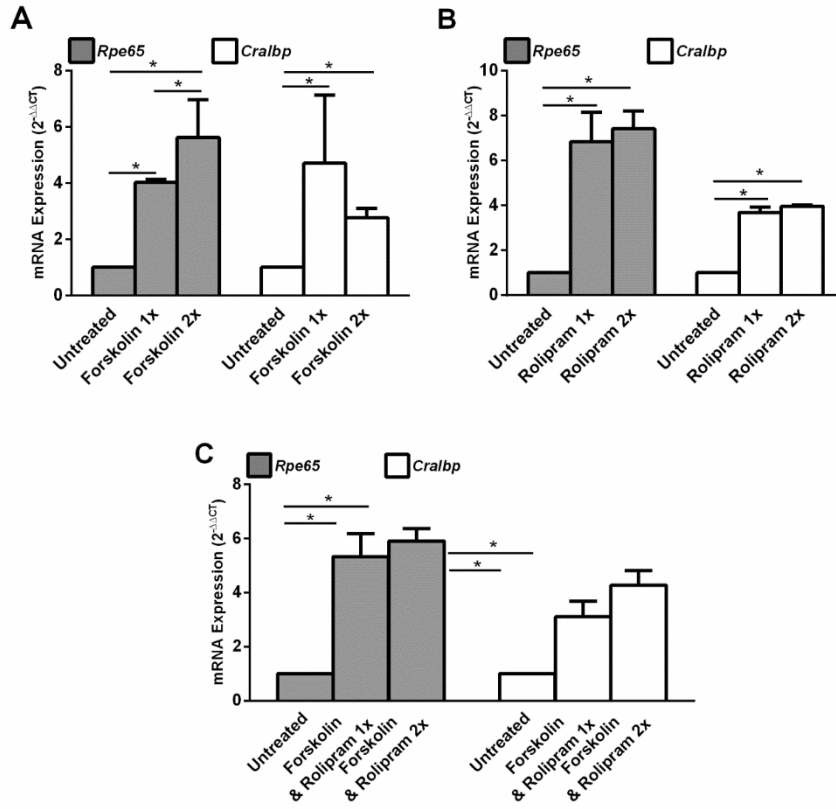


Figure 5.2. Forskolin and Rolipram Induce Expression of *RPE65* and *CRALBP* mRNA in Human BMDCs.

Human (CD34+) BMDCs were exposed to 10 $\mu\text{mol/l}$ Forskolin, 1 $\mu\text{mol/l}$ Rolipram, or a combination of 10 $\mu\text{mol/l}$ Forskolin and 1 $\mu\text{mol/l}$ Rolipram. Cells were either treated once, with drug-containing media left on the cells for 1 day prior to replacement with complete DMEM, or twice, with media replaced with a second treatment after 1 day and replaced with complete DMEM on the 3rd day. All cells were cultured for a total of 3 days. (A) Cells treated with Forskolin once expressed *RPE65* mRNA ~4-fold over control and *CRALBP* mRNA ~4.5-fold over control ($p < 0.05$). Cells treated twice expressed *Rpe65* mRNA ~6-fold over control and *Cralbp* mRNA ~3-fold over control ($p < 0.05$). (B) Cells treated with Rolipram once expressed *RPE65* mRNA ~7-fold over control and *CRALBP* mRNA ~4-fold over control ($p < 0.05$). Cells treated twice expressed *RPE65* mRNA ~7.5-fold over control and *CRALBP* mRNA ~4-fold over control ($p < 0.05$). (C) Cells treated with Forskolin and Rolipram once expressed *RPE65* mRNA ~5-fold over control and *CRALBP* mRNA ~3-fold over control ($p < 0.05$). Cells treated twice expressed *RPE65* mRNA ~6-fold over control and *CRALBP* mRNA ~4-fold over control ($p < 0.05$).

Inhibiting the Expression of Adenylate Cyclase Inhibits Murine and Human BMDC Differentiation *In Vitro*

To confirm the role of adenylate cyclase activation in the differentiation of murine and human BMDCs *in vitro*, we inhibited adenylate cyclase immediately prior to the treatment of cells with Forskolin, Rolipram, or ILV-*RPE65*. We first demonstrated that the inhibitors used – the transmembrane adenylate cyclase inhibitors BPIPP and NKY 80, and the soluble adenylate cyclase inhibitor KH7, did not influence expression of the *Rpe65* or *Cralbp* genes in murine BMDCs which had not been exposed to either adenylate cyclase activating drug Forskolin, or cAMP degradation inhibitor Rolipram (Figure 5.3A). No significant difference in expression was observed in murine BMDCs exposed to the vehicle used to deliver the drug, DMSO, or in response to any of the inhibitors (Figure 5.3A).

Next, we compared the efficacy of each inhibitor in downregulating the activation of *Rpe65* and *Cralbp* following exposure to Forskolin in murine BMDCs. When NKY 80 or BPIPP was added to cells treated with Forskolin individually, expression of *Rpe65* was ~2.5-fold ($p < 0.05$) over expression in control untreated cells, which is significantly lower than the ~6-fold ($p < 0.05$) increase in *Rpe65* expression in cells treated with Forskolin alone (Figure 5.3B). Combining inhibitors NKY 80 and BPIPP together further reduced *Rpe65* expression to a level similar to that observed in cells which had not been treated with Forskolin. While the KH7 inhibitor decreased *Rpe65* expression to approximately half that observed in cells

treated with Forskolin only, the level of inhibition is significantly different, indicating a role for non-transmembrane adenylate cyclase in the redifferentiation process (Figure 5.3B). Expression of *Cralbp* was significantly inhibited by treating Forskolin-exposed cells with NKY 80 or BPIPP alone (~0.1-fold and ~2.5-fold higher than the untreated control respectively, compared with a ~4-fold increase with Forskolin alone), and combining NKY 80 with BPIPP again resulted in a significantly lower expression of *Cralbp* than when BPIPP was used alone. Again, KH7 unexpectedly reduced *Cralbp* expression, further implicating soluble adenylate cyclase in the programming process (Figure 5.3B).

Inhibition of adenylate cyclase via these inhibitors resulted in a similar pattern of inhibition when combined with cellular treatment with Rolipram by itself, or where cells were treated with both Forskolin and Rolipram together (Figure 5.3C, D). NKY 80 and BPIPP consistently and significantly reduce expression of both *Rpe65* and *Cralbp*, with the strongest inhibition consistently observed when used in combination. KH7 also consistently results in reduced expression of both the *Rpe65* and *Cralbp* genes (Figure 5.3 C, D).

Since inhibiting adenylate cyclase significantly reduces expression of *Rpe65* and *Cralbp* in murine BMDCs, we next compared expression of *RPE65* and *CRALBP* in human donor BMDCs exposed to Forskolin or Rolipram with or without a combination of NKY 80 and BPIPP, or KH7. Interestingly, in human BMDCs, KH7 did not inhibit expression of *RPE65* or *CRALBP* to the same degree as this inhibitor

inhibited *Rpe65* and *Cralbp* in murine BMDCs (Figure 5.4). NKY 80 and BPIPP did, however, significantly reduce expression of both genes in human

Figure 5.3

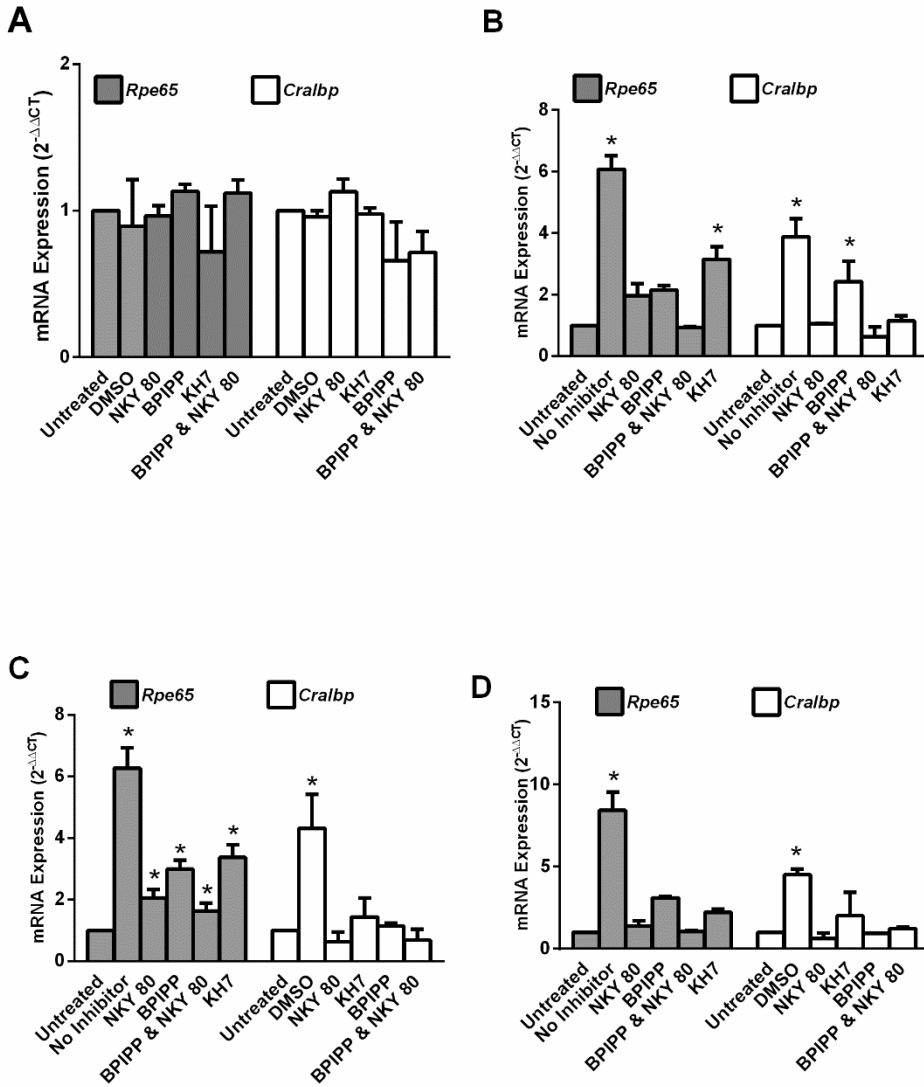


Figure 5.3. Adenylate Cyclase Inhibitors Block Expression of *Rpe65* and *Cralbp* in Forskolin and Rolipram-Treated Murine BMDCs.

BMDCs were exposed to 10 $\mu\text{mol/l}$ Forskolin, 1 $\mu\text{mol/l}$ Rolipram, or a combination of 10 $\mu\text{mol/l}$ Forskolin and 1 $\mu\text{mol/l}$ Rolipram in the presence or absence of 50 $\mu\text{mol/l}$ BPIPP, NKY 80, or KH7. (A) Cells treated with inhibitor vehicle DMSO, BPIPP, NKY 80, KH7, or a combination of BPIPP and NKY 80 did not significantly express *Rpe65* or *Cralbp* mRNA (B) Cells treated with Forskolin in the absence of any inhibitor expressed *Rpe65* mRNA ~6-fold over control and *Cralbp* mRNA ~4-fold over control ($p < 0.05$). *Rpe65* mRNA expression reduced to ~2-fold over control in cells treated with NKY 80 or BPIPP, approximately equal to control in cells treated with both NKY 80 and BPIPP, and ~3-fold over control in KH7-treated cells ($p < 0.05$). *Cralbp* mRNA expression was approximately equal to control in cells treated with NKY 80, KH7, or NKY 80 with BPIPP, and ~2-fold over control in cells treated with BPIPP. (C) Cells treated with Rolipram in the absence of any inhibitor expressed *Rpe65* mRNA ~6-fold over control and *Cralbp* mRNA ~4-fold over control ($p < 0.05$). *Rpe65* mRNA expression reduced to ~2-fold over control in NKY 80-treated cells, ~3-fold over control in BPIPP-treated cells, ~1.6-fold over control in NKY80 and BPIPP-treated cells, and ~3-fold over control in KH7-treated cells. *Cralbp* expression was reduced to approximately the same level as the untreated control in cells treated with all inhibitors. (D) Cells treated with Forskolin and Rolipram expressed *Rpe65* mRNA ~8-fold and ~4.5-fold over control ($p < 0.05$). In the presence of NKY 80 or a combination of BPIPP and NKY 80 reduced

expression of *Rpe65* to approximately that observed in the untreated control. BPIPP reduced *Rpe65* mRNA to ~3-fold over control, and KH7 ~2-fold over control ($p < 0.05$). *Cralbp* expression was reduced to approximately that of the untreated control in all conditions apart from KH7, in which expression was ~2-fold over the control. (*= $p < 0.05$; n(per experiment)=3, n(experiments)=3).

Figure 5.4

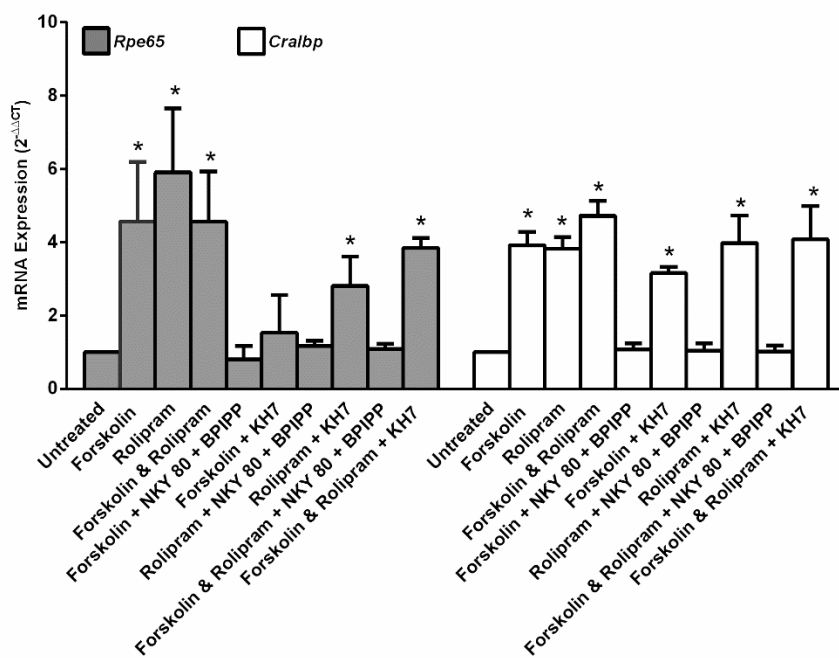


Figure 5.4. Adenylate Cyclase Inhibitors Block Expression of *RPE65* and *CRALBP* mRNA in Forskolin and Rolipram-Treated Human BMDCs.

BMDCs were exposed to 10 $\mu\text{mol/l}$ Forskolin, 1 $\mu\text{mol/l}$ Rolipram, or a combination of 10 $\mu\text{mol/l}$ Forskolin and 1 $\mu\text{mol/l}$ Rolipram in the presence or absence of 50 $\mu\text{mol/l}$ NKY 80/BPIPP, or KH7. In the presence of Forskolin, *RPE65* mRNA was ~4.5-fold over control ($p < 0.05$), reduced to approximately that of the control in the presence of NKY 80/BPIPP and ~1.5-fold over control in the presence of KH7. *CRALBP* mRNA levels were ~4-fold over control ($p < 0.05$), reduced to approximately that of the control in the presence of NKY 80/BPIPP and ~3-fold over control in the presence of KH7 ($p < 0.05$). In the presence of Rolipram, *RPE65* mRNA was ~6-fold over control ($p < 0.05$), reduced to approximately that of the control in the presence of NKY 80/BPIPP and ~3-fold over control in the presence of KH7 ($p < 0.05$). *CRALBP* mRNA levels were ~4-fold over control ($p < 0.05$), reduced to approximately that of the control in the presence of NKY 80/BPIPP and ~4-fold over control in the presence of KH7 ($p < 0.05$). In the presence of Forskolin and Rolipram, *RPE65* mRNA was ~4.5-fold over control ($p < 0.05$), reduced to approximately that of the control in the presence of NKY 80/BPIPP and ~4-fold over control in the presence of KH7. *CRALBP* mRNA levels were ~5-fold over control ($p < 0.05$) reduced to approximately that of the control in the presence of NKY 80/BPIPP and ~4-fold over control in the presence of KH7.

(*= $p < 0.05$; n(per experiment)=3, n(experiments)=3).

BMDCs treated with Forskolin, Rolipram, or a combination of Forskolin and Rolipram (Figure 5.4).

We next measured the effect of inhibiting adenylate cyclase on expression of *Rpe65*, *Cralbp*, and *CRALBP* in murine and human BMDCs infected with ILV3-*RPE65*. Exposure to NKY 80 and BPIPP, and to KH7, does not reduce expression of the lentiviral transgene *RPE65* (Figure 5.5). KH7 also does not inhibit expression of *Rpe65* or *Cralbp* in mouse cells treated with ILV-*RPE65* to the same level as it inhibits these genes in cells treated with Forskolin and Rolipram (Figure 5.5). KH7 also does not inhibit expression of *CRALBP* in human BMDCs. Consistent with our observations with inhibiting adenylate cyclase in Forskolin/Rolipram-treated cells, the combination of NKY 80 and BPIPP consistently reduced the expression of the murine *Rpe65* and *Cralbp* genes in murine ILV-*RPE65* infected BMDCs, and also inhibited expression of the human *CRALBP* gene in human ILV-*RPE65* infected cells (Figure 5.5).

These data support our hypothesis that expression of *RPE65/Rpe65* and *CRALBP/Cralbp* is almost completely inhibited by the inhibition of adenylate cyclase in both Forskolin/Rolipram treated cells and ILV-*RPE65*-treated cells. This suggests that adenylate cyclase activation is one of the earliest stages in the differentiation process, and confirms that the activation of adenylate cyclase precedes activation of the endogenous *Rpe65* gene, as *Rpe65* as well as *Cralbp* expression is inhibited by the inhibition of adenylate cyclase. This suggests that it

is the expression of the human *RPE65* gene in the murine BMDCs which initiates expression of adenylate cyclase in these cells, and that adenylate cyclase expression in turn results in expression of the endogenous *Rpe65* and *Cralbp* genes. If expression of the *RPE65* gene alone was sufficient to drive the up-regulation of *Rpe65* expression, we would expect to observe no inhibition of *Rpe65* expression in ILV-*RPE65*-treated cells exposed to the adenylate cyclase inhibitors. Although we observed significant similarities between the murine and human BMDCs in response to pharmacological activation of adenylate cyclase, murine and human BMDCs did differ in response to the soluble adenylate cyclase inhibitor, KH7. In murine BMDCs, KH7 unexpectedly inhibited expression of *Cralbp*. KH7 was expected to have no effect on expression of these genes due to the fact that the initial study implicated adenylate cyclases 1, 3, and 5 in the cellular programming process, which are all transmembrane adenylate cyclases. While the inhibition resulting from KH7 exposure was not as great as that observed when cells were treated with transmembrane adenylate cyclase inhibitors NKY 80 and BPIPP, the inhibition was significant, indicating that soluble adenylate cyclase may also play a role in murine BMDC programming. In contrast, in human BMDCs, inhibition of the soluble adenylate cyclase did not inhibit expression of *CRALBP*, indicating that there may be a difference in the number of adenylate cyclases involved in murine BMDC differentiation in comparison with human BMDC differentiation.

Figure 5.5

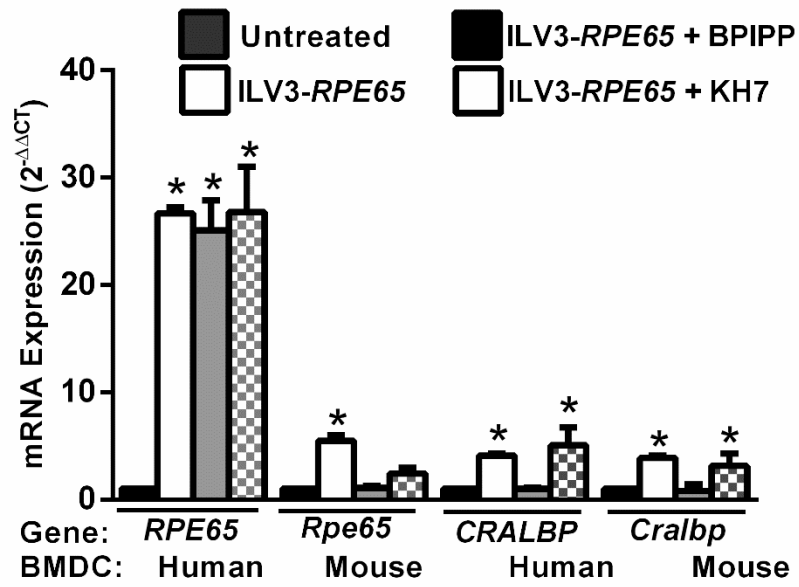


Figure 5.5. Adenylate Cyclase Inhibitors Block Expression of *Rpe65* and *Cralbp* mRNA in ILV3-*RPE65*-Infected Cells. Murine (*lin*⁻/*Sca1*⁺) or human (*CD34*⁺) BMDCs were infected with ILV3-*RPE65* at an MOI of 50 with or without inhibitors BPIPP or KH7. Control cells were not infected with virus. Expression of *RPE65* from the vector, and mouse *Rpe65* and *Cralbp* mRNA and human *CRALBP* mRNA were measured 4 hours after infection as previously described (Chapter 3). All cells infected with ILV3-*RPE65* expressed *RPE65*, with a ~26-fold, ~25 fold, and ~27-fold increase in *RPE65* mRNA observed in ILV3-*RPE65*, ILV3-*RPE65*+BPIPP, and ILV3-*RPE65*+KH7-treated cells respectively ($p < 0.05$). In mouse BMDCs, cells treated with ILV3-*RPE65* alone expressed *Rpe65* and *Cralbp* mRNA ~5- and ~4-fold over control respectively ($p < 0.05$). These levels reduced to ~1 and ~0.8 fold when BPIPP was added ($p < 0.05$), and to ~2 and ~3-fold when KH7 was added. In human BMDCs, *CRALBP* mRNA was expressed ~4-fold over control when cells were infected with ILV3-*RPE65* alone ($p < 0.05$). This reduced to ~1-fold when BPIPP was added ($p < 0.05$). In the presence of KH7, ILV3-*RPE65*-treated human BMDCs expressed *CRALBP* ~5-fold over control ($p < 0.05$). (*= $p < 0.05$; n(per experiment)=3; n(experiments)=3).

Murine BMDCs Programmed with Adenylate Cyclase Activators are Not Recruited to the RPE in Retinal Degeneration Murine Models

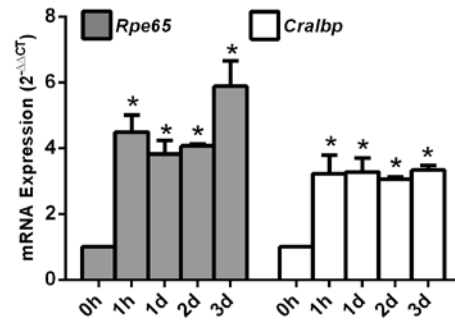
As we confirmed the role of adenylate cyclase in activating endogenous RPE-associated genes *in vitro*, and observed similar levels of activation of these genes following treatment with Forskolin and Rolipram as observed in murine BMDCs programmed with ILV-*RPE65* and IDLV-*RPE65*, it was thought that murine BMDCs exposed to Forskolin and Rolipram would also be recruited to and regenerate damaged RPE in the sodium iodate and SOD2-KD models of retinal degeneration. Due to the critical timing of injection of cells infected with the *RPE65* vectors, we first attempted to determine the best time of injection for BMDCs exposed to Forskolin. Murine BMDCs exposed to 10 $\mu\text{mol/l}$ Forskolin began expressing both the murine *Rpe65* and *Cralbp* genes within one hour post-exposure, with a ~ 4.2 -fold and ~ 3.5 -fold increase in expression of these genes compared with untreated cells ($p < 0.05$) (Figure 5.6A). Similar fold changes were observed consistently from 1 hour to 3 days in culture with 10 $\mu\text{mol/l}$ Forskolin, with an increase in *Rpe65* expression from ~ 4 -fold to ~ 6 -fold between 2 and 3 days ($p < 0.05$) but no significant increase in *Cralbp* expression (Figure 5.6A). Cells were injected into sodium iodate mice 8 hours after IP injection of sodium iodate, after 1 hour, 1 days, or 2 days of culture with 10 $\mu\text{mol/l}$ Forskolin. Cells treated with Forskolin alone expressed *Rpe65* ~ 4 -fold over the control, and *Cralbp* ~ 2.4 -fold. Cells treated with Rolipram demonstrated a ~ 3 -fold increase in expression of *Cralbp* and a ~ 4 -fold increase in expression of *Rpe65*. Cells treated with both Forskolin and Rolipram demonstrated

a ~3-fold increase in *Cralbp* expression and a ~4.4-fold increase in *Rpe65* expression (Figure 5.6B).

We did not observe GFP+ cells in the RPE layer in mice injected with BMDCs exposed to Forskolin at 1 hour, 1 day, or 2 days of culture with Forskolin (Figure 5.6C). Mice were sacrificed 7 days after injection. No GFP+ cells were observed in the RPE layer in mice injected with naïve BMDCs (Figure 5.6C). In contrast, several GFP+ cells were found in the RPE layer of mice injected with ILV3-*RPE65*, pictured here as a positive control. While some patches of green can be observed in the flat mounted RPEs of mice injected with BMDCs exposed to Forskolin for 1 hour or 1 day, these areas do not appear to be GFP+ cells. Instead, the green patches are likely to be autofluorescent particles occurring as a result of the sodium iodate induced RPE damage.

Figure 5.6

A



B

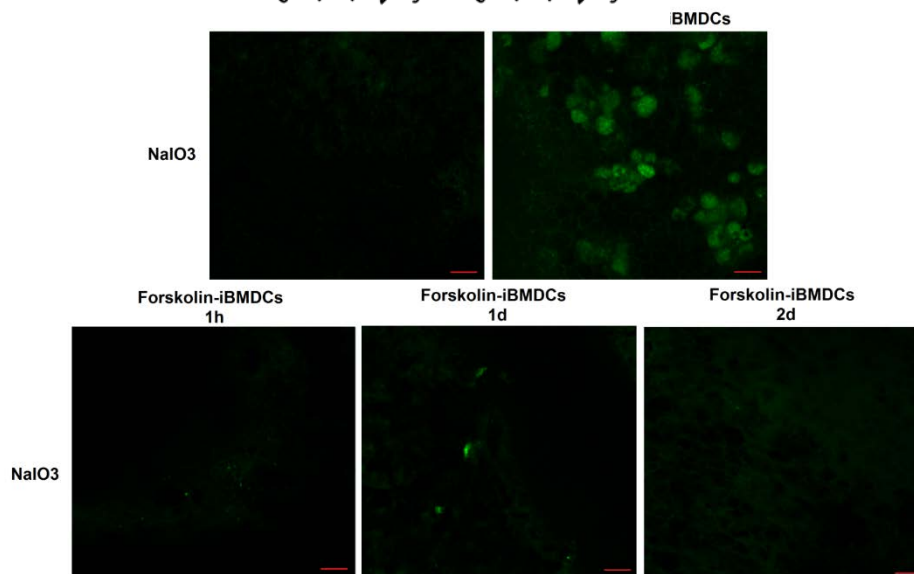


Figure 5.6. Forskolin and Rolipram-Treated Murine BMDCs Do Not Preserve Retinal Morphology in Murine Models of Retinal Degeneration.

Murine Lin⁻/Sca1⁺ BMDCs were isolated from the whole bone marrow of GFP⁺ C57BL6/J mice and treated with 10 μ mol/l Forskolin. Cells were kept in culture for 1h and 1-3 days after Forskolin treatment, and injected via tail vein 1h, 1d, and 2d after Forskolin treatment into wild type C57BL6/J mice, which had received 100mg/kg sodium iodate 1 day prior to injection with cells (50k cells/mouse). (A) *Rpe65* and *Cralbp* mRNA levels were measured in murine BMDCs treated with Forskolin at each injection time point (1 hour, and 1-3 days) to confirm gene expression in cells injected into Sodium Iodate mice. Prior to treatment with Forskolin, cells did not express *Rpe65* or *Cralbp*. At 1 hour post-exposure to Forskolin, cells *Rpe65* mRNA was increased ~4-fold over control, and *Cralbp* ~3-fold ($p < 0.05$). ~3-fold increase in *Cralbp* mRNA was consistent at each time point, and *Rpe65* mRNA was expressed ~4-fold over control at all time points apart from 3 days, at which *Rpe65* expression increased to ~6-fold over control ($p < 0.05$). (B) Flat mounted RPE/Choroid layers were examined by confocal microscopy for expression of GFP⁺ cells at each time point. In contrast to the large numbers of GFP⁺ cells observed in sodium iodate mice injected with ILV3-*RPE65*-treated cells, no expression of GFP was observed in any of the eyes from mice injected with Forskolin-treated BMDCs at any of the time points. Areas of green fluorescence were determined to be autofluorescent, not cellular, in nature and are

consistent with areas of autofluorescence observed in damaged RPE. (*= $p < 0.05$.

n=3)

Discussion

Programming BMDCs to RPE-like cells for therapeutic intervention in retinal degeneration with drugs instead of a LV vector approach is an attractive possibility due to the increased safety of the treatment. While we believe IDLV-based approaches are significantly safer than the previously used ILV approach,[13, 216] the use of a drug is more so, and may not only be cheaper and easier as a mechanism for programming cells, but also more likely to be quickly approved for use in human clinical trial. Forskolin is already FDA approved for treatment of conditions such as heart disease and glaucoma,[325] and Rolipram, while discontinued for its original purpose as an antidepressant, is also FDA approved and has been shown to be safe in human clinical trials.[326] Additionally, the drug(s) are used only to program the cells and are **not** injected along with the cells, unlike the LV approach, where the viral genome remains in the cells given back to the animal/patient. Where patients are not being directly exposed to the agent used for programming, the potential for dangerous side effects is significantly reduced. For this reason, further developing the BMDC-programming approach with Forskolin/Rolipram is advantageous and may allow for treatment of humans earlier than cells derived from the ILV/IDLV approach.

As Forskolin/Rolipram-treated cells express the same markers of programming as ILV3/IDLV3-*RPE65*-treated cells, *Rpe65/RPE65* and *Cralbp/CRALBP*, and as inhibition of expression of these mRNAs is inhibited on exposure to cAMP

inhibitors whether cells were treated with virus or drug(s), we are confident that the mechanism by which the cells express these mRNAs is the same. Expression of *Rpe65/RPE65* in particular indicates that the Forskolin/Rolipram-treated cells are at least beginning to differentiate into an RPE-like cell as this gene is specific to RPE cells and would not be expected to be expressed in the absence of programming to this cell type. The lack of Forskolin/Rolipram-treated BMDC migration to and regeneration of damaged RPE in both the sodium iodate and SOD2-KD retinal degeneration models, in our opinion, suggests that the ideal time point for treatment and subsequent injection of BMDCs may differ significantly from that used for ILV3/IDLV3-*RPE65*-treated cells. As shown in Chapter IV, cells cultured for 16 hours after ILV3-*RPE65* infection are also not recruited to and do not regenerate RPE in these models; however, this did not mean that ILV3-*RPE65*-treated cells were incapable of doing so. The problem was not with the cells, but the timing of the injection, as the cells are recruited and do regenerate RPE when injected immediately after infection. This highlighted the critical importance of selecting the optimum time point after treatment for injection. We therefore do not believe that the lack of migration and regeneration with Forskolin/Rolipram-treated cells at this stage in the study indicates that this treatment is not appropriate for generating therapeutic BMDCs. Instead, we think that identifying the best time at which to inject the cells following exposure to the drug(s) will result in BMDC repair of the RPE comparable to that achieved with ILV3-*RPE65*.

The one critical difference between cells programmed with ILV3/IDLV3-*RPE65* and cells programmed with Forskolin is the timeline of endogenous *Rpe65* and *Cralbp* mRNA expression. While these genes are found to be activated within 4 hours of infecting cells with ILV3/IDLV3-*RPE65*, their expression is detected within just one hour of exposure to Forskolin. In fact, when used in Förster resonance energy transfer (FRET) applications for *in vitro* imaging of biosensor activity, Forskolin activates cAMP pathways within 30 seconds of being added to the cells, with emission reaching its highest at just 2 minutes after Forskolin is added.[327] Comparatively, this activation is considerably faster than activation observed with the vector-transduced cells. As observed with the vector-transduced cells, there is a critical time window for injection which is most likely related to the time point at which endogenous genes become activated and, as treating the cells with Forskolin/Rolipram results in the expression of these genes at different times in comparison with the vector-transduced cells, it is likely that this time point will be different from the time point used with the vector-transduced cells.

When vector-transduced cells are injected into mice, they are effective only when they are injected at the time point where adenylate cyclase pathways are thought to have been activated or are in the process of being activated, but robust expression of *Rpe65* and *Cralbp* mRNA has yet to occur – vector-infected cells, when lysed immediately after infection, do not exhibit expression of these mRNAs, which occurs at the 2-3 hour time point after injection. In contrast, cells programmed with Forskolin/Rolipram already express *Rpe65* and *Cralbp*, even

when injected just one hour after treatment. We believe this difference in timing of expression is the key to understanding how to make functional BMDCs using Forskolin/Rolipram. Essentially, we hypothesize that pharmacologically-activated BMDCs may be too differentiated by the time they are injected into the mice, limiting their 'homing' capacity.

As expression of *Rpe65* and *Cralbp* increases over time, expression of the BMDC markers *Sca-1* decreases. Appendix 2). The most obvious explanation for cells not being recruited to the RPE after systemic injection would be that they have become too differentiated along a non-hematopoietic lineage and have lost expression of the markers that BMDCs require to be able to circulate in the blood and not be filtered out of the system. The cells may also begin to lose expression of markers involved in recruitment to the RPE after they become differentiated. While we have not measured CXCR4 expression, it is possible that the cells also lose expression of CXCR4 as they differentiate, which would significantly impair their ability to be recruited to and be retained in the retina following injection.[217] Future studies will focus on identifying the BMDC marker expression profile in comparison with the Forskolin/Rolipram activation timeline, in order to identify a time point at which the cells express the right markers for both differentiating into RPE-like cells, and migrating to the RPE from the bloodstream. It may be necessary to add the drug(s) directly to the cells immediately before injection into mice, which would make the treatment slightly riskier as the drugs would be injected along with the cells, but as

both have been shown to be safe in small doses, we do not expect that the amount of drug required to differentiate the cells would have an effect *in vivo*.

Overcoming this limitation would allow for rapid treatment of retinal degeneration, minimizing the amount of time the cells are required to be maintained *ex vivo*. This is beneficial, as it has been shown that maintaining cells *ex vivo* in ambient oxygen alters their phenotype and reduces the number of cells capable of engrafting.[328] In summary, pharmacological activation of adenylate cyclase and subsequent inhibition of this activation in both Forskolin/Rolipram-treated cells and ILV-*RPE56* treated cells confirms the role of adenylate cyclase in the programming of BMDCs to RPE-like cells, via activation of the endogenous *RPE65/Rpe65* and *CRALBP/Cralbp* mRNA expression. Modifications to the treatment and injection process may allow the use of pharmacologically differentiated cells *in vivo*.

CHAPTER VI: DISCUSSION AND FUTURE DIRECTIONS

The lack of therapeutically viable options for intervention in dry AMD is a significant concern, [12] as the prevalence of the disorder is increasing and expected to continue to increase, as life expectancy and human exposure to environmental factors which contribute to the development of the disorder increases. [1-4, 9, 329] There is a critical need for a therapy which can be given early in the progression of the disease to prevent, or at least delay, the development of geographical atrophy and loss of neural retinal integrity in dry AMD patients. [13, 216] No matter how effective an RPE replacement strategy is, there will be no preservation of central vision if the treatment is applied so late in the progression of the disorder that the neural retina, in particular the photoreceptors, along with the choroid, are already damaged.

Some of the main disadvantages in stem cell-based therapies which have been trialed in dry AMD – late-stage treatment, invasive cell delivery, and a lack of adequate ‘spreading’ of cells from the site of injection – can be overcome by delivering the cells systemically, avoiding the invasive protocols which limit cellular delivery to late-stage disease in adult RPE, iPSC and ESC-derived transplant strategies. [13, 216] Other disadvantages, such as the potential for iPSC and ESC-derived cells to become tumorigenic or form teratomas, [211] can be addressed by using an adult stem cell as the cell of origin, as adult stem cells lack the potential to become any cell type. BMSCs combine these two solutions in providing a cell

type that can be injected directly into the bloodstream, and which is also very unlikely to be tumorigenic in itself.

BMDCs can be differentiated into RPE-like cells which regenerate RPE and preserve vision in retinal degeneration mice. [13, 216] Here, we have expanded this approach to eliminate the need for an integrating lentiviral vector (ILV) in the production of RPE-like cells from BMDCs, avoiding any potential concerns associated with the integration of lentiviral vector particles into coding or regulatory regions of the genome. [330] We have generated an integrase-defective lentiviral vector (IDLV)-based system for programming BMDCs to RPE-like cells, including the development a method for optimizing the infection of BMDCs with this vector. Not only are IDLVs capable of programming murine BMDCs to RPE-like cells, infection with this vector also initiates programming of human BMDCs to RPE-like cells as evidenced by the cells' expression of *CRALBP* shortly after infection. Critically, RPE-like cells derived from BMDCs using the IDLV vector are as capable of regenerating the RPE and preserving visual function as cells programmed using the ILV, confirming that integration and permanent expression of the human *RPE65* gene from the infecting vector is not required for the programming of BMDCs to RPE-like cells. Finally, we have confirmed the role of adenylate cyclase in the process of BMDC programming to RPE-like cells, showing that adenylate cyclase activation is both necessary and sufficient for generating RPE-like cells from BMDCs.

Together, our studies provide invaluable insight into methods by which RPE-like cells can be derived from BMDCs without taking unnecessary risks in the use of ILVs, improving safety for human clinical trial. We have further confirmed that our previously published protocols [13, 216] for regenerating RPE function *in vivo*. To the best of our knowledge, this study is not only the first example of the use of a single IDLV being used to program an adult stem cell *in vitro*, but also the first to produce a new cell type from a lineage not usually generated by the cell of origin that acts as an effective tissue regeneration therapy when delivered *in vivo*. It is also the first evidence that human BMDCs can be programmed to become RPE-like cells, which is vital for the use of BMDC-derived RPE in human clinical trials. Several experiments are required to further assess the mechanisms by which differentiated BMDCs are recruited to and integrate into the RPE layer. Previously, we have conducted an experiment in which *RPE65* vector-transduced GFP+ BMDCs were injected into wild-type C57BL6/J mice, followed by harvest of the eye, lung, liver, spleen, and bone marrow 1 day, 7 days, and 28 days after injection. [13] Organs were then homogenized and qRT-PCR was used to determine the level of expression of GFP in each organ. While GFP expression was observed in all tissues 1 day after injection, by 7 days, GFP was detectable only in the spleen. By 28 days, expression was found only in the eye. This raises questions as to the mechanism behind which cells are recruited to the eye, as *RPE65*-transduced GFP cells are present in the eye of wild-type mice, whereas in our retinal degeneration studies involving the SOD2-KD model, the GFP+ cells are recruited predominantly to the injured eye and not to the eye which has not received SOD2-KD injury. This

suggests that the programmed cells are recruited to the eye in the absence of injury, but that the localization of the cells is specifically and significantly enhanced by the presence of injury at the RPE. One possible mechanism for this would be the relative expression levels of CXCR4 in the BMDCs and SDF-1 in the RPE cells, since it is known that BMDCs express CXCR4 and that the recruitment of cells to specific areas will be enhanced by the expression in those tissues of SDF-1. A comparison of SDF-1 expression in the presence and absence of injury to the retina would allow for determination of whether or not an upregulation of SDF-1 in the presence of injury could enhance the recruitment of the cells to the injured eye, and this may be confirmed by inhibiting SDF-1 in the and determining the effect on the recruitment of BMDCs. Additionally, measuring the expression level of CXCR4 in null vs. *RPE65*-programmed BMDCs may provide insight into how the CXCR4 pathway enhances the natural ability of the cells to be recruited to the eye in injury. If CXCR4 is upregulated in *RPE65*-programmed BMDCs in comparison with the null cells, this may account for the enhanced ability of the cells to be recruited to the RPE layer.

Further experiments to compare the role of injury with the role of the cells ability to be recruited to the eye specifically could compare the presence of *RPE65*-programmed BMDCs in, for example, the lung, liver, or spleen at the time points previously analyzed when those organs are injured as opposed to the injury being located in the eye. A lack of recruitment of these cells to other organs in the presence of injury would provide evidence to confirm that the recruitment to the

eye in our models, and, consequently, the reparative capabilities of the cells, is specific to the RPE. This may be important in the application of these cells in human clinical trials, as if the recruitment is *not* eye-specific, it would be important to determine that any off-target migration to other organs would not be detrimental to the patient. Long-term mouse studies evaluating *RPE65*-programmed cells in tissues other than the retina would be required to rule this out should these cells be recruited to other injured organs, including the isolation and characterization of cells localizing to other organs and histopathological analysis for the presence of changes in the organs.

It is worth noting that studies involving adult stem cells have, in the past, been associated with cell fusion to existing cells as opposed to the cells themselves providing a therapeutic effect, [331] and that we have previously determined that our BMDC-derived RPE-like cells do not fuse to existing RPE by using XY-FISH. [216] Lack of cell fusion indicates that the cells themselves are functioning as RPE cells *in vivo*. It does not, however, rule out the possibility that the cells are supporting and protecting existing RPE after they have integrated. It is entirely possible that the cells not only help preserve the retina by performing RPE cell functions, but also act to protect the existing RPE cells from further degeneration. This would be advantageous, as it is not clear that the BMDC-derived RPE-like cells are any more capable of cell division than native, terminally differentiated RPE in the RPE layer – an ability to protect and support existing RPE would result in longer-term preservation of vision or delay in the progression of dry AMD.

Our primary goal is to establish the outlined therapy for use in human clinical trials. Preliminary data showing preservation of vision in mice treated with human BMDC-derived RPE-like cells generated with ILV3-*RPE65* (Godoy *et al.*, personal communication) is encouraging; however, several issues need to be addressed prior to moving toward human clinical trials. Firstly, evaluation of human BMDC-derived RPE-like cells in a larger animal is necessary for a number of reasons, including determination of the number of cells required for RPE regeneration and preservation of vision in a larger animal.

The mouse retinal area is approximately 15.6mm^2 , [332] whereas a human eye is $\sim 1025\text{mm}^2$. [333] Based on the cell number used in this study, we inject approximately 3300 BMDC-derived RPE-like cells per mm^2 of retinal area in the mouse. To get the equivalent cell number in humans, 3.3 million cells would therefore be required. This is an extremely high cell number considering that only $\sim 150\text{k}$ CD34+ cells could be obtained from patient peripheral blood. Bringing more invasive techniques, such as bone marrow harvest, into the equation is not optimal, and it would be better for patients if such invasive methods could be avoided. Mobilization of CD34+ cells into the bloodstream using G-CSF and subsequent collection by apheresis is less invasive than bone marrow harvest, but has been found in rare cases to result in pulmonary complications. [334] Evaluating the therapy in a larger animal prior to use in humans may allow for this complication to be minimized, through injections of smaller numbers of cells to identify the lowest number necessary for visual recovery. It is possible that a number

significantly lower than 3.3 million will be required, based on the recovery of vision we have observed in mice treated with 5k cells. [216] Potentially, 300k or fewer cells may be sufficient. This would allow for the recovery of cells from peripheral blood of patients, keeping the invasiveness of the procedure at a minimum. In the event that a smaller cell number fails to adequately regenerate the RPE and preserve vision, other options for obtaining large numbers of cells are available. For example, it has been shown that CD34+ hematopoietic progenitor cells can be obtained from iPSCs, [335] which would be a viable alternative, as long as a screening mechanism was used to ensure the iPSC generation process had not generated cells with the potential to become tumorigenic. [212]

Studies on non-human primates are critical for another reason – the presence of a macula. [336] Murine models are appropriate for evaluating the ability of cells to regenerate RPE, but as mice do not have a macula, these models do not accurately represent human AMD, where the primary site of degeneration is around the macular region. Especially in the sodium iodate model, RPE damage is widespread across the entire RPE area, and in both this model and the SOD2-KD model, it is difficult to pinpoint any specific areas of RPE injury that the cells are recruited to. We can say that the injury promotes recruitment of the cells to the RPE layer as we find significant cell numbers in the injured eye in mice injected with the cells in comparison with the non-injured eye in the same mouse. We do not, however, know if focal areas of injury in the SOD2-KD model specifically recruit cells to that area or if the cells will spread across the RPE regardless of

where the RPE is most damaged. In human dry AMD, in order for the therapy to have the maximum effect on preservation of vision, we hypothesize that the majority of the recruited cells would need to localize around the macular region in order to protect that area of the retina from degeneration. Even if the cells also protect existing RPE, localization in this area is likely to be critical for sustained maintenance of central vision in dry AMD patients. Developing a model of retinal degeneration in a non-human primate would allow for testing the therapy in an animal that has a macula, if a model could be generated that affects that macular region in a similar way to human dry AMD, would determine whether or not the cells are likely to be recruited to the area of the RPE that requires the most regeneration and protection in dry AMD.

In addition to optimizing the therapy for a larger animal, there is also the potential for enhancing the therapeutic value of adult BMDCs in dry AMD by generating photoreceptor cells in addition to RPE-like cells for systemic injection. The photoreceptors are the most affected by dry AMD after the RPE cells, as the loss of function of RPE cells during the development of the disorder has a significant effect on the function of the photoreceptors. Replacing damaged RPE is only going to be effective if the overlying photoreceptors are still functional. While we are focusing on developing a therapy which can be delivered early in the progression of dry AMD, patients may not be diagnosed until some photoreceptor damage has already occurred, and in these cases, it would be advantageous to be able to regenerate photoreceptors at the same time as regenerating the RPE.

Theoretically, if BMDCs can be programmed to one non-hematopoietic retinal cell type, generating a second cell type should also be possible. In practice, it may be considerably more difficult to generate photoreceptors from BMDCs than it is to generate RPE-like cells. The reason for this is that, when programming BMDCs to RPE-like cells, we are not necessarily giving the cells a new function, but exploiting a capability they already have. Indeed, the naïve BMDCs' ability to be recruited to and regenerate RPE without any manipulation, albeit at a low level, is likely to be the reason why it is possible to generate our cells from BMDCs in the first place. [216] Other stem cell types, such as iPSC and ESC, have been differentiated into RPE cells with relative ease, indicating that non-retinal stem cells may be innately predisposed to being able to differentiate into RPE. That being said, however, with the right genes, it is not beyond possibility that photoreceptor cells could be generated from BMDC, and the significant advantage to the overall therapy that delivering both RPE and photoreceptor cells would provide makes it worthwhile to try to generate these cells in addition to RPE.

Another potential future direction is the use of BMDC-derived RPE-like cells as a preventive measure in patients identified as being at high risk for developing dry AMD. While not particularly viable with the current knowledge on the genetic basis for dry AMD development, as our understanding of the genetic components of the disorder increase, it may be possible in future to identify people at risk of developing the disorder before they develop it, and, in such cases, it may be beneficial to give the cells before any loss of vision occurs. We have demonstrated

that the cells are capable of migrating to the eye in a wild-type mouse, and that while they are present in all of the organs immediately after delivery, they preferentially localize to the eye and the spleen in the first 28 days post-injection. If cells that localize to the spleen can be retained there and then, at the onset of retinal injury, become recruited to the retina, injecting cells before significant retinal injury may provide a 'pool' of cells capable of regenerating that damage. This would be a relatively easy theory to test, as the cells could be given 1 week to 28 days prior to SOD2-KD injury to determine whether or not having the cells present prior to injury would be sufficient to promote their migration and repair of the damage.

Finally, early application of BMDC-derived RPE-like cells may also be applicable in inherited retinal disorders, for example, retinitis pigmentosa (RP) or leber congenital amaurosis – especially where the underlying cause of these disorders in a patient is mutations in the *RPE65* gene, which occurs in approximately 2% and 16% of cases. [337] Early identification through prenatal screening for these disorders would allow for rapid intervention at birth, utilizing autologous CD34+ cord blood cells as a cell source. Injecting RPE-like cells derived from these cord blood cells within the first few weeks of life may be sufficient to preserve vision before it is lost, particularly if BMDC-derived photoreceptor cells can be given at the same time. An IDLV-based approach would be unlikely to function for this application, however. Due to mutations in the existing *RPE65* gene, an ILV would be advantageous over an IDLV for these diseases as it would be performing a

second role in addition to programming the cells – replacing, and hopefully compensating for, a mutated gene. With the endogenous *Rpe65* activation in murine BMDCs following infection with *RPE65*-vectors occurring after adenylate cyclase activation, endogenous *RPE65* or at least sustained RPE65 expression from the ILV is likely to be required for the cells to be reparative and maintained in RP or LCA.

Conclusion

In conclusion, we have (Figure 1):

- (a) Generated an IDLV-based approach for reprogramming BMDCs to RPE-like cells which are recruited to and preserve vision in mouse models of retinal degeneration.
- (b) Improved the infection efficiency of IDLVs for short-term transgene expression in applications which only require transient expression.
- (c) Demonstrated that human BMDCs can be programmed to an RPE-like cell.
- (d) Confirmed the role of adenylate cyclase activation in BMDC programming to RPE-like cells.

Figure 6.1

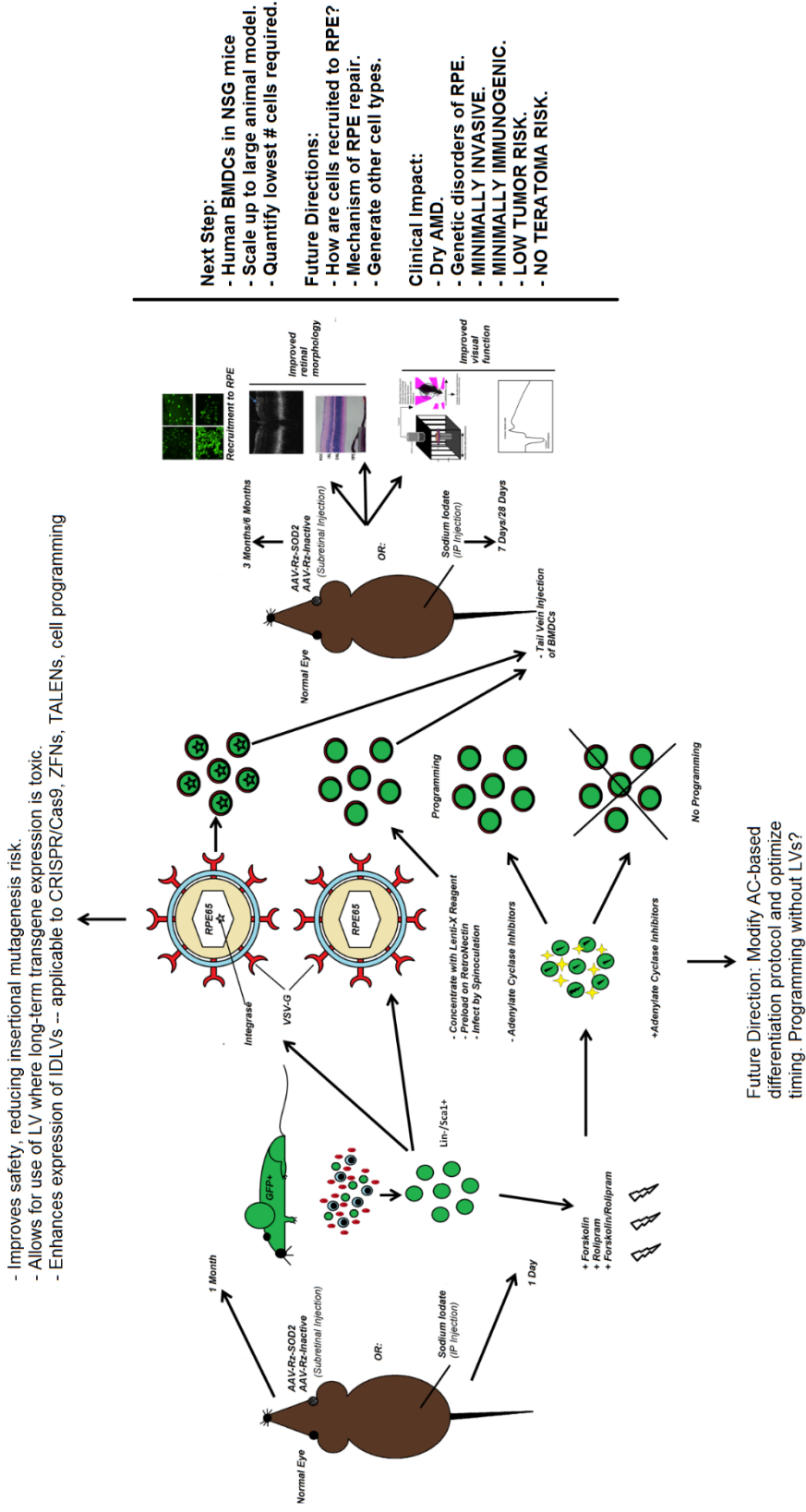


Figure 6.1. A Summary of the Current Study.

APPENDICES

Appendix 1: Plasmid Sequences

GeneArt *RPE65*

TCTAGAGCTAGCACCGGTAgtctatccagggtgagcatcctgctggtgtacaagaaactgttgaactgtggagga
 Actgtcctcgccgctcacagctcatgtaacaggcaggataaccctctggtcaccggcagctcctcgtatgtgggccag
 Gactcttgaagttggatctgagccatttaccacctgtttgatgggcaagccctcctgcacaagttgactttaaagaa
 Ggacatgtcacataccacagaaggtcatccgactgatcttacgtacgggcaatgactgagaaaaggatcgcataaac
 Agaattggcacctgtgcttccagatccctgcaagaatataatccagggtttttctacttccgaggagtagagg
 Ttactgacaatgccctgttaatgtctaccagtgggggaagattactacgctgcacagagaccaactttattacaag
 Attaatccagagacctggagacaattaagcaggtgatcttggcaactatgtctctgcaatggggccactgctcacc
 Ccacattgaaaatgatggaaccgtttacaatattgtaattgcttggaaaaaattttcaatgcctacaacattgtaa
 Agatcccaccactgcaagcagacaaggaatccaataagcaagtcagagatcgttgcattcccctgcagtgaccga
 tcaagccatcttacgtcatagtttggctgactcccaactataatcgttttgggagacaccagtcaaaattaaact
 gtcaagttccttctcatggagcttggggagccaactacatggattgttggagtcattgaaacatgggggtt
 ggctcatatgtcgaaaaaaaggaaaaagtaacctcaataataatacagaacttctcttcaacctctccatcac
 atcaacacctatgaagacaatgggttctgattgtgactctgtctgctggaaaggattgagttgttataaactt
 atatttagcaatttactgagaactgggaagaggtgaaaaaaatgccagaaaggctcccaacctgaagtaggagat
 atgtactccttgaatattgacaaggctgacacaggcaagaatttagtcacgctcccaatacaactgccactgcaatt
 ctgtgcagtgacgagactatctggctggagcctgaagttctctttcagggcctcgtcaagcattgagtttctcaaat
 caattaccagaagtattgggaaaccttacacatatgctgatggactggctgaatcattgttccagataggctct
 gtaagctgaatgcaaaactaaagaactgggttggcaagagcctgattcataccatcagaacctcttgttct
 caccagatgcttggaaagatgatgtgtgagttctgagttggtggtgagcccaggagcagagcaaaaagcctgctta
 tctctgatttgaatgcaaggactaagtaagttgcccgggctgaagtgagattaacatccctgtcaccttcatg
 gactgttcaaaaatctgatcaGTACAGGATCCGCGGCCGCgagaggaagcttctaactgcggtgacgtggagga
 gaatccggcccttccgCTCGAGGAATCAAGCTTGTCTGAC

Multiple Cloning Site

TTTCTGTTCTGCGCCGTTACAGATCCAAGCTGTGACCGGCGCCTACTCTAGAACCGGTGCCACCGAATT
 CTGTACAATTT
 AAATGCGGCCGCGAGGGCAGAGGAAGTCTTCTAACATGCGGTGACGTGGAGGAGAATCCCGGCCCTG
 GATCCCTTCCGGA
 ATGGAGAGCGACGAGAGCGGCCCTGCCCGCCATGGAGATCGAGTGCCGCATCACCG

pCDH-RPE65 (For ILV3-*RPE65* and IDLV3-*RPE65*)

acgcgtgtagtctttagcaactactctgtagtcttgaacatggtaacgatgagttagcaacatgccttacaaggagaga
 aaaagcaccgtgatgccgattggtggaagtaagtggtacgatcgtgccttattaggaaggcaacagacgggtctgaca
 tggattggacgaaccactgaattgccgcaatgcaagatattgtattaaagtgcttagctgatacaataaacgggtctc
 tctggttagaccagatctgagcctgggagctctctggtaactagggaaacctgcttaagcctcaataaagcttgcct
 tgagtgctcaagtagtgtgcccgtctgtgtgactctggttaactagagatccctcagacccttttagtcagtgtg
 gaaaatctctagcagtggtgcccgaacagggacctgaaagcgaagggaaccagagctctctcagcagcaggactcggc
 tgcgaagcgcgacggcaagagcggagggcggcactggtgagtagcgcacaaatattgactagcggaggctagaagg
 agagagatgggtgagagcgtcagttataagcgggggagaattagatcgcgatgggaaaaaattcggtaaggccaggg
 ggaagaaaaatataaataaaacatatagtagtgcaagcaggagctagaacgattcgcagttaatcctggcctgtt
 agaaacatcagaaggctgtagacaataactgggacagctacaacctccctcagacaggatcagaagaacttagatcat
 tataataacagtagcaaccctctattgtgcatcaaggatagagataaaagacaccaaggaagctttagacaagata
 gaggaagagcaaaaacaaagtaagaccaccgacagcaagcggccactgatctcagacctggaggaggagatagggg
 acaattggagaagtaattataaaatataaagtagtaaaaaatgaaccattaggagtagcaccaccaaggcaagaga
 agagttggtgcagagagaaaaaagcagcaggtggaataggagccttgggttctgggagcagcaggaagcactat
 gggcgcagcGtcaatgacgctgacggtacaggccagacaattattgtctgtatagtcagcagcagaacaattgtcga
 gggctattgaggcgaacagcatctgttgaaccacagctctgggcatcaagcagctccaggcaagaatcctggctgtg
 gaaagatacctaaaggatcaacagctcctgggatttgggtgtctctggaactcatttgcaccactgctgtgcctt
 gaatgctagttggagtaataatctctggaacagattTggaatcacacgacctggatggagttggagacagagaaattaaca
 attacacaagcttaatacactccttaattgaagaatgcacaaaccagcaagaaagaatgaacaagaattattggaatta

gataaatgggcaagttgtggaattggttaacataacaaattggctgtggtatataaaattattcataatgatagtagg
aggcttggtaggttaagaatagttttgctgtactttctatagtagaatagtaggtagggatattcaccattatcgt
ttcagaccacctcccacccccgaggggacccgacaggcccaaggaatagaagaagaaggtggagagagacagagac
agatccattcgtattagtaacggatctcgacggTATCGGTaaactttaaagaaaaggggggattgggggtacagtg
aggggaaagaatagtagacataatgcaacagacatacaactaaagaattcaaaaaaaattcaaaaattcaaaaatt
tatcgatactagtgatctgctgctccggtgcccgtcagtgggcagagcgcacatcgcccacagtccccgagaagtt
ggggggaggggtcgcaattgaacgggtgcttagagaaggtggcggggtaaactgggaaagtatgctgtactggtg
tccgcttttcccgaggggtggggagaaccgtatataagtgcagtagtgcctggaacgtttttcgcaacgggtt
gccgccagaacacagctgaagctcgaggggtcgcctctctcctcacgcgcccgcctacctgagggcccatcc
acggcgtgtagtgcgcttctccgctcccgctgtggtcctcctgaactgcgtccgcttaggtaagttaaagc
tcaggtcgagaccggcctttgctggcgtccctggagcctacctagactcagccgctctccacgcttgctgacc
ctgcttgcactacgctttgtttcgtttctgtctgcccgttacagatccaagctgtgaccggcgctacTct
agAGCTAGCACCGTAtgtctaccaggtgagcatcctgctggtggtacaagaactggtgaaactgtggaggaAct
gtcctcgccgtcacagctcatgtaacaggcaggatacccctggtcaccggcagctcctcctgagtggtggcagGac
tcttgaagttggtctgagccatttaccactgttggatgggcaagccctcctgcacaagttgactttaaagaaGga
catgtcacataccagaaggttcatccgactgatgcttacgctacggcaatgactgagaaaaggatcgtcataacAga
atttggacctgtgcttcccagatccctgcaagaatataatttccaggtttttcttacttgcaggagtagaggTta
ctgacaatgccctgttaattgctaccagtgggggaagattactcgttgcacagagaccaactttatacaaaagAtt
aatccagagacctggagacaattaagcaggtgatcttgcactatgctctgcaatggggccactgtcaccCca
cattgaaaatgatgaaaccgttacaatattgtaattgctttgaaaaaatttcaattgctacaacattgtaaAga
tcccaccctgcaagcagacaaggaagatccaataagcaagtcagagatcgttgccttccctgacgtgaccgattc
aagccatctacgttcatagtttggctgactcccaactatctgttttgggagacaccagtcaaaaataaccgtt
caagtcctttctcatggagctttggggagccaaactacatggattgtttgagccaatgaaaccatgggggttggc
ttcatattgctgacaaaaaaggaaaaagtaacctcaataataaacagaaacttctccttcaaccttccatcacatc
aacacctatgaagacaatgggttctgattgtggtatctgctgctggaagattgagttgttataattactata
tttagcaatttactgtagaactgggaagaggtgaaaaaaatgccagaaggtcccccaacctgaagttaggagatag
tacttcttgaataatgacaaggctgacacaggaagaatttagtcacgctccccatacaactgccaactgcaattctg
tgcagtcagagactcttggctggagcctgaagttctttcagggcctcgtcaagcatttgagttcctcaaatcaa
ttaccagaagtattgggaaaaactacacatagcgtatggactggtgctgaatcatttggccagataggctctgta
agctgaatgtcaaaactaaagaactgggttggcaagagcctgattcataccatcagaaccatcttgtttctcac
ccagatgcttgaagaagatgatggttagtctgagtggtgagcccaggagcaggacaaaagcctgctatct
cctgatctgaatgcaaggacttaagtgaagttgcccggctgaagtggaattaacacctgacaccttcatggac
tgttcaaaaatctgatcaTGACAGGATCCGCGGCCGCGcagaggaagcttctaacatgcccgtgacgtggaggaa
tccggcccttccgCTCAGGAAATTCAGCTTgctgacaatcaacctctggattcaaaaattgtgaaagattgactggt
attcttaactatgtgcttcttacgctatggtacgctgctttaaagccttctgtatcgtcttctccgctat
ggcttctatttctcctctgtataatcctggtgctgctctttagggagttgtggcccgttgcaggcaacgtg
gctggtgctgactggttctgctgacgcaacccccactggtggggcattgccaccactgtcagctccttccgggact
ttcgttccccctcctattgcccagcggaactcatcgcgctgcttgcctgcccgtgctggacaggggctcggctgtt
gggcactgacaattcctggtggttgcgggaaatcatcgtccttcttgcctgctcgcctgttggccactggattc
tgcgcccagctcttctgctacgctcctcggcccaatccagcggacctcctccgcccgtgctgcccgtctg
cggcctctccgctcttgccttcgccctcagacgagctggatctccttggggcgcctccccgctggtaccttaa
gaccaatgactacaagcagctgtagatcttagccacttttaaaagaaaaggggggactggaaggctaactactcc
caacgaaaataagactcttcttctgctgctgctgctgctgctgctgctgctgctgctgctgctgctgctgctgct
actaggaaccactgcttaagcctcaataaagctgctgagcttcaagtagtgtgcccgtctggtgctgact
ctggaactagagatccctcagaccctttagtctggtgaaatctctagcagtagtagtcatctattatt
cagttattataactgcaaaagaatgaaatcagagagtagaggaactgtttattgagctataatggttacaata
aagcaatgcatcacaatttcaaaaataaagcatttttctactgatttagtgtggttgcacaactcatcaatg
tatcttatcatgctgctctagctatcccggcccaactccgcccagttccgcccattcctcccccattggtgactaa
tttttttattatgagagggcagggccgctcggcctctgagctattccagaagttaggagggctttttggaggc
ctgactttgagagagcggccaaattcgtaatcatggtcatgctgttctctgtgaaattgtaiccgctcaaat
tccacacaacatacagccggaagcataaagttaaaagcctgggtgctaatgagtgagtaactcacattaattgct
tggcctcactgcccgtttccagtcgggaaacctgctgctgcaactgcaatgaaatgcaacgcgcccgggagagggc
ggtttgctattggcgcttccgctcctcctgctcactgactgctgctgctgctgctgctgctgctgctgctgctgct
agctactcaaaagcggtaatacgggtatccacagaatcaggggataacgcaggaaagaactgtgagcaaaaggccagc
aaaaggccaggaaccgtaaaaaggcggctgctgctgcttccataggctccgccccctgacgagcatcaaaaaat
cgacgctcaagtcagaggtggcgaaccggacaggaactataaagataccagggctttcccctggaagctccctgctg
ctcctcttccgaccctgcttaccgatacctgctcgccttctcccttccgggaagcgtggcgttctctatagct
cacgctgtaggtatctcagttcgtgtaggtcgtcctcaagctgggtgctgctgacgaacccccgttccagcccgac
cgctgctccttaccgtaactatcgtctgagttcaaccggtaagacacgacttatcgcactggcagcagccactgg
taacaggattagcagagcaggtatgtagggctgctacagagttcttgaagtggtgcttaactacggctactagaa
ggacagatttggatctgctctgctgaagcagttacctcggaaaaagagttgtagcttctgatccggcaaaaa
accaccgctgtagcgggtgtttttgttgaagcagcagattacgcgcagaaaaaaggatcacaagaagatcctt

gatctttctacggggtctgacgctcagtggaacgaaaactcacgtaaggatggtcatgagattatcaaaaagga
 tcttcacctagatccttttaaaataaaatgaagtttaaatcaatctaaagatatatgagtaaactggtctgacagt
 taccaatgcttaatcagtgaggcacctatctcagcgatctgtctatctcgttcatcatagttgctgactccccgctg
 gtgataactacgatacgggagggcttaccatctggcccagtgctgcaatgataccgagagaccacgctcaccggctc
 cagattatcagcaataaaccagccagccggaaggccgagcagaagtggtcctgcaactttatccgctccatccag
 tctattaattgtgcccgggaagctagagtaagtagttcggcagtaaatggttgcgcaacggttggccattgctacagg
 catcgtggtgacgctcgtctgttggatggctcattcagctccgggtcccaacgatcaaggcgagttacatgatccc
 ccatgttgcaaaaaagcggtagctcctcggctccgatcgtgtgcagaagtaagttggccgagttatcactc
 atggttatggcagcactgcataattccttactgcatgcatccgtaagatgcttttctgactggtgagtactcaac
 caagtcattctgagaatagtgtatgcgcgaccgagttgctctgcccggcgcaatacgggataataccgcccacata
 gcagaactttaaagtgctcatcattgaaaaagcttctcggggcgaaaactctcaaggatctaccgctgtgagatcc
 agttcagatgaaccactcgtgcaccaactgatcttcagcatctttactttcaccagcgtttctgggtgagcaaaaa
 aggaaggcaaaatgcccaaaaaggaataaaggcgacacggaaaatgtgaatactcactctccttttcaatatt
 attgaagcattatcaggggtattgtctcatgagcgggatacatattgaaatgattagaaaaataacaaataggggt
 ccgcgacatttcccgaagtgccactgacgtctaagaaaccattattatcatgacattaacctataaaaaatggcg
 taccagagcccttctcgtcgcggttctggatgacgggtgaaaacctctgacacatgacgtcccggagacggctca
 cagcttctgtgaagcggatccgggagcagacaagcccgcagggcgctcagcgggtgtggcgggtgctggggctg
 cttactatgcccacagagcagattgactgagagtgaccatatgcccgtgtgaaataccgcacagatgctgaaggag
 aaaataccgcatcagcggcattcgcattcaggctgcgcaactgttgggaaggcgatcgggtgcccgtctctcgtat
 tacgccagctggcgaagggggatgctgcaaggcgattaagttgggtaacgccagggtttccagtcacgacggtgt
 aaaacgacggccagtgccaagctg

pCDH-RPE65-MITF (For ILV3-RPE65-MITF and IDLV3-RPE65-MITF)

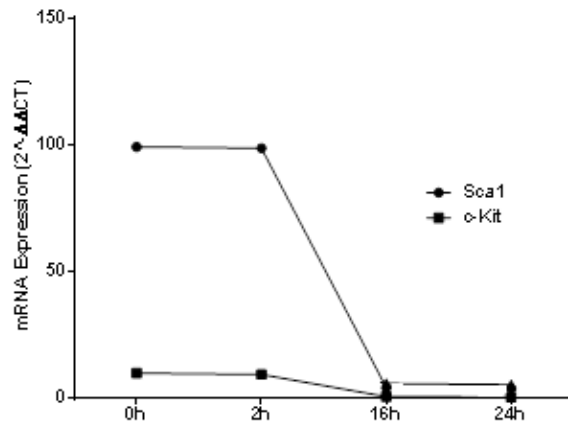
CATGCTGGAAATGCTAGAAATAATCACTATCAGGTGCAGACCCACCTCGAAAACCCACCAAGTACCA
 CATAACGCAAG
 CCCAACGGCAGCAGGTAAAGCAGTACCTTTCTACCACTTTAGCAAATAAACATGCCAACCAAGTCTCGA
 GCTTGCCATGT
 CCAAACCAGCCTGGCGATCATGTCATGCCACCGGTGCCGGGGAGCAGCGCACCCAACAGCCCCATGG
 CTATGCTTACGCT
 TAACTCCAAGTGTAAAAAGAGGGATTTTATAAGTTTGAAGAGCAAAACAGGGCAGAGAGCGAGTGCC
 CAGGCATGAACA
 CACATTCACGAGCGTCTGTATGCAGATGGATGATGTAATCGATGACATCATTAGCCTAGAATCAAGTT
 ATAATGAGGAA
 ATCTTGGGCTTGATGGATCCTGCTTTGCAAATGGCAAATACGTTGCCTGTCTCGGGAAACTTGATTGAT
 CTTTATGGAAA
 CCAAGGTCTGCCCCACCAGGCCTCACCATCAGCAACTCCTGTCCAGCCAACCTTCCCAACATAAAAA
 GGGAGCTCACAG
 AGTCTGAAGCAAGAGCACTGGCCAAAGAGAGGCAGAAAAAGACAATCACAACCTGATTGAACGAAGA
 AGAAGATTTAAC
 ATAAATGACCGCATTAAAGAACTAGGTACTTTGATTCCCAAGTCAAATGATCCAGACATGCGCTGGAAC
 AAGGGAACCAT
 CTTAAAAGCATCCGTGGACTATATCCGAAAGTTGCAACGAGAACAGCAACGCGCAAAAAGAACTTGAAAA
 CCGACAGAAGA
 AACTGGAGCACGCCAACCGGCATTTGTTGCTCAGAATACAGGAACTTGAAATGCAGGCTCGAGCTCAT
 GGACTTTCCCTT
 ATTCCATCCACGGGTCTCTGCTCTCCAGATTTGGTGAATCGGATCATCAAGCAAGAACCCGTTCTTGAG
 AACTGCAGCCA
 AGACCTCCTTCAGCATCATGCAGACCTAACCTGTACAACAACCTCTCGATCTCACGGATGGCACCATCAC
 CTTCAACAACA
 ACCTCGGAACTGGGACTGAGGCCAACCAAGCCTATAGTGTCCCACAAAAATGGGATCCAAACTGGAA
 GACATCCTGATG
 GACGACACCCTTTCTCCCGTCCGGTGTCACTGATCCACTCCTTTCTCAGTGTCCCCGGAGCTTCCAAA
 ACAAGCAGCCG
 GAGGAGCAGTATGAGCATGGAAGAGACGGAGCACACTTGTAgctTGtcgacaatcaacctctggattacaaaatttgg
 aaagattgactggtattcctaactatggtgctctttacgctatgtggatacgtctttaatgctttgatcatgct
 attgctcccgtatgcttcttctcctctgtataaatcctggtgctgctctttagaggagttgtggcccgt
 tgcaggcaacgtggcgtggtgctgactgtttgctgacgcaacccccactggtgggcaattgccaccacctgtcagc
 tctttccgggacttctccttccccctccatgtccacggcggaactcagccgctgcttcccgtgctggaca
 ggggctcggctgttggcactgacaattcgggtgtgtcgggaaatcatcgtccttctggtgctcgcctgtgt
 tgccactggtattctgcgggacgtcctctgctacgtccttccggcctcaatccagcgacattcctcccggcgc

tghtgcccgtctgcccctctccgctcttcgctctcgcctcagacgagtcggatctcccttggccgctccccg
 cctgttaccttaagaccaatgactacaaggcagctgtagatcttagccacttttaaaagaaaaagggggactggaag
 ggctaattcactcccaacgaaaataagatctgcttttgcctgtactggctctctggttagaccagatctgagcctgg
 gagctctctggtaactagggaaaccctgcttaagcctcaataaagcttgcttgagtgctcaagtagtggtgcccg
 tctgtgtgactctgtaactagagatccctcagacccttttagcagtggtgaaaatcttagcagtagtagtcat
 gtcaccttattacagtagttataactgcaaaagaaatgaatatcagagagtgagaggaaactgtttattgcagcttat
 aatggttacaaaataagcaatgcatcacaatcacaataaagcatttttactgcattctagttggtttgtc
 caaactcatcaatgatcttatcatgtctgctctagctatcccgccctaaactccgccagttccgccattctccgcc
 ccatggctgactaatttttttattatgacagaggccgagggccgctcctgagctattccagaagtagtgaggag
 gctttttggaggcctagacttttgacagagacgcccataatcgtaatcatggtcatagctgttctctgtgaaattgt
 tatccgctcacaattccacacaacatacagaccggaagcataaagtgtaaagcctggggtgctaatgagtgagtaact
 cacattaattgctgtgctcactgcccgtttccagtcgggaaacctgctgctgagctgcatatgaatcgccaac
 gcgcggggagaggcgtttgctgattggcgctctccgctcctcgtcactgactcgtcgtcgtcgtcgtcgtcgtc
 cggcgagcggatcagctcactcaaaaggcggtaatacgggtatccacagaatcaggggataacgcaggaaagacatgtg
 agcaaaaggccagcaaaaggccaggaaccgtaaaaaggccgctgtgctggcttttccataggctccgccccctgacg
 agcatcaaaaaatcagcgtcaagtcagaggtgcgaaaccgcagaggactataaagataaccaggcgttccccctgga
 agctccctcgtgctcctctcgtccgacctgcccgtaccggataacctgctccgcttctccctcgggaagcgtggc
 gctttctcatagctcagctgtaggtatctcagttcgtgtgagctgctcctcaagctgggctgtgtgcacgaacccc
 ccgtcagcccagcgtcgccttaccgtaactatcgtctgagccaacccggtaagacacgacttatcggcactg
 gcagcagcactgtaaacagattagcagagcaggtatgtagggctcagaggtgctacagagttctgaagtggtgacctacta
 cggctacactgaaagagcagtagttgtatctgcgctcgtgtaagccagttacctcggaaaaagagttgtagctctt
 gatccggcaaaacaaaccaccgctggtagcgggtgtttttgtgcaagcagcagattacgctcagaaaaaaggatct
 caagaagatcctttgatctttctacggggtgacgctcagtggaacgaaaactcagtttaagggtttgtcatgag
 attatcaaaaaggatctcactgtagcttttaataaaaaatgaagtttaatacaatcaaatatagtagtaaa
 ctggctgacagttaccaatgcttaacagtgaggcacctatctcagcgtctgctattctcattcatcattagttgccc
 tgactcccctgctgtagataactacgatacgggagggctaccatctggccccagtgctcaatgataccgcgagacc
 acgctaccggctccagattatcagcaataaacccagccagccggaaggccgagcgcagaagtggtcctgcaacttat
 ccgctccatccagctcttaattgtgcccgggaagctagagtaagtagttcgcgcaatagttgcaacggtgtt
 gccattgctacagcagctggtgtcagcctcgtctgtttggtatggctcattcagctccgggtccaacgatcaaggcg
 agttacatgacccccatgtgtgcaaaaaagcgttagctcctcgtcctccgatcgtgtcagaagtaagttggccg
 cagtggtactactcatggtatggcagcactgcataattctctactgcatgccatccgtaagatgctttctgtgact
 ggtgagtagtcaaccaagtcattctgagaatagtgatcggcgaccgagttgctctgcccggcgtaatacgggataa
 taccgcgccatagcagaactttaaaagtgctcatattggaacggttctcggggcgaaaaactcaaggatcttac
 cgctgtgagatccaagctgtagtaaccactcgtgcaccaactgatctcagcatctttactttaccagcgtttct
 gggtagcaaaaacagtgaaaggcaaaaatgccgcaaaaaaggaataagggcgacacggaatgtgtaatactatactct
 ccttttcaatattatgaagcattatcagggttattgtctcatgagcggatacatattgaatgattagaaaaata
 aacaaataggggttccgacacattccccgaaaagtgccacctgacgtctaagaaaccattatcatgacattaacc
 tataaaaataggcgtatcacgaggcccttctcgtcgcgcttctggtgatgacggtgaaaacctctgacacatgacgt
 ccgggagacggtcacagctgtctgtaagcggatgcccggagcagacaagcccgcagggcgctcagcgggtgtggcg
 ggtgtcggggctggcttaactatgcccagcagagcagattgactgagagtgaccatagcgggtgaaataaccgac
 agatgctgaaggagaaaaatccgcatcaggcgcattcgcattcaggctcgcgcaactgttgggaaggcgatcgggtcg
 ggctctcgtctattacggcagctggcgaagggggatgtgctgcaaggcgaattagttggtaacgcagggttttccc
 agtcacgagctgttaaacagcagcggcagtgcaaacgctgacgctgtagctttatgcaatactctgtagcttgcacaat
 ggtaacgatgagtagcaacatgcttacaaggagaaaaagcaccgtgcatgccattggtggaagtaagttgtagc
 atcgtgcttattaggaaggcaacagacgggtcagatggattggacgaaccactgaattgccgattgcagagatatt
 gtattaaagtgctagctgcatacaataaacgggtctctctggttagaccagatctgagcctgggagctctctggtaac
 tagggaaccactgcttaagcctcaataaagctgcttgagtgctcaagtagtggtgcccgtctgtgtgactct
 ggtaactagagatccctcagacccttttagcagtggtgaaaaatcttagcagtgggcccgcaacagggacctgaaagcg
 aaagggaaaccagagctctctcagcagcagcagcagcagcagcagcagcagcagcagcagcagcagcagcagcagc
 gagtacgcaaaaaattgactagcggaggctagaaggagagagatgggtgcgagagcgtcagtagttaaagcgggggagaa
 ttagatcggatgggaaaaaattcggtaaggccagggggaagaaaaataaaataaaacatatagtatgggcaagc
 agggagctagaacgattcagctaatcctggcgtttagaaacatcagaaggctgtagacaataactgggacagctaca
 accatccctcagacagatcagaagaacttagatcattataatacagtagcaaccctctattgtgtcatcaaaagga
 tagagataaaagacaccaaggaagctttagacaagatagaggaagagcaaaaacaaaagtaagaccaccgcagcaagcg
 gccactgatctcagaccctggaggaggatagtagggacaattggagaagtgaattataaaataaaagtagtaaaaa
 ttgaaccattaggtagaccccacaaaggcaaaagagaagtggtgcagagagaaaaagagcagtggaataggagct
 ttgttctgtgtcttgggagcagcaggaagcactatggcgagcGtcaatgacgctgacggtacagggcagacaat
 attgtctgttagtgtagcagcagcaaatgtctgagggctattgagggcaacagatctgtgcaactcagact
 ggggcatcaagcagctccaggcaagaatcctggctgtgaaagatacctaaaggatcaacagctcctgggattgggggt
 tgctctgaaaaactcattgaccactgctgtgcttgaatgtagttgagtaataatctctggaacagattTggaa
 tcacacgacctgtagtgaggacagagaaatcaacaattacaagcttaatacactccttaattgaagaatcgaaa
 accagcaagaaaagaatgaacaagaattattggaattagataaattgggcaagtttggaattggttaacatacaaat

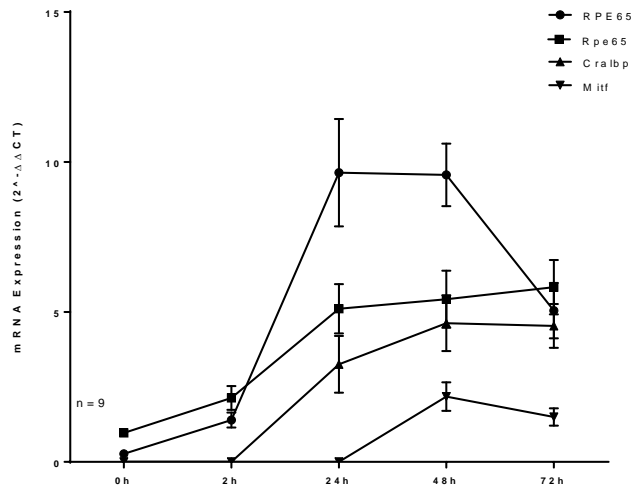
tggctgtggtatataaaaattattcataatgatagtaggaggcttggtaggtttaagaatagttttgctgtactttctat
 agtgaatagagtaggcaggatattcaccattatcgtttcagaccacctccaaccccgaggggacccgacaggcccg
 aaggaatagaagaagaagggtggagagagagacagagacagatcattcgattagtgaaacggatctcgacgggATCGGTta
 acttttaaaagaaaaggggggattgggggtacagtgcaggggaaagaatagtagacataatagcaacagacatacaaac
 taaagaattacaaaacaaattacaaaattcaaaatttatcgatactagtgatctgcatcgctccgggtgcccgtag
 tgggcagagcgcacatcgcccacagtccccgagaagtggggggaggggtcgcaattgaacgggtgcctagagaagggtg
 gcgggggtaaaactgggaaagtgtgctgtactggctccgcttttccgaggggtgggggagaaccgtatataagtg
 cagtagtgcgggtgaacgttcttttgcacacgggttccgcccagacacagctgaagctcgaggggctcgcatctct
 ccttcacgcggccgcccctacctgagggccatccacgcccgttgagtcgcttctgcccctcccctgtgggtgc
 ctctgaactgctgcccgtctaggttaagttaaagctcaggtcgagaccgggctttgtccggcctccctggagcc
 tacctagactcagccggctctccacgcttgcctgacctgctgtcaactctacgtctttgttctgtttctgttctg
 cgccgttacagatcaagctgtgaccggcgcctacTCTAGAGctagCACCGGTAtgtctatccagggtgagcatcctgct
 ggtggtacaagaactgttgaaactgtggaggaActgtcctcggctcacagctcatgtaacaggcaggataccct
 ctggctcaccggcagctcctcctgagtgggccagGactcttgaagttggatctgagccattttaccacctgtttgatg
 ggcaagccctcctgcacaagttgactttaagaaGgacatgtcacataccacagaaggtcatccgactgatgcttac
 gtacgggcaatgactgagaaaaggatgctataacAgaattggcacctgtctttccagatccctgcaagaatataat
 ttccagggttttcttactttcgaggagtagaggTtactgacaatgccctgttaatgtctaccagtgggggaagatt
 actacgctgacagagaccaactttattacaagAtaatccagagacctggagacaattaagcagggtgatctttgc
 aactatgtctctgtcaatggggccactgctcaccCcacattgaaaatgatggaaccggttacaatattgtaattgctt
 tggaaaaaattttcaattgctacaacattgtaaAgatcccaccactgcaagcagacaaggaagatccaataagcaagt
 cagagatcgttccaattcccctgcagtgaccgattcaagccatctacgttcatagtttggctgactccaactat
 atcgttttgggagacaccagtcaaaaataacctgtcaagttccttctcatggagtcttggggagccaactacat
 ggattgtttgagtccaatgaaaccatgggggttggctctatattgtgcaaaaaaaggaaaaagtacctcaataata
 aatacagaactctccttcaacctctccatcacatcaacacctatgaagacaatgggttctgattgtggatctctgc
 tgcgtgaaaggattgagittgttataattacttatattagccaattacgtgagaactgggagagggtaaaaaaaa
 tgccagaaaggctcccaacctgaagttaggagatagtacttcttgaatattgacaaggctgacacaggcaagaatt
 tagtcacgctcccaatacaactgccactgcaattctgtcagtgacgagactatctggctggagcctgaagttctctt
 tcaggccctcgtcaagcattgagtttccctcaaatcaattaccagaagtattgtggaaaccttacacatatgctgatgg
 actggcttgaatcactttgtccagataggctctgtaagctgaatgtcaaaaactaaagaactgggttggcaagagc
 ctgattcataccatcagaaccatcttctcaccagatgcttggagaagatgatggtgtagttctgagtggtg
 gtggtgagcccaggagcaggacaaaagcctgcttctcctgattctgaatgccaaggacttaagtgaagttgccgggc
 tgaagtgagattaacatccctgtcaccttctgactgtcaaaaatcttgatcaTGTACAGGATCCGCGGCCGCGc
 agaggaagcttctaactatcggtgacgtggaggagaatccccggcctccgCTCGAGGaatt

Appendix 2: Gene Expression Over Time

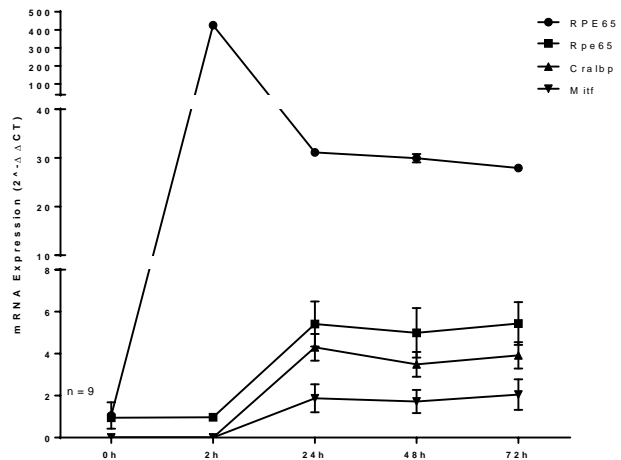
Gene Expression in BMDC Transduced with pCDH-RPE65



Gene Expression in BMDC Transduced with Non-Integrating pCDH-RPE65



Gene Expression in BMDC Transduced with Integrating pCDH-RPE65



Appendix 2: Expression of cKit and Sca1 in FACS sorted Lin-Sca1+ cells decreases after *RPE65*, *Rpe65* and *Cralbp* expression is initiated, approximately 2 hours after treatment with ILV3-*RPE65* or IDLV3-*RPE65*.

REFERENCES

1. Hayflick, L., *The not-so-close relationship between biological aging and age-associated pathologies in humans*. J Gerontol A Biol Sci Med Sci, 2004. **59**(6): p. B547-50; discussion 551-3.
2. Rizzuto, D., et al., *Effect of the Interplay Between Genetic and Behavioral Risks on Survival After Age 75*. J Am Geriatr Soc, 2016. **64**(12): p. 2440-2447.
3. Hung, M., et al., *The relationship between family support; pain and depression in elderly with arthritis*. Psychol Health Med, 2017. **22**(1): p. 75-86.
4. Hickman, R.A., A. Faustin, and T. Wisniewski, *Alzheimer Disease and Its Growing Epidemic: Risk Factors, Biomarkers, and the Urgent Need for Therapeutics*. Neurol Clin, 2016. **34**(4): p. 941-953.
5. Lee, A. and R.M. Gilbert, *Epidemiology of Parkinson Disease*. Neurol Clin, 2016. **34**(4): p. 955-965.
6. Violan, C., et al., *The burden of cardiovascular morbidity in a European Mediterranean population with multimorbidity: a cross-sectional study*. BMC Fam Pract, 2016. **17**(1): p. 150.
7. Mattei, F., et al., *Exposure to chlorinated solvents and lung cancer: results of the ICARE study*. Occup Environ Med, 2014. **71**(10): p. 681-9.
8. Huang, N.Q., et al., *TLR4 is a link between diabetes and Alzheimer's disease*. Behav Brain Res, 2017. **316**: p. 234-244.
9. Sorensen, S., et al., *The macular degeneration and aging study: Design and research protocol of a randomized trial for a psychosocial intervention with macular degeneration patients*. Contemp Clin Trials, 2015. **42**: p. 68-77.
10. Wong, W.L., et al., *Global prevalence of age-related macular degeneration and disease burden projection for 2020 and 2040: a systematic review and meta-analysis*. Lancet Glob Health, 2014. **2**(2): p. e106-16.
11. Meyer, C.H. and F.G. Holz, *Preclinical aspects of anti-VEGF agents for the treatment of wet AMD: ranibizumab and bevacizumab*. Eye (Lond), 2011. **25**(6): p. 661-72.
12. Forest, D.L., L.V. Johnson, and D.O. Clegg, *Cellular models and therapies for age-related macular degeneration*. Dis Model Mech, 2015. **8**(5): p. 421-7.
13. Qi, X., et al., *Systemic Injection of RPE65-Programmed Bone Marrow-Derived Cells Prevents Progression of Chronic Retinal Degeneration*. Mol Ther, 2017.
14. Alvarez Palomo, A.B., et al., *Prospects for clinical use of reprogrammed cells for autologous treatment of macular degeneration*. Fibrogenesis Tissue Repair, 2015. **8**: p. 9.
15. Kamao, H., et al., *Characterization of human induced pluripotent stem cell-derived retinal pigment epithelium cell sheets aiming for clinical application*. Stem Cell Reports, 2014. **2**(2): p. 205-18.

16. Afshari, F.T. and J.W. Fawcett, *Improving RPE adhesion to Bruch's membrane*. Eye (Lond), 2009. **23**(10): p. 1890-3.
17. Ramsden, C.M., et al., *Stem cells in retinal regeneration: past, present and future*. Development, 2013. **140**(12): p. 2576-85.
18. Bedel, A., et al., *Preventing Pluripotent Cell Teratoma in Regenerative Medicine Applied to Hematology Disorders*. Stem Cells Transl Med, 2017. **6**(2): p. 382-393.
19. Garber, K., *RIKEN suspends first clinical trial involving induced pluripotent stem cells*. Nat Biotechnol, 2015. **33**(9): p. 890-1.
20. Land, M.F. and R.D. Fernald, *The evolution of eyes*. Annu Rev Neurosci, 1992. **15**: p. 1-29.
21. Hohmann-Marriott, M.F. and R.E. Blankenship, *Evolution of photosynthesis*. Annu Rev Plant Biol, 2011. **62**: p. 515-48.
22. Tang, K.H., Y.J. Tang, and R.E. Blankenship, *Carbon metabolic pathways in phototrophic bacteria and their broader evolutionary implications*. Front Microbiol, 2011. **2**: p. 165.
23. Kolb, H., *Simple Anatomy of the Retina*, in *Webvision: The Organization of the Retina and Visual System*, H. Kolb, E. Fernandez, and R. Nelson, Editors. 1995: Salt Lake City (UT).
24. Purves D, A.G., Fitzpatrick D, Katz LC, LaMantia AS, McNamara J, Williams SM, *Neuroscience*. Sunderland (MA): Sinauer Associates, 2001. **2nd Edition**.
25. Rashid, A., et al., *RPE Cell and Sheet Properties in Normal and Diseased Eyes*. Adv Exp Med Biol, 2016. **854**: p. 757-63.
26. Panda-Jonas, S., J.B. Jonas, and M. Jakobczyk-Zmija, *Retinal pigment epithelial cell count, distribution, and correlations in normal human eyes*. Am J Ophthalmol, 1996. **121**(2): p. 181-9.
27. la Cour, M., *ACTA-EVER lecture 2007. The retinal pigment epithelium: friend or foe?* Acta Ophthalmol, 2008. **86**(6): p. 593-7.
28. Rizzolo, L.J., *Development and role of tight junctions in the retinal pigment epithelium*. Int Rev Cytol, 2007. **258**: p. 195-234.
29. Simo, R., et al., *The retinal pigment epithelium: something more than a constituent of the blood-retinal barrier--implications for the pathogenesis of diabetic retinopathy*. J Biomed Biotechnol, 2010. **2010**: p. 190724.
30. Ishikawa, M., Y. Sawada, and T. Yoshitomi, *Structure and function of the interphotoreceptor matrix surrounding retinal photoreceptor cells*. Exp Eye Res, 2015. **133**: p. 3-18.
31. Sparrow, J.R., D. Hicks, and C.P. Hamel, *The retinal pigment epithelium in health and disease*. Curr Mol Med, 2010. **10**(9): p. 802-23.
32. Altunay, H., *Fine structure of the retinal pigment epithelium, Bruch's membrane and choriocapillaris in the horse*. Anat Histol Embryol, 2000. **29**(3): p. 135-9.
33. Boulton, M. and P. Dayhaw-Barker, *The role of the retinal pigment epithelium: topographical variation and ageing changes*. Eye (Lond), 2001. **15**(Pt 3): p. 384-9.

34. Chen, M., et al., *Retinal pigment epithelial cell multinucleation in the aging eye - a mechanism to repair damage and maintain homeostasis*. Aging Cell, 2016. **15**(3): p. 436-45.
35. Stern, J. and S. Temple, *Retinal pigment epithelial cell proliferation*. Exp Biol Med (Maywood), 2015. **240**(8): p. 1079-86.
36. Osusky, R. and S.J. Ryan, *Retinal pigment epithelial cell proliferation: potentiation by monocytes and serum*. Graefes Arch Clin Exp Ophthalmol, 1996. **234 Suppl 1**: p. S76-82.
37. Parrales, A., et al., *Thrombin stimulates RPE cell proliferation by promoting c-Fos-mediated cyclin D1 expression*. J Cell Physiol, 2010. **222**(2): p. 302-12.
38. Marmorstein, A.D., *The polarity of the retinal pigment epithelium*. Traffic, 2001. **2**(12): p. 867-72.
39. Krigel, A., M.P. Felder-Schmittbuhl, and D. Hicks, *Circadian-clock driven cone-like photoreceptor phagocytosis in the neural retina leucine zipper gene knockout mouse*. Mol Vis, 2010. **16**: p. 2873-81.
40. Stamer, W.D., et al., *Aquaporin-1 channels in human retinal pigment epithelium: role in transepithelial water movement*. Invest Ophthalmol Vis Sci, 2003. **44**(6): p. 2803-8.
41. Gundersen, D., J. Orłowski, and E. Rodriguez-Boulan, *Apical polarity of Na,K-ATPase in retinal pigment epithelium is linked to a reversal of the ankyrin-fodrin submembrane cytoskeleton*. J Cell Biol, 1991. **112**(5): p. 863-72.
42. Marmorstein, A.D., et al., *Apical polarity of N-CAM and EMMPRIN in retinal pigment epithelium resulting from suppression of basolateral signal recognition*. J Cell Biol, 1998. **142**(3): p. 697-710.
43. Guo, H., et al., *EMMPRIN (CD147), an inducer of matrix metalloproteinase synthesis, also binds interstitial collagenase to the tumor cell surface*. Cancer Res, 2000. **60**(4): p. 888-91.
44. Bonilha, V.L., et al., *The retinal pigment epithelium apical microvilli and retinal function*. Adv Exp Med Biol, 2006. **572**: p. 519-24.
45. Lehmann, G.L., et al., *Plasma membrane protein polarity and trafficking in RPE cells: past, present and future*. Exp Eye Res, 2014. **126**: p. 5-15.
46. Ou, B., et al., *Ultrastructural study of basal lamina of retinal pigment epithelium*. Ophthalmic Res, 1995. **27**(3): p. 158-62.
47. Palisson, A., A. Courcoul, and B. Durand, *Analysis of the Spatial Organization of Pastures as a Contact Network, Implications for Potential Disease Spread and Biosecurity in Livestock, France, 2010*. PLoS One, 2017. **12**(1): p. e0169881.
48. Booiij, J.C., et al., *The dynamic nature of Bruch's membrane*. Prog Retin Eye Res, 2010. **29**(1): p. 1-18.
49. Guymer, R., P. Luthert, and A. Bird, *Changes in Bruch's membrane and related structures with age*. Prog Retin Eye Res, 1999. **18**(1): p. 59-90.
50. Chen, L., et al., *Distribution of the collagen IV isoforms in human Bruch's membrane*. Br J Ophthalmol, 2003. **87**(2): p. 212-5.

51. Bai, X., et al., *Developmental distribution of collagen IV isoforms and relevance to ocular diseases*. *Matrix Biol*, 2009. **28**(4): p. 194-201.
52. Aisenbrey, S., et al., *Retinal pigment epithelial cells synthesize laminins, including laminin 5, and adhere to them through alpha3- and alpha6-containing integrins*. *Invest Ophthalmol Vis Sci*, 2006. **47**(12): p. 5537-44.
53. Opas, M. and V.I. Kalnins, *Light-microscopical analysis of focal adhesions of retinal pigmented epithelial cells*. *Invest Ophthalmol Vis Sci*, 1986. **27**(11): p. 1622-33.
54. Sarna, M., et al., *The nanomechanical role of melanin granules in the retinal pigment epithelium*. *Nanomedicine*, 2016. **13**(3): p. 801-807.
55. Weiter, J.J., et al., *Retinal pigment epithelial lipofuscin and melanin and choroidal melanin in human eyes*. *Invest Ophthalmol Vis Sci*, 1986. **27**(2): p. 145-52.
56. Sinha, D., et al., *Lysosomes: Regulators of autophagy in the retinal pigmented epithelium*. *Exp Eye Res*, 2016. **144**: p. 46-53.
57. Bosch, E., J. Horwitz, and D. Bok, *Phagocytosis of outer segments by retinal pigment epithelium: phagosome-lysosome interaction*. *J Histochem Cytochem*, 1993. **41**(2): p. 253-63.
58. Robison, W.G., Jr. and T. Kuwabara, *Microperoxisomes in retinal pigment epithelium*. *Invest Ophthalmol*, 1975. **14**(11): p. 866-72.
59. Futter, C.E., *The molecular regulation of organelle transport in mammalian retinal pigment epithelial cells*. *Pigment Cell Res*, 2006. **19**(2): p. 104-11.
60. Jin, M., et al., *Regulation of RPE intercellular junction integrity and function by hepatocyte growth factor*. *Invest Ophthalmol Vis Sci*, 2002. **43**(8): p. 2782-90.
61. Mese, G., G. Richard, and T.W. White, *Gap junctions: basic structure and function*. *J Invest Dermatol*, 2007. **127**(11): p. 2516-24.
62. Malfait, M., et al., *Effects of hyperglycemia and protein kinase C on connexin43 expression in cultured rat retinal pigment epithelial cells*. *J Membr Biol*, 2001. **181**(1): p. 31-40.
63. Zhang, Y. and W. Wang, *Effects of bone marrow mesenchymal stem cell transplantation on light-damaged retina*. *Invest Ophthalmol Vis Sci*, 2010. **51**(7): p. 3742-8.
64. Strauss, O., *The retinal pigment epithelium in visual function*. *Physiol Rev*, 2005. **85**(3): p. 845-81.
65. Seagle, B.L., et al., *Melanin photoprotection in the human retinal pigment epithelium and its correlation with light-induced cell apoptosis*. *Proc Natl Acad Sci U S A*, 2005. **102**(25): p. 8978-83.
66. Mitter, S.K., et al., *Dysregulated autophagy in the RPE is associated with increased susceptibility to oxidative stress and AMD*. *Autophagy*, 2014. **10**(11): p. 1989-2005.
67. Burke, J.M., et al., *Dynamic analyses reveal cytoprotection by RPE melanosomes against non-photoc stress*. *Mol Vis*, 2011. **17**: p. 2864-77.
68. Kaczara, P., et al., *Melanosome-iron interactions within retinal pigment epithelium-derived cells*. *Pigment Cell Melanoma Res*, 2012. **25**(6): p. 804-14.

69. Sparrow, J.R. and M. Boulton, *RPE lipofuscin and its role in retinal pathobiology*. Exp Eye Res, 2005. **80**(5): p. 595-606.
70. Flood, M.T., P. Gouras, and H. Kjeldbye, *Growth characteristics and ultrastructure of human retinal pigment epithelium in vitro*. Invest Ophthalmol Vis Sci, 1980. **19**(11): p. 1309-20.
71. Young, R.W., *The renewal of photoreceptor cell outer segments*. J Cell Biol, 1967. **33**(1): p. 61-72.
72. Bazan, N.G., *Homeostatic regulation of photoreceptor cell integrity: significance of the potent mediator neuroprotectin D1 biosynthesized from docosahexaenoic acid: the Proctor Lecture*. Invest Ophthalmol Vis Sci, 2007. **48**(11): p. 4866-81; biography 4864-5.
73. Kevany, B.M. and K. Palczewski, *Phagocytosis of retinal rod and cone photoreceptors*. Physiology (Bethesda), 2010. **25**(1): p. 8-15.
74. Grace, M.S., A. Chiba, and M. Menaker, *Circadian control of photoreceptor outer segment membrane turnover in mice genetically incapable of melatonin synthesis*. Vis Neurosci, 1999. **16**(5): p. 909-18.
75. Nguyen-Legros, J. and D. Hicks, *Renewal of photoreceptor outer segments and their phagocytosis by the retinal pigment epithelium*. Int Rev Cytol, 2000. **196**: p. 245-313.
76. Finnemann, S.C., et al., *Phagocytosis of rod outer segments by retinal pigment epithelial cells requires alpha(v)beta5 integrin for binding but not for internalization*. Proc Natl Acad Sci U S A, 1997. **94**(24): p. 12932-7.
77. Nandrot, E.F., et al., *Loss of synchronized retinal phagocytosis and age-related blindness in mice lacking alphavbeta5 integrin*. J Exp Med, 2004. **200**(12): p. 1539-45.
78. Chang, Y. and S.C. Finnemann, *Tetraspanin CD81 is required for the alpha v beta5-integrin-dependent particle-binding step of RPE phagocytosis*. J Cell Sci, 2007. **120**(Pt 17): p. 3053-63.
79. Nandrot, E.F., et al., *Essential role for MFG-E8 as ligand for alphavbeta5 integrin in diurnal retinal phagocytosis*. Proc Natl Acad Sci U S A, 2007. **104**(29): p. 12005-10.
80. Finnemann, S.C., *Focal adhesion kinase signaling promotes phagocytosis of integrin-bound photoreceptors*. EMBO J, 2003. **22**(16): p. 4143-54.
81. Law, A.L., et al., *Annexin A2 regulates phagocytosis of photoreceptor outer segments in the mouse retina*. Mol Biol Cell, 2009. **20**(17): p. 3896-904.
82. Vollrath, D., et al., *Correction of the retinal dystrophy phenotype of the RCS rat by viral gene transfer of Mertk*. Proc Natl Acad Sci U S A, 2001. **98**(22): p. 12584-9.
83. Duncan, J.L., et al., *An RCS-like retinal dystrophy phenotype in mer knockout mice*. Invest Ophthalmol Vis Sci, 2003. **44**(2): p. 826-38.
84. Burstyn-Cohen, T., et al., *Genetic dissection of TAM receptor-ligand interaction in retinal pigment epithelial cell phagocytosis*. Neuron, 2012. **76**(6): p. 1123-32.
85. Caberoy, N.B., Y. Zhou, and W. Li, *Tubby and tubby-like protein 1 are new MerTK ligands for phagocytosis*. EMBO J, 2010. **29**(23): p. 3898-910.

86. Hall, M.O., et al., *Both protein S and Gas6 stimulate outer segment phagocytosis by cultured rat retinal pigment epithelial cells*. *Exp Eye Res*, 2005. **81**(5): p. 581-91.
87. Gibbs, D., J. Kitamoto, and D.S. Williams, *Abnormal phagocytosis by retinal pigmented epithelium that lacks myosin VIIa, the Usher syndrome 1B protein*. *Proc Natl Acad Sci U S A*, 2003. **100**(11): p. 6481-6.
88. Sethna, S., et al., *Regulation of Phagolysosomal Digestion by Caveolin-1 of the Retinal Pigment Epithelium Is Essential for Vision*. *J Biol Chem*, 2016. **291**(12): p. 6494-506.
89. Baylor, D., *How photons start vision*. *Proc Natl Acad Sci U S A*, 1996. **93**(2): p. 560-5.
90. Lamb, T.D., *Evolution of vertebrate retinal photoreception*. *Philos Trans R Soc Lond B Biol Sci*, 2009. **364**(1531): p. 2911-24.
91. Kusakabe, T.G., et al., *Evolution and the origin of the visual retinoid cycle in vertebrates*. *Philos Trans R Soc Lond B Biol Sci*, 2009. **364**(1531): p. 2897-910.
92. Miyazono, S., et al., *Highly efficient retinal metabolism in cones*. *Proc Natl Acad Sci U S A*, 2008. **105**(41): p. 16051-6.
93. Steinberg, R.H., R. Schmidt, and K.T. Brown, *Intracellular responses to light from cat pigment epithelium: origin of the electroretinogram c-wave*. *Nature*, 1970. **227**(5259): p. 728-30.
94. Steinberg, R.H., R.A. Linsenmeier, and E.R. Griff, *Three light-evoked responses of the retinal pigment epithelium*. *Vision Res*, 1983. **23**(11): p. 1315-23.
95. Oakley, B., 2nd and D.G. Green, *Correlation of light-induced changes in retinal extracellular potassium concentration with c-wave of the electroretinogram*. *J Neurophysiol*, 1976. **39**(5): p. 1117-33.
96. Kusaka, S., et al., *Functional Kir7.1 channels localized at the root of apical processes in rat retinal pigment epithelium*. *J Physiol*, 2001. **531**(Pt 1): p. 27-36.
97. Kusaka, S., et al., *Expression and polarized distribution of an inwardly rectifying K⁺ channel, Kir4.1, in rat retinal pigment epithelium*. *J Physiol*, 1999. **520 Pt 2**: p. 373-81.
98. Shimura, M., et al., *Expression and permeation properties of the K⁽⁺⁾ channel Kir7.1 in the retinal pigment epithelium*. *J Physiol*, 2001. **531**(Pt 2): p. 329-46.
99. Oakley, B., 2nd, *Potassium and the photoreceptor-dependent pigment epithelial hyperpolarization*. *J Gen Physiol*, 1977. **70**(4): p. 405-25.
100. Rover, J. and M. Bach, *C-wave versus electrooculogram in diseases of the retinal pigment epithelium*. *Doc Ophthalmol*, 1987. **65**(3): p. 385-91.
101. Bazan, N.G., W.C. Gordon, and E.B. Rodriguez de Turco, *Docosahexaenoic acid uptake and metabolism in photoreceptors: retinal conservation by an efficient retinal pigment epithelial cell-mediated recycling process*. *Adv Exp Med Biol*, 1992. **318**: p. 295-306.

102. Mukherjee, P.K., et al., *Neuroprotectin D1: a docosahexaenoic acid-derived docosatriene protects human retinal pigment epithelial cells from oxidative stress*. Proc Natl Acad Sci U S A, 2004. **101**(22): p. 8491-6.
103. Bazan, N.G., *Neurotrophins induce neuroprotective signaling in the retinal pigment epithelial cell by activating the synthesis of the anti-inflammatory and anti-apoptotic neuroprotectin D1*. Adv Exp Med Biol, 2008. **613**: p. 39-44.
104. Hamann, S., *Molecular mechanisms of water transport in the eye*. Int Rev Cytol, 2002. **215**: p. 395-431.
105. Rizzolo, L.J., *Polarization of the Na⁺, K(+)-ATPase in epithelia derived from the neuroepithelium*. Int Rev Cytol, 1999. **185**: p. 195-235.
106. Rizzolo, L.J., *The distribution of Na⁺,K(+)-ATPase in the retinal pigmented epithelium from chicken embryo is polarized in vivo but not in primary cell culture*. Exp Eye Res, 1990. **51**(4): p. 435-46.
107. Zhou, R. and R.R. Caspi, *Ocular immune privilege*. F1000 Biol Rep, 2010. **2**.
108. Wenkel, H. and J.W. Streilein, *Evidence that retinal pigment epithelium functions as an immune-privileged tissue*. Invest Ophthalmol Vis Sci, 2000. **41**(11): p. 3467-73.
109. Knickelbein, J.E., et al., *Modulation of Immune Responses by Extracellular Vesicles From Retinal Pigment Epithelium*. Invest Ophthalmol Vis Sci, 2016. **57**(10): p. 4101-7.
110. Tanihara, H., et al., *Identification of transforming growth factor-beta expressed in cultured human retinal pigment epithelial cells*. Invest Ophthalmol Vis Sci, 1993. **34**(2): p. 413-9.
111. Ishida, K., et al., *Participation of pigment epithelium in ocular immune privilege. 3. Epithelia cultured from iris, ciliary body, and retina suppress T-cell activation by partially non-overlapping mechanisms*. Ocul Immunol Inflamm, 2003. **11**(2): p. 91-105.
112. Holtkamp, G.M., et al., *Expression of multiple forms of IL-1 receptor antagonist (IL-1ra) by human retinal pigment epithelial cells: identification of a new IL-1ra exon*. Eur J Immunol, 1999. **29**(1): p. 215-24.
113. Jorgensen, A., et al., *Human retinal pigment epithelial cell-induced apoptosis in activated T cells*. Invest Ophthalmol Vis Sci, 1998. **39**(9): p. 1590-9.
114. Kim, Y.H., et al., *Regulated secretion of complement factor H by RPE and its role in RPE migration*. Graefes Arch Clin Exp Ophthalmol, 2009. **247**(5): p. 651-9.
115. Streeten, B.W., *Development of the human retinal pigment epithelium and the posterior segment*. Arch Ophthalmol, 1969. **81**(3): p. 383-94.
116. Hogan MJ, A.J., Weddell JE, *Histology of the human eye : an atlas and textbook*. Philadelphia, London, Saunders., 1971.
117. Cabral, L., et al., *Regional distribution of lysosomal enzymes in the canine retinal pigment epithelium*. Invest Ophthalmol Vis Sci, 1990. **31**(4): p. 670-6.

118. Burke, J.M. and S.S. Twining, *Regional comparisons of cathepsin D activity in bovine retinal pigment epithelium*. Invest Ophthalmol Vis Sci, 1988. **29**(12): p. 1789-93.
119. Burke, J.M., B.S. McKay, and G.J. Jaffe, *Retinal pigment epithelial cells of the posterior pole have fewer Na/K adenosine triphosphatase pumps than peripheral cells*. Invest Ophthalmol Vis Sci, 1991. **32**(7): p. 2042-6.
120. Del Priore, L.V., Y.H. Kuo, and T.H. Tezel, *Age-related changes in human RPE cell density and apoptosis proportion in situ*. Invest Ophthalmol Vis Sci, 2002. **43**(10): p. 3312-8.
121. Feeney-Burns, L., E.S. Hilderbrand, and S. Eldridge, *Aging human RPE: morphometric analysis of macular, equatorial, and peripheral cells*. Invest Ophthalmol Vis Sci, 1984. **25**(2): p. 195-200.
122. Feher, J., et al., *Mitochondrial alterations of retinal pigment epithelium in age-related macular degeneration*. Neurobiol Aging, 2006. **27**(7): p. 983-93.
123. Wang, A.L., et al., *Increased mitochondrial DNA damage and down-regulation of DNA repair enzymes in aged rodent retinal pigment epithelium and choroid*. Mol Vis, 2008. **14**: p. 644-51.
124. Wang, A.L., et al., *Age-related increase in mitochondrial DNA damage and loss of DNA repair capacity in the neural retina*. Neurobiol Aging, 2010. **31**(11): p. 2002-10.
125. Bird, A.C., *Therapeutic targets in age-related macular disease*. J Clin Invest, 2010. **120**(9): p. 3033-41.
126. Alamouti, B. and J. Funk, *Retinal thickness decreases with age: an OCT study*. Br J Ophthalmol, 2003. **87**(7): p. 899-901.
127. Eriksson, U. and A. Alm, *Macular thickness decreases with age in normal eyes: a study on the macular thickness map protocol in the Stratus OCT*. Br J Ophthalmol, 2009. **93**(11): p. 1448-52.
128. Feuer, W.J., et al., *Topographic differences in the age-related changes in the retinal nerve fiber layer of normal eyes measured by Stratus optical coherence tomography*. J Glaucoma, 2011. **20**(3): p. 133-8.
129. Garway-Heath, D.F., G. Wollstein, and R.A. Hitchings, *Aging changes of the optic nerve head in relation to open angle glaucoma*. Br J Ophthalmol, 1997. **81**(10): p. 840-5.
130. Panda-Jonas, S., J.B. Jonas, and M. Jakobczyk-Zmija, *Retinal photoreceptor density decreases with age*. Ophthalmology, 1995. **102**(12): p. 1853-9.
131. Curcio, C.A., N.E. Medeiros, and C.L. Millican, *Photoreceptor loss in age-related macular degeneration*. Invest Ophthalmol Vis Sci, 1996. **37**(7): p. 1236-49.
132. Klein, R., et al., *The prevalence of age-related macular degeneration and associated risk factors*. Arch Ophthalmol, 2010. **128**(6): p. 750-8.
133. Klein, R., B.E. Klein, and S.E. Moss, *Diabetes, hyperglycemia, and age-related maculopathy. The Beaver Dam Eye Study*. Ophthalmology, 1992. **99**(10): p. 1527-34.

134. Klein, R., B.E. Klein, and K.L. Linton, *Prevalence of age-related maculopathy. The Beaver Dam Eye Study*. Ophthalmology, 1992. **99**(6): p. 933-43.
135. Mitchell, P., W. Smith, and J.J. Wang, *Iris color, skin sun sensitivity, and age-related maculopathy. The Blue Mountains Eye Study*. Ophthalmology, 1998. **105**(8): p. 1359-63.
136. Stone, E.M., V.C. Sheffield, and G.S. Hageman, *Molecular genetics of age-related macular degeneration*. Hum Mol Genet, 2001. **10**(20): p. 2285-92.
137. Sergejeva, O., et al., *Genetic factors associated with the development of age-related macular degeneration*. Medicina (Kaunas), 2016. **52**(2): p. 79-88.
138. Khan, J.C., et al., *Smoking and age related macular degeneration: the number of pack years of cigarette smoking is a major determinant of risk for both geographic atrophy and choroidal neovascularisation*. Br J Ophthalmol, 2006. **90**(1): p. 75-80.
139. Sperduto, R.D. and R. Hiller, *Systemic hypertension and age-related maculopathy in the Framingham Study*. Arch Ophthalmol, 1986. **104**(2): p. 216-9.
140. Klein, R., et al., *Ten-year incidence of age-related maculopathy and smoking and drinking: the Beaver Dam Eye Study*. Am J Epidemiol, 2002. **156**(7): p. 589-98.
141. Zhang, J., et al., *Alterations of the classic pathway of complement in adipose tissue of obesity and insulin resistance*. Am J Physiol Endocrinol Metab, 2007. **292**(5): p. E1433-40.
142. Bartlett, H. and F. Eperjesi, *Age-related macular degeneration and nutritional supplementation: a review of randomised controlled trials*. Ophthalmic Physiol Opt, 2003. **23**(5): p. 383-99.
143. Lima, V.C., R.B. Rosen, and M. Farah, *Macular pigment in retinal health and disease*. Int J Retina Vitreous, 2016. **2**: p. 19.
144. Bowes Rickman, C., et al., *Dry age-related macular degeneration: mechanisms, therapeutic targets, and imaging*. Invest Ophthalmol Vis Sci, 2013. **54**(14): p. ORSF68-80.
145. Quillen, D.A., *Common causes of vision loss in elderly patients*. Am Fam Physician, 1999. **60**(1): p. 99-108.
146. Gangnon, R.E., et al., *Severity of age-related macular degeneration in 1 eye and the incidence and progression of age-related macular degeneration in the fellow eye: the Beaver Dam Eye Study*. JAMA Ophthalmol, 2015. **133**(2): p. 125-32.
147. Wu, G., *Retina: The Fundamentals*. Philadelphia, PA: W.B. Saunders Company, 1995.
148. Curcio, C.A. and C.L. Millican, *Basal linear deposit and large drusen are specific for early age-related maculopathy*. Arch Ophthalmol, 1999. **117**(3): p. 329-39.
149. Kamei, M. and J.G. Hollyfield, *TIMP-3 in Bruch's membrane: changes during aging and in age-related macular degeneration*. Invest Ophthalmol Vis Sci, 1999. **40**(10): p. 2367-75.

150. Nita, M., et al., *Age-related macular degeneration and changes in the extracellular matrix*. Med Sci Monit, 2014. **20**: p. 1003-16.
151. Salvi, S.M., S. Akhtar, and Z. Currie, *Ageing changes in the eye*. Postgrad Med J, 2006. **82**(971): p. 581-7.
152. Klein, R.J., et al., *Complement factor H polymorphism in age-related macular degeneration*. Science, 2005. **308**(5720): p. 385-9.
153. Jager, R.D., W.F. Mieler, and J.W. Miller, *Age-related macular degeneration*. N Engl J Med, 2008. **358**(24): p. 2606-17.
154. Hogg, R.E., *Reticular pseudodrusen in age-related macular degeneration*. Optom Vis Sci, 2014. **91**(8): p. 854-9.
155. Hageman, G.S. and R.F. Mullins, *Molecular composition of drusen as related to substructural phenotype*. Mol Vis, 1999. **5**: p. 28.
156. Rudolf, M., et al., *Prevalence and morphology of druse types in the macula and periphery of eyes with age-related maculopathy*. Invest Ophthalmol Vis Sci, 2008. **49**(3): p. 1200-9.
157. Curcio, C.A., et al., *The oil spill in ageing Bruch membrane*. Br J Ophthalmol, 2011. **95**(12): p. 1638-45.
158. Dentchev, T., et al., *Amyloid-beta is found in drusen from some age-related macular degeneration retinas, but not in drusen from normal retinas*. Mol Vis, 2003. **9**: p. 184-90.
159. Ferris, F.L., 3rd, et al., *Clinical classification of age-related macular degeneration*. Ophthalmology, 2013. **120**(4): p. 844-51.
160. Nowak, J.Z., *Age-related macular degeneration (AMD): pathogenesis and therapy*. Pharmacol Rep, 2006. **58**(3): p. 353-63.
161. Blasiak, J., et al., *Oxidative stress, hypoxia, and autophagy in the neovascular processes of age-related macular degeneration*. Biomed Res Int, 2014. **2014**: p. 768026.
162. Ambati, J., J.P. Atkinson, and B.D. Gelfand, *Immunology of age-related macular degeneration*. Nat Rev Immunol, 2013. **13**(6): p. 438-51.
163. Berger JW, F.S., Maguire MG, *Age-Related Macular Degeneration*. Mosby, 1999.
164. Schmitz-Valckenberg, S., et al., *In vivo imaging of foveal sparing in geographic atrophy secondary to age-related macular degeneration*. Invest Ophthalmol Vis Sci, 2009. **50**(8): p. 3915-21.
165. Hageman GS, G.K., Johnson LV, Anderson D, *Age-Related Macular Degeneration (AMD)*. Webvision: The Organization of the Retina and Visual System, 2008.
166. Cahill, M.T., et al., *Recurrence of retinal pigment epithelial changes after macular translocation with 360 degrees peripheral retinectomy for geographic atrophy*. Arch Ophthalmol, 2005. **123**(7): p. 935-8.
167. da Cruz, L., et al., *Five-Year Safety and Performance Results from the Argus II Retinal Prosthesis System Clinical Trial*. Ophthalmology, 2016. **123**(10): p. 2248-54.
168. Dang, Y., C. Zhang, and Y. Zhu, *Stem cell therapies for age-related macular degeneration: the past, present, and future*. Clin Interv Aging, 2015. **10**: p. 255-64.

169. Alexander, P., et al., *Retinal pigment epithelium transplantation: concepts, challenges, and future prospects*. Eye (Lond), 2015. **29**(8): p. 992-1002.
170. Age-Related Eye Disease Study Research, G., *A randomized, placebo-controlled, clinical trial of high-dose supplementation with vitamins C and E, beta carotene, and zinc for age-related macular degeneration and vision loss: AREDS report no. 8*. Arch Ophthalmol, 2001. **119**(10): p. 1417-36.
171. van Meurs, J.C., et al., *Autologous peripheral retinal pigment epithelium translocation in patients with subfoveal neovascular membranes*. Br J Ophthalmol, 2004. **88**(1): p. 110-3.
172. Peyman, G.A., et al., *A technique for retinal pigment epithelium transplantation for age-related macular degeneration secondary to extensive subfoveal scarring*. Ophthalmic Surg, 1991. **22**(2): p. 102-8.
173. Stanga, P.E., et al., *Retinal pigment epithelium translocation and central visual function in age related macular degeneration: preliminary results*. Int Ophthalmol, 2001. **23**(4-6): p. 297-307.
174. van Meurs, J.C. and P.R. Van Den Biesen, *Autologous retinal pigment epithelium and choroid translocation in patients with exudative age-related macular degeneration: short-term follow-up*. Am J Ophthalmol, 2003. **136**(4): p. 688-95.
175. Binder, S., et al., *Transplantation of autologous retinal pigment epithelium in eyes with foveal neovascularization resulting from age-related macular degeneration: a pilot study*. Am J Ophthalmol, 2002. **133**(2): p. 215-25.
176. Algere, P.V., et al., *Transplantation of RPE in age-related macular degeneration: observations in disciform lesions and dry RPE atrophy*. Graefes Arch Clin Exp Ophthalmol, 1997. **235**(3): p. 149-58.
177. Weisz, J.M., et al., *Allogenic fetal retinal pigment epithelial cell transplant in a patient with geographic atrophy*. Retina, 1999. **19**(6): p. 540-5.
178. Tezel, T.H., et al., *Adult retinal pigment epithelial transplantation in exudative age-related macular degeneration*. Am J Ophthalmol, 2007. **143**(4): p. 584-95.
179. Maya-Vetencourt, J.F., et al., *A fully organic retinal prosthesis restores vision in a rat model of degenerative blindness*. Nat Mater, 2017.
180. Schwartz, S.D., et al., *Embryonic stem cell trials for macular degeneration: a preliminary report*. Lancet, 2012. **379**(9817): p. 713-20.
181. Mandai, M., et al., *Autologous Induced Stem-Cell-Derived Retinal Cells for Macular Degeneration*. N Engl J Med, 2017. **376**(11): p. 1038-1046.
182. Abe, T., et al., *Auto iris pigment epithelial cell transplantation in patients with age-related macular degeneration: short-term results*. Tohoku J Exp Med, 2000. **191**(1): p. 7-20.
183. Mahmoudzadeh, R., S. Heidari-Keshel, and A. Lashay, *Schwann Cell-Mediated Preservation of Vision in Retinal Degenerative Diseases via the Reduction of Oxidative Stress: A Possible Mechanism*. Med Hypothesis Discov Innov Ophthalmol, 2016. **5**(2): p. 47-52.
184. Oner, A., et al., *Subretinal adipose tissue-derived mesenchymal stem cell implantation in advanced stage retinitis pigmentosa: a phase I clinical safety study*. Stem Cell Res Ther, 2016. **7**(1): p. 178.

185. Kuriyan, A.E., et al., *Vision Loss after Intravitreal Injection of Autologous "Stem Cells" for AMD*. N Engl J Med, 2017. **376**(11): p. 1047-1053.
186. Schwartz, S.D., et al., *Human embryonic stem cell-derived retinal pigment epithelium in patients with age-related macular degeneration and Stargardt's macular dystrophy: follow-up of two open-label phase 1/2 studies*. Lancet, 2015. **385**(9967): p. 509-16.
187. Sengupta, N., et al., *The role of adult bone marrow-derived stem cells in choroidal neovascularization*. Invest Ophthalmol Vis Sci, 2003. **44**(11): p. 4908-13.
188. Wan, J. and D. Goldman, *Retina regeneration in zebrafish*. Curr Opin Genet Dev, 2016. **40**: p. 41-47.
189. Mitashov, V.I., *Retinal regeneration in amphibians*. Int J Dev Biol, 1997. **41**(6): p. 893-905.
190. Wilken, M.S. and T.A. Reh, *Retinal regeneration in birds and mice*. Curr Opin Genet Dev, 2016. **40**: p. 57-64.
191. Otteson, D.C., *Talkin' about my (re)generation: The who of intrinsic retinal stem cells*. Neuroscience, 2017. **346**: p. 447-449.
192. Webster, M.K., et al., *Evidence of BrdU-positive retinal neurons after application of an Alpha7 nicotinic acetylcholine receptor agonist*. Neuroscience, 2017. **346**: p. 437-446.
193. Das, A.V., et al., *Neural stem cell properties of Muller glia in the mammalian retina: regulation by Notch and Wnt signaling*. Dev Biol, 2006. **299**(1): p. 283-302.
194. Lawrence, J.M., et al., *MIO-M1 cells and similar muller glial cell lines derived from adult human retina exhibit neural stem cell characteristics*. Stem Cells, 2007. **25**(8): p. 2033-43.
195. Saini, J.S., S. Temple, and J.H. Stern, *Human Retinal Pigment Epithelium Stem Cell (RPESC)*. Adv Exp Med Biol, 2016. **854**: p. 557-62.
196. Stanzel, B.V., et al., *Human RPE stem cells grown into polarized RPE monolayers on a polyester matrix are maintained after grafting into rabbit subretinal space*. Stem Cell Reports, 2014. **2**(1): p. 64-77.
197. Martello, G. and A. Smith, *The nature of embryonic stem cells*. Annu Rev Cell Dev Biol, 2014. **30**: p. 647-75.
198. Henon, P.R., *Human embryonic or adult stem cells: an overview on ethics and perspectives for tissue engineering*. Adv Exp Med Biol, 2003. **534**: p. 27-45.
199. van der Torren, C.R., et al., *Immunogenicity of human embryonic stem cell-derived beta cells*. Diabetologia, 2017. **60**(1): p. 126-133.
200. Myint, A., et al., *Strongyloides hyperinfection syndrome in an immunocompetent host resulting in bacteremia and death*. BMJ Case Rep, 2017. **2017**.
201. Fabiani, S., et al., *Allogeneic hematopoietic stem cell transplant recipients and parasitic diseases: A review of the literature of clinical cases and perspectives to screen and follow-up active and latent chronic infections*. Transpl Infect Dis, 2017.

202. Gallagher, M.P., et al., *Long-term cancer risk of immunosuppressive regimens after kidney transplantation*. J Am Soc Nephrol, 2010. **21**(5): p. 852-8.
203. Guillemin, A., et al., *[De novo cancer after solid organ transplantation: Epidemiology, prognosis and management]*. Bull Cancer, 2017. **104**(3): p. 245-257.
204. Song, W.K., et al., *Treatment of macular degeneration using embryonic stem cell-derived retinal pigment epithelium: preliminary results in Asian patients*. Stem Cell Reports, 2015. **4**(5): p. 860-72.
205. Atala, A., *Human embryonic stem cells: early hints on safety and efficacy*. Lancet, 2012. **379**(9817): p. 689-90.
206. Zhang, G.Y., et al., *Stem cells in age-related macular degeneration and Stargardt's macular dystrophy*. Lancet, 2015. **386**(9988): p. 29-30.
207. Patel, P.J., et al., *Intersession repeatability of contrast sensitivity scores in age-related macular degeneration*. Invest Ophthalmol Vis Sci, 2009. **50**(6): p. 2621-5.
208. Huang, J., et al., *Embryonic stem-cell-derived retinal pigment epithelial cells for macular degeneration*. Lancet, 2012. **379**(9831): p. 2050; author reply 2050-1.
209. Schulze-Bonsel, K., et al., *Visual acuities "hand motion" and "counting fingers" can be quantified with the freiburg visual acuity test*. Invest Ophthalmol Vis Sci, 2006. **47**(3): p. 1236-40.
210. Liao, J., et al., *Enhanced efficiency of generating induced pluripotent stem (iPS) cells from human somatic cells by a combination of six transcription factors*. Cell Res, 2008. **18**(5): p. 600-3.
211. Riggs, J.W., et al., *Induced pluripotency and oncogenic transformation are related processes*. Stem Cells Dev, 2013. **22**(1): p. 37-50.
212. Liu, W., et al., *Reevaluation of the safety of induced pluripotent stem cells: a call from somatic mosaicism*. Protein Cell, 2013. **4**(2): p. 83-5.
213. Huang, C., et al., *Combination of retinal pigment epithelium cell-conditioned medium and photoreceptor outer segments stimulate mesenchymal stem cell differentiation toward a functional retinal pigment epithelium cell phenotype*. J Cell Biochem, 2012. **113**(2): p. 590-8.
214. Gong, L., et al., *Differentiation of rat mesenchymal stem cells transplanted into the subretinal space of sodium iodate-injected rats*. Clin Exp Ophthalmol, 2008. **36**(7): p. 666-71.
215. Tomita, M., et al., *Bone marrow-derived stem cells can differentiate into retinal cells in injured rat retina*. Stem Cells, 2002. **20**(4): p. 279-83.
216. Sengupta, N., et al., *Regulation of Adult Hematopoietic Stem Cells Fate for Enhanced Tissue-specific Repair*. Mol Ther, 2009. **17**(9): p. 1594-1604.
217. Wyderka, R., et al., *Mobilization of CD34+CXCR4+ stem/progenitor cells and the parameters of left ventricular function and remodeling in 1-year follow-up of patients with acute myocardial infarction*. Mediators Inflamm, 2012. **2012**: p. 564027.
218. Wright, D.E., et al., *Hematopoietic stem cells are uniquely selective in their migratory response to chemokines*. J Exp Med, 2002. **195**(9): p. 1145-54.

219. Bhutto, I.A., et al., *Localisation of SDF-1 and its receptor CXCR4 in retina and choroid of aged human eyes and in eyes with age related macular degeneration*. Br J Ophthalmol, 2006. **90**(7): p. 906-10.
220. Harris, J.R., et al., *Bone marrow-derived cells home to and regenerate retinal pigment epithelium after injury*. Invest Ophthalmol Vis Sci, 2006. **47**(5): p. 2108-13.
221. Maier, P., C. von Kalle, and S. Laufs, *Retroviral vectors for gene therapy*. Future Microbiol, 2010. **5**(10): p. 1507-23.
222. Lombardo, A., et al., *Gene editing in human stem cells using zinc finger nucleases and integrase-defective lentiviral vector delivery*. Nat Biotechnol, 2007. **25**(11): p. 1298-306.
223. Provasi, E., et al., *Editing T cell specificity towards leukemia by zinc finger nucleases and lentiviral gene transfer*. Nat Med, 2012. **18**(5): p. 807-15.
224. Joglekar, A.V., et al., *Integrase-defective lentiviral vectors as a delivery platform for targeted modification of adenosine deaminase locus*. Mol Ther, 2013. **21**(9): p. 1705-17.
225. Verma, I.M. and N. Somia, *Gene therapy -- promises, problems and prospects*. Nature, 1997. **389**(6648): p. 239-42.
226. Kumar, M., et al., *Systematic determination of the packaging limit of lentiviral vectors*. Hum Gene Ther, 2001. **12**(15): p. 1893-905.
227. Zufferey, R., et al., *Self-inactivating lentivirus vector for safe and efficient in vivo gene delivery*. J Virol, 1998. **72**(12): p. 9873-80.
228. Cronin, J., X.Y. Zhang, and J. Reiser, *Altering the tropism of lentiviral vectors through pseudotyping*. Curr Gene Ther, 2005. **5**(4): p. 387-98.
229. Coleman, A. and J.E. Gern, *Lentiviral hematopoietic stem cell gene therapy in patients with wiskott-Aldrich syndrome*. Pediatrics, 2014. **134** Suppl 3: p. S182-3.
230. Kafri, T., et al., *Sustained expression of genes delivered directly into liver and muscle by lentiviral vectors*. Nat Genet, 1997. **17**(3): p. 314-7.
231. Blomer, U., et al., *Highly efficient and sustained gene transfer in adult neurons with a lentivirus vector*. J Virol, 1997. **71**(9): p. 6641-9.
232. Miyoshi, H., et al., *Stable and efficient gene transfer into the retina using an HIV-based lentiviral vector*. Proc Natl Acad Sci U S A, 1997. **94**(19): p. 10319-23.
233. Porter, D.L., et al., *Chimeric antigen receptor-modified T cells in chronic lymphoid leukemia*. N Engl J Med, 2011. **365**(8): p. 725-33.
234. Dull, T., et al., *A third-generation lentivirus vector with a conditional packaging system*. J Virol, 1998. **72**(11): p. 8463-71.
235. Miyoshi, H., et al., *Development of a self-inactivating lentivirus vector*. J Virol, 1998. **72**(10): p. 8150-7.
236. Segall, H.I., E. Yoo, and R.E. Sutton, *Characterization and detection of artificial replication-competent lentivirus of altered host range*. Mol Ther, 2003. **8**(1): p. 118-29.
237. Delenda, C., M. Audit, and O. Danos, *Biosafety issues in lentivector production*. Curr Top Microbiol Immunol, 2002. **261**: p. 123-41.

238. Mautino, M.R., et al., *Modified human immunodeficiency virus-based lentiviral vectors display decreased sensitivity to trans-dominant Rev*. Hum Gene Ther, 2000. **11**(6): p. 895-908.
239. Cornetta, K., et al., *Replication-competent lentivirus analysis of clinical grade vector products*. Mol Ther, 2011. **19**(3): p. 557-66.
240. Barry, S.C., et al., *Lentivirus vectors encoding both central polypurine tract and posttranscriptional regulatory element provide enhanced transduction and transgene expression*. Hum Gene Ther, 2001. **12**(9): p. 1103-8.
241. Garg, S., et al., *The hybrid cytomegalovirus enhancer/chicken beta-actin promoter along with woodchuck hepatitis virus posttranscriptional regulatory element enhances the protective efficacy of DNA vaccines*. J Immunol, 2004. **173**(1): p. 550-8.
242. Zufferey, R., et al., *Woodchuck hepatitis virus posttranscriptional regulatory element enhances expression of transgenes delivered by retroviral vectors*. J Virol, 1999. **73**(4): p. 2886-92.
243. Burns, J.C., et al., *Vesicular stomatitis virus G glycoprotein pseudotyped retroviral vectors: concentration to very high titer and efficient gene transfer into mammalian and nonmammalian cells*. Proc Natl Acad Sci U S A, 1993. **90**(17): p. 8033-7.
244. Huang, F., et al., *RNA helicase MOV10 functions as a co-factor of HIV-1 Rev to facilitate Rev/RRE-dependent nuclear export of viral mRNAs*. Virology, 2015. **486**: p. 15-26.
245. Naldini, L., et al., *In vivo gene delivery and stable transduction of nondividing cells by a lentiviral vector*. Science, 1996. **272**(5259): p. 263-7.
246. Cartier, N., et al., *Hematopoietic stem cell gene therapy with a lentiviral vector in X-linked adrenoleukodystrophy*. Science, 2009. **326**(5954): p. 818-23.
247. Cavazzana-Calvo, M., et al., *Transfusion independence and HMGA2 activation after gene therapy of human beta-thalassaemia*. Nature, 2010. **467**(7313): p. 318-22.
248. Aiuti, A., et al., *Lentiviral hematopoietic stem cell gene therapy in patients with Wiskott-Aldrich syndrome*. Science, 2013. **341**(6148): p. 1233151.
249. Biffi, A., et al., *Lentiviral hematopoietic stem cell gene therapy benefits metachromatic leukodystrophy*. Science, 2013. **341**(6148): p. 1233158.
250. Zhang, T., et al., *Efficiency of CD19 chimeric antigen receptor-modified T cells for treatment of B cell malignancies in phase I clinical trials: a meta-analysis*. Oncotarget, 2015. **6**(32): p. 33961-71.
251. Turtle, C.J., S.R. Riddell, and D.G. Maloney, *CD19-Targeted chimeric antigen receptor-modified T-cell immunotherapy for B-cell malignancies*. Clin Pharmacol Ther, 2016. **100**(3): p. 252-8.
252. Hay, K.A. and C.J. Turtle, *Chimeric Antigen Receptor (CAR) T Cells: Lessons Learned from Targeting of CD19 in B-Cell Malignancies*. Drugs, 2017. **77**(3): p. 237-245.
253. Hacein-Bey-Abina, S., et al., *A serious adverse event after successful gene therapy for X-linked severe combined immunodeficiency*. N Engl J Med, 2003. **348**(3): p. 255-6.

254. Sibbald, B., *Death but one unintended consequence of gene-therapy trial*. CMAJ, 2001. **164**(11): p. 1612.
255. Abordo-Adesida, E., et al., *Stability of lentiviral vector-mediated transgene expression in the brain in the presence of systemic antivector immune responses*. Hum Gene Ther, 2005. **16**(6): p. 741-51.
256. Lopez-Gordo, E., et al., *Circumventing antivector immunity: potential use of nonhuman adenoviral vectors*. Hum Gene Ther, 2014. **25**(4): p. 285-300.
257. Jin, C., et al., *Safe engineering of CAR T cells for adoptive cell therapy of cancer using long-term episomal gene transfer*. EMBO Mol Med, 2016. **8**(7): p. 702-11.
258. Ranzani, M., et al., *Cancer gene discovery: exploiting insertional mutagenesis*. Mol Cancer Res, 2013. **11**(10): p. 1141-58.
259. Zhang, R., et al., *Long non-coding RNA PTENP1 functions as a ceRNA to modulate PTEN level by decoying miR-106b and miR-93 in gastric cancer*. Oncotarget, 2017.
260. Zhuo, C., et al., *Genomic Editing of Non-Coding RNA Genes with CRISPR/Cas9 Ushers in a Potential Novel Approach to Study and Treat Schizophrenia*. Front Mol Neurosci, 2017. **10**: p. 28.
261. Mortezaei, Z., H. Lanjanian, and A. Masoudi-Nejad, *Candidate novel long noncoding RNAs, MicroRNAs and putative drugs for Parkinson's disease using a robust and efficient genome-wide association study*. Genomics, 2017.
262. Zhu, K., C. Dobard, and S.A. Chow, *Requirement for integrase during reverse transcription of human immunodeficiency virus type 1 and the effect of cysteine mutations of integrase on its interactions with reverse transcriptase*. J Virol, 2004. **78**(10): p. 5045-55.
263. Das, S., *Integrase interactor 1 in health and disease*. Curr Protein Pept Sci, 2015. **16**(6): p. 478-90.
264. Ramezani, A. and R.G. Hawley, *Overview of the HIV-1 Lentiviral Vector System*. Curr Protoc Mol Biol, 2002. **Chapter 16**: p. Unit 16 21.
265. Yung, E., et al., *Inhibition of HIV-1 virion production by a transdominant mutant of integrase interactor 1*. Nat Med, 2001. **7**(8): p. 920-6.
266. Katz, R.A., et al., *The avian retroviral IN protein is both necessary and sufficient for integrative recombination in vitro*. Cell, 1990. **63**(1): p. 87-95.
267. Englund, G., et al., *Integration is required for productive infection of monocyte-derived macrophages by human immunodeficiency virus type 1*. J Virol, 1995. **69**(5): p. 3216-9.
268. Mochizuki, H., et al., *High-titer human immunodeficiency virus type 1-based vector systems for gene delivery into nondividing cells*. J Virol, 1998. **72**(11): p. 8873-83.
269. Wang, X. and M. McManus, *Lentivirus production*. J Vis Exp, 2009(32).
270. Zhang, X.Y., V.F. La Russa, and J. Reiser, *Transduction of bone-marrow-derived mesenchymal stem cells by using lentivirus vectors pseudotyped with modified RD114 envelope glycoproteins*. J Virol, 2004. **78**(3): p. 1219-29.

271. Shaw, A.M., et al., *Differences in vector-genome processing and illegitimate integration of non-integrating lentiviral vectors*. *Gene Ther*, 2017. **24**(1): p. 12-20.
272. Wang, Y., et al., *Integration-defective lentiviral vector mediates efficient gene editing through homology-directed repair in human embryonic stem cells*. *Nucleic Acids Res*, 2016.
273. Rio, P., et al., *Targeted gene therapy and cell reprogramming in Fanconi anemia*. *EMBO Mol Med*, 2014. **6**(6): p. 835-48.
274. Maeder, M.L. and C.A. Gersbach, *Genome-editing Technologies for Gene and Cell Therapy*. *Mol Ther*, 2016. **24**(3): p. 430-46.
275. Cornu, T.I. and T. Cathomen, *Targeted genome modifications using integrase-deficient lentiviral vectors*. *Mol Ther*, 2007. **15**(12): p. 2107-13.
276. Prakash, V., M. Moore, and R.J. Yanez-Munoz, *Current Progress in Therapeutic Gene Editing for Monogenic Diseases*. *Mol Ther*, 2016. **24**(3): p. 465-74.
277. Justilien, V., et al., *SOD2 knockdown mouse model of early AMD*. *Invest Ophthalmol Vis Sci*, 2007. **48**(10): p. 4407-20.
278. Schachat AP, W.C., Hinton DR, Sadda SE, Wiedemann P, *Ryan's Retina*. Elsevier, 2018. **1**(6th Edition).
279. Schambach, A., et al., *Biosafety features of lentiviral vectors*. *Hum Gene Ther*, 2013. **24**(2): p. 132-42.
280. Bayer, M., et al., *A large U3 deletion causes increased in vivo expression from a nonintegrating lentiviral vector*. *Mol Ther*, 2008. **16**(12): p. 1968-76.
281. Hanenberg, H., et al., *Optimization of fibronectin-assisted retroviral gene transfer into human CD34+ hematopoietic cells*. *Hum Gene Ther*, 1997. **8**(18): p. 2193-206.
282. Philippe, S., et al., *Lentiviral vectors with a defective integrase allow efficient and sustained transgene expression in vitro and in vivo*. *Proc Natl Acad Sci U S A*, 2006. **103**(47): p. 17684-9.
283. Dutt, P., et al., *A recombinant human fibronectin fragment facilitates retroviral mediated gene transfer into human hematopoietic progenitor cells*. *Biochem Mol Biol Int*, 1997. **42**(5): p. 909-17.
284. Wanisch, K. and R.J. Yanez-Munoz, *Integration-deficient lentiviral vectors: a slow coming of age*. *Mol Ther*, 2009. **17**(8): p. 1316-32.
285. Di Stasi, A., et al., *Inducible apoptosis as a safety switch for adoptive cell therapy*. *N Engl J Med*, 2011. **365**(18): p. 1673-83.
286. Zhou, X. and M.K. Brenner, *Improving the safety of T-Cell therapies using an inducible caspase-9 gene*. *Exp Hematol*, 2016. **44**(11): p. 1013-1019.
287. Case, S.S., et al., *Stable transduction of quiescent CD34(+)CD38(-) human hematopoietic cells by HIV-1-based lentiviral vectors*. *Proc Natl Acad Sci U S A*, 1999. **96**(6): p. 2988-93.
288. Haas, D.L., et al., *Critical factors influencing stable transduction of human CD34(+) cells with HIV-1-derived lentiviral vectors*. *Mol Ther*, 2000. **2**(1): p. 71-80.
289. Vargas, J., Jr., et al., *Novel integrase-defective lentiviral episomal vectors for gene transfer*. *Hum Gene Ther*, 2004. **15**(4): p. 361-72.

290. Suwanmanee, T., et al., *Integration-deficient lentiviral vectors expressing codon-optimized R338L human FIX restore normal hemostasis in Hemophilia B mice*. Mol Ther, 2014. **22**(3): p. 567-74.
291. Negri, D.R., et al., *Successful immunization with a single injection of non-integrating lentiviral vector*. Mol Ther, 2007. **15**(9): p. 1716-23.
292. Vargas, J., Jr., M.E. Klotman, and A. Cara, *Conditionally replicating lentiviral-hybrid episomal vectors for suicide gene therapy*. Antiviral Res, 2008. **80**(3): p. 288-94.
293. Teschendorf, C., et al., *Comparison of the EF-1 alpha and the CMV promoter for engineering stable tumor cell lines using recombinant adeno-associated virus*. Anticancer Res, 2002. **22**(6A): p. 3325-30.
294. Berger, G., et al., *SIVMAC Vpx improves the transduction of dendritic cells with nonintegrative HIV-1-derived vectors*. Gene Ther, 2009. **16**(1): p. 159-63.
295. Negri, D.R., et al., *Simian immunodeficiency virus-Vpx for improving integrase defective lentiviral vector-based vaccines*. Retrovirology, 2012. **9**: p. 69.
296. Paul, R.W., et al., *Increased viral titer through concentration of viral harvests from retroviral packaging lines*. Hum Gene Ther, 1993. **4**(5): p. 609-15.
297. Sanes, J.R., J.L. Rubenstein, and J.F. Nicolas, *Use of a recombinant retrovirus to study post-implantation cell lineage in mouse embryos*. EMBO J, 1986. **5**(12): p. 3133-42.
298. Chuck, A.S., M.F. Clarke, and B.O. Palsson, *Retroviral infection is limited by Brownian motion*. Hum Gene Ther, 1996. **7**(13): p. 1527-34.
299. Moritz, T., et al., *Fibronectin improves transduction of reconstituting hematopoietic stem cells by retroviral vectors: evidence of direct viral binding to chymotryptic carboxy-terminal fragments*. Blood, 1996. **88**(3): p. 855-62.
300. Hanenberg, H., et al., *Colocalization of retrovirus and target cells on specific fibronectin fragments increases genetic transduction of mammalian cells*. Nat Med, 1996. **2**(8): p. 876-82.
301. Kiem, H.P., et al., *Improved gene transfer into baboon marrow repopulating cells using recombinant human fibronectin fragment CH-296 in combination with interleukin-6, stem cell factor, FLT-3 ligand, and megakaryocyte growth and development factor*. Blood, 1998. **92**(6): p. 1878-86.
302. Donahue, R.E. and C.E. Dunbar, *Update on the use of nonhuman primate models for preclinical testing of gene therapy approaches targeting hematopoietic cells*. Hum Gene Ther, 2001. **12**(6): p. 607-17.
303. Neff, T., et al., *Methylguanine methyltransferase-mediated in vivo selection and chemoprotection of allogeneic stem cells in a large-animal model*. J Clin Invest, 2003. **112**(10): p. 1581-8.
304. Cornetta, K. and W.F. Anderson, *Protamine sulfate as an effective alternative to polybrene in retroviral-mediated gene-transfer: implications for human gene therapy*. J Virol Methods, 1989. **23**(2): p. 187-94.

305. Bharti, K., et al., *Alternative promoter use in eye development: the complex role and regulation of the transcription factor MITF*. *Development*, 2008. **135**(6): p. 1169-78.
306. Maruotti, J., et al., *MITF-M, a 'melanocyte-specific' isoform, is expressed in the adult retinal pigment epithelium*. *Pigment Cell Melanoma Res*, 2012. **25**(5): p. 641-4.
307. Adijanto, J., et al., *Microphthalmia-associated transcription factor (MITF) promotes differentiation of human retinal pigment epithelium (RPE) by regulating microRNAs-204/211 expression*. *J Biol Chem*, 2012. **287**(24): p. 20491-503.
308. Bharti, K., et al., *A regulatory loop involving PAX6, MITF, and WNT signaling controls retinal pigment epithelium development*. *PLoS Genet*, 2012. **8**(7): p. e1002757.
309. Wei, B., et al., *Cilostazol promotes production of melanin by activating the microphthalmia-associated transcription factor (MITF)*. *Biochem Biophys Res Commun*, 2014. **443**(2): p. 617-21.
310. Kiuchi, K., et al., *Morphologic characteristics of retinal degeneration induced by sodium iodate in mice*. *Curr Eye Res*, 2002. **25**(6): p. 373-9.
311. Michelini, Z., D. Negri, and A. Cara, *Integrase defective, nonintegrating lentiviral vectors*. *Methods Mol Biol*, 2010. **614**: p. 101-10.
312. Wang, X., et al., *Unbiased detection of off-target cleavage by CRISPR-Cas9 and TALENs using integrase-defective lentiviral vectors*. *Nat Biotechnol*, 2015. **33**(2): p. 175-8.
313. Kim, J., et al., *Liver cell line derived conditioned medium enhances myofibril organization of primary rat cardiomyocytes*. *Mol Cells*, 2012. **34**(2): p. 149-58.
314. Li, Q., et al., *Regenerative and reparative effects of human chorion-derived stem cell conditioned medium on photo-aged epidermal cells*. *Cell Cycle*, 2016. **15**(8): p. 1144-55.
315. Xing, X., et al., *Differentiation of human umbilical cord mesenchymal stem cells into steroidogenic cells in vitro*. *Exp Ther Med*, 2016. **12**(6): p. 3527-3534.
316. Cantinieaux, D., et al., *Conditioned medium from bone marrow-derived mesenchymal stem cells improves recovery after spinal cord injury in rats: an original strategy to avoid cell transplantation*. *PLoS One*, 2013. **8**(8): p. e69515.
317. Chen, L., et al., *Conditioned medium from hypoxic bone marrow-derived mesenchymal stem cells enhances wound healing in mice*. *PLoS One*, 2014. **9**(4): p. e96161.
318. Heino, T.J., T.A. Hentunen, and H.K. Vaananen, *Conditioned medium from osteocytes stimulates the proliferation of bone marrow mesenchymal stem cells and their differentiation into osteoblasts*. *Exp Cell Res*, 2004. **294**(2): p. 458-68.
319. Baraniak, P.R. and T.C. McDevitt, *Stem cell paracrine actions and tissue regeneration*. *Regen Med*, 2010. **5**(1): p. 121-43.

320. Johnson, T.V., et al., *Neuroprotective effects of intravitreal mesenchymal stem cell transplantation in experimental glaucoma*. Invest Ophthalmol Vis Sci, 2010. **51**(4): p. 2051-9.
321. Jung, G., et al., *Genetically modified neural stem cells for a local and sustained delivery of neuroprotective factors to the dystrophic mouse retina*. Stem Cells Transl Med, 2013. **2**(12): p. 1001-10.
322. Kots, A.Y., et al., *Pyridopyrimidine derivatives as inhibitors of cyclic nucleotide synthesis: Application for treatment of diarrhea*. Proc Natl Acad Sci U S A, 2008. **105**(24): p. 8440-5.
323. Onda, T., et al., *Type-specific regulation of adenylyl cyclase. Selective pharmacological stimulation and inhibition of adenylyl cyclase isoforms*. J Biol Chem, 2001. **276**(51): p. 47785-93.
324. Pierre, S., et al., *Capturing adenylyl cyclases as potential drug targets*. Nat Rev Drug Discov, 2009. **8**(4): p. 321-35.
325. Sapio, L., et al., *The Natural cAMP Elevating Compound Forskolin in Cancer Therapy: Is It Time?* J Cell Physiol, 2017. **232**(5): p. 922-927.
326. Bielekova, B., et al., *Treatment with the phosphodiesterase type-4 inhibitor rolipram fails to inhibit blood--brain barrier disruption in multiple sclerosis*. Mult Scler, 2009. **15**(10): p. 1206-14.
327. Day, R.N., W. Tao, and K.W. Dunn, *A simple approach for measuring FRET in fluorescent biosensors using two-photon microscopy*. Nat Protoc, 2016. **11**(11): p. 2066-80.
328. Mantel, C.R., et al., *Enhancing Hematopoietic Stem Cell Transplantation Efficacy by Mitigating Oxygen Shock*. Cell, 2015. **161**(7): p. 1553-65.
329. Fritsche, L.G., et al., *Seven new loci associated with age-related macular degeneration*. Nat Genet, 2013. **45**(4): p. 433-9, 439e1-2.
330. Banasik, M.B. and P.B. McCray, Jr., *Integrase-defective lentiviral vectors: progress and applications*. Gene Ther, 2010. **17**(2): p. 150-7.
331. Wang, X., et al., *Cell fusion is the principal source of bone-marrow-derived hepatocytes*. Nature, 2003. **422**(6934): p. 897-901.
332. Jeon, C.J., E. Strettoi, and R.H. Masland, *The major cell populations of the mouse retina*. J Neurosci, 1998. **18**(21): p. 8936-46.
333. Panda-Jonas, S., et al., *Retinal photoreceptor count, retinal surface area, and optic disc size in normal human eyes*. Ophthalmology, 1994. **101**(3): p. 519-23.
334. Arimura, K., et al., *Acute lung Injury in a healthy donor during mobilization of peripheral blood stem cells using granulocyte-colony stimulating factor alone*. Haematologica, 2005. **90**(3): p. ECR10.
335. Gori, J.L., et al., *Efficient generation, purification, and expansion of CD34(+) hematopoietic progenitor cells from nonhuman primate-induced pluripotent stem cells*. Blood, 2012. **120**(13): p. e35-44.
336. Pennesi, M.E., M. Neuringer, and R.J. Courtney, *Animal models of age related macular degeneration*. Mol Aspects Med, 2012. **33**(4): p. 487-509.
337. Morimura, H., et al., *Mutations in the RPE65 gene in patients with autosomal recessive retinitis pigmentosa or leber congenital amaurosis*. Proc Natl Acad Sci U S A, 1998. **95**(6): p. 3088-93.

CURRICULUM VITAE

S. Louise Pay

EDUCATION

- 2005-2007 **HNC, Arts and Social Sciences**, University of Aberdeen, Aberdeen, United Kingdom.
- 2007-2011 **BSc (Hons) First Class, Biomedical Sciences**, Edinburgh Napier University, Edinburgh, United Kingdom.
Honours Thesis: “Chitosan-Mediated Inhibition of *Pseudomonas Aeruginosa* Biofilm Formation in Polyethylene Catheter Tubing”.
Research Mentors: Dr. Douglas Fraser-Pitt (Novabiotics Ltd, Aberdeen, UK), Dr. Brandi L. Baros (Pennsylvania State University).
- 2011-2017 **PhD**, Department of Medical and Molecular Genetics, Indiana University, Indiana University- Purdue University Indianapolis Indianapolis, Indiana, USA **Major: Medical and Molecular Genetics**
Minor: Life Sciences
Thesis Topic: “A Systemically-Delivered Stem Cell Therapy for Dry Age-Related Macular Degeneration”.

Research Mentors: Dr. Michael E. Boulton and Dr. Maria B. Grant

Committee Members: Dr. Hal E. Broxmeyer, Dr. Janaiah Kota, Dr. Nuria Morral

Collaborations/Additional Projects: Dr. Fletcher White and Dr. Todd McKinley (analysis of circulating cell-free DNA), Dr. Maria Grant and Dr. Murray Korc (A Bi-Specific Chimeric Antigen Receptor T-Cell for Pancreatic Cancer), Dr. Maria Grant (stem cells obtained via acupuncture for treatment of equine injuries).

RESEARCH AND TRAINING EXPERIENCE

2007-2009

Technical Research Assistant, Center for Timber Engineering, Edinburgh Napier University, Edinburgh, United Kingdom.

Project: Development of a novel cellulose-based advanced material. A confidentiality agreement prevents further disclosure of project details.

Supervisor: Dr. Simon Curling

Director: Professor Philip Turner.

- 2009-2011 **Research Assistant**, School of Life, Sport and Social Sciences, Department of Microbiology and Biotechnology, Edinburgh Napier University, Edinburgh, United Kingdom.
Project: Characterization of a Putative ABC-Transporter in *Salmonella enterica* sv. Typhimurium.
Supervisor: Dr. Clare M. Taylor
- 2012-2013 **Graduate Research**, Herman B Wells Center for Pediatric Research, Indiana University School of Medicine, Indianapolis, Indiana, USA.
Project(s): Optimization of lentiviral vector infection protocols with fibronectin, a cre-recombinase lentiviral based system for excising floxed genes *in vitro*, and the use of a novel suicide gene system in Graft-versus-Host disease and chimeric antigen receptor T-cell therapies.
Research Mentor: Dr. Helmut Hanenberg.

TEACHING EXPERIENCE

- 2010-2011 **Problem-Based Learning Facilitator**, University of Edinburgh Medical School, University of Edinburgh, Edinburgh, United Kingdom.
Job Description: Taught small groups of 1st and 2nd year Medical students, covering: cardiovascular disease,

immunology, genetics, cancer, clinical medicine, sports injuries, infectious disease, and gastrointestinal disorders.

2013-2017 Mentoring summer students and undergraduates in laboratory research, Indiana University School of Medicine, Indianapolis, Indiana, USA.

ACADEMIC ACTIVITIES

2012-2014 ***Student Representative***, Department of Medical and Molecular Genetics, Indiana University School of Medicine, Indianapolis, Indiana, USA.

Responsibilities: Attending faculty meetings, organizing events, coordinating a student journal club, and promoting student networking within the department.

2012-2014 ***Medical and Molecular Genetics Representative***, IU School of Medicine Student Representative Committee, Indiana University School of Medicine, Indianapolis, Indiana, USA.

Responsibilities: Meeting with representatives from all departments to discuss student issues, organizing student events, reviewing student travel grant applications, and

attending Graduate and Professional Student Government meetings.

- 2014 **Careers Event Coordinator**, Graduate Division, Indiana University School of Medicine, Indianapolis, Indiana, USA.
Responsibilities: Organized speakers, venue, and program for a careers event for graduate students and postdocs at the IU School of Medicine held in Spring 2014.

POSTER PRESENTATIONS

- 2012 11th General Meeting of the American Society for Microbiology, San Francisco, California, USA. **Pay SL**, Baros BL, Fraser-Pitt D. “Chitosan-Mediated Inhibition of *Pseudomonas aeruginosa* Biofilm Formation in Polyethylene Catheter Tubing”. (Poster)
- 2013 4th Eugene and Marion Glick Eye Institute Vision Research Symposium, Indianapolis, Indiana, USA. **Pay SL**, Wurm M, Leurs C, Lindemann D, Hanenberg H. “Retroviral Gene Therapy: May the Fibronectin be With You” (Poster)
- 2014 Department of Medical and Molecular Genetics Poster Session, Indianapolis, Indiana, USA. **Pay SL**, Yan Y, Shaw L, Lewin A, Grant MB, Boulton ME. Bone Marrow Progenitor

Cells Expressing *RPE65* Repopulate the RPE in the SOD2-KD Model of Early Age-Related Macular Degeneration.

(Poster)

2015

IU Simon Cancer Center Cancer Research Day, Indianapolis, Indiana, USA. **Pay SL**, Korc M, Grant MB. A Bi-Specific Chimeric Antigen Receptor T-Cell for Targeting Pancreatic Cancer. (Poster)

2015

Department of Medical and Molecular Genetics Poster Session. Indianapolis, Indiana, USA. **Pay, SL**, Willard JF, Grant MB, Boulton ME. An Integrase-Deficient Lentiviral Vector for Reprogramming Bone Marrow-Derived Cells. (Poster)

2016

2nd Annual Symposium on Cell Therapy and Regenerative Medicine, Indianapolis, Indiana, USA. **Pay SL**, Quigley J, Qi X, Willard J, Grant MB, Boulton ME. Bone Marrow-Derived Cells as a Therapy for Retinal Degeneration. (Poster)

ORAL PRESENTATIONS

2014

Department of Medical and Molecular Genetics Seminar Series. Indianapolis, Indiana, USA **Pay, SL**, Grant MB,

Boulton ME. A Novel Non-Invasive Cell-Based Therapy for Retinal Degeneration. (Presentation).

2016 Sigma Xi Graduate Student Research Competition, Indianapolis, Indiana, USA. **Pay, SL.** A Non-Invasive Therapy for Dry Age-Related Macular Degeneration.

AWARDS

2016 Robert C. Miller Award for Excellence in Vascular Research, Pre-Doctoral Level. 2nd Annual Symposium on Cell Therapy and Regenerative Medicine, Indianapolis, Indiana, USA

2016 1st Place: Sigma Xi Graduate Student Research Division, Senior Graduate Student Level. Indianapolis, Indiana, USA.

PEER-REVIEWED PUBLICATIONS

Qi, X, Pay SL, Yan Y, Fajardo D, Mao H, Lewin AS, Chang LJ, Grant MB, Boulton ME (2017). Systemic Injection of *RPE65*-Programmed Bone Marrow-Derived Cells Prevents Progression of Chronic Retinal Degeneration. *Molecular Therapy*. Published Online: January 23rd 2017.

Qian Q, Mitter SK, Pay SL, Qi X, Rickman CB, Grant MB, Boulton ME (2016) A Non-Canonical Role for Beta-Secretase in the Retina. *Adv Exp Med Biol*. 854: 333-339

Blue EK, Digioseppe R, Derr-Yellin E, Acosta JC, Pay SL, Hanenberg H, Schellinger MM, Quinney SK, Mund JA, Case J, Haneline LS (2014). Gestational Diabetes Induces Alterations in the Function of Neonatal Endothelial Colony Forming Cells. *Pediatr Res.* 75(2): 266-272

BOOK CHAPTERS

Boulton ME, Mitter SK, **Pay SL.** (2017) Cell Death, Apoptosis, and Autophagy in Retinal Injury. Ryan SJ *Retina (6th Edition)*, Saunders. (Not yet in print)

MANUSCRIPTS UNDER REVIEW

Pay SL, Qi X, Willard J, Sankhavaram K, Horton R, Mitter S, Quigley J, Chang LJ, Grant MB, Boulton ME. Improving the Infection of Bone Marrow-Derived Cells with an Integrase-Defective Lentiviral Vector. Submitted to *Human Gene Therapy* in May 2017.

MANUSCRIPTS IN PREPARATION

Pay, SL, Qi X, Quigley J, Willard J, Chang LJ, Grant MB, Boulton ME. Bone Marrow-Derived Cells Programmed with *RPE65*-Expressing Non-Integrating Lentiviral Vectors Prevent Progression of Retinal Degeneration.

Hato T, Zollman A, Plotkin Z, El-Achkar T, Maier B, **Pay SL,** Graham P, Dube S, Cabral P, Yoshimoto M, McClintick J, Dagher P. Endotoxin Preconditioning-Induced Protective Gene and Metabolic Reprogramming in Sepsis.

CURRICULUM VITAE

S. Louise Pay

EDUCATION

- 2005-2007 **HNC, Arts and Social Sciences**, University of Aberdeen, Aberdeen, United Kingdom.
- 2007-2011 **BSc (Hons) First Class, Biomedical Sciences**, Edinburgh Napier University, Edinburgh, United Kingdom.
Honours Thesis: “Chitosan-Mediated Inhibition of *Pseudomonas Aeruginosa* Biofilm Formation in Polyethylene Catheter Tubing”.
Research Mentors: Dr. Douglas Fraser-Pitt (Novabiotics Ltd, Aberdeen, UK), Dr. Brandi L. Baros (Pennsylvania State University).
- 2011-2017 **PhD**, Department of Medical and Molecular Genetics, Indiana University, Indiana University- Purdue University Indianapolis Indianapolis, Indiana, USA **Major: Medical and Molecular Genetics**
Minor: Life Sciences
Thesis Topic: “A Systemically-Delivered Stem Cell Therapy for Dry Age-Related Macular Degeneration”.

Research Mentors: Dr. Michael E. Boulton and Dr. Maria B. Grant

Committee Members: Dr. Hal E. Broxmeyer, Dr. Janaiah Kota, Dr. Nuria Morral

Collaborations/Additional Projects: Dr. Fletcher White and Dr. Todd McKinley (analysis of circulating cell-free DNA), Dr. Maria Grant and Dr. Murray Korc (A Bi-Specific Chimeric Antigen Receptor T-Cell for Pancreatic Cancer), Dr. Maria Grant (stem cells obtained via acupuncture for treatment of equine injuries).

RESEARCH AND TRAINING EXPERIENCE

2007-2009

Technical Research Assistant, Center for Timber Engineering, Edinburgh Napier University, Edinburgh, United Kingdom.

Project: Development of a novel cellulose-based advanced material. A confidentiality agreement prevents further disclosure of project details.

Supervisor: Dr. Simon Curling

Director: Professor Philip Turner.

- 2009-2011 **Research Assistant**, School of Life, Sport and Social Sciences, Department of Microbiology and Biotechnology, Edinburgh Napier University, Edinburgh, United Kingdom.
Project: Characterization of a Putative ABC-Transporter in *Salmonella enterica* sv. Typhimurium.
Supervisor: Dr. Clare M. Taylor
- 2012-2013 **Graduate Research**, Herman B Wells Center for Pediatric Research, Indiana University School of Medicine, Indianapolis, Indiana, USA.
Project(s): Optimization of lentiviral vector infection protocols with fibronectin, a cre-recombinase lentiviral based system for excising floxed genes *in vitro*, and the use of a novel suicide gene system in Graft-versus-Host disease and chimeric antigen receptor T-cell therapies.
Research Mentor: Dr. Helmut Hanenberg.

TEACHING EXPERIENCE

- 2010-2011 **Problem-Based Learning Facilitator**, University of Edinburgh Medical School, University of Edinburgh, Edinburgh, United Kingdom.
Job Description: Taught small groups of 1st and 2nd year Medical students, covering: cardiovascular disease,

immunology, genetics, cancer, clinical medicine, sports injuries, infectious disease, and gastrointestinal disorders.

2013-2017 Mentoring summer students and undergraduates in laboratory research, Indiana University School of Medicine, Indianapolis, Indiana, USA.

ACADEMIC ACTIVITIES

2012-2014 ***Student Representative***, Department of Medical and Molecular Genetics, Indiana University School of Medicine, Indianapolis, Indiana, USA.

Responsibilities: Attending faculty meetings, organizing events, coordinating a student journal club, and promoting student networking within the department.

2012-2014 ***Medical and Molecular Genetics Representative***, IU School of Medicine Student Representative Committee, Indiana University School of Medicine, Indianapolis, Indiana, USA.

Responsibilities: Meeting with representatives from all departments to discuss student issues, organizing student events, reviewing student travel grant applications, and

attending Graduate and Professional Student Government meetings.

- 2014 **Careers Event Coordinator**, Graduate Division, Indiana University School of Medicine, Indianapolis, Indiana, USA.
Responsibilities: Organized speakers, venue, and program for a careers event for graduate students and postdocs at the IU School of Medicine held in Spring 2014.

POSTER PRESENTATIONS

- 2012 11th General Meeting of the American Society for Microbiology, San Francisco, California, USA. **Pay SL**, Baros BL, Fraser-Pitt D. “Chitosan-Mediated Inhibition of *Pseudomonas aeruginosa* Biofilm Formation in Polyethylene Catheter Tubing”. (Poster)
- 2013 4th Eugene and Marion Glick Eye Institute Vision Research Symposium, Indianapolis, Indiana, USA. **Pay SL**, Wurm M, Leurs C, Lindemann D, Hanenberg H. “Retroviral Gene Therapy: May the Fibronectin be With You” (Poster)
- 2014 Department of Medical and Molecular Genetics Poster Session, Indianapolis, Indiana, USA. **Pay SL**, Yan Y, Shaw L, Lewin A, Grant MB, Boulton ME. Bone Marrow Progenitor

Cells Expressing *RPE65* Repopulate the RPE in the SOD2-KD Model of Early Age-Related Macular Degeneration.

(Poster)

2015

IU Simon Cancer Center Cancer Research Day, Indianapolis, Indiana, USA. **Pay SL**, Korc M, Grant MB. A Bi-Specific Chimeric Antigen Receptor T-Cell for Targeting Pancreatic Cancer. (Poster)

2015

Department of Medical and Molecular Genetics Poster Session. Indianapolis, Indiana, USA. **Pay, SL**, Willard JF, Grant MB, Boulton ME. An Integrase-Deficient Lentiviral Vector for Reprogramming Bone Marrow-Derived Cells. (Poster)

2016

2nd Annual Symposium on Cell Therapy and Regenerative Medicine, Indianapolis, Indiana, USA. **Pay SL**, Quigley J, Qi X, Willard J, Grant MB, Boulton ME. Bone Marrow-Derived Cells as a Therapy for Retinal Degeneration. (Poster)

ORAL PRESENTATIONS

2014

Department of Medical and Molecular Genetics Seminar Series. Indianapolis, Indiana, USA **Pay, SL**, Grant MB,

Boulton ME. A Novel Non-Invasive Cell-Based Therapy for Retinal Degeneration. (Presentation).

2016 Sigma Xi Graduate Student Research Competition, Indianapolis, Indiana, USA. **Pay, SL.** A Non-Invasive Therapy for Dry Age-Related Macular Degeneration.

AWARDS

2016 Robert C. Miller Award for Excellence in Vascular Research, Pre-Doctoral Level. 2nd Annual Symposium on Cell Therapy and Regenerative Medicine, Indianapolis, Indiana, USA

2016 1st Place: Sigma Xi Graduate Student Research Division, Senior Graduate Student Level. Indianapolis, Indiana, USA.

PEER-REVIEWED PUBLICATIONS

Qi, X, Pay SL, Yan Y, Fajardo D, Mao H, Lewin AS, Chang LJ, Grant MB, Boulton ME (2017). Systemic Injection of *RPE65*-Programmed Bone Marrow-Derived Cells Prevents Progression of Chronic Retinal Degeneration. *Molecular Therapy*. Published Online: January 23rd 2017.

Qian Q, Mitter SK, Pay SL, Qi X, Rickman CB, Grant MB, Boulton ME (2016) A Non-Canonical Role for Beta-Secretase in the Retina. *Adv Exp Med Biol*. 854: 333-339

Blue EK, Diguseppe R, Derr-Yellin E, Acosta JC, Pay SL, Hanenberg H, Schellinger MM, Quinney SK, Mund JA, Case J, Haneline LS (2014). Gestational Diabetes Induces Alterations in the Function of Neonatal Endothelial Colony Forming Cells. *Pediatr Res.* 75(2): 266-272

BOOK CHAPTERS

Boulton ME, Mitter SK, **Pay SL.** (2017) Cell Death, Apoptosis, and Autophagy in Retinal Injury. Ryan SJ *Retina (6th Edition)*, Saunders. (Not yet in print)

MANUSCRIPTS UNDER REVIEW

Pay SL, Qi X, Willard J, Sankhavaram K, Horton R, Mitter S, Quigley J, Chang LJ, Grant MB, Boulton ME. Improving the Infection of Bone Marrow-Derived Cells with an Integrase-Defective Lentiviral Vector. Submitted to *Human Gene Therapy* in May 2017.

MANUSCRIPTS IN PREPARATION

Pay, SL, Qi X, Quigley J, Willard J, Chang LJ, Grant MB, Boulton ME. Bone Marrow-Derived Cells Programmed with *RPE65*-Expressing Non-Integrating Lentiviral Vectors Prevent Progression of Retinal Degeneration.

Hato T, Zollman A, Plotkin Z, El-Achkar T, Maier B, **Pay SL,** Graham P, Dube S, Cabral P, Yoshimoto M, McClintick J, Dagher P. Endotoxin Preconditioning-Induced Protective Gene and Metabolic Reprogramming in Sepsis.